Ministry of Higher Education and Scientific Research

Djillali Liabes University
of Sidi Bel-Abbes

*Faculty of Electrical Engineering*

# JDGE'2023

## Fourth Doctoral Days in Electrical Engineering

# Abstract's Book

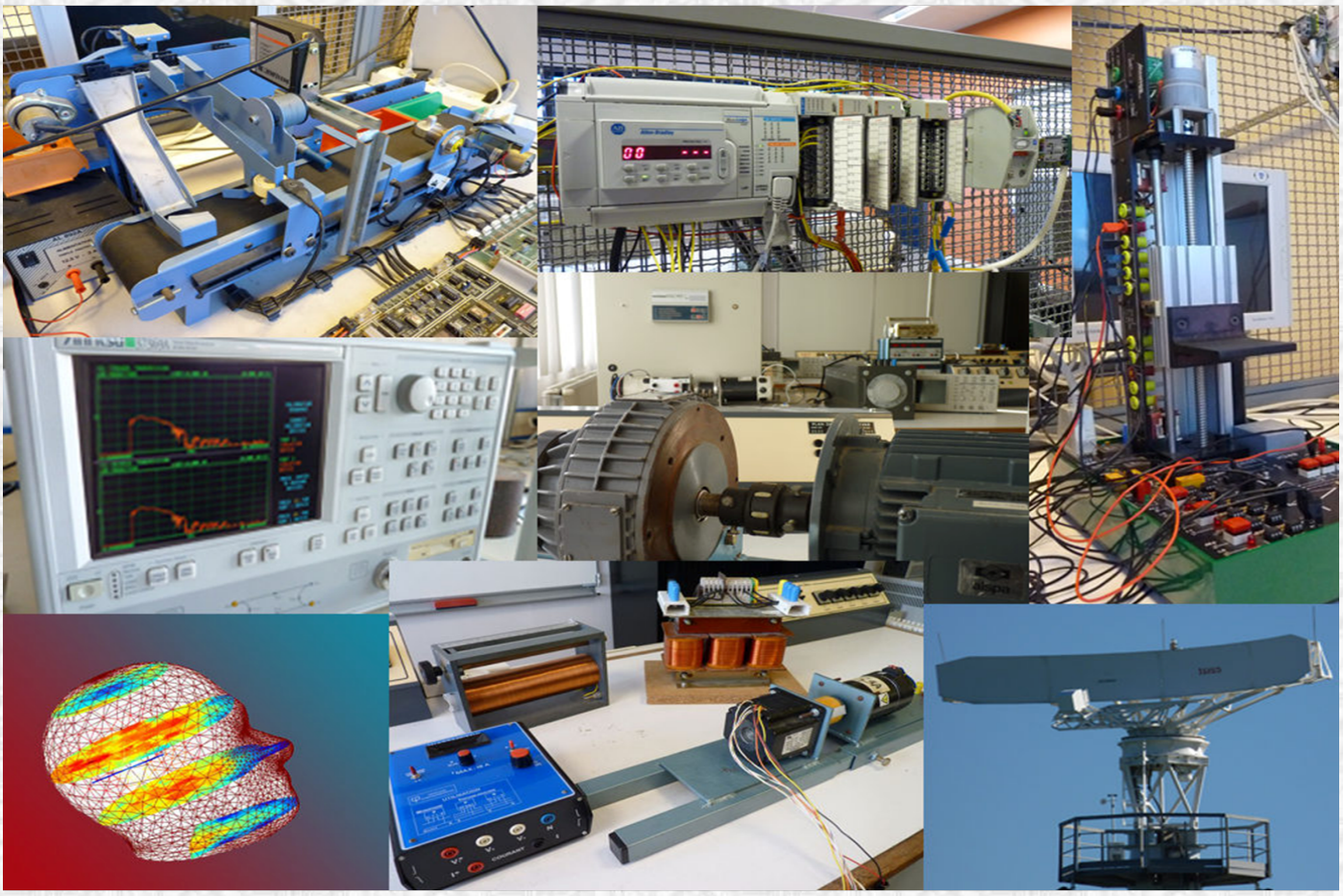

**Sidi Bel-Abbes, November, 28-29, 2023**

**Présidents d'honneur**
Pr. BOUZIANI Merahi
Recteur de l'université de Sidi Bel Abbès

Pr. KHADRAOUI Mohamed
Doyen de la Faculté de Génie Electrique

**Président du Workshop**
Pr. BENDAOUD Abdelber

**Comité d'organisation**
Dr. KACHA Arselane Hatem
Dr. KANDOUCI Chahinaz
Pr. MAHDJOUB Zoubir
Mr. SEKKAL Sidi Mohamed
Dr. JBILOU Mokhtaria
Dr. TOLBI Bilal
Dr. ALAMI Ahmed
Pr. TALBI Abassia
Dr. BECHEKIR Seif Eddine
Dr. OUAHAB Iman

**Comité scientifique**
Pr. ANANI Macho
Pr. TILMATINE Amar
Pr. ABID Hamza
Pr. ABID Mohamed
Pr. BENAMARA Zineb
Pr. BRAHAMI Mostéfa
Pr. KHADRAOUI Mohammed
Pr. MAHDJOUB Zoubir
Pr. TALEB Nasreddine
Pr. DJEBBARI Ali

# Sommaire

# Génération d'un MPD/MPEG-DASH

**A. BENHASSAINI[1], S. A. CHOUAKRI[1], F. MESKINE[2]**

[1] *Laboratoire Télécommunications et Traitement Numérique du Signal (LTTNS)*
[2]*Réseaux de Communications, Architectures et Multimédia(RCAM)*
*Email : benhassainiabdelatif@gmail.com*

**ABSTRACT**

La diffusion adaptative de vidéos en continu est devenue un pilier majeur de l'industrie de la diffusion en ligne. MPEG-DASH est l'un des protocoles de streaming vidéo les plus populaires et est largement utilisé pour diffuser des médias via la vidéo à la demande (VOD) ou la diffusion en direct. En MPEG-DASH, une vidéo est divisée en segments encodés d'une façon qui permet de s'adapter aux contraintes du réseau et aux limites des équipements des utilisateurs finaux ; ces informations caractéristiques sont enregistré dans un fichier appelé manifeste ou MPD (Media Présentation Description).Le MPD est d'abord transmis au lecteur, qui l'utilise pour demander des segments du débit binaire et de la résolution appropriée en fonction de diverses conditions pour garantir une expérience de visionnage fluide et de plus haute qualité possible. La génération d'un MPD en utilisant la norme MPEG-DASH implique plusieurs étapes essentielles. Tout d'abord, l'encodage du contenu vidéo est effectué pour créer des fichiers de médias adaptatifs. Ensuite, ces fichiers sont segmentés en segments vidéo et audio de courte durée. Une fois les segments créés, un fichier MPD est généré pour décrire la structure de présentation, les résolutions disponibles, les débits et les adresses URL des segments. Le MPD inclut également des informations sur les règles de streaming adaptatif. Enfin, le MPD et les segments sont hébergés sur un serveur de streaming pour être accessible aux clients. Pour approfondir la description de présentation multimédia DASH (MPD), telle que définie dans la norme ISO/IEC 23009-1. L'objectif de ce travail est de permettre de mieux comprendre les différentes parties d'un MPD DASH, à quoi elles servent et comment elles sont générées. On éxplore une approche de génération de MPD statique pour les services VOD, l'organigrame de cette approche est décrit dans la figure 1. En utilisant des outils open source largement adoptés, tels que FFMPEG, GPAC et MP4Box pour la partie préparation du contenu DASH figure 2. Le manifeste résultant est décrit dans la figure 3 ; La conformité de ce dernier au schéma de base de MPD MPEG-DASH doit être testée ; pour cela, dans la figure 4, le Validateur DASH de la boîte à outils du consensus « conformance.dashif.org » est utilisé, dont le résultat de la partie MPD est décrit à la figure 5 qui nous conduit dans les futurs travaux à la recherche de la conformité avec les autres schémas MPD MPEG-DASH. La lecture du contenu par des lecteurs compatibles DASH -tel que MP4Box dans notre cas- garantit le bon fonctionnement du contenu lors du streaming.

**Keywords:**MPEG-DASH; MPD; Manifest; VoD; FFMPEG; GPAC.

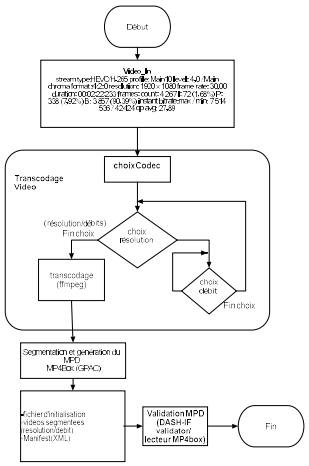


*Fig 1:Organigrame de génération de contenu DASH*

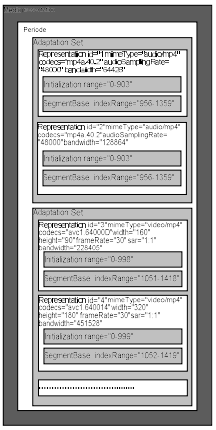

*Fig 2:Model résultant de données DASH de haut niveau*

*Fig 3:Manifest résultant*

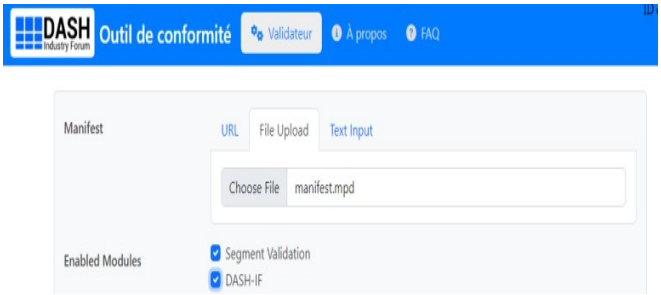


*Fig 4:Validation du Manifest résultant*


*Fig 5:Partie MPD du resultat de validation du Manifest résultant*

## References

[1] ISO/IEC 23009-1 Information technology — Dynamic adaptive streaming over HTTP (DASH) — Part 1: Media presentation description and segment formats,2022.

[2] İren, Ecem & Kantarci, Aylin. (2022). Content Aware Video Streaming with MPEG DASH Technology. TEM Journal. 11. 611-619. 10.18421/TEM112-15.

[3] MP4Box. https://gpac.wp.mines-telecom.fr/mp4box/. [last visited, Oct. 1, 2023].

[4] Subhash, V.. (2023). Starting with FFmpeg. 10.1007/978-1-4842-8701-9_2.

# Performance Analysis of Window Functions in Filtered OFDM Systems for 5G and Beyond

S. BENIEDDI, S. A. ELAHMAR

*Telecommunications and Digital Signal Processing Laboratory, University of Djillali Liabes, Sidi Bel-Abbes, Algeria.*
*Email : benieddisofiane@gmail.com, silahmar@yahoo.fr*

**ABSTRACT**

The evolution of wireless communication systems for the fifth generation (5G) and beyond requires low latency and high-speed connectivity to support a large number of users. Traditional orthogonal multiple access (OMA) systems like TDMA have limitations due to resource constraints. Non-orthogonal multiple access (NOMA) emerges as a solution, offering non-orthogonal resource sharing that enhances throughput, spectrum efficiency, and user fairness while reducing latency [1, 2]. Waveform selection is critical for NOMA's efficacy, with orthogonal frequency division multiplexing (OFDM) being a preferred choice, although it has challenges like out-of-band emission (OOBE) and high peak to average power ratio (PAPR). Filtered-Orthogonal Frequency Division Multiplexing (F-OFDM) is proposed as an optimal solution due to its high spectral efficiency, backward compatibility with OFDM systems, and flexible resource allocation for 5G networks [3, 4, 5]. This study aims to compare different windows used in F-OFDM in terms of OOBE, bit error rate (BER), and computational complexity.

**Keywords : 5G; OMA; NOMA; OOBE; F-OFDM; BER.**

As the 5G network prepares to connect an ever-growing number of users, it faces the challenge of providing rapid connectivity with low latency. Traditional OMA methods like Time Division Multiple Access (TDMA), while offering low interference, fall short in scalability for this new era. NOMA emerges as a solution, allowing users to share resources and utilizing techniques like superposition coding and successive interference cancellation (SIC) to manage interference, thus improving throughput, efficiency, and fairness.

Waveform selection remains crucial for NOMA's performance, with OFDM being a common choice. However, its drawbacks, such as OOBE and PAPR, have led to the exploration of alternative waveforms like F-OFDM, which offers improved spectral efficiency and compatibility with existing systems. Against other proposed waveforms like Generalized Frequency Division Multiplexing (GFDM), Filter Bank Multi-Carrier Modulation (FBMC), Universal Filtered Multi-Carrier (UFMC) , F-OFDM stands out for its balance between performance and operational simplicity, which is essential for practical 5G deployment.

This study compares the effectiveness of various windowing techniques Hanning, Hamming, Blackman, Blackman-Harris and Kaiser proposed for F-OFDM using MATLAB. Our analysis focuses on their impacts on OOBE, BER, and computational complexity, aiming to identify the optimal windowing method for f-OFDM in the context of 5G communications.

We present in below the simulation results of different windows used in F-OFDM.

Figure 1 illustrates the comparative Power Spectral Density (PSD) profiles for an OFDM and F-OFDM system with difirent windowing techniques. The OFDM signal shows the highest side lobes, indicating a risk of interference. The implementation of Hanning and Hamming windowing methods results in noticeable side lobe

suppression, enhancing spectral efficiency. The Blackman-Harris window further reduces side lobes, while Kaiser exhibit the most significant side lobe attenuation, indicating their superior effectiveness in minimizing spectral leakage. These results underscore the trade-off between spectral containment and system performance

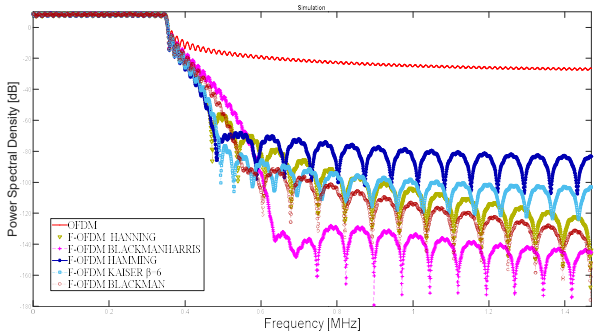


*Fig 1: PSD of defirent filters for F-OFDM system.*

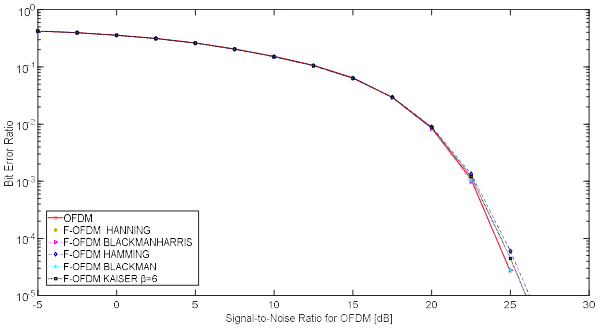


*Fig 2: BER of defirent filters for F-OFDM system*

Figure 2 compares the BER performance of different filters in F-OFDM systems as Signal to Noise Ratio (SNR) increases. The results indicate that Blackman-Harris, Hanning, and Kaiser windows marginally enhance BER at high SNR compared to traditional OFDM, suggesting their potential advantage for improving signal quality in noisy conditions.

## References

[1] M. Saideh, Y. Alsaba , I. Dayoub and M. Berbineau, "Joint Interference Cancellation for Multi-Carrier Modulation Based Non-Orthogonal Multiple Access," *IEEE Communications Letters,* vol. 23, no. 11, pp. 2114-2117, November 2019.

[2] L. Dai, B. Wang, Y. Yuan, S. Han, I. Chih-lin and Z. Wang, "Non-orthogonal multiple access for 5G: solutions, challenges, opportunities, and future research trends," *EEE Communications Magazine,* vol. 53, no. 9, pp. 74-81, September 2015.

[3] L. Zhang, A. Ijaz, P. Xiao, M. M. Molu and R. Tafazolli, "Filtered OFDM Systems, Algorithms, and Performance Analysis for 5G and Beyond," *IEEE Transactions On Communications,* vol. 66, no. 3, pp. 1205-1218, March 2018.

[4] A. Benieddi, S. A. Elahmar, . I. Dayoub and S. Haxha, "Blind adaptive low-complexity time-domain equalizer for 100-gb/s direct-detection optical OFDM systems over long-reach SSMF," *IEEE Systems Journal,* vol. 15, no. 3, pp. 3841-3847, June 2020.

[5] X. Huang, J. A. Zhang and Y. Jay Guo, "Out-of-band emission reduction and a unified framework for precoded OFDM," *IEEE Communications Magazine,* vol. 53, no. 6, pp. 151-159, June 2015.

# Analyse et comparaison des protocoles de routage dans un réseau VANET

**N. BERREKHCHI BERRAHMA[1], M. BOUZIANI[1]**

[1]*Laboratoire de Télécommunications et Traitement Numérique du Signal, Université Djillali Liabes, Sidi Bel Abbes, Algeria*
*Email : neilabekhchiberrahma@gmail.com , bouzi.mera@gmail.com*

**RESUME**

Les Réseaux Ad hoc pour Véhicules (VANET) se démarquent comme une catégorie bien définie parmi les réseaux ad hoc mobiles (MANET). Bien que les nœuds de ces deux types de réseaux partagent des caractéristiques de mobilité, la mobilité rapide et imprévisible ainsi que les changements de topologie des VANET les différencient significativement des MANET. Les VANET sont conçus pour permettre aux véhicules de transmettre de manière efficace des informations cruciales concernant le trafic et l'état des routes, nécessitant l'utilisation de protocoles de routage spécifiquement adaptés à cette dynamique. Dans le cadre de cette étude comparative, nous procédons à une analyse approfondie des performances de deux protocoles de routage réactifs, à savoir l'Ad hoc On Demand Distance Vector (AODV) et l'Ad hoc On Demand Multipath Distance Vector (AOMDV), dans des environnements variés, incluant les autoroutes et les zones urbaines en utilisant le logiciel NS2.35.

L'environnement urbain est défini comme un réseau routier composé d'intersections et de points d'arrêt (feux de circulation, panneaux d'arrêt, cédez le passage, etc.). Cette environnement est caractérisé par un modèle de mobilité complexe, une forte densité de véhicules et une vitesse faible (moins de 60 km/h). Dans notre cas, nous avons utilisé des vitesses de 30 à 40 km/h et un nombre de véhicules qui varie entre 28 et 150, la figure ci-dessous montre notre environnement :

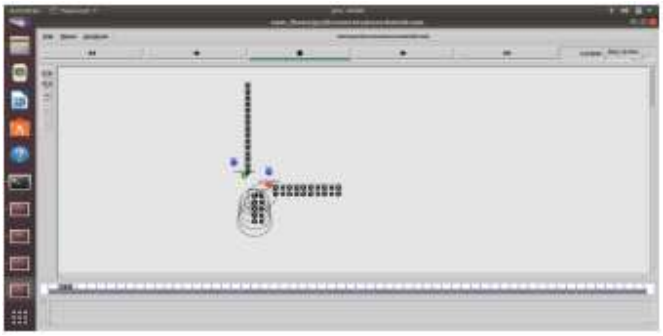

*Fig 1 :Environnement urbain*

Nous mesurons l'efficacité des deux protocoles en fonction de plusieurs paramètres de performance, tels que le débit qui représente le taux de transfert maximal de données entre deux nœuds d'un réseau, et le délai moyen de bout en bout, qui permet de calculer le temps total compté nécessaire pour livrer un paquet du nœud d'origine à la destination souhaitée, en prenant en compte les variations de densité du réseau, les figures ci-dessous représentent les différents résultats obtenus.

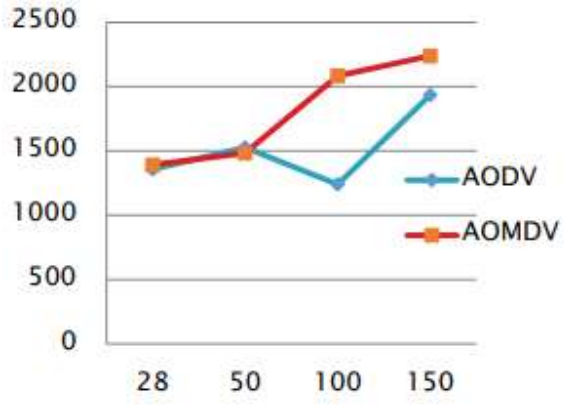


*Fig 2 : Le débit moyen*

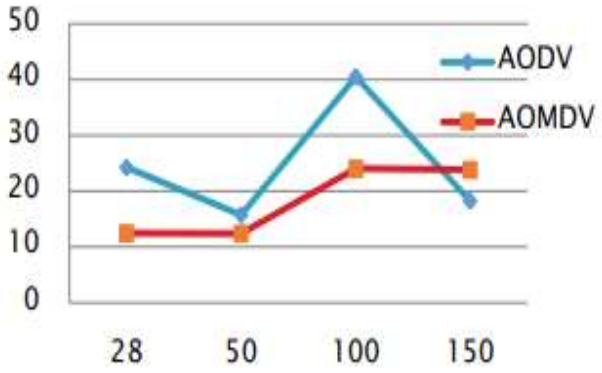


*Fig 3 : Le délai de bout en bout moyen*

La figure 2 montre la variation du débit pour AODV et AOMDV en fonction des différentes densités. On observe que l'AOMDV a un débit plus élevé que l'AODV. Par conséquent, les résultats de la simulation prouvent que l'AOMDV est plus adapté à différentes densités de véhicules que l'AODV.

La figure 3 montre les résultats du délai E2E pour AODV et AOMDV dans différentes densités. Nous notons qu'AOMDV a un meilleur délai moyen que AODV en raison du fait que si une rupture de lien se produit dans la topologie actuelle, AOMDV tentera de trouver un chemin alternatif parmi les routes de sauvegarde entre les nœuds source et de destination sont paires une fois. Contairement à AODV qui se caractérise par des tentatives uniques de découverte d'itinéraire, si une rupture de lien se produit, le paquet n'atteindra pas la destination en raison de l'indisponibilité d'un autre chemin de la source à la destination.

Nos résultats démontrent de manière concluante que le protocole AOMDV surpasse le protocole AODV en termes d'efficacité, de robustesse et de fiabilité. En particulier, l'AOMDV offre une livraison de paquets plus fiable , un débit plus constant,et un délai réduit même lorsque la densité du réseau fluctue. Ces conclusions mettent en évidence l'importance cruciale de la sélection du protocole de routage approprié pour optimiser les performances des VANET, en particulier dans des environnements exigeants tels que les autoroutes et les zones urbaines, où la communication efficace entre les véhicules est essentielle pour la sécurité routière et l'amélioration de la circulation.

**Mots clés:** AODV, AOMDV, NS2, VANET

**References**

[1] F·Belamri , S·Boulfekhar , D· Aissani , "A survey on QoS routing protocols in Vehicular Ad Hoc Network (VANET)," Springer Nature 2021,in press.

[2] S·Singh ,P· Kumari ,S·Agrawal ,"Comparative Analysis of Various Routing Protocols in VANET," 2015 Fifth International Conference on Advanced Computing & Communication Technologies.

[3] R· Anggoro , T· Kitasuka , R· Nakamura ,M· Aritsug,"Performance Evaluation of AODV and AOMDV with Probabilistic Relay in VANET Environments,"IEEE Kumamoto University,PP 259-263 [Third International Conference on Networking and Computing,2012].

[4] A· Al-Ahwal ,R. A. Mahmoud ,"Performance Evaluation and Discrimination of AODV and AOMDV VANET

# Enhancing NOMA Performance in 5G Downlink communication with Multi-Carrier Modulation and Adaptive Time Domain Equalization

**Nour El Houda BOUDA[1], Sid Ahmed ELAHMAR[1]**

[1] *Telecommunications and Digital Signal Processing Laboratory Djillali Liabes University of Sidi Bel Abbes Sidi Bel Abbes, Algeria*
*Emai : boudanoor@gmail.com, silahmar@yahoo.fr*

**ABSTRACT**

In the 5G downlink, consider the use of a Non-Orthogonal Multiple Access (NOMA) system based on Multi-Carrier Modulation (MCM) in order to benefit from both technologies' advantages for a high-frequency selective channel (ITU-VehicularB). Through the utilization of the power domain, NOMA allocates time, frequency, and code resources simultaneously to multiple users, resulting in improved spectral efficiency. User distinctions in NOMA are based on their respective channel conditions at the NOMA Base Station. Users with favorable channel conditions receive lower power allocations compared to those with less favorable conditions. The construction of the NOMA communication system entails the implementation of two key processes, Superposition Coding (SC) and Successive Interference Cancellation (SIC), at both the Base Station (BS) and user terminals. Conversely, a key waveform of the MCM is Orthogonal Frequency Division Multiplexing (OFDM), known for its robustness and widespread use in communication systems. Its extension, Cyclic Prefix (CP)-OFDM, significantly improves the system's resistance in multipath channels. However, ensuring interference-free transmission with CP-OFDM requires the insertion of a cyclic prefix longer than the channel impulse response (CIR), which can lead to inefficiencies due to a large delay spread within the channel. On the other hand, the CP length can become larger than the useful information, resulting in a reduction in the throughput and the spectral efficiency. To overcome these drawbacks, a blind adaptive Time domain Equalizer (TEQ) is proposed to shorten the effective channel, hence reducing the need for an extensive CP. Two Low-complexity TEQ methods are considered, Sum-Squared Autocorrelation Minimization TEQ (LSAM) and Minimization of Correlation of Adjacent Samples (MCAS). These algorithms are an addition to the family of several existing autocorrelation-based methods, which can achieve similar or better performance at lower complexity when compared to alternative algorithms. Unfortunately, once the CP length is reduced, Inter Symbol Interference (ISI) as well as Inter User Interference (IUI) occur. To enhance the system's performance, an adaptive blind TEQ with iterative interference cancellation (It-IC) is proposed. Therefore, the aim of this paper is to compare the performance of LSAM-TEQ and MCAS-TEQ by referring to the bit error rate (BER) versus the Signal-to Noise Ratio (SNR). The input and output data, as well as the filter tap weights, are handled as complex values. Simulation of a NOMA based OFDM system using It-IC with both LSAM-TEQ and MCAS-TEQ is executed under the ITU-VehicularB model. The simulation results reveal significant performance enhancements through the implementation of TEQ, even in the presence of selective fading channel. Fig. 1 illustrates the BER performance in both cases. As predicted, our proposed approach outperforms conventional detection methods. Furthermore, it's worth noting that LSAM-TEQ surpasses the performance of iterative interference cancellation when the SNR reaches 10 dB. However, MCAS-TEQ demonstrates faster convergence and superior performance, even at lower SNR levels.

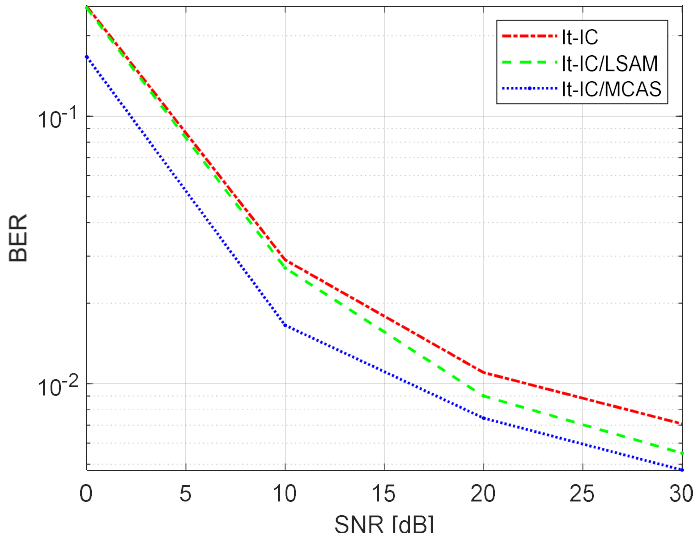


**Fig. 1** Bit Error Rate (BER) Analysis for NOMA-based OFDM with Iterative Interference Cancellation: LSAM-TEQ vs. MCAS under Varying SNR

**Index Terms s:** Non-Orthogonal Multiple Access, Multi-Carrier Modulation, blind adaptive Time domain Equalizer, Inter Symbol Interference, Inter User Interference.

**REFERENCES**

[1] M. Saideh, Y. Alsaba, I. Dayoub and M. Berbineau, "Joint Interference Cancellation for Multi-Carrier Modulation-Based Non-Orthogonal Multiple Access," *IEEE Communications Letters,* vol. 23, no. 11, pp. 2114-2117, 2019.

[2] R. Nissel and M. Rupp, "OFDM and FBMC-OQAM in DoublySelective Channels: Calculating the Bit Error Probability," *IEEE Communications Letters,* vol. 21, no. 6, pp. 1297-1300, 2017.

[3] I. G. Muhammad, E. Abdel-Raheem and K. Tepe, "Efficient blind adaptive channel shortening algorithm for multicarrier modulation systems," *2009 IEEE International Symposium on Signal Processing and Information Technology (ISSPIT)*, Ajman, United Arab Emirates, 2009, pp. 293-296, doi: 10.1109/ISSPIT.2009.5407505.

[4] A. Benieddi, S. Elahmar, I. Dayoub and S. Haxha, "Blind adaptive low-complexity time-domain equalizer for 100-gb/s direct-detection optical OFDM systems over long-reach SSMF," *IEEE Systems Journal,* vol. 15, no. 3, pp. 3841-3847, 2020.

[5] A. Hamza, I. Dayoub, I. Alouani and A. Amrouche, "Enabling user relaying in MCM-NOMA under doubly selective channels using iterative interference cancellation schemes for wireless IoT networks," *IEEE Sensors Letters,* vol. 6, no. 3, pp. 1-4, 2022.

[6] N. Bouda, S. Elahmar and I. Dayoub, "Adaptive Receiver for MCM Based NOMA in Doubly Selective Channels," in *2nd International Conference on Advanced Electrical Engineering (ICAEE)*, Constantine, 2022.

# Enhancing Visible Light Communication Systems through Luminescent Nanomaterials : A Paradigm Shift in Illumination and Data Transmission

**H. Chahed[1], B. Fassi[1], S. Driz[1]**

[1]*Telecommunications and Digital Signal Processing Laboratory, Faculty of Electrical Engineering, University of Djillali Liabes, Sidi Bel Abbes 22000, Algeria*
*Email :* halima.chahed@univ-sba.dz fassibenattou@yahoo.fr samia.driz@univ-sba.dz

**ABSTRACT**

Visible Light Communication (VLC) has emerged as a dynamic frontier in next-generation data transmission, leveraging the widespread presence of artificial lighting systems for dual purpose – illumination and high-speed wireless data transfer. However, to fully harness the potential of VLC and seamlessly integrate it into our connected world, it is essential to address the conundrum of increasing system complexity and costs. This research investigates the integration of emerging luminescent nanomaterials to boost the efficiency and data-carrying capacity of VLC emitters, specifically Light- Emitting Diodes (LEDs) [1].

The quest to design and develop VLC systems that rival the efficiency and ubiquity of Wi-Fi networks has often involved augmenting traditional light sources and communication equipment with complex modulators and signal processing technologies. This addition, although effective in expanding data transfer capabilities, invariably introduce operational intricacies and elevated infrastructure costs. By contrast, the incorporation of luminescent nanomaterials within the light source themselves promises to be a game-changing strategy for enhancing VLC while preserving simplicity and cost-effectiveness [1,2].

This research embarks on a comprehensive exploration of the vast potential of luminescent nanomaterials in the context of light emitters used in VLC systems. We explore the synthesis, and structural characterization of these emerging nanomaterials, including colloidal quantum dots and perovskite nanocrystals as potential emitter materials in VLC systems [3,4]. Our research delves into the optical properties of these nanomaterials, including their emission spectra, Photoluminescence Quantum Yield (PLQY), External Quantum Efficiency (EQE), photostability, and their Full Width at the Half Maximum (FWHM) which are helpful for manufacturing performant LEDs. In the table below we present some emergent luminescent nanomaterials according to their optical properties which may vary depending on specific LED designs, chemical structure, and manufacturing procedures [3,4,5].

**Table 1**: Emerging luminescent nanomaterials-based LEDs

| *Emergent luminescent materials* | *PLQY (%)* | *EQE (%)* | *FWHM (nm)* |
|---|---|---|---|
| PbS/CdS | ~52 | 20 | ~10 |
| $CuInS_2/ZnS$ | 85.06 | 5-10 | 20-40 |
| ZnO/ZnS | 30-60 | 0.1-5 | 20-80 |
| $MAPbBr_3$ | 80-90 | 10-20 | 10-40 |
| $CsPbI_3$ | 30-70 | 1-10 | 30-60 |
| $MA_3Bi_2Br_9$ | ~55 | ≤10 | 20-60 |
| $Cs_3Sb_2Br_9$ | 20-60 | 0.2-10 | 20-40 |
| $Co_2FeSi$ | 60-80 | 10-20 | 30-40 |

Our findings reveal that the integration of luminescent nanomaterials leads to significant enhancements in VLC performance. These nanomaterials exhibit narrow emission spectra, allowing for precise wavelength tuning to match the requirements of efficient data encoding and transmission. Their exceptional quantum yields result in brighter and more efficient light emitters such as LEDs. Moreover, their robust photostability ensures extended operational lifetime making them an ideal choice for long-term, real-world VLC deployments [4]. This attribute enhances the reliability and sustainability of VLC, which is paramount for its adoption in various applications. As well As, the integration of those luminescent nanomaterials in LEDs promises to deliver VLC systems that operate effectively consolidating illumination and data transmission into a single, cost-effective infrastructure [6].

Overall, this study underscores the potential of luminescent nanomaterials in revolutionizing VLC technology. By exploiting the unique properties of these emerging materials, through their narrow emission spectra, high photoluminescence quantum yield, and extended photostability, we pave the way for VLC systems that offer higher data rates, improved energy efficiency, and enhanced communication robustness with cost-effective infrastructure [2,4]. The integration of luminescent nanomaterials into VLC light- emitters promises to accelerate the adoption of VLC in various applications, ranging from intelligent lighting systems capable of simultaneously illuminating spaces and transferring data to highly secure wireless communication networks in environments sensitive to electromagnetic interference [3,5,6,7].

**Keywords:** VLC; Luminescent nanomaterials; LEDs; Wireless communications.

**References**

[1] Lopez-Fraguas, E., Arredondo, B., Vega-Colado, C., del Pozo, G., Najafi, M., Martin-Martin, D. et al., Visible Light Communication system using an organic emitter and a perovskite photodetector. *Organic Electronics*, vol. 73, pp. 292–298, 2019. https://doi.org/10.1016/j.orgel.2019.06.028

[2] Chen Chen & Cuiwei He. A Review of Advanced Transceiver Technologies in Visible Light Communications. *Photonics*, vol. 10, no. 6, pp. 1-12, 2023. https://doi.org/10.3390/photonics10060648

[3] Pavlos P.; Yoshida, Kou; Turnbull, Graham A. & Samuel, Ifor D. W.. Manousiadis, Organic semiconductors for visible light communications. *Philosophical Transactions of the Royal Society*, vol. 378, no. 2169, pp. 1-18, 2020. http://dx.doi.org/10.1098/rsta.2019.0186

[4] Ren, A., Wang, H., Zhang, W., Wu, J., Wang, Z., Penty, R. V., & White, I. H. Emerging light-emitting diodes for next-generation data communications. *Nature Electronics*, vol.4, no.8, pp.559–572, 2021. https://doi.org/10.1038/s41928-021-00624-7

[5] Zhuangzhuang M, Zhifeng S , Xu C, Di W , Xinjian L, and Chongxin S, Recent Advances and Opportunities of Lead-Free Perovskite Nanocrystal for Optoelectronic Application. *Energy Material Advances*, vol. 2021, 2021. https://doi.org/10.34133/2021/5198145

[6] Martínez, J., Osorio-Roman, I., & Gualdrón-Reyes, A. F. Progress of Organic/Inorganic Luminescent Materials for Optical Wireless Communication Systems. *Photonics*, vol.10, no.6, pp.1-17, 2023. https://doi.org/10.3390/photonics10060659

[7] Xue, D., Ruan, C., Zhang, Y., Chen, H., Chen, X., Wu, C. et al. Enhanced bandwidth of white light communication using nanomaterial phosphors. *Nanotechnology,* vol. 29, no.45, pp.1-9, 2018. https://doi.org/10.1088/1361-6528/aaddc0

# In-service Monitoring of Passive Optical Networks: Investigating Performance and Interference Challenges of Periodic Codes Among Close-Proximity Encoders

**Ahmed El Amine Cheikr El Mezouar[1], Mouad Addad[1], Ali Djebbari[1]**

[1] *Telecommunications and digital Signal Processing Laboratory, Djillali Liabes University, Sidi Bel Abbes, 22000, Algeria*
*Email : cheikrelmezouar@outlook.com*

**Abstract**

In the dynamic landscape of telecommunications, Passive Optical Networks (PONs) have assumed the role of a foundational pillar in modern fiber networks. Their capacity to deliver high-speed, cost-effective broadband services to an ever-expanding clientele is indisputable. As the demand for seamless connectivity continues to surge, the reliability and uninterrupted operation of PONs have emerged as paramount prerequisites, underpinning their role in fulfilling the connectivity needs of our digital age [1-3].

Recognizing the pivotal role of PONs in today's evolving technological infrastructure has led to the development of advanced monitoring mechanisms, designed to swiftly responding to network anomalies, facilitating rapid recovery, and minimizing service disruptions. As a result, they reinforce the reliability of PONs, making them an integral part of the modern communication networks [2,4-6].

Although a variety of monitoring techniques have been developed, systems based on Periodic Codes (PCs) have surfaced as a promising solution to adderss challenges posed by traditional methods [4,7]. This communication presents a comprehensive evaluation of the performance and feasibility of PCs in the context of PON monitoring systems. The primary focus of our investigation centers on understanding the effectiveness of PCs in scenarios characterized by constrained geographical distributions.

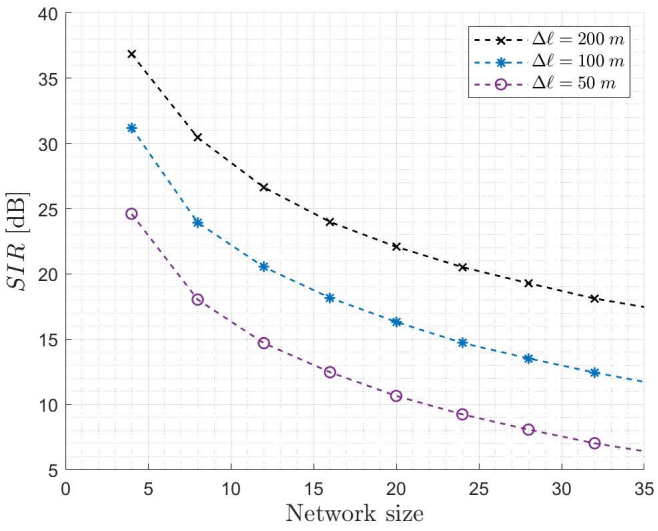


*Fig 1: Illustration of the interference impact on the monitoring system for different geographical constraints.*

To achieve this, we employ numerical analysis, specifically utilizing the Monte Carlo method. This approach quantifies the cumulative impact of interference arising from undesired reflections within the monitored network. We express our results through the Signal-to-Interference Ratio (*SIR*), with a particular emphasis on the maximum relative separation distance $\Delta\ell$ between encoders and network size. This analytical approach provides valuable insights into the challenges of network scalability, especially when confronted with increased network density.
In the broader context, our work is dedicated to refining the application of modern monitoring systems and providing pragmatic guidance for identifying their prevailing limitations and shortcomings. This endeavor serves as a catalyst for further enhancements or the exploration of alternative techniques that are less susceptible to the issues presented. Ultimately, our aim consists into strengthening the reliability of deployed PONs, ensuring their uninterrupted provision of high-speed broadband services, irrespective of the network complexities and the environmental constraints.

**Keywords:** Passive optical network; Fault monitoring; Optical coding; Optical time domain reflectometer.

## References

[1] J. S. Wey, "The Outlook for PON Standardization: A Tutorial," *Journal of Lightwave Technology*, vol. 38, no. 1, pp. 31–42, Jan. 2020.

[2] B. Mukherjee, I. Tomkos, M. Tornatore, P. Winzer, and Y. Zhao, Eds., Springer *Handbook of Optical Networks* (Springer Handbooks). Springer International Publishing, 2020.

[3] M. H. Ali, H. M. ALkargole, and T. A. Hassan, "A Review of immigration obstacles to PON-FTTH and its evolution around the world," *TELKOMNIKA (Telecommunication Computing Electronics and Control)*, vol. 19, no. 2, pp. 645–663, 2 Apr. 1, 2021.

[4] M. A. Esmail and H. Fathallah, "Physical Layer Monitoring Techniques for TDM-Passive Optical Networks: A Survey," *IEEE Communications Surveys & Tutorials*, vol. 15, no. 2, pp. 943–958, 2013.

[5] A. Usman, N. Zulkifli, M. R. Salim, K. Khairi, and A. I. Azmi, "Optical link monitoring in fibre-to-the-x passive optical network (FTTx PON): A comprehensive survey," *Optical Switching and Networking*, vol. 39, p. 100 596, Nov. 1, 2020.

[6] H. S. Abbas and M. A. Gregory, "The next generation of passive optical networks: A review," *Journal of Network and Computer Applications*, vol. 67, pp. 53–74, May 1, 2016.

[7] H. Fathallah, M. M. Rad, and L. A. Rusch, "PON Monitoring: Periodic Encoders With Low Capital and Operational Cost," *IEEE Photonics Technology Letters*, vol. 20, no. 24, pp. 2039–2041, Dec. 2008.

# An Exploration of the MF-TDMA Technique in DVB-RCS2 Systems

**Meryem Romaissa DJELLOULI[1], Sid Ahmed CHOUAKRI[2], Abdelkrim GHAZ[3]**
[1] *Telecommunications and Digital Signal Processing Laboratory, Djillali Liabes University, Sidi Bel Abbes, Algeria*
[2] *Telecommunications and Digital Signal Processing Laboratory, Djillali Liabes University, Sidi Bel Abbes, Algeria*
[3] *Communications Networks Architecture and Multimedia Laboratory, Djillali Liabes University, Sidi Bel Abbes, Algeria*

*Email : meryemromaissa1@gmail.com*

**ABSTRACT**

Within the domain of multi-user communication systems, resource optimization is essential. The present research delineates the efficacy of the Multi-Frequency Time Division Multiple Access (MF-TDMA) technique for concurrent signal multiplexing across varied frequencies and temporal domains. A simulation, utilizing 1,000 samples, evidenced modulation of five distinct users, each allocated specific frequency bands and temporal slots, underscoring the MF-TDMA's prowess in spectrum optimization. Each signal, conforming to the DVB-RCS2 standard, employed Quadrature Phase Shift Keying (QPSK) modulation with a 2/3 turbo coding rate. The resultant composite channel manifests the sophistication of MF-TDMA multiplexing, cementing its prominence in maximizing spectrum efficiency in high-density communication environments.
**Keywords: multi-user communications; QPSK; MF-TDMA; DVB-RCS2.**

## INTRODUCTION

In satellite communication, optimal spectrum use and resource allocation are key for high-quality transmissions. The Multi-Frequency Time Division Multiple Access (MF-TDMA) stands out as a method for multiplexing signals over varied frequencies and times. The MATLAB script demonstrates this by integrating MF-TDMA within a DVB-RCS2 framework, using QPSK modulation and a 2/3 turbo coding rate. It showcases waveform generation for multiple users and visualizes the combined signals on a composite channel, highlighting the benefits of blending MF-TDMA with DVB-RCS2 for spectrum efficiency.

## WAVEFORME GENERATION DVB-RCS2

In Figure 1, raw data is transformed into DVB-RCS2 waveforms through processes that include structuring into PDUs, CRC error detection, FEC coding for resilience, interleaving against burst errors, QPSK modulation into symbols, and upconversion for satellite transmission.

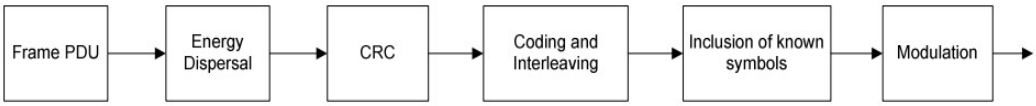


**Figure 1:** DVB-RCS2 burst waveform generation.

## MF-TDMA in DVB-RCS2 Systems: A Paradigm Shift in Satellite Multiplexing

Integrating Multi-Frequency Time Division Multiple Access (MF-TDMA) with DVB-RCS2 has revolutionized satellite communications. This union boosts spectrum efficiency and redefines satellite multiplexing, meeting challenges of dense traffic and dynamic bandwidth allocation with unprecedented efficacy.

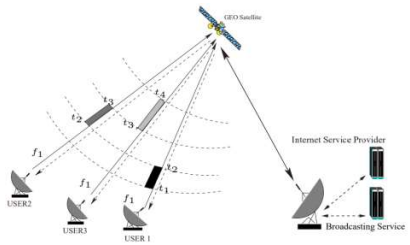


**Figure 2:** MF-TDMA in DVB-RCS2 Systems

## IMPLEMENTATION via SIMULATION

In a MATLAB simulation, DVB-RCS2 waveform generation, over 1,000 samples, facilitated multi-user communication. Five users were allocated time slots and frequencies via MF-TDMA, with data processed using QPSK modulation and 2/3 turbo coding, illustrating the MF-TDMA's synergy with turbo-coded DVB-RCS2.

## RESULTS AND DISCUSSIONS

In the context of modulation techniques, the decision to utilize a 1,000-sample waveform is of paramount importance. This allocation ensures an optimal representation of modulated data from five distinct users, mitigating potential signal overlap and interference. The structure not only exemplifies the multifaceted capabilities of MF-TDMA multiplexing but also accentuates the synergy between MF-TDMA's operational efficiency and the resilience of turbo-coded DVB-RCS2. The discernible partitions within these samples underscore the methodology's precision, hinting at its potential applicability in dense satellite communication scenarios.

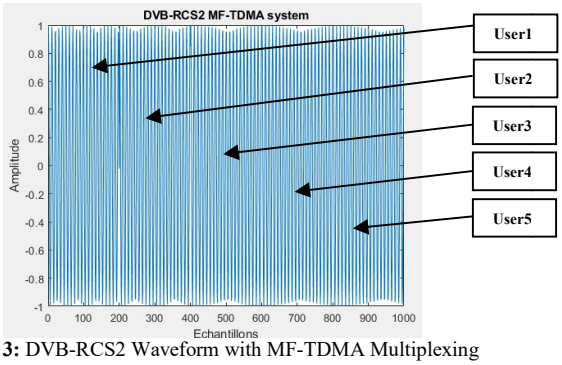


**Figure 3:** DVB-RCS2 Waveform with MF-TDMA Multiplexing

## CONCLUSION

The MATLAB simulation was assessed on its precise integration of MF-TDMA, ensuring accurate time slot and frequency allocations for each user, along with generating waveforms adhering to the DVB-RCS2 standard with QPSK modulation. Additional evaluation metrics included the effectiveness of the turbo coding, absence of interference in the composite signal, visualization clarity, code cleanliness, and adherence to given parameters. This evaluation underscores the significance of this integration in enhancing satellite communications.

## References

[1] A.B. SatComm, R.Y. Linker, "Utilizing DVB-RCS2 Waveform Generation in MF-TDMA Systems: An Experimental Approach," J. Satellite Comm. Res., 18 (2017) 32.
[2] C.D. Modulate, F.G. Transfer, "Simulation Techniques for Understanding Multi-User Communication Dynamics in MF-TDMA," Adv. Telecomm. Tech., 15 (2019) 45.
[3] H.I. Synthesize, J.K. Channelize, "Efficient Resource Allocation using MF-TDMA in Conjunction with Turbo-Coded DVB-RCS2," Satellite Comm. Insights, 20 (2021) 60.
[4] L.M. Frequency, N.O. Time, "Exploring QPSK Modulation in DVB-RCS2: A MATLAB-based Approach," Aerospace Signal Process., 14 (2018) 29.
[5] P.Q. Allocator, R.S. Scheduler, "From Time Slots to Frequencies: A Deep Dive into MF-TDMA Systems," Comm. System Rev., 19 (2020) 50.

# Image quality assessment in FSO communication system: Mitigating Haze weather-induced challenges through beam divergence and receiver aperture

**A. Djir[1], F. Meskine[2], M.L. Tayebi[1]**

[1] *Telecommunications and Digital Signal Processing Laboratory (LTTNS), Djillali LiabesUniversity, Sidi Bel-Abbes, 22000 Algeria*
[2] *Communication Networks, Architectures and Multimedia Laboratory (RCAM), Djillali LiabesUniversity, Sidi Bel-Abbes, 22000 Algeria*
*Email : djir_amina@yahoo.com*

## ABSTRACT

The Free Space Optical (FSO) communication system is a wireless communication technology that utilizes a modulated narrow optical laser beam to transmit digital data from a transmitter to a receiver. It has emerged as a prominent wireless communication technology, experiencing a significant surge in interest and substantial development over the past decade [1-3]. However, as optical radiation traverses the atmosphere, it encounters various phenomena, including absorption and scattering [4, 5]. These effects change over time and are contingent on the prevailing local and weather conditions. In practical FSO systems, optimization involves considering trade-offs between factors like range, spot size, receiver size and atmospheric conditions to achieve the best compromise for the specific application and environmental conditions. This research examines the transmission of RGB images over an intensity modulation/direct detection (IM/DD) communication-oriented FSO system under the influence of haze weather atmospheric attenuations. The aim of this study is to identify the best system's characteristics for practical FSO deployment in the presence of haze conditions. Our analysis seeks to strike a balance between receiver aperture diameter, beam divergence angle, and range. We consider the advantages and disadvantages of large receiver apertures, taking into account their potential to collect more signal power but also to capture more background noise. By identifying the ideal combination of FSO characteristics, this study attempts to provide valuable guidelines for practical FSO deployments in regions prone to haze, with a specific focus on ensuring reliable and high-quality RGB image transmission.

**Keywords:** Free Space Optics (FSO); Image quality; Beam divergence; Receiver aperture size; Hazy weather conditions; Structure Similarity Index (SSIM).

## RESULTS AND DATA ANALYSIS

Beam divergence refers to the spreading of the optical beam as it propagates through the atmosphere [4]. The further the beam propagates, the more it spreads out. By carefully adjusting the divergence angle, it is possible to minimize the effects of atmospheric losses caused by hazy weather conditions. Receiver aperture optimization, on the other hand, involves optimizing the size of the receiver aperture to maximize the collection of optical signals. These strategies combined can greatly enhance FSO image quality assessment, leading to more reliable data transmission. Figure 1(a) and 1(b) provide a visual representation of how receiver aperture size, beam divergence angle, haze conditions and image quality are interrelated. By examining the bars across varying receiver aperture sizes and different haze conditions, valuable insights emerge regarding their influence on image quality. The graphical results depict a notable trend: as the receiver aperture size increases, there is a significant improvement in SSIM values, as illustrated by the

ascending bar height. Similarly, when analyzing the bars across different beam divergence angles and various haze conditions, the shifts in image quality become apparent. The graphical findings demonstrate that an increase in beam divergence corresponds to a gradual decline in SSIM values, as the bars decrease in height. Moreover, this increased divergence is concurrently linked to a reduction in the maximum achievable range for the optical communication system. On the other hand, haze conditions have a clear impact on image quality. In general, as the haze level intensifies, there is a consistent reduction in SSIM values. This implies that adverse atmospheric conditions, particularly heavy haze, severely affect the quality of transmitted images.

Based on the findings presented in Figures 1(a) and 2(b), several critical conclusions can be drawn. Increasing the receiver aperture size substantially enhances SSIM values, improving image quality. However, larger apertures also capture more background noise, impacting the signal-to-noise ratio (SNR). Beam divergence inversely affects SSIM values, highlighting the need to control it for high-quality image transmission. Moreover, an increase in divergence is associated with a reduced maximum communication range. Haze conditions consistently degrade image quality, emphasizing the necessity for advanced strategies to mitigate atmospheric impact on image transmission. In summary, selecting the optimal balanced between divergence, receiver size and range is critical for achieving high-quality image transmission under varying haze scenarios for reliable and robust FSO communication system.

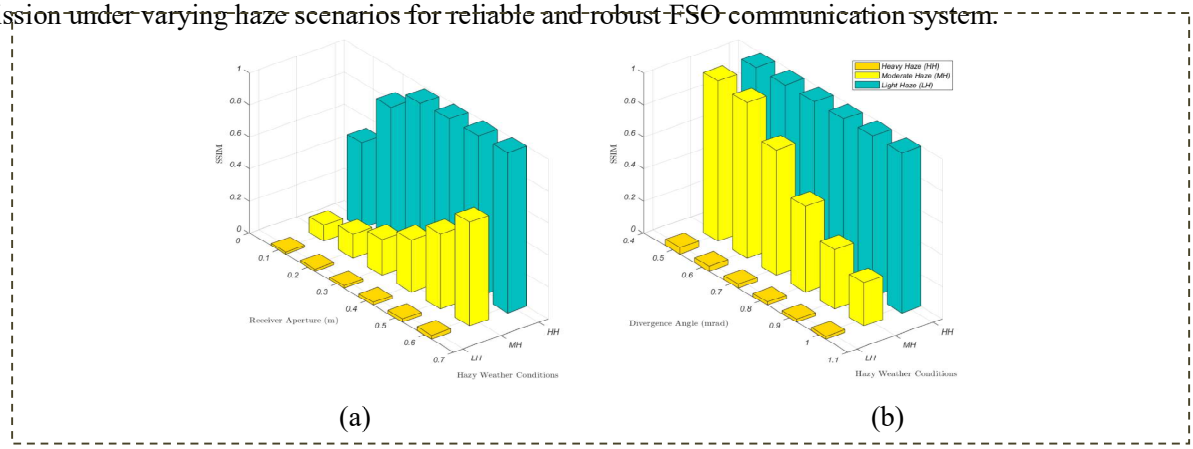


(a) (b)

*Fig 1: (a) SSIM vs. receiver aperture size in light, moderate, and heavy haze –(b) SSIM vs. divergence angle in light, moderate, and heavy haze.*

**References**

[1] H. Henniger, O. Wilfert, An introduction to free-space optical communications. Radioengineering, 19 (2010), 203-212.
[2] S.A. Al-Gailani, M.F.M. Salleh, A.A. Salem, R.Q. Shaddad, U.U. Sheikh, N.A. Algeelani, T.A. Almohamad, A Survey of Free Space Optics (FSO) communication systems, links, and networks. IEEE Access, 9 (2020) 7353-7373.
[3] H. Willebrand, B.S. Ghuman, Free-Space Optics: enabling optical connectivity in today's networks. SAMS Publishing, 2001.
[4] Ghassemlooy, W. Popoola, S. Rajbhandari, Optical wireless communications: system and channel modelling with MATLAB®. 2nd ed. Taylor & Francis Group, 2018.
[5] D. Anandkumar, RG. Sangeetha, A survey on performance enhancement in free space optical communication system through channel models and modulation techniques. Optical and Quantum Electronics, 53 (2021) 1-39.

# Contribution to Improving the Performances of a Modified Reconfigurable Patch Antenna for Sub-6 Bands Applications

**Nour El Houda FROUDA[1], Abdellatif BERKAT[2], Salima AZZAZ RAHMANI[3]**

[1] *Laboratory of telecommunications and digital signal processing(LTTNS), Faculty of Electrical Engineering, University of Sidi Bel Abbes, Algeria.*
[2]*Laboratory of Telecommunication-Tlemcen (LTT), Faculty of Techology, University of Tlemcen, Algeria.*
[3] *Laboratory of Telecommunication-Tlemcen (LTT), Faculty of Electrical Engineering, University of Sidi Bel Abbes, Algeria.*
*Email : frouda.nour@gmail.com*

**ABSTRACT**

In this contribution, a modified reconfigurable patch antenna for Sub-6 bands applications has been designed and simulated. The proposed patch antenna is based on a single layer FR4 substrate with a partial ground. The gain can be up to 3.85 dBi at 5.8 GHz and can get 2.93 dBi and 3.7 dBi at 3.4 GHz and 6.1 GHz respectively. The radiation pattern is quasi-omnidirectional on the greater part of the working band. The envisaged reconfigurable antenna is currently being validated through practical implementation and validation of measurements. The proposed antenna can be applied where Sub-6 band is needed citing 5G and medical communications.

**Keywords:** Patch antenna; Reconfigurable antenna; Smart antenna; Sub-6 frequency band.

## ANTENNA STRUCTURE AND RESULTS

The proposed reconfigurable antenna was simulated using a software package CST Microwave on FR4 substrate. The simulated and measured S11 characteristics of the antenna are depicted in Fig. 1. The S11 result of the antenna operates for Sub-6 bands. The major advantage of this latter structure antenna is resumed in its small size and lost cost profile.

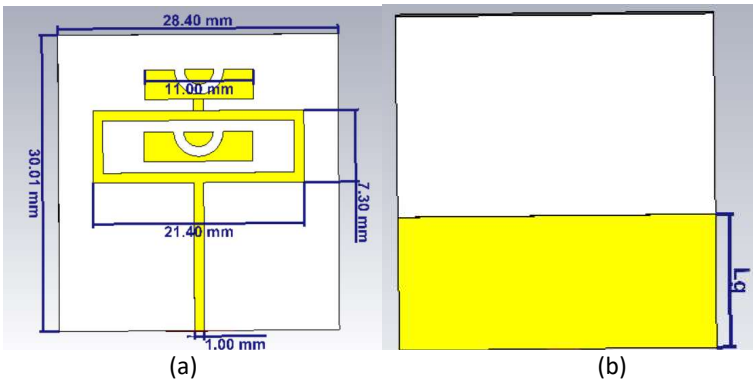


Fig1. The proposed antenna model, (a) front view, (b) bottom view.

Fig. 2 shows the variation effect of the length (Lg) in the ground of the proposed structure on the reflection coefficient results. The simulated S11 result obtained with Lg= 12mm operate at 5.8 GHz, and Lg=15mm operates at 3.4 GHz and 6.1 GHz.

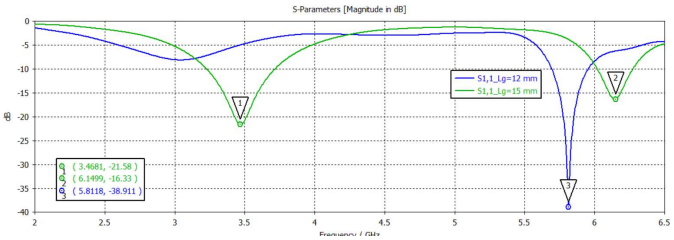


Fig 2. S11 of the reconfigurable antenna for Lg=12mm and Lg=15mm.

Fig. 3 from(a) to (f) show the simulated far-field 3D and the current distribution of the antenna at 5.8 GHz, 3.4 GHz and 6.1 GHz respectively. Full wave simulation was carried out using CST software. These results in Fig. 3 (a), Fig. 3 (c) and Fig. 11 (e) are simulated at 5.8 GHz, 3.4 GHz and 6.1 GHz giving a maximum gain of 3.85 dBi, 2.93 dBi, and 3.7 dBi respectively. Fig. 3 (b), Fig. 3 (d) and Fig. 3 (f) shows the surface current distribution of the reconfigurable antenna at all frequencies resonance. The maximum current is concentrated in the center of the patch, and it is also observed that the maximum current can be produced due to the increase the size of the ground at 15mm.

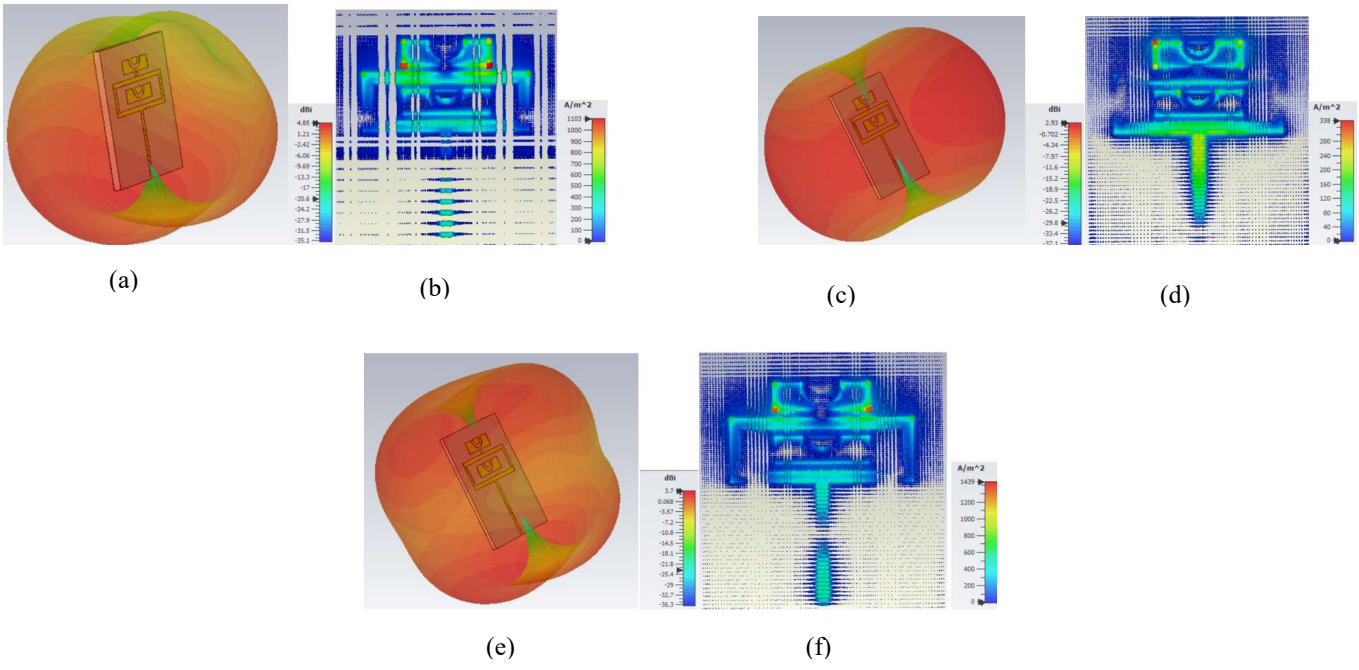


Fig 3. Simulated 3D radiation patterns and surface current distribution of the proposed reconfigurable antenna at 5.8 GHz (a and b), 3.4 GHz (c and d) and 6.1 GHz (e and f) respectively.

**References**

[1] Y. Liu, Q. Wang, Y. Jia and P. Zhu, "A Frequency- and Polarization-Reconfigurable Slot Antenna Using Liquid Metal", *IEEE Transactions on Antennas and Propagation*, vol. 68, no. 11, pp. 7630-7635, Nov. 2020.

[2] W. Li, Y. M. Wang, Y. Hei, B. Li and X. Shi, "A Compact Low-Profile Reconfigurable Metasurface Antenna with Polarization and Pattern Diversities", IEEE Antennas and Wireless Propagation Letters, vol. 20, no. 7, pp. 1170-1174, July 2021.

[3] W. Li, Y. M. Wang, Y. Hei, B. Li and X. Shi, "A Compact Low-Profile Reconfigurable Metasurface Antenna with Polarization and Pattern Diversities", in IEEE Antennas and Wireless Propagation Letters, vol. 20, no. 7, pp. 1170-1174, July 2021.

# Re-imagining Telecommunication Optical Systems: Leveraging Machine Learning Approach for Enhanced Intelligence

**R. Kebaili [1], S. Driz[1], B. Fassi[1]**

[1] *Telecommunications and digital signal processing laboratory, Faculty of Electrical Engineering, University of Djillali LiabesSidi Bel Abbes 22000, Algeria.*
*Email : rima.kebaili@univ-sba.dzsamia.driz@univ-sba.dz fassibenattou@yahoo.fr*

**ABSTRACT**

In the face of rapid growth in data demand and pivotal role of telecommunication networks, the optimization of optical systems has become a paramount concern. This research endeavors to redefine the landscape of next-generation telecommunication optical systems by harnessing the power of Machine Learning (ML), ushering in a new era of intelligent and adaptive network architectures. Through a systematic and comprehensive investigation, this study delves into the transformative potential of integrating machine learning approaches to augment the intelligence of telecommunication optical systems. Machine Learning, with its ability to analyze large datasets and derive actionable insights, emerges as a key catalyst in revolutionizing the efficiency and responsiveness of these systems [1].

The research places a significant emphasis on the practical applications of machine learning, elucidating its role in various critical facets of telecommunication optical systems. By integrating predictive maintenance models, the study demonstrates how machine learning can empower proactive system monitoring, enabling the timely identification and rectification of potential faults and issues, thus minimizing downtimes and ensuring uninterrupted service delivery. Furthermore, the study highlights the pivotal role of machine learning in facilitating intelligent resource allocation, optimizing the utilization of bandwidth and power to enhance the overall efficiency and performance of telecommunication networks [2, 3].

Notably, our application of the SVM algorithm to classify modulation formats resulted in an impressive accuracy of 99.2%. Accuracy is calculated by comparing the number of correct classifications to the total classifications made, illustrating the precision and effectiveness of our approach. In addition, scatter plots provide visual representations of data distribution (Fig. 1a), aiding in the identification of patterns and outliers. Also, confusion matrices (Fig. 1b) offer a comprehensive view of classification results, highlighting true positives, true negatives, false positives, and false negatives. These tools play a crucial role in fine-tuning the model and enhancing its real-world applicability and impact.

By harnessing the potential of machine learning, this research endeavors to achieve a series of objectives, including the identification of existing shortcomings within optical systems and the evaluation of the practical impact of machine learning models on system performance and intelligence. Our goal is not only to ameliorate issues but to empower optical systems to adapt and self-optimize in real time, thereby making them intelligent

Our comprehensive research methodology incorporates a multifaceted approach, integrating data collection and system analysis using advanced machine learning models. Our analysis is firmly grounded in real-world data acquired from operational optical systems, forming the cornerstone of our research investigation. To imbue optical systems with heightened intelligence and performance optimization, we deploy a diverse array of machine learning techniques, including deep neural networks, recurrent neural networks, and ensemble learning. These sophisticated models are meticulously crafted to empower the optimization of optical system functionality and efficacy. Employing supervised learning models, we proactively predict and identify potential system issues, allowing for preemptive mitigation

strategies to be implemented. Furthermore, our utilization of unsupervised learning methodologies enables us to uncover latent patterns and subtle opportunities for system enhancement and refinement, contributing to the continual improvement and evolution of our research findings. By leveraging this comprehensive approach, our research endeavors to propel the development of highly efficient and intelligent optical systems that are primed to meet the dynamic demands of modern telecommunications networks [4, 5].

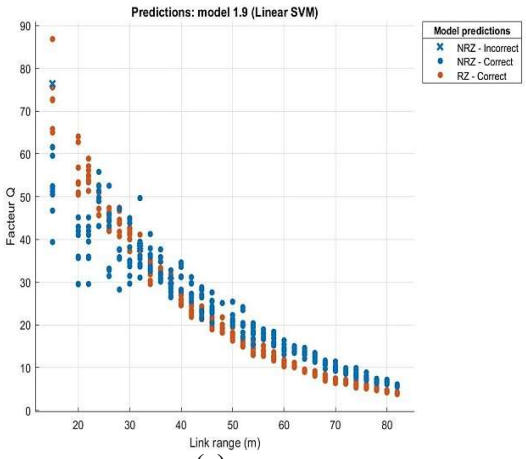


(a)

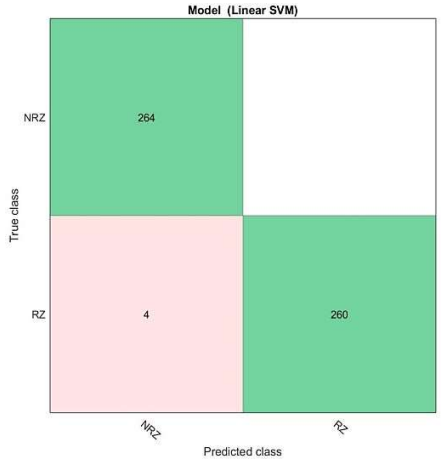


(b)

**Fig. 1.** (a) scatter plot (b) confusion matrix

Overall, the pivotal role that machine learning plays in the ongoing evolution of telecommunication optical systems, particularly in endowing these systems with intelligence, is highlighted. In an era where seamless data connectivity is paramount, our findings offer innovative solutions to boost system performance and reliability while making optical systems intelligent. The integration of of machine learning as cutting-edge technology and advanced research methodologies marks a profound shift in telecommunication, promising a future of more efficient and resilient optical systems with unprecedented intelligence.

**Keywords:** Machine Learning (ML); Intelligent optical systems ; Next generation.

## References

[1] Samanta, R. K., Sadhukhan, B., Samaddar, H., Sarkar, S., Koner, C., & Ghosh, M. Scope of machine learning applications for addressing the challenges in next-generation wireless networks. *CAAI Transactions on Intelligence Technology*, vol.7, no.3, pp.395-418, 2022. https://doi.org/10.1049/cit2.12114

[2] Möhring, H. C., Wiederkehr, P., Erkorkmaz, K., & Kakinuma, Y. Self-optimizing machining systems. *CIRP Annals*, vol.69, no.2, pp.740-763, 2020. https://doi.org/10.1016/j.cirp.2020.05.007

[3] Musumeci, F., Rottondi, C., Nag, A., Macaluso, I., Zibar, D., Ruffini, M., & Tornatore, M. An overview on application of machine learning techniques in optical networks. *IEEE Communications Surveys & Tutorials*, vol.21, no.2, pp.1383-1408, 2018. 10.1109/COMST.2018.2880039

[4] Gu, R., Yang, Z., & Ji, Y. Machine learning for intelligent optical networks: A comprehensive survey. *Journal of Network and Computer Applications*, vol.157, pp.1-51, 2020. https://doi.org/10.1016/j.jnca.2020.102576

[5] Ahammed, T. B., Patgiri, R., & Nayak, S. A vision on the artificial intelligence for 6G communication. *ICT Express*, vol.9, no.2, pp.197-210, 2023. https://doi.org/10.1016/j.icte.2022.05.005

# Deploying Content Stores in Named Data Networking (NDN)

**A. KECHKECHE[1], M. BOUZIANI[1], H. BELKHIRA[2]**

[1]*Department of Telecommunications, Faculty of Electrical Engineering, Djillali Liabes University, Sidi Bel Abbes (Algeria)*
[2] *Department of Telecommunications, Faculty of Technology, Nour Bachir University, El Bayadh (Algeria)*
*Email : kechkeche.amal.rt@gmail.com ; mbouziani2014@gmail.com ;belkhira.hichem@gmail.com*

**ABSTRACT**

The Named-Data-Networking (NDN) architecture consists of a network of caches, enabling nodes to store data as it traverses the network to satisfy upcoming requests. The memory required at each node, known as the Content Store, represents a significant portion of the infrastructure cost. This article aims to explore the potential advantages of implementing Content Stores for all nodes in order to enhance the performance of NDN architecture. In order to achieve this, we will examine the effects of both the size and placement of Content Stores within an NDN topology, specifically referred to as "Topo-11-Node-Two-Bottelencks". Our objective is to assess its performance metrics, with a primary focus on the Server Hit Reduction Ratio (SHR), the Average Retrieval Delay (ARD) and the Average Retrieval Hop Count (AHC). By conducting a series of extensive simulation experiments using NS-3 and its ndnSIM module, our study reveals that the Named Data Networking (NDN) architecture achieves optimal performance when nodes situated at the network's edge, in proximity to end-consumers, possess substantial Content Stores. This is an important finding for network operators as it indicates that NDN architecture can be deployed with reduced infrastructure costs.

**Keywords:** Named-Data-Networking; Content Store; Caching; NDN remplacement policy; Topo-11-node-two-bottelencks; ndnSIM.

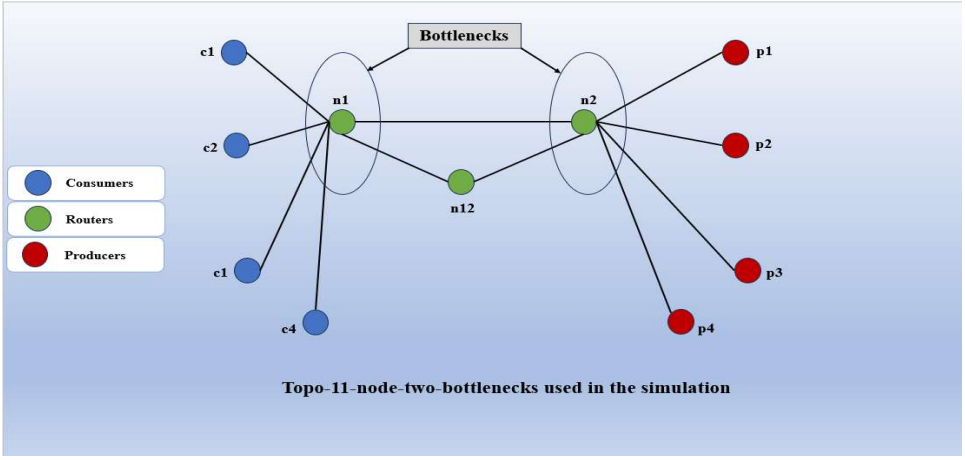


*Fig 1 Topo-11-node-two-bottlenecks used in the simulation*

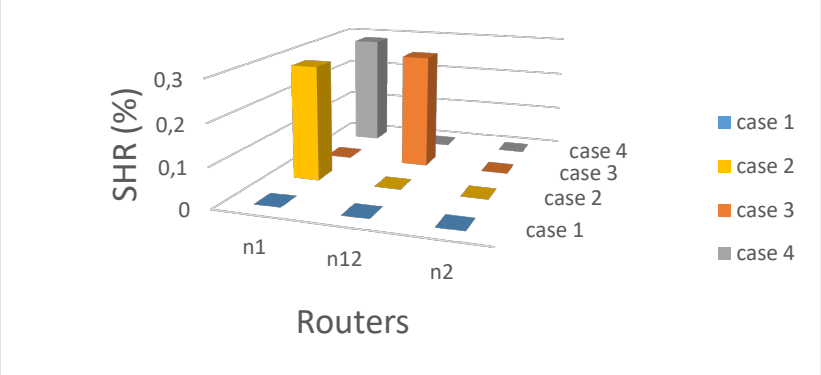


*Fig 2 The Server Hit Reduction (SHR) at the level of routers n1, n12 and n2*

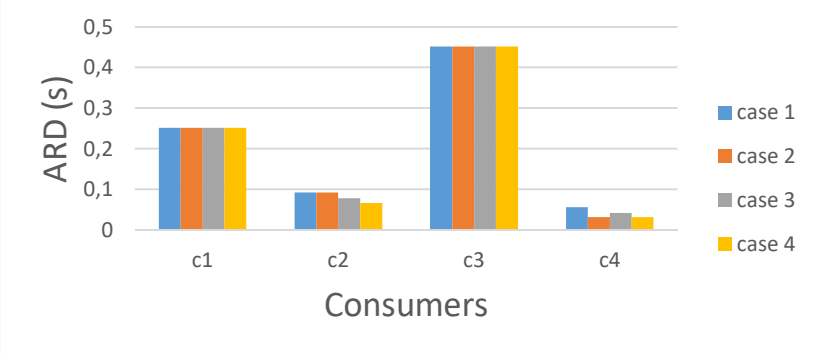


*Fig 3 The Average Retrievel Delay (ARD) at the level of Consumers*

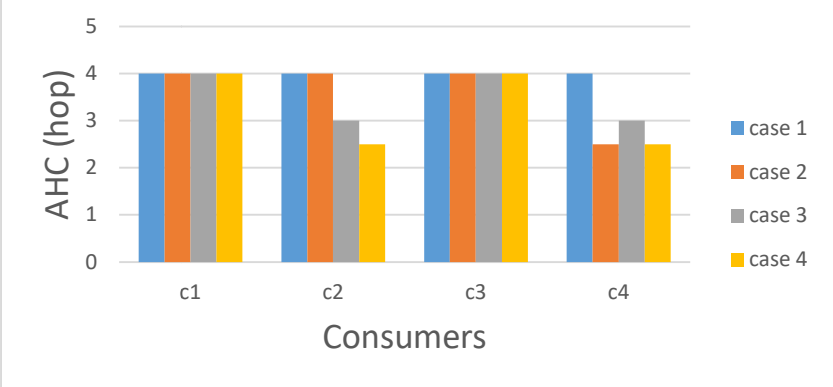


*Fig 4 The Average Retrievel Hop Count (AHC) at the level of Consumers*

**References**

[1] Putra, M. A. P., Kim, D. S., & Lee, J. M. (2022). Adaptive LRFU replacement policy for named data network in industrial IoT. *ICT Express*, *8*(2), 258-263.

[2] Gupta, D., Rani, S., Ahmed, S. H., & Hussain, R. (2020). Caching policies in NDN-IoT architecture. *Integration of WSN and IoT for Smart Cities*, 43-64.

[3] Alduayji, S., Belghith, A., Gazdar, A., & Al-Ahmadi, S. (2023). PF-EdgeCache: Popularity and freshness aware edge caching scheme for NDN/IoT networks. *Pervasive and Mobile Computing*, *91*, 101782.

# A Comparative Analysis of Two TCP Congestion Control Algorithms in the Current State of the Art

**LEBID Sadjida[1], ZOUAOUI Chakib.M.A[2] , DJEBBAR Ahmed Bouzidi [1]**

[1] *Telecommunications and Digital Signal Processing Laboratory*
[2] *Communication Networks, Architectures and Multimedia Laboratory*
*Djillali Liabes University of Sidi Bel-Abbes 22000, Algeria*
*Email: sadjida.lebid@univ-sba.dz*

**ABSTRACT**

The transmission control protocol (TCP) is fundamental to reliable data transmission in computer networks. Two notable TCP congestion control algorithms, TCP BBR (Bottleneck Bandwidth and Round-trip propagation time) [1] and TCP CUBIC [2]have gained significant attention for their unique approaches to mitigating network congestion. This study aims to provide an in-depth comparative analysis of TCP BBR and TCP CUBIC, our analysis is primarily based on a selection of key research papers [1] [3] that were identified as particularly relevant and intriguing within the current state of the art with a focus on their performance, adaptability, and relevance to modern network environments. The selected algorithms, extracted from the latest literature and research findings, represent the cutting edge of congestion control solutions, catering to the evolving demands of contemporary networks.

TCP BBR, known for its innovative approach, aims to optimize network performance by continuously probing for the available bandwidth and maintaining low queue sizes at the bottleneck link. It prioritizes achieving high throughput and low latency, making it particularly suitable for high-speed, low-latency networks.

On the other hand, TCP CUBIC employs a more traditional cubic function to regulate congestion, periodically doubling the congestion window. It offers steady, predictable behavior but can be less aggressive in exploring available bandwidth. TCP CUBIC has been widely deployed and well-studied, making it a useful benchmark for comparison.

This research leverages both simulations and practical experiments to evaluate TCP BBR and TCP CUBIC across various network conditions. Drawing from recent studies and advancements, we delve into the specifics of their design, implementation, and real-world applications. Through rigorous analysis, we provide insights into how these algorithms perform under the latest network scenarios and conditions.

The comparative analysis reveals that TCP BBR often outperforms TCP CUBIC in terms of achieving higher throughput and reduced latency, particularly in networks with high bandwidth and low round-trip times. However, TCP BBR's aggressive behavior can lead to unfair resource allocation when competing with TCP CUBIC and other congestion control algorithms, which tend to maintain fair sharing of network resources.

The findings from this research offer valuable insights for network administrators and researchers when selecting the most appropriate congestion control algorithm for specific network environments and objectives. The choice between TCP BBR and TCP CUBIC depends on the network's characteristics, traffic patterns, and performance requirements.

In summary, this comparative analysis sheds light on the strengths and weaknesses of TCP BBR and TCP CUBIC, helping to make informed decisions regarding congestion control algorithm selection in various networking applications. Understanding the trade-offs between throughput, latency, and fairness is essential for optimizing network performance and delivering improved user experiences in the face of network congestion challenges.

**Keywords:** TCP BBR; TCP Cubic; Comparative study; Network performance.

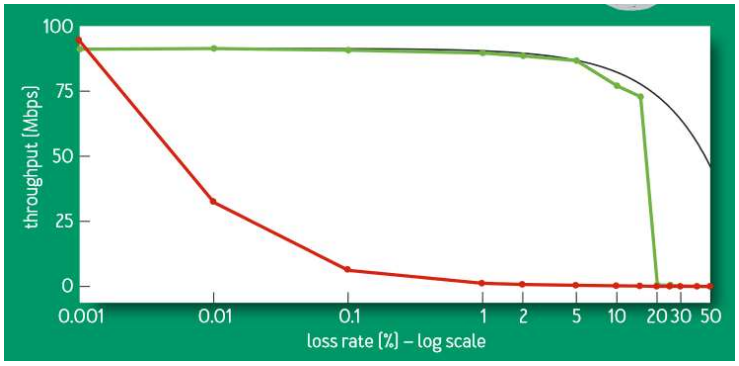


*Fig 1: BBR vs cubic goodput under loss*

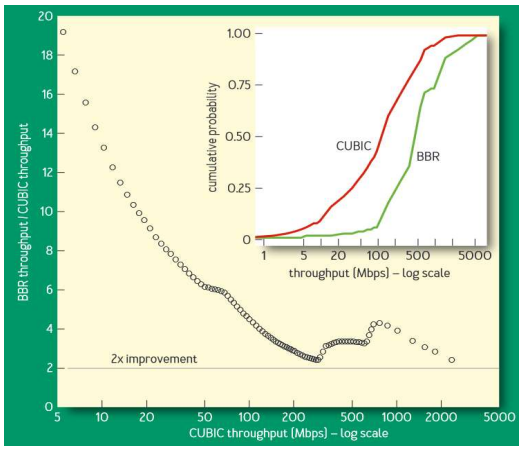


*Fig 2: BBr vs cubic throughput*

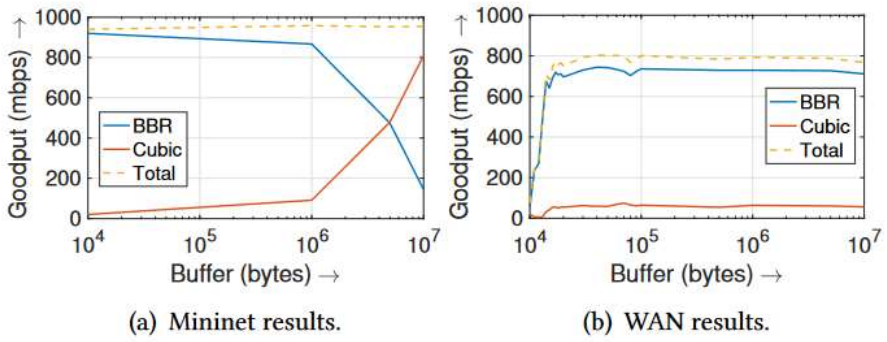


*Fig 3: BBR and Cubic's bandwidth share under 1Gbps BW, 20ms RTT, and different buffer sizes.*

## References

[1] N. Cardwell, Y. Cheng, C. S. Gunn, S. H. Yeganeh and V. Jacobson, "BBR: congestion-based congestion control," *ACM queue,* pp. 20-53, 2016.

[2] I. R. Sangtae Ha and L. Xu, "CUBIC: A New TCP-Friendly High-Speed TCP Variant ∗," *ACM SIGOPS,* vol. 42, no. 5, pp. 64-74, 2008.

[3] Y. Cao, A. Jain, K. Sharma, A. Balasubramanian and A. Gamdhi, "When to Use and When Not to Use BBR: An Empirical Analysis and Evaluation Study," in *IMC '19: Proceedings of the Internet Measurement Conference*, Amsterdam , 2019.

# Effect of Velocity and Power Budget on Performance of V2V-VLC System in Safety Application

**Aicha Meghraoui[1], Mohamed L. Tayebi[1]**

[1] *LTTNS Laboratory, University of Djillali Liabes, Sidi bel Abbes, Algeria*
*E-mail: Aicha.Meghraoui@univ-sba.dz*

## ABSTRACT

Lane change is one of applications were considered as a hard safety, and a high performance requirements, which needs a good driving environment. This paper studies the use of visible light communication (VLC) system in lane change application, using non-sequential ray channel modeling approach. The headlamps and the taillights of the vehicle serve as wireless transmitters while photodetectors located in front end and/or rear end the others vehicles to act as wireless receivers. We investigate the effect of velocity and power budget on the bit error rate (BER) for varying inter-vehicle distance and lateral shift.The results demonstrated that VLC could be qualified for exchanging data between the cars for a safe lane change.

**Keywords:** lane change application; visible light communication.

## INTRODUCTION

Intelligent Transportation Systems (ITS) have gained attention as an effective way for improving road safety [1]. Vehicular communication as essential elements of the ITS. Lane changing application was identified as the highest priority safety services [2]. In this application, vehicular visible light communication (VVLC) enables neighbouring vehicles to communicate with each other using light signals, and this can help drivers to make more informed decisions during the lane change process, reducing the risk of collisions and improving road safety. This paper investigates the performance of VLC in lane change applications, we consider multi-links V2V communications where the subject vehicle communicates with several surrounding vehicles to do lane changing as practical scenario.

In the simulation study, we investigate the effect of velocity on the V2V VLC system's for different inter-vehicle distances and lateral shifts on the BER at various transmitting power is also investigated .

## SYSTEM MODEL

As illustrated in Fig. 1, we consider a V2V scenario in a two-lane road, and each lane has a width of W. We assume that vehicle D intends to change its lane and vehicle C is the leading vehicle in its existing lane. Meanwhile, vehicles A and B lead and follow vehicles in the target lane. Assuming that these vehicles are travelling at a constant velocity V and the distance between A and B are large enough to make room for D to change lanes. All vehicles are positioned at the centre of their respective lanes with a separation distance of $d_i$ and a lateral shift of y.

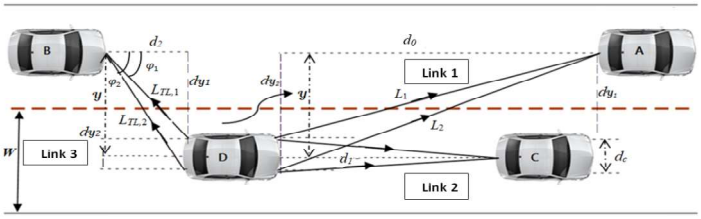


Fig. 1: Vehicle-to-vehicle scenario.

## SIMULATION RESULTS AND DISCUSSION

Fig. 2 shows how the vehicle's velocity has influenced the BER data communication performance on link 1 between vehicular D and A. As the velocity of the vehicles increases, it becomes necessary to maintain a larger safe distance between the vehicles to ensure sufficient time for proper braking and manoeuvring. However, it is observed that this increase in safety distance, due to vehicle velocity, has an adverse effect on the BER performance of the communication system. For example, consider the mid-time of the process (t = T/2) at a transmit power of 25 dBm, the BER for V = 10 m/s, V= 15 m/s, and V = 20 m/s are given by $10^{-11}$, $2.5\times10^{-5}$, $8.5\times10^{-3}$, respectively. It also showed that when t increases, the BER reduces due to the reduction in the communication distance. For example, consider a transmit power of 25 dBm and V = 15 m/s. The BER values are given for starting time (t = 0), mid-time (t = T/2), and end-time of the process (t = T) as $8\times10^{-3}$, $2.5\times10^{-5}$, and $\ll10^{-10}$ , respectively. Additionally, the results demonstrate necessity of factoring in an power budget to account for the heightened velocity, ensuring dependable communication throughout the lane change process.

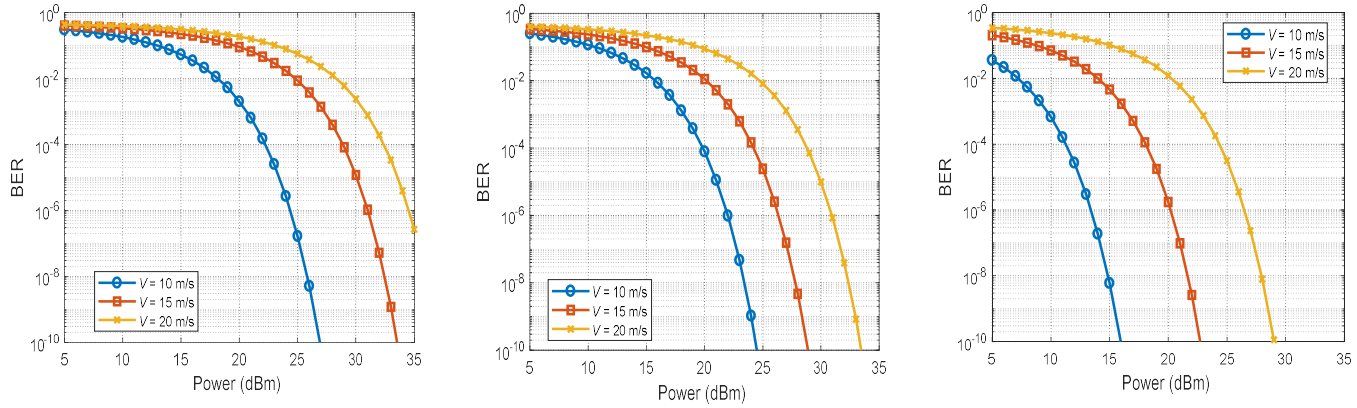


Fig. 2: Effect of velocity and power budget on BER for link 1 (a) Starting time t = 0, (b) Mid time t = T/2, and (c) End time t = T.

## CONCLUSION

In this paper, we investigated the performance of VLC based V2V system during a lane change process as practical scenario. The bit error rate for different inter-vehicle distances and lateral shifts was investigated, the impact of vehicle velocity was also addressed, and the required power budget to compensate for its effect is finally obtained.
The results demonstrated that VLC could be qualified for exchanging data between the cars for a safe lane change.

## References

[1] J. Zhang et al., "Data-driven intelligent transportation systems: A survey," IEEE Trans. Intell. Transp. Syst., Jul. 2011.
[2] A.-M. Cailean et al., "A survey on the usage of DSRC and VLC in communication-based vehicle safety applications," Netherlands: IEEE, 2014.

# Comparative Study of Caching Strategies for NDN Topologies: Analysis and Performance

**SEGHIER Meftah[1], BOUZIANI Merahi[1], KANDOUCI Chahinaz[1]**

[1] *Laboratory of telecommunication and digital signal processing , university of Djilali Liabes, Sidi Bel Abbes, Algeria.*
*Email: meftah.seghier45@gmail.com ; mbouziani2014@gmail.com ; chahinazkandouci@gmail.com*

**Abstract:**

In recent years, researchers have begun to change the communication unit in the IP architecture from an end-to-end channel between two endpoint identifiers specified by IP addresses to naming the content block in a new architecture called Named Data Networking (NDN). This is an example of a broader web research direction called Information-Centric Networking (ICN), under which different architectural designs have emerged.

Within (NDN), caching holds significant importance for network efficiency. Managing caching in NDN networks is crucial to ensure effective data storage. Cache management policies define the rules and strategies for deciding which data should be cached, how to manage limited cache space (cache placement), and how to handle data updates in the cache (cache replacement).

We presented a comparative study among different topologies of the NDN architecture (Abilene and Grid) by varying various caching strategies (placement and replacement) and an analysis of this study based on several metrics. Finally, we conclude by defining the suitable topology for the proposed architecture based on the metrics measured during.

**Keywords:** Information Contents Networking **(ICN),** Content-Centric Networking **(CCN),** Named Data Networking **(NDN),** caching.

**Table 1.** Comparison based on delay of the two topologies using LRU and FIFO strategies.

| | abilene | grid |
|---|---|---|
| LRU | 62790 | 84201 |
| FIFO | 79460 | 93821 |

**References**

[1] V. Jacobson, D. K. Smetters, J. D. Thornton, M. F. Plass, N.H. Briggs, and R. L. Braynard, Networking Named Content,ACM CoNEXT, 2009.

[2] Léonce MEKINDA, Cache, Process and Forward in Information-Centric Networking , Ecole de l'Institut Mines-Télécom - Membre de ParisTech,2016

[3] Giuseppe Rossini , Design and Analysis of Forwarding Strategies for Host and Content Centric Networking, Ecole de l'Institut Mines-Télécom - Membre de ParisTech, Janvier 2014

[4] Leanna Vidya Yovita, Nana Rachmana Syambas ,Caching on Named Data Network: a Survey and Future Research

School of Electrical Engineering and Informatics, Bandung Institute of Technology, Indonesia,2018.

[5] Adrien Thibaud, Julien Fasson, Fabrice Arnal, Renaud Sallantin, Emmanuel Dubois, and Emmanuel Chaput. An analysis of NDN Congestion Control challenges. In International Conference on Hot Information-Centric Networking (HotICN 2019), Chongqing, China, December 2019.

[6] Abdelali Kerrouche. Routing Named Data in Information-Centric Networks. Networking and Internet Architecture [cs.NI]. Université Paris-Est, 2017. E

[7] Fatima Zahra Saadaoui, état d'art sur les protocoles en temps réel pour l'internet des objets sous le réseau NDN, Ecole Supérieure de Technologie de Casablanca (Maroc), Institut Universitaire de Technologie d'Aix-Marseille (France), Jun 2019, CASABLANCA, Maroc.

[8] S. Mastorakis and al. ndnSIM 2 : An updated NDN simulator for NS-3. Technical Report NDN-0028, Revision 2, NDN, November 2016.

[9] Hammad Zafar , An Effective Fairness Scheme for Named Data Networking, Department of Electrical Engineering, Air University, Aerospace and Aviation Campus, Kamra 43570, Pakistan.

[10] Yusung Kim, Younghoon Kim, Jun Bi, and Ikjun Yeom, Differentiated Forwarding and Caching in Named-Data Networking, Journal of Network and Computer Applications, http://dx.doi.org/10.1016/j.jnca.2015.09.011

[11] Firman Chandra Alamsyah , the Effect of Content Population and Frequency Interest for Named Data Networking with Modified-Optimal Replacement Algorithm Networking, Microprocessor and Interfacing Assistant Lab School of Electrical Engineering, Telkom University Bandung, Indonesia,2021.

[12] Shahid Md. Asif Iqbal cache-MCDM: A Hybrid Caching Scheme in Mobile Named Data Networks based on Multi-Criteria Decision Making , Department of Computer Science & Engineering, Premier University, 44, Hazari Lane, Kotwali, Chattogram, 4000, Chattogram, Bangladesh

[13] Xavier Marchal. Architectures et fonctions avancées pour le déploiement progressif de réseaux orientés contenus. Réseaux et télécommunications [cs.NI]. Université de Lorraine, 2019.

[14] Elian Aubry, Thomas Silverston, Isabelle Chrisment. Croissance Verte dans NDN: Déploiement des Content Stores. ALGOTEL 2016

# Fault Diagnosis in Electric Cables by Chaos Time Domain Reflectometry

**Yasmina Tabouri [1], Mouad Addad [1], Ali Djebbari [1]**

[1] *Telecommunications and Digital Signal Processing Laboratory, Djillali Liabes University , Sidi Bel Abbes, 22000, Algeria*
*Email: yasminou776@gmail.com*

**ABSTRACT**

In the realm of cable fault diagnosis, traditional methods like Time-Domain Reflectometry (TDR) have long been instrumental in identifying cable issues [1]. However, the advent of innovative techniques, notably Chaos Time Domain Reflectometry (CTDR), has ushered in a new era of fault detection [2].

This work focuses on the use of CTDR for diagnosing faults in cables, addressing both hard and soft defects. Hard defects, such as obvious cable problems like open and short circuits [3], stand in totally contrast to soft defects [4], which encompass subtler anomalies such as small impedance variations. The objective is to assess the effectiveness of CTDR as a valuable tool for proactively managing cable-related issues.

**Keywords:** Reflectometry; Chaotic sequences; Hard defects; Soft defects; Cable.

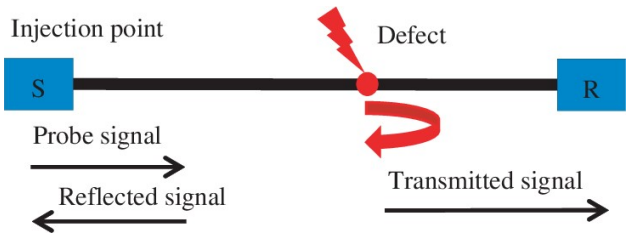


*Fig 1: Principle of reflectometry*

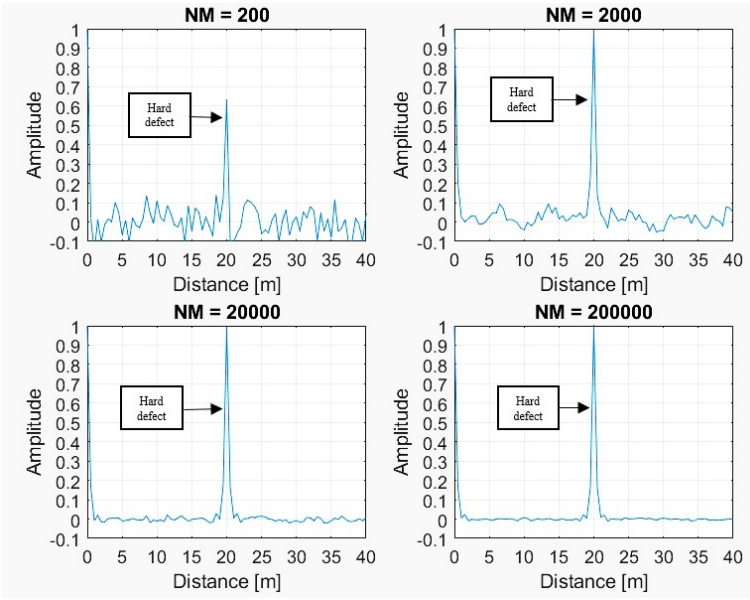


*Fig 2: Simulation of CTDR generated using logistic-Bernoulli maps with various sample sizes (NM)*

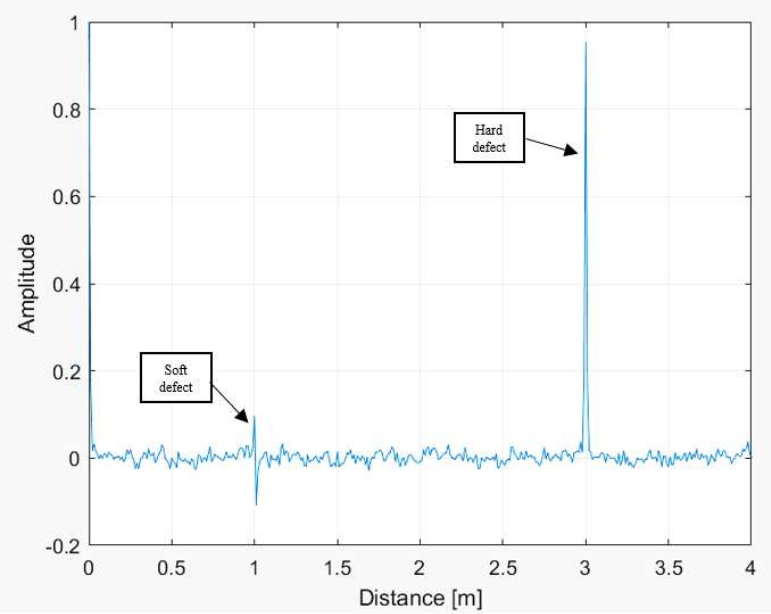


*Fig 3: Simulation of soft defect using CTDR*

**References**

[1] S. Sallem, and O. Osman, L. Sommervogel, and M. O. Carrion, "Wired network distributed diagnosis and sensors communications by multi-carrier time domain reflectometry" in Proc. IEEE Intell. Syst. Conf., London, U.K., Sep. 2018.

[2] Auzanneau. F, Ravot. N, Incarbone. L, "Chaos Time Domain Reflectometry for Online Defect Detection in Noisy Wired Networks". IEEE Sens. J. 2016.

[3] Auzanneau. F, Ravot. N, "Defects detection and localization in complex topology wired networks" Annals of Telecommunications, vol. 62, pp. 193–213, Feb. 2007.

[4] N. Taki, "Diagnosis of soft faults in complex wired networks" Ph.D. dissertation, Université Paris-Saclay, 2022.

# Comparison between Superimposed Training (ST) and Data Dependent Superimposed training (DDST) Channel Estimation Methods

**Hanane Meriem Toaba[1], Mouad Addad[1], Ali Djebbari[1]**

[1] *Telecommunications and Digital Signal Processing Laboratory Djillali Liabes University of Sidi Bel Abbes Sidi Bel Abbes, Algeria*
*Email: hanane_tm@live.fr*

**ABSTRACT**

Channel estimation is an important module in any modern communication system. It can provides information about distortion of the transmitted signal when it propagates through the channel. Then the information is used by equalizers so that any distortion such as fading effects or interferences can be removed and the transmitted signal can be restored [1].

One of the most practical channel estimation methods is based on Superimposed Training (ST) [2] [3] [4].In the latter method, a periodic training sequence known to the receiver is arithmetically added to the data sequence instead of being allocated to an empty time slot [5]. This way, contrary to the conventional training approaches, no bandwidth is lost. In addition, due to the periodicity of training sequence, cyclostationarity characteristics are induced in the received signal and can be exploited to estimate channel via only first- order statistics [6]. However, the ST method suffer from the interference between the data sequence and the training sequence. To remove the interference, a modified ST method called Data- Dependent Superimposed Training (DDST) was proposed in [7]. It consists in adding a data-dependent sequence unknown to the receiver, which cancels the effects of data on the channel estimation performance. The conditions imposed on the training sequence in the ST method remain applicable for the DDST method.

In this paper, a comparison between the two training based channel estimation methods: ST and DDST is presented. where the estimation performance analysis is detailed and the expressions of the ST and DDST channel estimarion error-variance are deduced and given as follow

$$\sigma^2_{e_h(\boldsymbol{DDST})} = \frac{1}{N_P}\frac{\sigma_n^2}{\sigma_c^2} \quad (1)$$

$$\sigma^2_{e_h(\boldsymbol{ST})} = \frac{1}{N_P}\frac{\sigma_b^2+\sigma_n^2}{\sigma_c^2} \quad (2)$$

The expressions above will be given as functions of the signal-to-noise ratio $SNR = \left(\sigma_b^2 + \sigma_c^2\right)/\sigma_{n_r}^2$ and the power loss factor $\alpha = \sigma_b^2/\sigma_b^2 + \sigma_c^2$, and will be represented by a Matlab figure in order to observe the comparison.

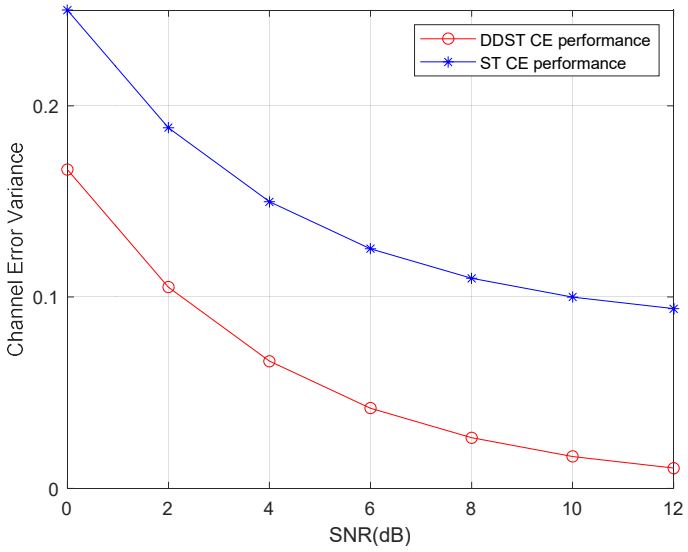


***Fig 1.*** Channel estimation error-variance vs. SNR for ST and DDST schemes.

**Keywords:** Channel Estimation Performance, DDST, ST, Training sequences.

**References**

[1] P.-Y. T. I.-W. L. Tzi-Dar Chiueh, Baseband Receiver Design for Wireless MIMO-OFDM Communications, 2nd ed., J. W. &. Sons, Ed., Singapore: Wiley, IEEE, 2012.

[2] Y. Zhang, H. Zhao, W. Xia, J. Zhang, L. Yang and H. Zhu, "Wireless- Powered Cell-Free Massive MIMO with Superimposed Pilot Transmission," *IEEE Communications Letters,* vol. 26, no. 07, pp. 1688 - 1692, 2022.

[3] N. Garg, H. Ge and T. Ratnarajah, "Generalized Superimposed Training Scheme In IRS-assisted Cell-free Massive MIMO Systems," *IEEE Journal of Selected Topics in Signal Processing,* vol. 16, no. 05, p. 1157, 2022.

[4] H. Zhang and B. Sheng, "An Enhanced Partial-Data Superimposed Training Scheme for OFDM Systems," *IEEE Communications Letters,* vol. 24, no. 08, pp. 1804 - 1807, 2020.

[5] A. Orozco-Lug, M. Lara and D. McLernon, "Channel estimation using implicit training," *IEEE Transactions on Signal Processing,* vol. 52, no. 01, pp. 240 - 254, 2004.

[6] E. Alameda-Hernandez, D. McLernon, A. G. Orozco-Lugo, M. M. Lara and M. Ghogho, "Frame/Training Sequence Synchronization and DC-Offset Removal for (Data-Dependent) Superimposed Training Based Channel Estimation," *IEEE Transactions on Signal Processing,* vol. 55, no. 06, pp. 2557 - 2569, 2007.

[7] M. Ghogho, D. McLernon, E. Alameda-Hernandez and A. Swami, "Channel estimation and symbol detection for block transmission using data-dependent superimposed training," *IEEE Signal Processing Letters,* vol. 12, no. 03, pp. 226 - 229, 2005.

# Optimizing Free-Space Optical Communications: Overcoming Atmospheric Turbulence for Enhanced System Performance

**A. Tou[1], S. Driz[1], B. Fassi[1]**

[1]*Telecommunications and Digital Signal Processing Laboratory, Faculty of Electrical Engineering, University of Djillali Liabes, Sidi Bel Abbes 22000, Algeria*
*Email : amar.tou@gmail.com ; samia.driz@univ-sba.dz ; fassibenattou@yahoo.fr*

**ABSTRACT**
The advancement of Free-Space Optical (FSO) communications has emerged as a promising solution to meet the escalating demands of high-speed data transmission, offering the potential for high bandwidth and secure communication. However, the detrimental impact of atmospheric turbulence on the stability, reliability and performance of FSO systems has posed a significant challenge [1, 2]. This research endeavors to address this issue by proposing effective strategies to mitigate the adverse effects of atmospheric turbulence, thereby enhancing the resilience and efficiency of FSO communications in challenging environments. Through an in-depth analysis of the underlying causes and implications of atmospheric turbulence, this study sheds light on the complexities and intricacies associated with maintaining stable optical communication links. In addition, the research highlights the adverse effects of scintillation, spectrum broadening and beam wandering induced by atmospheric turbulence, leading to signal distortion and decreased transmission quality. Leveraging advanced techniques and innovative methodologies, the research presents a comprehensive approach to optimize FSO communications, focusing on the development of robust solutions capable of countering the disruptive effects of atmospheric turbulence.

By offering a comprehensive analysis of turbulence effects and introducing innovative solutions, this research lays the groundwork for the development of a more resilient and efficient optical communication infrastructure. The proposed methodologies not only mitigate the challenges posed by atmospheric turbulence but also pave the way for the seamless integration of FSO systems in diverse operational environments, fostering a more reliable and secure communication network for the future [3, 4].

Furthermore, the impact of choosing optimal modulation formats is introduced to underscore the crucial role of strategic modulation schemes in ensuring robust data transmission and mitigating the impact of atmospheric turbulence on signal quality [5]. In the landscape of FSO communication systems, the Differential Phase-Shift Keying (DPSK) modulation scheme stands out as a resilient modulation technique renowned for its ability to combat the adverse effects of atmospheric turbulence. Operating on the principle of encoding data by the phase difference between successive symbols, DPSK demonstrates enhanced tolerance to phase fluctuations induced by turbulent atmospheric conditions, thereby ensuring more robust and reliable signal transmission [6].

This research delves into the fundamental attributes and operational mechanisms of the Differential Quadrature Phase Shift Keying (DQPSK) modulation scheme, elucidating its unique capacity to mitigate the detrimental impact of turbulence-induced phase distortions. By leveraging the inherent advantages of DQPSK, including its resistance to phase noise and its capability to maintain signal integrity under challenging environmental circumstances, the study highlights the potential of DQPSK as a key enabler for ensuring stable and efficient data transmission in FSO communication systems. A performance analysis of DQPSK formats in 10 Gb/s FSO communication, under the influence of weak, moderate and strong atmospheric turbulences is illustrated in Figure 1.

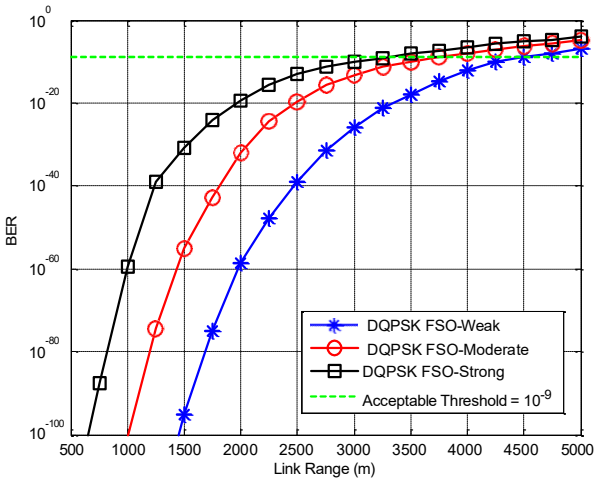


**Fig. 1.** Performance analysis of DQPSK formats in various atmospheric turbulence scenarios.

Overall, this study underscores the potential of leveraging advanced modulation techniques, such as DQPSK, to fortify FSO communication systems against the disruptive effects of atmospheric turbulence. By delving into the robust capabilities of DQPSK in maintaining signal integrity and minimizing the impact of turbulence-induced phase distortions, the research contributes to a comprehensive framework for enhancing the resilience and efficiency of optical communication networks. This study's findings advocate for the strategic integration of DQPSK modulation as a viable solution to mitigate the challenges posed by atmospheric turbulence, paving the way for the development of more resilient and efficient FSO communication systems capable of meeting the demands of modern data transmission requirements.

**Keywords:** FSO; Advanced modulation format; DQPSK ; Optical wireless communications.

**References**

[1] Miglani, R., & Malhotra, J. S. An innovative approach for performance enhancement of 320 Gbps free space optical communication system over turbulent channel. *Optical and Quantum Electronics*, vol.51, pp.1-26, 2019. https://doi.org/10.1007/s11082-019-2004-8

[2] Zafar, S., & Khalid, H. Free space optical networks: applications, challenges and research directions. *Wireless Personal Communications*, vol.121, no.1, pp.429-457, 2021. https://doi.org/10.1007/s11277-021-08644-4

[3] Xu, Z., Xu, G., & Zheng, Z. BER and channel capacity performance of an FSO communication system over atmospheric turbulence with different types of noise. *Sensors*, vol.21, no.10, pp.1-14, 2021. https://doi.org/10.3390/s21103454

[4] Sridhar, B., Sridhar, S., & Nanchariah, V. Performance Evaluation of FSO System under Atmospheric Turbulence and Noise. *Journal of The Institution of Engineers (India): Series B*, vol.103, no.6, pp.2085-2095, 2022. https://doi.org/10.1007/s40031-022-00789-5

[5] Hayal, M. R., Yousif, B. B., & Azim, M. A. Performance enhancement of DWDM-FSO optical fiber communication systems based on hybrid modulation techniques under atmospheric turbulence channel. In *Photonics*, vol.8, no.11, pp. 1-17, 2021. https://doi.org/10.3390/photonics8110464

[6] Kathpal, N., Garg, A. K., Goyal, P., & Awasthi, Y. K. Design of 16× 100 Gbps free-space optical system using advanced modulation techniques. *Journal of Optics*, vol.52, no.3, pp.1584-1601, 2023. https://doi.org/10.1007/s12596-022-01072-y

# Effect of the temperature on the electrical characteristics of the Ti/6H–SiC (n) Schottky diode

**A. Bekaddour, S.Tizi[1], B. Zebentout[1], E. Bounab[1], Z. Benamara[1]**
[1]*Laboratoire de Micro-électronique Appliquée, Université Djillali Liabès de Sidi Bel Abbès, BP 89, 22000, Sidi Bel Abbès,*
*Email: abdelrahmane.bekaddour1995@gmail.com*

**ABSTRACT**

Thanks to its wide bandgap, good thermal conductivity and high chemical and physical stability, as well as a higher breakdown field than Si, solid silicon carbide SiC is an innovative success in components that operate at high temperatures. SiC also has interesting mechanical properties due to its hardness, its high resistance to heat.

SiC Schottky rectifiers are also of considerable relevance for research due to the Schottky diode inhomogeneity. The barrier height inhomogeneity manifests itself in different forms in the static characteristics of a Schottky diode. The most frequent case is the double barrier. The interface states play a critical role for device characteristics; it is considered that the doping impurities, defects, dislocations, micropipes, and inclusions of different polytypes in the epitaxial layers existing in SiC are responsible for Schottky barrier inhomogeneities.

In this work, we investigated the electrical behavior of Ti/6H–SiC(n) diode using (I-V-T) current-voltage-temperature measurements. Generally, it is well established that the (I–V-T) characteristics attempt to extract first the proper Schottky parameters such as ($\Phi B_n$, n, $R_s$), the homogeneous barrier height, and the Richardson constant. In fact, Werner's inhomogeneous model is used to understand anomalies in electrical parameters retrieved and to approach the Richardson constant value A* which is compatible with the value provided by the theory and it is near about 146 $A/K^2$ $cm^2$.

Ti/6H–SiC(n) Schottky diode was prepared. Temperature-dependent I(V) measurements were performed either by a heating system and its cooling with liquid nitrogen during construction. The temperature may be adjusted from 77 to 500 K. The HP4145B "Semiconductor Parameter Analyzer" was used to measure current; each SMU may be configured to create a potential between 0 and ± 100 V.

The first results clearly show that the I(V) characteristics deviate from thermionic behavior as the temperature decreases. The appearance of the double barrier is visible. The barrier height shows an increase with an increase in temperature, while the ideality factor decreases with an increase in temperature.

At low temperature, when T =77 K, the values of the high and low barrier heights are respectively ${\Phi_{Bn}}^H = 0.67eV$ and ${\Phi_{Bn}}^L = 0.49eV$. The high part ideality factor $n^H$ was close to 1.78 showing that the conduction is dominated by the generation–recombination at deep centers. Also, the value of low part ideality factor $n^L$ is equal to 1.67 showing that the conduction mechanism was then dominated by a tunneling current assisted by default.

A similar phenomenon has been reported by other researchers on silicon carbide Schottky diodes, especially for 6H–SiC and 4H–SiC polytypes in contact with metals such as (Ni, Ti, Mo, Au …). It was highlighted that this non-ideal behavior of the I–V-T characteristics is due to interface inhomogeneities. Furthermore, this double barrier was more common at lower temperatures, which was explained by barrier height inhomogeneities.

**Keywords:** Ti/SiC-6H diode; silicon carbide; Barrier height; I-V-T

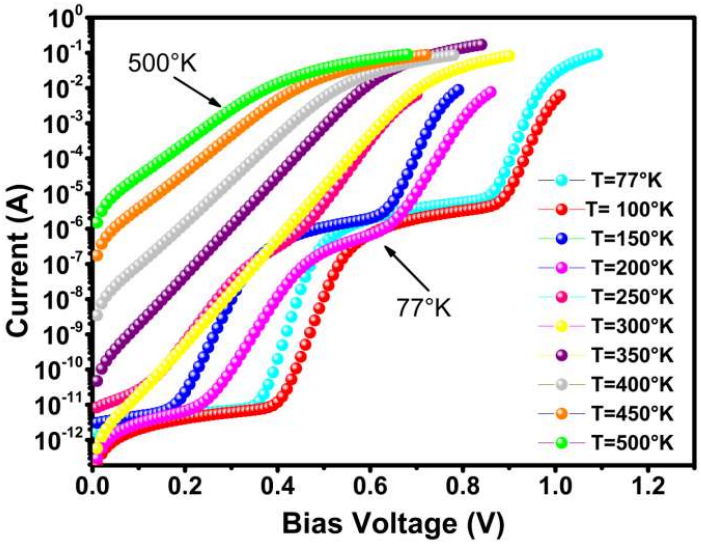


Fig: Measurements of the forward I–V-T characteristics of a Ti/6H–SiC Schottky diode at temperatures between 77 K and 500 K

**References**

[1] S. Duman, A. Turut, S. Dogan, Thermal sensitivity and barrier height inhomogeneity in thermally annealed and un-annealed Ni/n-6H-SiC Schottky diodes, Sensor Actuator Phys. 338 (2022), 113457.

[2] S.M. Sze, Y. Li, K.K. Ng, Physics of Semiconductor Devices, John wiley& sons, (2021).

[3] M.H. Ziko, A. Koel, T. Rang, J. Toompuu, Analysis of barrier inhomogeneities of p-type Al/4H-SiC Schottky barrier diodes, in: Materials Science Forum, vol. 1004, Trans Tech Publications Ltd, (2020), pp. 960–972.

[4] T.Güzel, A.K. Bilgili, M. Ozer, Investigation of inhomogeneous barrier height for Au/n-type 6H-SiC Schottky diodes in a wide temperature range, Superlattice. Microst. 124 (2018) 30–40

# Simulation of current-voltage electrical characteristics in the dark and under illumination of a GaAs-based photodetector

**B. BENELDJEMOUI[1], A. H. KACHA[1], B. AKKAL[1], M. ANANI[2], Z. BENAMARA[1]**

[1] *Laboratoire de microélectronique appliquée, Universsité Djillali Liabes de Sidi Bel Abbes, BP89, Sidi Bel aAbbes, 22000 Algérie*

[2] *Département d'électronique, Universsité Djillali Liabes de Sidi Bel Abbes, BP89, Sidi Bel aAbbes, 22000 Algérie*

*Email: bachir2111@gmail.com*

**ABSTRACT:**

GaAs is a semiconductor material widely used in various electronic and optoelectronic devices due to its unique properties. Among the promising devices made from this material are photodetectors [1]. These devices are designed to react according to the illumination, thus enabling their use for various applications. The purpose of this work is to study and simulate the current-voltage characteristics of these photodetectors in the dark and under illumination in order to define their response and study the photoelectric parameters of the structures. An analytical simulation was performed using MATLAB, allowing for precise control and manipulation of simulation parameters such as ideality factor, saturation current, barrier height, series resistance, and the wavelength of the illumination. The I-V characteristics of GaAs were simulated by varying the wavelength of the incident light, ranging from ultraviolet to infrared. The simulations were performed both in the dark and under illumination, mimicking real-world scenarios. The studied structures are Au/GaAs Schottky diodes. The electrical parameters of these diodes were inspired by previous experimental studies [2], taking into account the manufacturing technological constraints [3]. The simulation results revealed interesting and significant findings. In the dark, the I-V curve of GaAs exhibited typical diode behavior, with an exponential increase in current as the applied voltage increased. However, under illumination, the behavior of GaAs varied depending on the wavelength of the incident light. It was observed that GaAs exhibited a higher current response when illuminated by shorter wavelengths, such as ultraviolet, compared to longer wavelengths such as infrared. This wavelength-dependent behavior can be attributed to the energy band gap of GaAs, which determines the absorption and generation of electron-hole pairs under illumination. Furthermore, the simulations highlighted the importance of considering the effects of light intensity on the I-V characteristics of GaAs. It was observed that increasing the intensity of the incident light led to a higher current response, indicating the influence of light intensity on the generation and recombination of charge carriers within GaAs. This simulation allowed for the plotting of surface photovoltaic (SPV) curves [5-7] of the studied structures as a function of illumination from the simulated current-voltage (I-V) curves, thus studying the influence of illumination on photoelectric parameters such as excess charge concentration and interface state density of these structures.

**Keywords :** GaAs ; Schottky ; illumination ; Simulation.

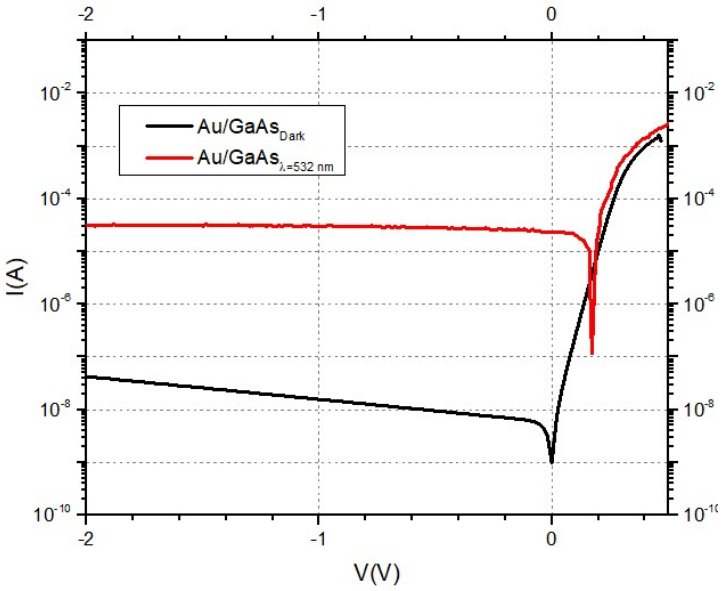


Figure 1 : Simulated I(V) characteristics in dark and under illumination

**References :**

[1]. A. H. Kacha, B. Akkal, Z. Benamara, C. Robert-Goumet, G. Monier and B. Gruzza. MOL. CRYST. LIQ. CRYST. VOL. 627 (2016) 66-73

[2]. A. H. Kacha, M. N. Amroun, B. Akkal. Z. Benamara. Semiconductors 2021, Vol 55. Suppl. 1, pp S54-S61

[3]. H. Mehdi, F. Reveret, C, Bougerol, C. Robert-Goumet, P. E. Hoggan, L. Bideux, B. Gruzza, J. Leymarie, G. Monier. Applied Surface Science 495 (2019) 143586

[4]. L. Kronik, Y. Shapira. Surf. Sci. Rep. 37 (1999), 1.

[5]. L. Kronik, Y. Shapira. Surf. Interface Anal. 31 (2001), 954-965.

[6]. D. Cavalcoli, B. Fraboni, A Cavallini. Semiconductors and Semimetals, 91 (2015), 251–278.

# Study of Reverse-Bias Leakage Current Mechanisme in Metal/GaN Nano-Schottky Diodes

**S. Benykrelef[1], S. Mansouri [1], A. Joti [1] , Z. Benamara[1]**
[1] *Laboratoire de Micro-électronique Appliquée, Université Djillali Liabés de Sidi Bel Abbés, BP 89, Sidi Bel Abbés, 22000, Algeria*

*Email: sbenyekhlef22@gmail0com*

**ABSTRACT**

GaN is a wide direct bandgap semiconductor that has unique applications in the manufacturing of blue light-emitting diodes (LEDs), lasers, ultraviolet detectors, etc. The metal-semiconductor contact is one of the most widely used rectifying contacts in electronics industry. However, GaN-based Schottky contacts suffer from abnormal reverse-bias leakage currents, which currently limit the performance of devices.

Due to the technological importance of Schottky diodes, a comprehensive understanding of the nature of their electrical characteristics is of great interest. GaN-bases nano-Schottky diodes have gained significant attention in recent years. Therfore, our study focuses on simulating Metal/GaN nano-Schottky diodes as a function of temperature using the phonon-assisted tunneling model whith the SILVACO Atlas simulation tool in a temperature range from 80K to 500K. This is done to demonstrate the temperature-dependent reverse-bias leakage current, which can be caused by electron trapping at the metal-semiconductor interface during their transition to the conduction band.

The Silvaco-Atlas software takes into account all of the electrical properties of n-GaN and its contacts, such as forbidden band properties Eg, electron affinity χ, dielectric constant ε, density of conductance states $N_c$, density of valance states $N_v$, electron mobility $\mu_n$, hole mobility $\mu_p$, work function of the metals $\Phi_m$, etc., and uses the Poisson equation and the Continuity equation for electrons and holes as basic equations for the transport mechanisms.

The models used in this simulation are the Shockley-Read-Hall (SRH) recombination . Auger recombination rate (Auger), PIPINYS model and concentration dependent mobility (CONMOB). The numerical resolution methods are the Gummel and Newton methods. Finally, the temperature is varied from 80° to 500° K with a step of ΔT = 100 K.

The current across the Schottky contacts is the classical thermionic emission mechanism, which is expressed by :

$$I = I_s\left(exp\left(\frac{q(V-IR_s)}{nkT}\right)-1\right)$$

where $I_s$ is the saturation current expressed as:

$$I_S = AA^*T^2exp\left(-\frac{q\Phi_b}{kT}\right)$$

where$R_s$ is the series resistance, $n$ is the ideality factor, $k$ is the Boltzmann constant, $T$ is the temperature, $A$ is the effective diode area equal $2.8\times10^{-5}$ $cm^{-2}$, $\Phi_b$ is the barrier height and $A^*$ is the effective Richardson constant.

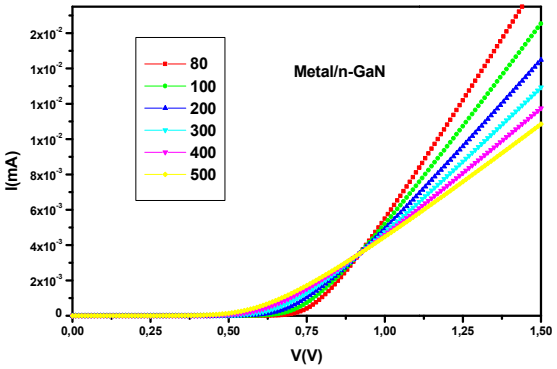


Figure 1. (a) Linear forward bias I-V characteristics of n-GaN Nano-Schottky for different temperatures

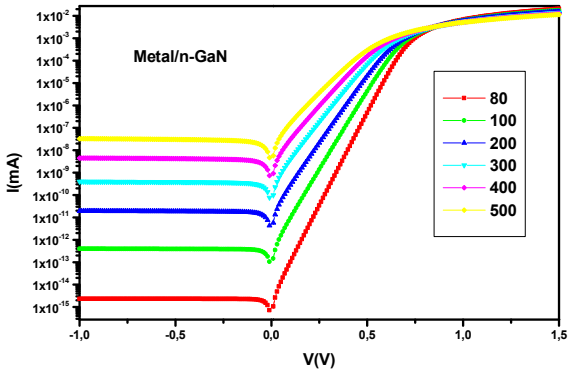


Figure 2. Semi-logarithmic I-V characteristics of n-GaN Nano-Schottky for different temperatures

**Keywords:** GaN; Silvaco-Atlas; Schottky diode; the I–V characteristic

**References**

[1] ATLAS User's Manual DEVICE SIMULATION SOFTWARE", Silvaco, Santa clara, California, USA, 2014.
[2] B. Akkal, Z. Benamara, H. Abid, A. Talbi, and B. Gruzza, "Electrical characterization of Au/n-GaN Schottky diodes," Materials chemistry and physics, vol. 85, pp. 27-31, 2004.
[3] P. Pipinys and V. Lapeika, "Temperature dependence of reverse-bias leakage current in GaN Schottky diodes as a consequence of phonon-assisted tunneling," Journal of Applied Physics, vol. 99, no. 9, Article ID 093709, 2006.
[4] Werner JH, Güttler HH. Barrier inhomogeneities at Schottky contacts. Journal of applied physics. 1991;69:1522-33.

# Study and investigation of reverse I-V-T measurements of Ti/6H-SiC(n) Schottkydiode for three area contacts

**E. Bounab[1], S. Tizi[1], B. Zebentout[1], A. Rabehi [2] , A. Bekaddour[1], Z. Benamara[1]**
[1]*Laboratoire de Micro-électronique Appliquee, UniversiteDjillaliLiabes de Sidi Bel Abbes, BP 89, 22000, Sidi Bel Abbes, Algeria*
[2]*University of Ziane Achor, Djelfa, 17000, Algeria*
*Contact: bounabelhachani@gmail.com*

**ABSTRACT**

As the evolution of electronic components continues, we are currently at the limit of the physical and the electrical properties of silicon in certain application areas. This limit has motivated the search for new materials with a wide bandgap that can offer superior performance to that of silicon.

Silicon carbide SiC is a promising semiconductor material for harsh environment sensing applications thanks its remarkable properties such as wide band gap, high thermal conductivity, high breakdown field, high saturation electron drift velocity, high chemical stability, and great mechanical strength. Because of these properties, SiC has been developed as a semiconductor for high-power and hightemperature electronics.

The M/S Schottky contact is one of the most important components of modern integrated devices. In particular, ohmic contacts with low contact resistance and Schottky contacts with controlled barrier height between SiC and metal are critical points that can compromise the manufacturing quality of devices.

The interface states play a critical role for device characteristics. The doping impurities, defects, dislocations, micropipes, and inclusions of different polytypes in the epitaxial layers existing in SiC are responsible for Schottky barrier inhomogeneities. Therefore, it is vital to identify these electrically active defects in the grown epitaxial layers and to know how they affect the detector performance in terms of leakage current, Schottky barrier inhomogeneities.

In this work, three different sizes (1.6 × 1.6, 1.6 × 0.4 and 0.4 × 0.4 $mm^2$) of Ti Schottky diodes on n-type 6H–SiC epitaxial layers were fabricated.

A "Semiconductor Parameter Analyzer" model HP4145B was utilized in order to obtain accurate readings of the electrical current. Each SMU is capable of being configured to generate an electrical potential ranging from 0V to ± 50 V.The reverse bias I-V characteristics are investigated at different temperatures for an extensive analysis.

To achieve an understanding of thecommon transport mechanisms (thermoionic current; tunneling current,… ) in the study diodes, we compare the measured I-V characteristics with theoretical ones through the Matlab environment.

Whatever the type of diode, we note an increase in leakage current with temperature but this increase varies from one diode to another. In big area diodes, the increase in leakage current with temperature is continuous.When the size of the diode is reduced in the medium and the small diode, the leakage current becomes more independent of temperature.

The authors attributed this phenomenon to the presence of non-ionized impurities in the semiconductor.When the voltage becomes greater, these impurities emit carriers in the permitted bands which gives rise to an excess current, which destroys the diode.The additional heating further leads to faster ionization of impurities which in turn produces more current. It is deduced that for SiC components, a minimum temperature and reduced dimension are required to optimize performance if a low leakage current is required.

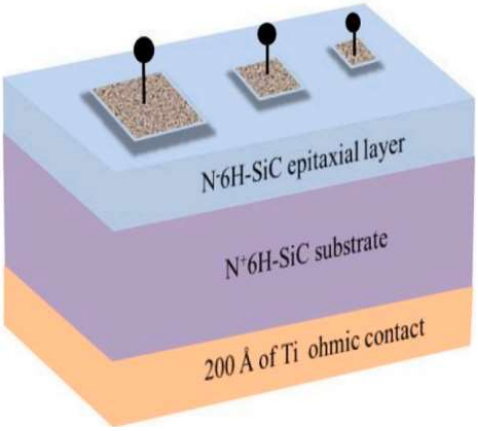


Fig. 1. Schematic section of a Ti/6H-SiC Schottky diode.

**Keywords:** Schottky diode; SiC semiconductor; Titanium metal; I-V-T characterization; leakage current.

**References**

[1] K. Zekentes (Ed.), Advancing Silicon Carbide Electronics Technology: Metal Contacts to Silicon Carbide: Physics, Technology, Applications, Materials Research Forum LLC, (2018), September.

[2] S.M. Sze, Y. Li, K.K. Ng, Physics of Semiconductor Devices, John wiley& sons, (2021).

[3] A. Rabehi, B. Akkal, M. Amrani, S. Tizi, Z. Benamara, H. Helal, A. Ziane, Current-Voltage, Capacitance-Voltage-Temperature, and DLTS studies of Ni| 6H-SiC Schottky diode, Semiconductors 55 (4) (2021) 446-454.

[4] P.G. Neudeck, C.Fazi, High field fast rise time pukse failure in 4H and 6H-SiC pn Junction diode, J.Appl.Phys.Vol.80, pp.1219-1225, (1996).

# A Simulation Study to the Effects of Doping Concentration and Region Thickness on the Performance of InGaN Single Junction-Based Solar Cells

**Amine Hadjouni[1], Boudali Akkal[1], Zineb Benamara[1], Arslane Hatem Kacha[1].**
[1] *Laboratoire de MicroElectronique Appliqué, Faculté de Génie Electronique , Université de sidi bel abbes ,Algerie*
*Email: hadjouni-amine@hotmail.com*

**ABSTRACT**

The Silvaco ATLAS simulation program was used to examine the effect of doping concentration and thickness of the n-InGaN and p-InGaN regions on the power conversion efficiency of single junction-based InGaN solar cells. For the n-InGaN and p-InGaN areas, the doping concentrations of 5e19 $cm^{-3}$ and 3e15 $cm^{-3}$, respectively, were optimized. Both n-InGaN and p-InGaN areas were tuned for a thickness of 470 nm and 430 nm . respectively. At optimal values of doping concentration and thickness of n-InGaN and p-InGaN regions of InGaN solar cells, the greatest efficiency of 23,47% with $J_{sc}$ = 41,9 mA/cm2, $V_{oc}$ = 0,7 V, and FF = 79% were attained. Comparison of these results with other workhighlights the usefulness of Silvaco's ATLAS simulation tool and the optimization of the doping concentration and thickness of the n-InGaN and p-InGaN regions for solar cells, This would make the creation of highly effective InGaN solar cells both affordable and effective.

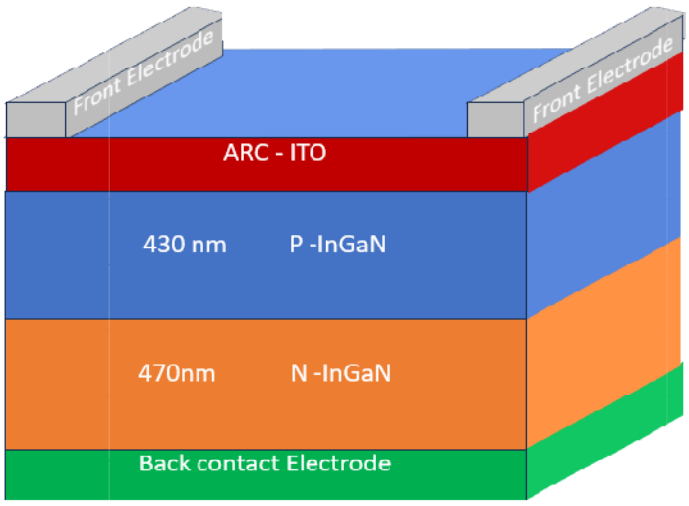


Fig1. InGaN-based Single-junction solar cell

**Table1. InGaN structure parameters.**

| Parameters | p-InGaN | n-InGaN |
|---|---|---|
| Thickness (µm) | 430 | 470 |
| Donor concentration $N_d$ ($cm^{-3}$) | | $5.10^{19}$ |
| Acceptor concentration $N_a$($cm^{-3}$) | $3.10^{15}$ | |

**Table2. Simulation results.**

| Results | $J_{sc}$=41.9 | $V_{oc}$= 0.7 | FF=79% | η=23.47% |
|---|---|---|---|---|

**Keywords:** GaN, III-V, SILVACO, Solar Cells, 2D simulation.

**References**

[1] D. Parajuli, D. K. Shah, D. KC, S. Kumar, M. Park, et B. Pant, « Influence of Doping Concentration and Thickness of Regions on the Performance of InGaN Single Junction- Based Solar Cells: A Simulation Approach »,*Electrochem*, vol. 3, n° 3, p. 407‑415, 2022.

# Optimizing InGaN-Based Solar Cells for Enhanced Sustainability

**Ibrahim Sofiane Herir[1], Abdelaziz Rabehi[1,2], Baya Zebentout[1], Zineb Benamara[1]**

[1]*Laboratoire de microélectronique appliquée, Université Djillali Liabes de Sidi Bel Abbes, BP89, Sidi Bel Abbes, 22000 Algérie*
[2]*Telecommunications and smart systems Laboratory, University of Ziane Achour, Djelfa 17000, Algeria.*
*Email: brahim.herir@univ-sba.dz*

## ABSTRACT

This investigation delves into harnessing the yet-untapped potential of InGaN material to enhance solar cell efficiency. GaN and high-bandgap InGaN solar cells demonstrate promising features, including open-circuit voltages up to 2.4 V and internal quantum efficiencies of 60%[1]. Despite the industry achieving over 40% energy conversion efficiency with III-V semiconductor compounds by 2012[2], a persistent challenge remains in the insufficient indium composition of current devices.

To tackle this challenge, our research focuses on refining the indium composition using the InN/GaN material system. Building upon prior studies identifying a peak efficiency of $\eta = 58.25\%$ with specific layer thicknesses [3], Silvaco Atlas TCAD simulations are employed to extend the boundaries of InGaN solar cell technology. The primary objective is a substantial enhancement of the indium composition, thereby advancing sustainable energy solutions.

The bandgap energies of the InGaN alloy system span the entire air-mass-1.5 solar spectrum, effectively depicted in Fig. 1. Notably, InxGa1−xN films exhibit robust photoluminescence, even when cultivated on lattice-mismatched substrates. Furthermore, these films demonstrate remarkable resistance to high-energy (2 MeV) photon irradiation, outperforming traditional PV materials like GaAs and GaInP. This resilience positions InGaN alloys as promising candidates for radiation-hard high-efficiency solar cells, particularly in space applications.

Moreover, InGaN alloys boast advantages such as high carrier mobility, drift velocity, thermal conductivity, and temperature resistance. These attributes collectively contribute to realizing highly efficient solar cells suitable for concentrated sunlight conditions. Consequently, solar cells based on group-III-nitride materials emerge as strong contenders for operation in challenging environments, where conventional Si solar cells may face difficulties. A nuanced comprehension of InGaN's distinct properties places it at the forefront of advanced solar cell technology development, applicable both on Earth and in space.

**Keywords:** GaN, III-V, SILVACO, photodetectors, 2D simulation. optimization.

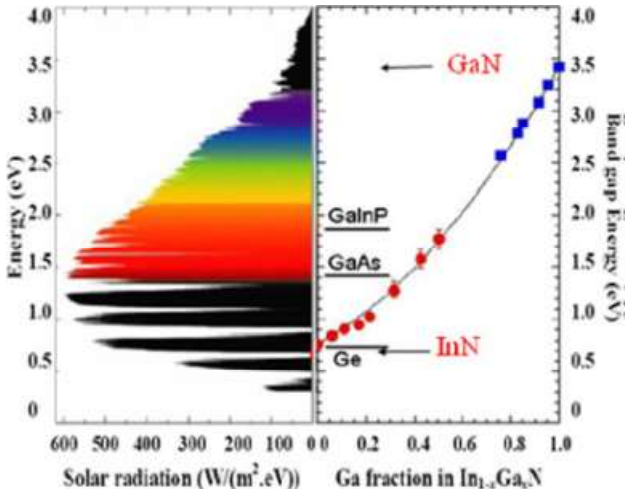


**Fig . 1** Comprehensive Coverage of the Air-Mass-1.5 Solar Spectrum by Bandgap Energies in the InGaN Alloy System

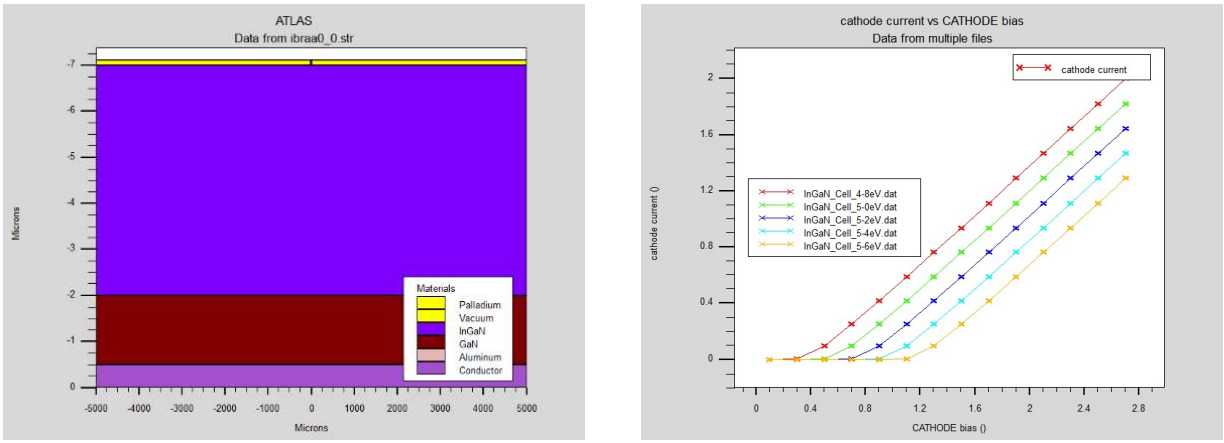


**Fig .2** InGaN/GaN solar-cell device structure with the corresponding I-V characteristics.

**References**

[1] O. Jani, I. Ferguson, C. Honsberg, and S. Kurtz, "Design and characterization of gan/ingan solar cells," Applied Physics Letters, vol. 91, pp. 132 117–132 117, Sep. 2007. doi: 10.1063/1.2793180.

[2] A. Bhuiyan, K. Sugita, A. Hashimoto, and A. Yamamoto, "Ingan solar cells: Present state of the art and important challenges," Photovoltaics, IEEE Journal of, vol. 2, pp. 276–293, Jul. 2012. doi: 10.1109/JPHOTOV.2012.2193384.

[3] L. Pérez, A. Aouami, K. Feddi, et al.,"Parameters optimization of intermediate band solar cells: Cases of pbte/cdte, pbse/znte and inn/gan quantum dots," Crystals, vol. 12, p. 1002, Jul. 2022. doi: 10.3390/cryst12071002.

[4] J. Wu, W. Walukiewicz, K. M. Yu, W. Shan, J. W. Ager III, E. E. Haller, Hai Lu, W. J. Schaff, W. K. Metzger, and S. Kurtz, "Superior radiationresistance of In1−x GaxN alloys: Full-solar-spectrum photovoltaicmaterial system," J. Appl. Phys., vol. 94, no. 10, pp. 6477–6482, Nov.2003.

# Study of electrical parameters of III-V based Schottky diodes for photovoltaic applications

**H. KHALES[1], A. H. KACHA[1], B. AKKAL[1], Z. BENAMARA[1]**

[1] *Laboratoire de miucroélectronique appliquée, Universsité Djillali Liabes de Sidi Bel Abbes, BP89, Sidi Bel aAbbes, 22000 Algérie*
*Email: h_khales@hotmail.com*

**ABSTRACT**

Schottky diode-based cells are appealing due to the simplicity of their fabrication process [1]. They lend themselves well to manufacturing using simple chemical methods [2] and are well-suited for the production of large-area solar cells [3], as well as for implementation on flexible substrates [4]. In this context, nitride GaAs Schottky diodes [8-10] are strong candidates, with their performance depending on the quality of the metal-semiconductor interface passivation. Numerous studies [9-12] have focused on understanding the operational phenomena of these types of structures. This study presents the influence of Schottky diode parameters on the performance of a solar diode. Indeed, the crucial parameters characterizing the Schottky diode, namely the diode ideality factor (n), barrier height ($\emptyset_{b_n}$), saturation current (Is), and series resistance (Rs), significantly impact the properties of a solar diode. Analytical solutions serve as an effective method for understanding the interaction of each of these parameters with the open-circuit voltage (Vco), short-circuit current density (Jsc), conversion efficiency (η), and fill factor (FF), which collectively characterize a photovoltaic cell. By using the Scilab numerical simulation software, we obtain the characteristic (I-V) with the characteristic parameters of a Schottky diode, and the variation of these parameters elucidates their influence on the performance of a photovoltaic cell. The conversion efficiency of a Schottky diode for photovoltaic applications is dependent on these electrical parameters. In summary, high values of series resistance lead to a degradation of efficiency. Additionally, although analytically the open-circuit voltage (Vco) increases with the ideality factor, the efficiency is reduced by the increase in the latter, which is accompanied by an increase in the saturation current. Finally, the higher the barrier height, the higher the open-circuit voltage, fill factor, and conversion efficiency.

**Keywords:** Shottky diodes; Electrical characterization; photoelectrical characterization, III-V materials.

**Analytical models :**

The variation of current density in a photovoltaic diode follows the following relationship :

$$J = J_s \left( e^{\frac{q}{n\,k\,T}(V - Rs\ I)} - 1 \right) - J_L ,$$

Where the saturation current density is given by : $J_s = A^*\ T^2\ e^{\left(-\frac{q\,\emptyset_{bn}}{k\,T}\right)}$

To obtain the parameters of the photovoltaic cell, the following equations must be solved :

The open circuit voltage: $V_{oc} = \frac{nKT}{q} ln\left(\frac{J_L}{J_s} + 1\right) \approx \frac{nKT}{q}\left[ln\left(\frac{J_L}{AT^2}\right) + \frac{q\emptyset_{bn}}{KT}\right]$,

And the maximum voltage $V_{oc} = V_{max} - R_s J_{max} + \frac{nKT}{q} ln\left(1 + \frac{qV_{max}}{nKT}\right)$,

To obtain the fill factor (FF) $FF = \frac{J_{max}V_{max}}{J_{sc}V_{oc}}$,

And the conversion effeciency $\eta = \frac{J_{max}V_{max}}{P_{in}} = \frac{FF\ J_{sc}\ V_{oc}}{P_{in}}$

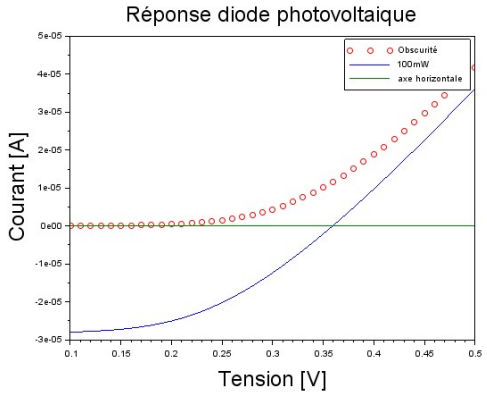


**Figure 1 :** Electrical response of a GaAs Shottky diode [8].

**Figure 2 :** Evolution of conversion effeciency and fill factor for a GaAs Schottky diode

**References**

[1] A. Ghods, « A Review of Schottky Junction Solar Cells ». Special issue of IEEE-HKN The Bridge Magazine, 2021.

[2] X. Kong *et al.*, « Graphene/Si Schottky solar cells: a review of recent advances and prospects », *RSC Adv.*, vol. 9, n° 2, p. 863‑877, 2019, doi: 10.1039/C8RA08035F.

[3] K. M. Islam, T. Ismael, C. Luthy, O. Kizilkaya, et M. D. Escarra, « Large-Area, High-Specific-Power Schottky-Junction Photovoltaics from CVD-Grown Monolayer MoS ₂ », *ACS Appl. Mater. Interfaces*, vol. 14, n° 21, p. 24281‑24289, juin 2022, doi: 10.1021/acsami.2c01650.

[4] X. Li, P. Li, Z. Wu, D. Luo, H.-Y. Yu, et Z.-H. Lu, « Review and perspective of materials for flexible solar cells », *Mater. Rep. Energy*, vol. 1, n° 1, p. 100001, févr. 2021, doi: 10.1016/j.matre.2020.09.001.

[5] A. H. Kacha *et al.*, « Effect of metallic contacts diffusion on Au/GaAs and Au/GaN/GaAs SBDs electrical quality during their fabrication process », *J. Alloys Compd.*, vol. 876, p. 159596, sept. 2021, doi: 10.1016/j.jallcom.2021.159596.

[6] H. Helal *et al.*, « Electrical characterization of Au/GaN/n-GaAs Schottky nano-structures in a wide temperature range ».

[7] A. M. Benamara, A. H. Kacha, A. Talbi, B. Akkal, Z. Benamara, et S. Belarouci, « Electrical Study of Au/GaN/GaAs (100) Structures as a Function of Frequency », *J. Nano- Electron. Phys.*, vol. 14, n° 2, p. 02008-1-02008‑4, 2022, doi: 10.21272/jnep.14(2).02008.

[8] M. Soylu et F. Yakuphanoglu, « Photovoltaic and interface state density properties of the Au/n-GaAs Schottky barrier solar cell », *Thin Solid Films*, vol. 519, n° 6, p. 1950‑1954, janv. 2011, doi: 10.1016/j.tsf.2010.10.030.

# Ideal and real behavior of the I-V curves of polytype-SiC based schottky diode for a wide range of metal contact

**Fayssal Mekaret, B. Zebentout, S. Tizi, Z. Benamara**

*Applied Microelectronic Laboratory, Djillali Liabès University of Sidi Bel Abbess, BP 89, 22000, Algeria*
*Email: mekaretf@gmail.com*

## ABSTRACT

Silicon carbide is a promising semiconductor material for harsh environment sensing applications thanks to its superior material properties compared with silicon and other semiconductor materials. The wide bandgap, high thermal conductivity, and high breakdown field allow SiC based devices to work under extreme conditions, therefore many researchers have studied the properties of SiC Schottky rectifiers on 3C–SiC , then on 6H–SiC , and more recently on 4H–SiC .The objectif of this work is to compare the I(V) curves of Schottky diodes based on the three SiC prototypes for a wide range of metal's work function values ranging from 3.65 eV to 5.65 eV for both ideal and real case via a Matlab simulation. The charge transport mechanism in a Schottky contact consists of four models: thermionic emission, diffusion, tunneling, and generation-recombination, however, the diffusion, tunneling, and generation-recombination currents will be neglected due to the low n doping (Nd=$5\times10^{15}$ $cm^{-3}$) and the large bandgap width for the three prototypes ( 2.2eV for 3C, 3 eV for 6H, and 3.2 eV for 4H), therefore only the thermoionic current ($I_{thermoionic}$) will be taken into consideration, $I_{thermoionic}= Io\left(e^{\frac{q(V-Rs\times I)}{nkT}}-1\right)+\frac{V-Rs\times I}{R_p}$; $I_0$ is the saturation current $= A^*T^2exp\left(-\frac{q\Phi_{Bn}}{kT}\right)$, $R_s$ and $R_p$ are respectively the series and parallel resistances, $A^*$ is the richardsson constant= $4\pi m^*qk^2/h^3$, $m^*$ is the effective masse of electron , n is the factor ideality and $\Phi_{Bn}$ is the schottky barrier high.In the ideal case the barrier height is calculated directly as the difference between the metal's work function $\Phi_m$ and the semiconductor's electron affinity $\chi_{sc}$ (3.2 eV for 3C, 3.5 eV for 6H, and 4 eV for 4H) $q\Phi_{Bn(ideal)}=q\Phi_m-q\chi_{sc}$, in the reel situation the calculation of the Schottky barrier height takes into account the interface states ($N_{SS}$), the thickness of the native oxide layer formed at the interface ($D_{OX}$), the barrier height reduction $\Delta\Phi$ due to the image force (mirror effect) and the leakage current ,$\Phi_{Bn(reel)}= \gamma(\Phi m-\chi sc)+(1-\gamma)(\frac{Eg}{q}-\phi_0)-\Delta\Phi$ , $\Delta\Phi=\sqrt{\frac{qE}{4\pi\varepsilon_{SC}}}$ where $\gamma=\frac{\varepsilon i}{\varepsilon_{ox}+q.\varepsilon_{Si}.Nss}$ , $\varepsilon_{ox}$ and $\varepsilon_{SC}$ are the semiconductor and the oxyde layer permittivity.

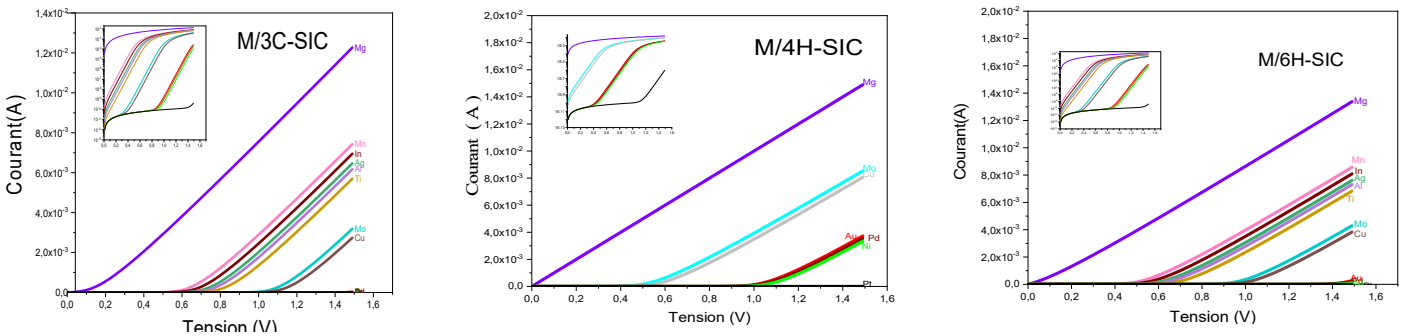


Fig 1: The effect of the metal on the I-V characteristic at 300K in the reel case fot the three prototypes SiC.

The I-V characteristics curves analyse for a SiC prototypes based Schottky diode using a wide range of metals in both real and ideal cases at room temperature T=300K reveal that for 3C and 6H we have good rectification within a range of metal works function from 4.15 to 4.65eV ,for lower values we have an ohmic contact, and for higher values we have the double barrier phenomenon,in the case of 4H, for good rectification, the range of metals that ensures good rectification is from 4.6 to 5.15 eV. , and we can see that Titanium (qΦm=4.33eV) provides the better rectification for 3C-SiC and 6H-SiC, whileit is the Nickel for 4H-SiC(Figure1).To better visualize the difference between the two studied cases (ideal and real), both currents are plotted on the same graph in Figure 2. It is apparent that the margin between the two currents varies depending on the chosen prototype,therefore we can conclude that due to the differences in physical properties among the three prototypes, such as energy bandgap, charge mobility, effective state density and the richardson's constant, the quality of Schottky rectification is not the same, and the choice of metal is crucial.

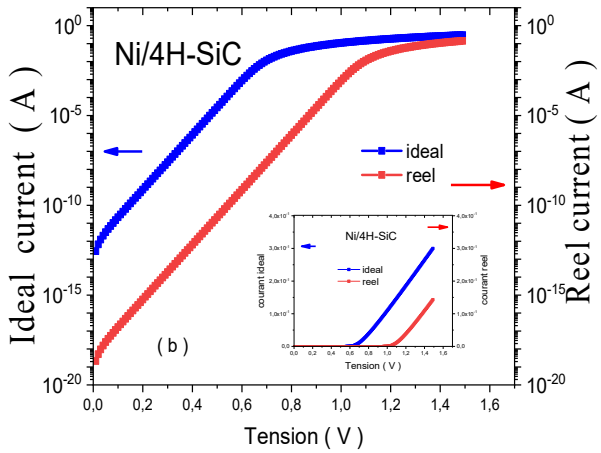


Fig 2: I-V characteristic for Ni/4H-SiC in ideal and reel case.

**Keywords:** SiC; Reel; Ideal; Barrier hight,Thermoionic

## REFERENCES

[1] H. Helal, Z. Benamara, M. B. Arbia, A. Rabehi, A. C. Chaouche, et H. Maaref, « Electrical behavior of N-GAAS based Schottky diode for different contacts: Temperature dependence of c URRENT-VOLTAGE », *Int J Numerical Modelling*, vol. 34, n° 6, p. e2916, nov. 2021, doi: 10.1002/jnm.2916.

[2] K. Zeghdar, « Simulation et Analyse des caractéristiques électriques de la diode à barrière de Schottky (SBD) Métal/Carbure de Silicium »,Universite mohamed khider,Biskra,Algerie,2019.

[3] A. Bekaddour, A. Rabehi, S. Tizi, B. Zebentout, B. Akkal, et Z. Benamara, « Effect of the contact area on the electrical characteristics of the Ti/6H–SiC (n) Schottky diode », *Micro and Nanostructures*, vol. 173, p. 207464, janv. 2023, doi: 10.1016/j.micrna.2022.207464.

[4] A. Chvála *et al.*, « Characterization and evaluation of current transport properties of power SiC Schottky diode », *Materials Today: Proceedings*, vol. 53, p. 285‑288, 2022.

[5] J. H. Zhao, K. Sheng, et R. C. Lebron-Velilla, « Silicon carbide schottky barrier diode », *International journal of high speed electronics and systems*, vol. 15, n° 04, p. 821‑866, 2005.

# I-V and AFM analysis of Au/n-GaAs Schottky contacts for different GaAs thickness

**S. Taibi[1], Z. Benamara[1], M. A. Benamara[1], H. Helal[2], I. Demir[3], D. Zappa[2], E. Comini[2]**

[1]*Laboratoire de MicroélectroniqueAppliquée, Université de Sidi Bel Abbès, BP 89, 22000, Sidi Bel Abbes, Algérie*
[2]*Sensor Laboratory University of Brescia, Via D. Valotti 9, 25133 Brescia, Italy*
[3]*Nanophotonics Research and Application Center, Sivas Cumhuriyet University, 58140, Sivas, Turkey*
*Email: soumiaaiboudi27@gmail.com*

**ABSTRACT**

Thispaper presents a study of the Au/n-GaAs Schottky diode fabricated byMetal Organic Chemical Vapor Deposition (MOCVD) technic. The GaAs layer was grown for different thicknesses, 1, 3, and 8µm for samples A, B, and C progressively. The topography of the GaAs surfaces was analyzed using Atomic force microscopy, where the samples present a good topography with a low roughness.The electrical properties were characterized and the electrical parameters were extracted at room temperature. The comparison of results shows that sample B gives the best characteristics with a low ideality factor and low resistance.
**Keywords:**GaAs; MOCVD; AFM; I-V; Schottky; ideality factor;

## INTRODUCTION

The Schottky contacts Metal-Semiconductor MS have attracted much attention. This is due to the potential application in various electronic and optoelectronic devices, such as high-frequency field effect transistors, microwave FETs, RF detectors, photodiodes, laser diodes, and solar cells[1]. In this work, we fabricated Au/n–GaAs Schottky contacts using MOCVDfor different thicknesses of the GaAs layer. The samples were analyzed by AFM microscopy and the electrical properties were investigated at room temperature.

## EXPERIMENTAL PART

The GaAs layers were grown using MOCVD on Si-GaAs highly doped for different thicknesses, 1, 3, and 8 µm for samples A, B, and C progressively. The deposition was at a temperature of 650 °Cand 1nm/s rate. Au plots were deposited using Sputtering technic at 300°C under $5 \times 10^{-4}$Torr and 7 Sccm flow of nitrogen and 75Watt power for 3 minutes and 20s, to obtain100nm of Au thickness. The surface topography was analyzed using AFM microscopy using a Scanning Probe Microscope (SPM) SmartSPM-1000 on 10×10 µm surface by non-contact mode. The current-voltage characteristics were investigated at room temperature.

## RESULTS

Figure 1 shows the AFM topography of samples A,B, and C on 10×10 µm surface.They show a lowroughness of 0.34, 0.49, and 1.78 nm, respectively. The roughness increases with the increase of the growing layer. As well known, for a Schottky contact, the roughness of the interface directly affects the electrical performance and should be as low as possible.

The classical model of the thermionic emission current for non-ideal Schottky contacts is expressed as:

$I = I_s \exp\left(\frac{q(V-R_sI)}{nkT}\right)$ *(1)*

where $k$ is the Boltzmann constant,$A$ is the effective diode area, $A^*$ is the effective Richardson constant.

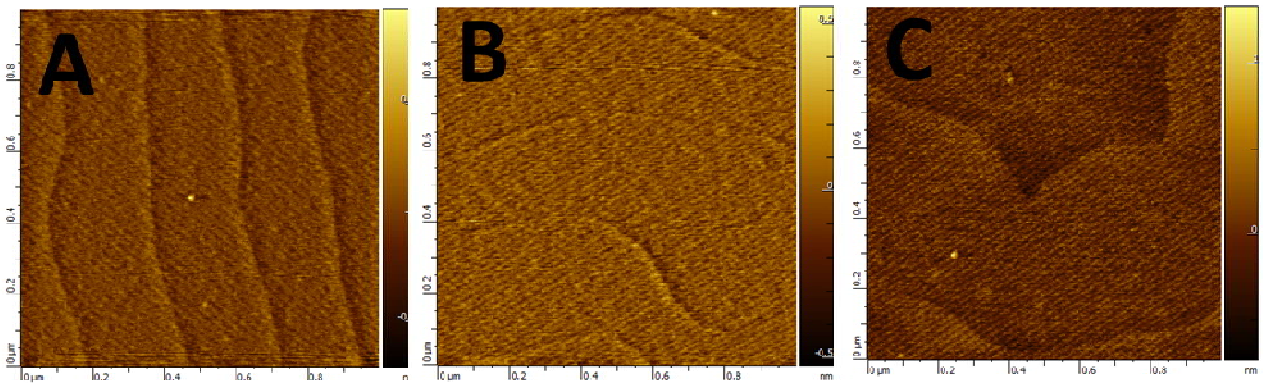


Fig 1: AFM topography of samples A,B, and C with roughness of 0.34, 0.49, and 1.78 nm, respectively .

The electrical parameters are extracted using Cheung and Cheung method [2].

The I-V curves are shown in Figure 2 and the electrical parameters extracted from the I-V characteristicsare shown in Table 1.

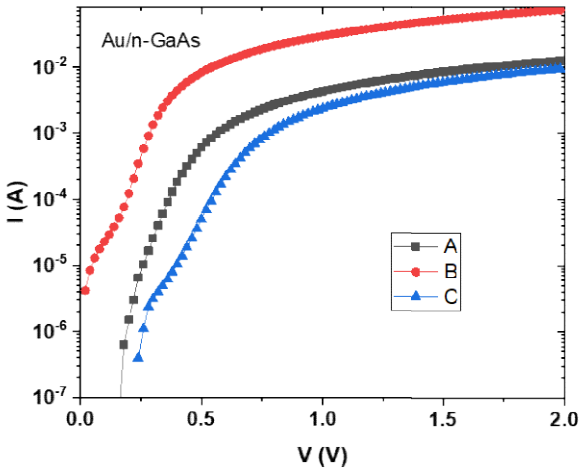


Fig 2:I-V characteristics of samples A, B, and C.

| Samples | R ($\Omega$) | n | $\phi_b$(eV) | Is (A) |
|---|---|---|---|---|
| A | 114 | 1.76 | 0.71 | $1.07\times 10^{-7}$ |
| B | 22 | 1.22 | 0.65 | $9.12\times 10^{-7}$ |
| C | 130 | 2.01 | 0.77 | $1.25\times 10^{-8}$ |

Tible 1: Electrical parameters of samples A, B, and C.

From Tible 1, we can conclude that sample B gives the best characteristics with a low ideality factor and low resistance. Also, it gives a an acceptable saturation current of $9.12\times \mathbf{10^{-7}}$A,and a Shottky barrier height of 0.65 eV.

**References**

[1] Helal, H., Benamara, Z., Kacha, A. H., Amrani, M., Rabehi, A., Akkal, B., ... & Robert-Goumet, C. (2019). Comparative study of ionic bombardment and heat treatment on the electrical behavior of Au/GaN/n-GaAs Schottky diodes. Superlattices and Microstructures, 135, 106276.

[2]Cheung S, Cheung N. Extraction of Schottky diode parameters from forward current-voltage characteristics. Appl Phys Lett. 1986;49:85-87.

# Effect of contact metal on the electrical parameters of Au/n-GaAs Shottky barrier diodes

**H. Toumi[1], M. A. Benamara[1], A. Talbi[1], Z. Benamara[1]**

[1]*Laboratory of Applied Micro Electronics University Djillali Liabes of Sidi Bel Abbes, 22000 Sidi Bel Abbes, Algeria*
*e-mail:* hayattoumi97eln@gmail.com

**ABSTRACT**

The III-V binary GaAs semiconductor has been flourished as a promising material for micro and nanoelectronic devices This is due to high physical and electrical properties such as wide band gap, excellent transport, high saturation electron velocity, high thermal conductivity, high breakdown voltage, and chemical inertness [1]. We report on the electrical behavior of Metal/n-GaAs Schottky structure, using Silvaco-Atlas software. To study the effect of metal work function ϕm on the performance of various parameters such as saturation current Is, ideality factor n, and barrier height ϕb, we examine a large number of contact materials having different ϕm at room temperature (300k). sructure is investigated for different Schottky contacts, such as Cr (4.60), W (4.63), Ag (4.64), Cu (4.94), Au (5.10), Pt (5.12), and Ni (5.31). At room temperature. In order to explore the impact of metal working on the different electrical parameters of n-GaAs SBDs, the current-voltage characteristics were simulated as a function of temperature using the Silvaco Atlas program. The simulated structure is designed in a three-dimensional mesh.The simulated structure is designed in a three-dimensional mesh. The GaAs semiconductor is specified as a 400 µm substrate layer. Once the structure is defined, Silvaco-Atlas takes into account all the electrical and optical properties such as the energy band gap (Eg = 1.42 eV), the electron affinity (χ = 4.07 eV) and the constant dielectric (ε = 13.2). GaAs is defined as n-type doping and concentration $N_d$= 1 × $10^{16}$$cm^{-3}$. The results show a significant dependence between ϕm and the electrical parameters. We observe that the smallest values of the threshold voltage Vi are obtained for low ϕm.

**Keywords:** Schottky barrier diodes; Metal/n-GaAs; Electrical characterization;Silvaco Atlas.

figure 1 show Cross-sectional curve of the simulated Metal/n-GaAs structure.

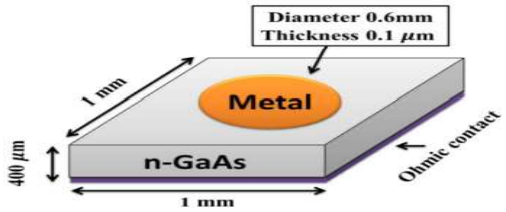


**Fig. 1.** General view of the simulated Metal/n-GaAs SBDs.

Electrical parameters such as ideality factor n, saturation current $I_s$ and barrier height $\phi_b$ and series resistance $R_s$ were then extracted from the simulated curves using the thermionic model.The general expression for the current flowing through a diode is:

$$I = I_s\left(\exp\left(\frac{q(v-IR_s)}{nkt}\right) - 1\right) \quad (1) \qquad [2]$$

Where V is the applied bias voltage, $I_s$ the saturation current, $R_s$ the series resistance, n the ideality factor, k the Boltzmann constant, T the temperature and q the electron charge.

Figure 2 show the linear and the semi- logarithmic scale of the forward bias I-V characteristics of Metal/n-GaAs Schottky structure at room temperature.

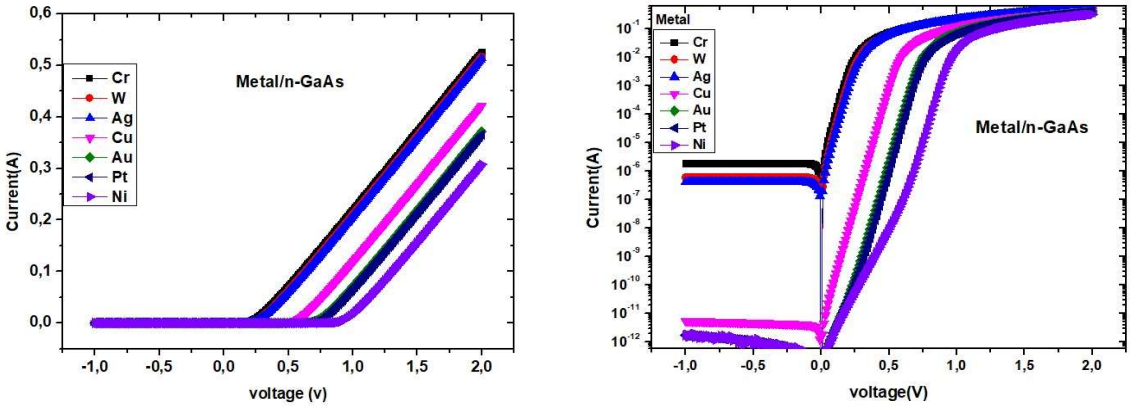


**Fig.2.**Current-tension simulated curves of Metal/nGaAs using Silvaco-Atlas.

When observing the semi-log characteristics and applying a reverse bias voltage, it becomes evident that a lower metal work function results in a significant reverse current**.** However, this reverse current diminishes as the metal work function increases from 4.60 eV to 5.31 eV. (Fig 2).When a forward bias voltage is applied, the Schottky characteristic behavior is observed regardless of the value of ϕm. Specifically, for bias voltages V <~ 0.8 V, the current shows a linear increase as the bias voltage increases. However, as ϕm increases, the current gradually decreases. The results obtained are satisfactory and in good agreement with the literature [3], the results of this work present a first part of a series of simulations aimed at proposing high quality SBDs that can be used in electronic and optoelectronic applications under optimal or hostile conditions.

**References**

[1] Akkal B, Benamara Z, Abid H, Talbi A, Gruzza B. Electrical characterization of au/n-GaN Schottky diodes. Mater Chem Phys. 2004; 85: 27-31.

[2] S. M. Sze, Kwok K. NG, "Physics of Semiconductor Devices", Third Edition, JOHN Wiley & Sons, JNC, 2007.

[3] Helal,H. Benamara,Z. Ben Arbia,M. Rabehi,A. Chabane Chaouche,A. Maaref,H. 2021, may. Electrical behavior of n-GaAs based Schottky diode for different contacts: Temperature dependence of currentvoltage ,Helal,H. 2021 John Wiley & Sons Ltd .DOI: 10.1002/jnm.2916.

# The structural and electronic properties of (001) growth axis(BSb)n/$(BN)_n$ superlattices

**Belghoul Hafida[1], Oukli Mimouna[1], Abid H[1]**

[1] *Applied Materials Laboratory (A.M.L), Faculté de Genie Electrique, University DjillaliLiabes of Sidi Bel Abbes, 2200 Sidi Bel Abbes Algeria*

**ABSTRACT**

**Keywords:** FP-LMTO, Growth axis, Superlattices, BN BSb,Electronic structure,optical properties.

The investigation of the structural, electronic, and optical attributes of BSb, BN, and their corresponding superlattices (SLs) (BSb)n/(BN)n was conducted using the ab initio full potential linear muffin-tin orbital method. The full potential linear muffin-tin orbitals method (FPLMTO) was used, which is incorporated in the new version LMTART computer code within the generalized gradient approximation (GGA96) and using the parameterization of Perdew et al. The calculated structural properties of BSb and BN compounds were compared to available experimental and theoretical data, showing good agreement. An indirect fundamental band gap was found in BSb, BN, and their alloys, with the fundamental band gap decreasing as the number of monolayers n increased. The optical properties analysis showed that the static dielectric constant significantly decreased in superlattices when compared to their binary compounds.

**FIGURE**

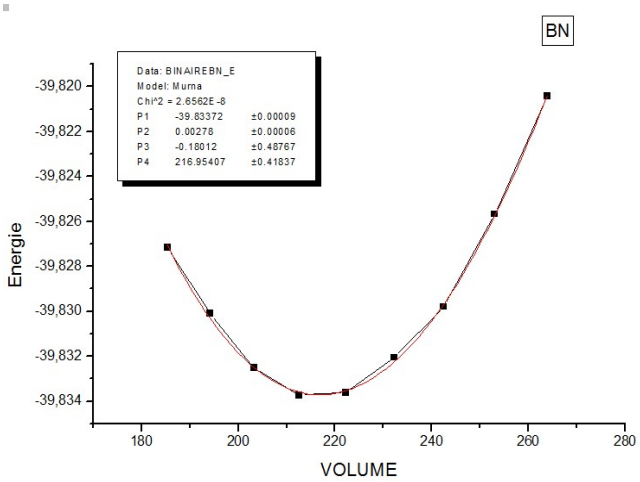


Fig. 1. Variation of the total energy versus volume atomic of BN for zinc blende.

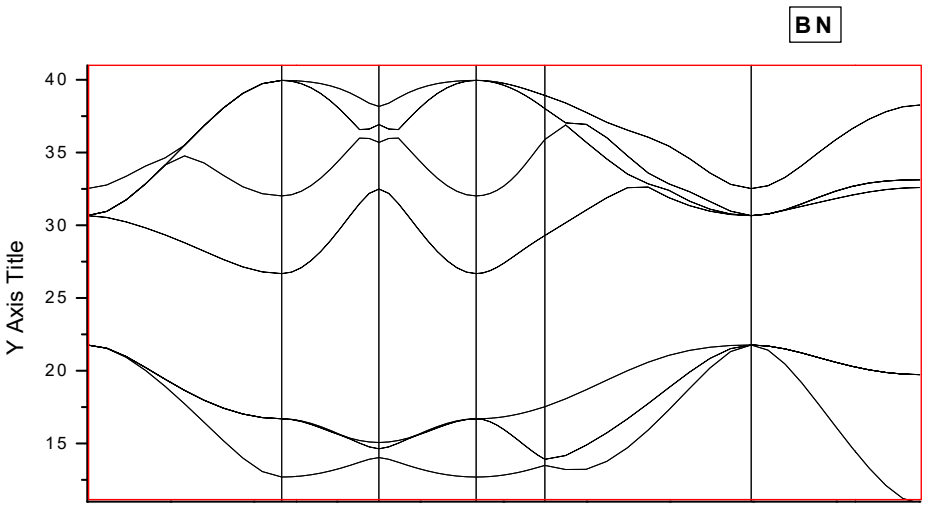


Fig. 4. Band-structures of zinc blende for the BN.

**References**

[1] T.O. Seeyou, N.X. May, I.N. Kyoto, Hope. For. Success, 5 (2016) 22.
[2]L. Djoudi, A. Lachebi, B. Merabet and H. AbidACTA PHYSICA POLONICA AVol. 122 (2012)

[3]:M. Ustundag, M. Aslan, Battal G. Yalcin Computational Materials Science 81 (2014) 471–477

[4] K. Bencherif, A. Yakoubi and H. Mebtouche Vol. 131 (2017) ACTA PHYSICA POLONICA A

[5] M. Guemoua,n, A.Abdiche b, R.Riane b, R.Khenata c PhysicaB436(2014)33–40
[6]E. Knittle, R.M. Wenzcovitch, R. Jeansloz, M.L. Cohen, Nature 337 (1989) 349–352
[7]:SalahDaoud&NoudjoudLebga International Journal of Physical Research, 4 (1) (2016) 1-5

[8]:M. Guemou, A. Abdiche, R. Riane, R. KhenataPhysica B 436 (2014) 33–40

[9] Mimouna Oukli, NoureddineMehnane, Nabila Oukli, BachirBachirBouiadjra,HafidaBelghoulPhysica E: Low-dimensional Systems and Nanostructures 114 (2019) 113653

[10] N. Mehnane, N. Oukli, M. Ouki, Chin. J. Phys. 55 (2017) 1275–1283.

[11] M. Xie, S. Zhang,B. Cai, Z. Zhu, Y. Zou and H. Zeng, *Nanoscale*, 2016, DOI: 10.1039/C6NR02923J.

# Etude, Simulation et Realisation d'un Suiveur de Soleil avec Convertisseur Integré Optimisé

HOUHOU Aimad Abdel Illah[(1)] , ABID Hamza[(2)] , BENABADJI Noureddine[(3)]

(2) Laboratoire des Matériaux Appliqués (AML)
(3) Laboratoire d'Analyse et des Applications du Rayonnement (LAAR)
[1]h_imad2002@yahoo.fr, [2]abid_hamza@yahoo.fr, [3]benanour2000@yahoo.com
Département électronique Université Djillali Liabes de Sidi Bel Abbes

**Résumé :**

L'optimisation du rendement des générateurs photovoltaïques (GPV) reste encore un sujet d'étude. Fabrication d'un matériau avec un rendement élevé et dépourvu de défauts, L'adaptation d'impédance entre un générateur PV et une charge, l'augmentation la quantité des rayons incidents sur les panneaux tous sont question à résolus.

En ce travail, nous évoluons une stratégie pour l'optimisation dynamique des systèmes de suiveur photovoltaïques. La tâche principale dans l'optimisation est de maximiser le gain énergique en augmentant le rayonnement solaire incident et en réduisant au minimum la consommation d'énergie pour le cheminement. Cette stratégie est possible en développant un prototype du système de suiveur, qui est une boucle de control composé par le modèle mécanique lié au modèle dynamique des relais et au modèle de contrôleur.

De cette façon, nous pouvons optimiser le mécanisme de poursuite, choisir les relais appropriés, et concevoir le contrôleur optimal.

Nous rappelons les généralités sur l'énergie solaire photovoltaïque ainsi que les principales caractéristiques de fonctionnement d'un générateur PV à sa puissance maximale, ensuite on présente les cordonnés astronomiques et les angles correspondantes la trajectoire du soleil dans la sphère céleste pour repérer sa position dans le ciel, nous présentons aussi une méthode algorithmique pour calculer cette position, ainsi on parle sur les différentes conceptions du suiveur solaire et le principe de fonctionnement de chacun, une simulation a été menée pour mettre en évidence la comparaison entre eux du coté énergétique, après une simulation d'un suiveur en boucle fermée basé sur la détection des photocellules a été étudiée avec des contrôleurs P, PI, PID et un contrôleur FLOU sous MATLAB ;Enfin on va entamer la conception d'un système de suiveur solaire a un mode basé sur la détection des photocellules, et le deuxième mode basé sur les calcules des positions du soleil, ainsi une optimisation possible du système en incluant une commande de MPPT.

**Mots-clés :** Energie solaire, générateur photovoltaïque, suiveur solaire, MPPT, Cellules solaires, optimisation de l'énergie photovoltaïque.

**Bibliographie:**

[1] M. Hamdaoui, K. Kassmi, F.Olivié, 'Conception et modélisation d'un système photovoltaïque adapté par une commande MPPT analogique', Revue des Energies Renouvelables Vol. 10 N°4, pp. 451 – 462, Décembre 2007.

[2] M. Angel Cid Pastor, 'Conception et réalisation de modules photovoltaïques électroniques' Institut National des Sciences Appliquées de Toulouse, septembre 2007.

[3] Mohanad Alata , M.A. Al-Nimr, Yousef Qaroush 'Developing a multipurpose sun tracking system using fuzzy control',juin 2004.

[4] A. Trombe,B. Lacarrière ,J.C. Fourès, 'Consommations énergétiques de ponts thermiques',Mars 2004.

[5] M.L. Roderick, 'Methods for Calculating Solar Position and Day Length including Computer Programs and Subroutines', Division of Resource Management Technical Report No. 137, Western Australian Department of Agriculture, Perth, pp.22, 2004.

[6] Kevin danel ' Génération du disque solaire des communes de l'Ouest', Août 2008

# Study of the physical and optical properties of the (CsPbBr3) perovskite

**H. B. Kaarour[1], B. Soudini[1], H. Abid[1]**
[1] *Applied Material laboratory (AML), Djillali Liabes University of Sidi Bel Abbes 22000, Algeria .*
*Email: hadjbarkatkaarour@gmail.com*

**ABSTRACT**

In 2014, a groundbreaking achievement was made when researchers demonstrated the first high-brightness infrared and visible electroluminescence (EL) using solution-processed perovskite materials at room temperature **[1].** These exceptional characteristics, in addition to other distinctive electrical and optical properties, position perovskite materials as ideal candidates for the development of high-performance, cost-effective, and large-scale LEDs **[1, 2]**. Notably, the remarkable color purity of perovskite materials, with a full width at half maximum (FWHM) of less than 20 nm, sets PeLEDs apart from traditional LEDs and makes them promising contenders for the future of LED technology **[2].** This study delves into the examination and optimization of perovskite light emitting diodes PeLEDs (CsPbBr3) through a two-dimensional simulation SILVACO TCAD (figure 2). We explore how the device's performance varies with the thickness of the perovskite layer serving as the active component. Our findings suggest that the most pronounced luminescent output can be attained when the perovskite layer's thickness falls within the 2 nm range (figure 3) , We also discover the effect of the intensity of the electrical voltage on the luminous power, as we find that the luminous power increases with the increase in the intensity of the electrical voltage from 2 to 10 volts (figure 4). Additionally, we highlight the significance of the density of trap states as a pivotal parameter for enhancing the efficiency of PeLEDs, as it reflects the quality of the active layer. Moreover, we undertook a comparative examination, contrasting these simulations with the findings from recent hands-on experiments (figure 1). These experiments were conducted during our recent scientific discourse, focusing on the study of perovskite (CsPbBr3). During this discourse, we performed experiments involving the exposure of perovskite to ultraviolet lasers, from which we derived a wavelength curve.

**Keywords:** Semiconductors; Perovskite ; PeLED.

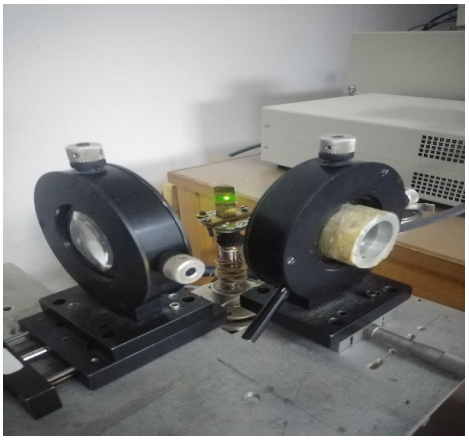

*figure.1: The experimental study that has been conducted*

*figure.2 : The device architecture of PeLED used in simulation with CsPbBr3 as an active layer.*

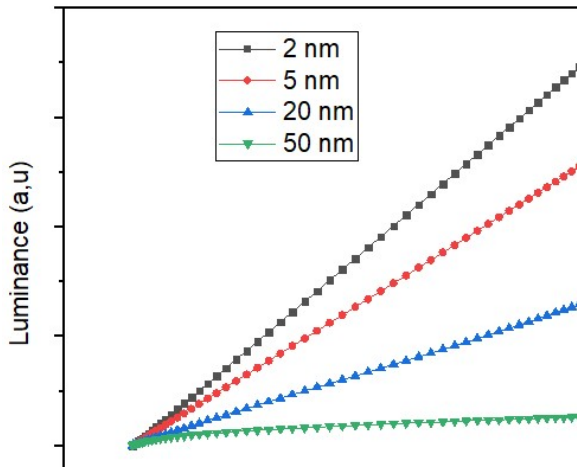


*figure.3: The luminous-current curves for different perovskite thicknesses.*

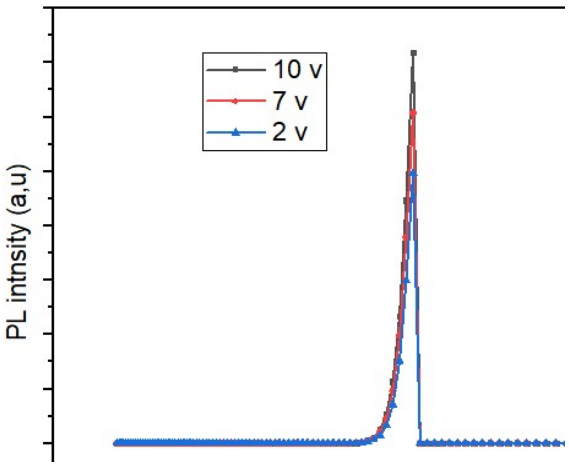


*figure 4: The effect of electrical voltage on luminicense power*

**References**

[1] Z.-K. Tan, R. S. Moghaddam, M. L. Lai, P. Docampo, R. Higler, F. Deschler, et al., "Bright light-emitting diodes based on organometal halide perovskite," Nat Nano, vol. 9, pp. 687-692, 09//print 2014.
[2] Y.-H. Kim, H. Cho, and T.-W. Lee, "Metal halide perovskite light emitters," Proceedings of the National Academy of Sciences, vol. 113, pp. 11694-11702, October 18, 2016 2016.

# Structural ,electronic and optical properties of $Al_xGa_y In_{1-x-y}As_zSb_{1-z}$ quinary alloys

**Mohammed Amine BOULEKBACHE[1], Miloud BENCHEHIMA [*,1,2], Abdelhadi LACHABI[1] , Hamza ABID[1]**

[1]*Applied Materials Laboratory, Research Center (CFTE), Sidi Bel Abbès Djillali Liabes University, 22000, Algeria*
[2]*Electronic Department University of Sciences and Technology of Oran, Mohamed Boudiaf (USTO), El M'nouar BP 1505, Oran, Algeria*
Email : amine-29-med@hotmail.com

**ABSTRACT**

The motivation of our study is to examine the physical properties of $Al_xGa_{1-x} In_{1-x-y}As_zSb_{1-z}$ quinary alloys to explore their usefulness for optoelectronic devices. Structural ,electronic and optical properties of $Al_xGa_{1-x} In_{1-x-y}As_zSb_{1-z}$ quinary alloys are investigated via the (FP-LAPW) method within the density functional theory (DFT) [1, 2]. where different generalized gradient approximations are used for approximating the exchange-correlation effects. For analyzing electronic and optical properties, the exchange–correlation energy was handled using the Wu-Cohen generalized gradient approximation (WC-GGA) [3] approach and (TB-mBJ) [4] was also used.

**Keywords**: Binary compounds; $Al_xGa_{1-x} In_{1-x-y}As_zSb_{1-z}$ quinary alloys; optoelectronic properties; Wien2k program; (TB-mBJ) approach;

## Results and discution

### Structural propertiees

We have analyzed the structural properties of the quinary alloys $Al_xGa_y In_{1-x-y}As_zSb_{1-z}$ in the zinc blende structure. The structural parameters have been optimized using (WC-GGA) approach [3] for the exchange-correlation functional. Murnaghan's equation of state (EOS) [5, 6] has been employed to minimizing the total energy with respect to the unit cell volume. The composition dependence of the calculated lattice constant and bulk modulus of $Al_xGa_y In_{1-x-y}As_zSb_{1-z}$ quinary alloys, using (GGA-WC) approach are schown in Fig.1

### Optoelectronic properties

The electronic properties of the quinaries and their end binaries have been calculated by utilizing our optimized lattice parameters (a $^{(WC\text{-}GGA)}$) within (GGA-WC) and Tran Blaha modified Becke–Johnson (TB-mBJ) [23] schemes. Table 1 summarizes the calculated band gap values of binaries and quinary alloys.

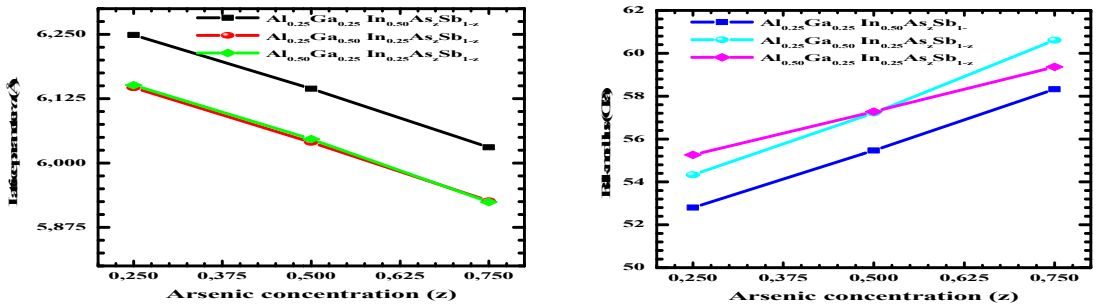


**Fig**.1. Composition dependence of the calculated lattice constant and bulk modulus of $Al_xGa_y In_{1-x-y}As_zSb_{1-z}$

Table 1 .electronic band gap values of binaries quinarys alloys.

| | Energy band gap (Eg) in eV | | | |
|---|---|---|---|---|
| **Material** | **Present work** | **Theo. studies** | | **Exp.** |
| | TB-mBJ | LDA | TB-mBJ | |
| **AlAs** | 2.157 | 1.434 [7] | 2.12 [8] | 2.24 [9] |
| **AlSb** | 1.765 | 1.052 [7] | 1.768 [6] | 1.696 [9] |
| **InAs** | 0.566 | - | 0.587 [10] | 0.417 [9] |
| **InSb** | 0.322 | - | 0.48 [8] | 0.235 [9] |
| **GaAs** | 1.565 | 0.342 [11] | 1.579 [11] | 1.519 [9] |
| **GaSb** | 0.851 | - | - | 0.812 [9] |
| $Al_{0.25}Ga_{0.25}In_{0.50}As_{0.25}Sb_{0.75}$ | 0.763 | - | - | - |
| $Al_{0.25}Ga_{0.25}In_{0.50}As_{0.50}Sb_{0.50}$ | 0.827 | - | - | - |
| $Al_{0.25}Ga_{0.25}In_{0.50}As_{0.75}Sb_{0.25}$ | 0.978 | - | - | - |
| $Al_{0.25}Ga_{0.50}In_{0.25}As_{0.25}Sb_{0.75}$ | 0.880 | - | - | - |
| $Al_{0.25}Ga_{0.50}In_{0.25}As_{0.50}Sb_{0.50}$ | 0.978 | - | - | - |
| $Al_{0.25}Ga_{0.50}In_{0.25}As_{0.75}Sb_{0.25}$ | 1.161 | - | - | - |

**Conclusion**

In this investigation, we have employed the FP-LAPW method to conduct a first-principles examination the optoelectronic properties of $Al_xGa_y\ In_{1-x-y}As_zSb_{1-z}$ quinary alloys.Our obtained results are in excellent agreement with the existing data in literature. The calculation endorses that the $Al_xGa_y\ In_{1-x-y}As_zSb_{1-z}$ is a promising candidate for photovoltaic application

**References**

[1] W. Kohn, L.J. Sham, Physical review, 140 (1965) A1133.
[2] D. Koelling, B. Harmon, Journal of Physics C: Solid State Physics, 10 (1977) 3107.
[3] Z. Wu, R.E. Cohen, Physical Review B, 73 (2006) 235116.
[4] F. Tran, P. Blaha, Physical review letters, 102 (2009) 226401.
[5] F. Murnaghan, Proceedings of the national academy of sciences of the United States of America, 30 (1944) 244.
[6] M. Benchehima, H. Abid, A.C. Chaouche, A. Resfa, The European Physical Journal Applied Physics, 77 (2017) 30101.
[7] A. Gazhulina, M. Marychev, Journal of alloys and compounds, 623 (2015) 413-437.
[8] G. Rehman, M. Shafiq, R. Ahmad, S. Jalali-Asadabadi, M. Maqbool, I. Khan, H. Rahnamaye-Aliabad, I. Ahmad, Journal of Electronic Materials, 45 (2016) 3314-3323.
[9] I. Vurgaftman, J.á. Meyer, L.á. Ram-Mohan, Journal of applied physics, 89 (2001) 5815-5875.
[10] E. Khennous, H. Abid, M. Benchehima, A. Benzina, Optik, 165 (2018) 248-258.
[11] M.H. Hachemi, M. Benchehima, K. Bencherif, H. Abid, Optik, (2022) 169282.

# Optoelectronic properties of $Zn_{0.750}Cd_{0.250}Se$ and $Be_{0.750}Cd_{0.250}Se$ ternaries ZnO binary in zinc blende phase: Photovoltaic Application

**Abdelhafid Said BOUROUMI [1], Miloud BENCHEHIMA [*,1,2], kada BENCHIKH, Hamza ABID[1]**
[1]*Applied Materials Laboratory, Research Center (CFTE), Sidi Bel Abbès Djillali Liabes University, 22000, Algeria*
[2]*Electronic Department University of Sciences and Technology of Oran, Mohamed Boudiaf (USTO), El M'nouar BP 1505, Oran, Algeria*
*Contact: samir40575@gmail.com*

**ABSTRACT**

We present an Ab-initio investigation of optoelectronic properties of $Be_{0.750}Cd_{0.250}Se$ and $Zn_{0.750}Cd_{0.250}Se$ ternaries and their end binary comound (BeSe, ZnSe and CdSe ). These properties have been calculated using the first-principles calculations based on the density functional theory. Generalized gradient approximation of Wu and Cohen (GGA-WC) has been used to compute their structural properties. However, in order to calculate the electronic and properties we employed the (LDA) and the recently (TB-m BJ) approaches. The obtained results of structural parameters and electronic band gap for for binaries and both ternaries agree with experimental values and theoretical data available in the literature. Finally, we calculated and analyzed in detail the optical properties of $MgS_xO_{1-x}$ ternary alloys. Our obtained results are in excellent agreement with the existing data in literature. Based on our obtained results, direct band gaps and optical parameters, both ternaries are very for manufacturing different microelectronic and, optoelectronic devices.

**Keywords: II-VI** semiconductor compounds; Density Functional Theory; Ternary Alloys; optoelectronic properties**;** (TB-m BJ) approache;

**Results and discution**

**Structeral and optoelectronic propertes**

The obtained results of the lattice parameter ( a) and the bulk modulus of $Be_{0.750}Cd_{0.250}Se$ and $Zn_{0.750}Cd_{0.250}Se$ ternaries and (BeSe, ZnSe and CdSe ) binaries in zinc blende structure are summarized in Table 1.

**Table 1**.Calculated structural parameters of ternary alloys.

| Compound | This work | | | Other calculations | | | Experiment | | |
|---|---|---|---|---|---|---|---|---|---|
| | a(Å) | B (GPa) | B' | a(Å) | B(GPa) | B' | a(Å) | B (GPa) | B' |
| **BeSe** | 5.1384 | 79.5366 | 4.0916 | 5.13 [1] | 75.86 [1] | | 5.137 [2] | 92.2 [2] | |
| **ZnSe** | 5.6505 | 66.1177 | 4.7570 | 5.69[3], 5.642 [4] | 67.05[3] 64.21[4] | 4.938[4] | 5.668 [5, 6] | 64.7[7] | 4.77[7] |
| **CdSe** | 6.0925 | 52.7657 | 4.6181 | 6.09 [3] | 55.91[3], 55.59 [8] | 4.492 [8] | 6.05 [9] | 53.0[10] | |
| **$Zn_{0.750}Cd_{0.250}Se$** | 5.7822 | 61.4977 | 4.9797 | 5.70 [3] | - | - | - | - | - |
| **$Be_{0.750}Cd_{0.250}Se$** | 5.5057 | 71.6365 | 4.8575 | 5.49[1], | 68.93[1], | 4.888 [8] | - | - | - |

5.472 [8] 72.94[8]

**Table 2**. Calculated band gap ( $E_g$ ) of $Be_{0.750}Cd_{0.250}Se$ and $Zn_{0.750}Cd_{0.250}Se$ ternaries and their binaries with (LDA) and (TB- mBJ) compared to experimental and other theoretical studies.

| | This work | | Other calculations. | | Experiment |
|---|---|---|---|---|---|
| | LDA | TB-mBJ | LDA | TB-mBJ | |
| **BeSe** | 2.467 | 3.484 | | 3.714[11] | 4-4.5[12] |
| **ZnSe** | 1.060 | 2.761 | 1.24 [3], 1.19 [13] | 2.67 [14], 2.74 [13], 2.829 [4] | 2.69 [5], 2.721[15], 2.82 [16] |
| **CdSe** | 0.316 | 1.935 | 0.38 [13] | 1.89[14], 1.87[17], 1.89[18] | 1.70 [6], 1.90 [19] |
| **$Zn_{0.750}Cd_{0.250}Se$** | 0.755 | 2.441 | | | 2,515[a] |
| **$Be_{0.750}Cd_{0.250}Se$** | 2.260 | 3.649 | | 3.321[8] | 3,475[a] |

**Conclusion**

We have employed the (FP-LAPW) method to calculate the optoelectronic properties of of $Be_{0.750}Cd_{0.250}Se$ and $Zn_{0.750}Cd_{0.250}Se$ ternaries their binaries alloys.Our obtained results are in excellent agreement with the existing data in literature. The calculation endorses that the both ternaries are a promising candidate for photovoltaic application

**References**

[1] N. Noor, W. Tahir, F. Aslam, A. Shaukat, Physica B: Condensed Matter, 407 (2012) 943-952.
[2] H. Luo, K. Ghandehari, R. Greene, A. Ruoff, S. Trail, F. DiSalvo, Physical Review B, 52 (1995) 7058.
[3] N. Korozlu, K. Colakoglu, E. Deligoz, Y. Ciftci, Optics Communications, 284 (2011) 1863-1867.
[4] U. Sarkar, B. Debnath, M. Debbarma, D. Ghosh, S. Chanda, R. Bhattacharjee, S. Chattopadhyaya, Materials Chemistry and Physics, (2019).
[5] N. Troullier, J.L. Martins, Physical review B, 43 (1991) 1993.
[6] H. Okuyama, Y. Kishita, A. Ishibashi, Physical Review B, 57 (1998) 2257.
[7] R. Casali, N. Christensen, Solid State Communications, 108 (1998) 793-798.
[8] S. Chattopadhyaya, U. Sarkar, B. Debnath, M. Debbarma, D. Ghosh, S. Chanda, R. Bhattacharjee, Physica B: Condensed Matter, (2019).
[9] I. Broser, R. Broser, H. Finkenrath, R. Galazka, H. Gumlich, A. Hoffmann, J. Kossut, E. Mollwo, H. Nelkowski, G. Nimtz, Physics of II-VI and I-VII Compounds, Semimagnetic Semiconductors/Physik Der II-VI und I-VII-Verbindungen, Semimagnetische Halbleiter Elemente, Springer Science & Business Media, 1982.
[10] H. Weiss, M. Schulz, O. Madelung, in, Springer-Verlag, Berlin, 1982.
[11] S. Chattopadhyaya, U. Sarkar, B. Debnath, M. Debbarma, D. Ghosh, S. Chanda, R. Bhattacharjee, Computational Condensed Matter, (2019) e00384.
[12] W. Yim, J. Dismukes, E. Stofko, R. Paff, Journal of Physics and Chemistry of Solids, 33 (1972) 501-505.

# Enhancing Conversion Efficiency in InGaP/Si Double-Junction Solar Cells through the Integration of a Double Back Surface Field (BSF) Layer

**I. Zidani[1], Z. Bensaad[1], H. Abid[1]**
[1] *Applied Materials Laboratory, sidi bel abbes, 22000, Algeria*
*Email: zidaikram@gmail.com*

## ABSTRACT

The efficiency of solar energy capture has significantly increased with dual-junction solar cells. This is attributed to the use of III-V semiconductor materials with different band gaps, resulting in higher absorption of the solar spectrum and, consequently, higher efficiency. In recent years, extensive research has been conducted to develop reliable techniques for thestructural optimization of these devices. In this study, we present a simulation and optimization of an $In_{0.5}Ga_{0.5}P$/Si dual-junction solar cell [1]. The studied structure includes a double back surface field (BSF) layer in the upper cell. Simulation results show an increase in efficiency compared to cells that do not use this double BSF layer. Indeed, the BSF layer helps block the diffusion of minority carrier holes, thereby reducing surface recombination and increasing the short-circuit current [2]. The AlInP material was used for the BSF layer with varying thicknesses (20-220)nm for the upper dual BSF cells. The study presents simulation results of current-voltage (J-V) density, external quantum efficiency (EQE), conversion-voltage efficiency, and characteristics obtained using the Silvaco ATLAS TCAD simulation tool, based on the ASTM-certified global AM1.5G spectrum [3]. Result show that optimal thickness of the upper dual BSF layer is determined at 160nm provide an improvement of a short-circuit current 18.371 to 23.853 mA/cm², a conversion efficiency 32.163 to 40.122% illustrated in fig2 and fig3. This structure are obtained **Jsc=23.853 mA/cm², Voc=2.017 V, FF=83.387%, η=40.122%.** These results could open new opportunities for improving the production of high-efficiency, low-cost III-V solar cells on lower silicon cells. Finally, the performance of InGaP/Si tandem solar cells is compared to previously published results [4].

**Keywords:** Tandem solar cell; Back surface field (BSF); Silvaco Atlas; Optimization

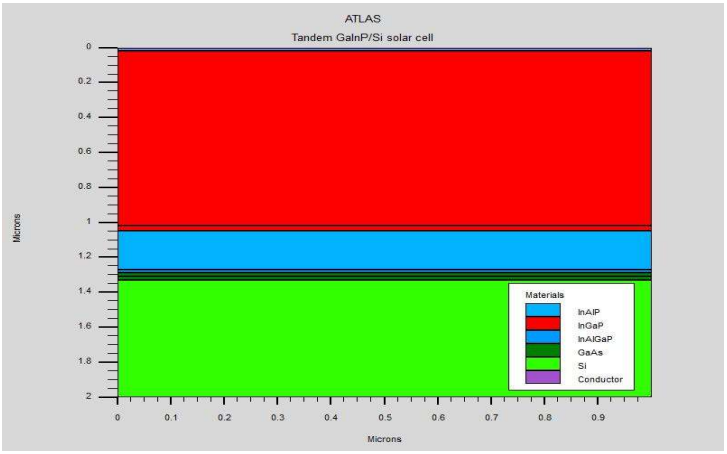


**Figure1:** Structure of InGaP/Si tandem SC with double BSF layer

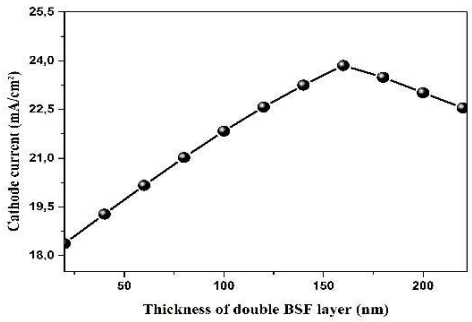


**Figure2:** Effect of DBSF layer on the Jsc

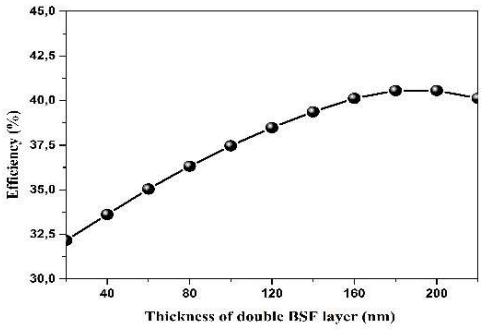


**Figure3:** Effect of DBSF layer on the efficiency

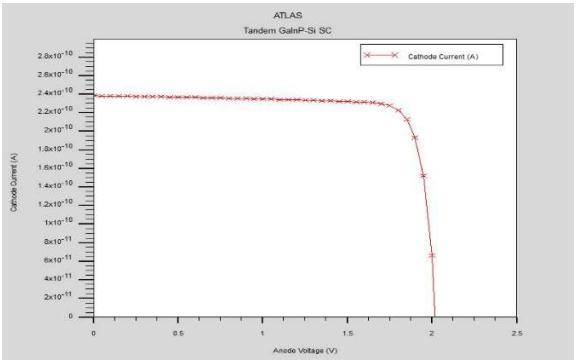


**Figure4:** I-V Charactristic of tandem solar cell

## References

[1] S.Essig, S.Ward, A. Myles.Steiner. Progress towards a 30% efficient GaInP/Si tandem solar cell.Energy Procedia, 77 (2015) 464-469.
[2] Singh, k.Jolson,Sarkar, ,S.K. Sarkar.Highly efficient ARC less InGaP/GaAs DJ solar cell numerical modeling using optimized InAlGaP BSF layers. Optical and Quantum Electronics, 43 (2012) 1-21.
[3] Silvaco Data Systems Inc: Silvaco ATLAS User's Manual (2018).
[4] Verma, Manish, G.P. Mishra. An integrated GaInP/Si dual-junctionsolar cell with enhanced efficiency using TOPCon technology. Applied Physics A 126 (2020) 1-13.

# Effects of sulfur incorporation on the optoelectronic properties of ZnO binary compound in rock salt phase : Photovoltaic Application

**Nadir HASSANI[1], Miloud BENCHEHIMA [*,1,2], Kada BENCHIKH, Hamza ABID[1], Amer DJILI[1]**

[1]*Applied Materials Laboratory, Research Center (CFTE), Sidi Bel Abbès Djillali Liabes University, 22000, Algeria*
[2]*Electronic Department University of Sciences and Technology of Oran, Mohamed Boudiaf (USTO), El M'nouar BP 1505, Oran, Algeria*
*Email : nadir902017@gmail.com*

**ABSTRACT**

We present a theoretical study on the structural and optoelectronic properties of $MgS_xO_{1-x}$ ternary alloys in rock salt phase. These properties have been described using the full-potential linearized augmented plane wave (FP-LAPW) formalism [1] within the framework of density functional theory (DFT) [2]. Structural properties and total energies of $MgS_xO_{1-x}$ ternaries have been calculated using generalized gradient approximation of Wu and Cohen (WC-GGA) approach [3] for different concentrations (x). Based on the regular solution model [4-7], we have determined the thermodynamic stability of $MgS_xO_{1-x}$. In addition to (WC-GGA) approach, we have employed the modified Becke-Johnson scheme proposed by Tran and Blaha (TB-mBJ) approach [8] to calculated the electronic and optical properties for the ternaries. Finally, we calculated and analyzed in detail the optical properties of $MgS_xO_{1-x}$ ternary alloys. Our obtained results are in excellent agreement with the existing data in literature. The calculation endorses that the $MgS_xO_{1-x}$ ternary alloys is a promising candidate for photovoltaic application

**Keywords:** $MgS_xO_{1-x}$ ternary alloys**;** Density functional theory (DFT); Rock salt phase; Lattice constant; optical properties;

**Results and discution**

**Structeral and optoelectronic propertes**

At room temperature, MgO and SO binaries are most stable in rocksalt phase with space group (F- 34m) [9] Therefore, in this work, the rock salt phase is adopted for $MgS_xO_{1-x}$ for different compositions x ($0 \leq x \leq 1$ ). The equilibrium structural parameters (lattice parameter (a) and bulk modulus (B)) are calculated by employing the (WC-GGA) approach. The obtained results of the lattice parameter ( a) and the bulk modulus of for $MgS_xO_{1-x}$ ternaries and their end binaries in rock salt structure are summarized in Table 1. In Figs. 1, we illustrate the dependence of the lattice parameters and bulk modulus as function of (x) compositions of $MgS_xO_{1-x}$ ternaries. Based on our predicted lattice parameter, the electronic properties of $MgS_xO_{1-x}$ in rock salt structure are computed within (WC-GGA) and (TB-mBJ) approaches. The results for the band gap energy ($Eg$) inferred by using both approaches are summarized in Table 2. Fig. 2 shows plots of the dependence of band gaps as a function of S content calculated with (WC-GGA) and (TB- mBJ) approaches.

| $MgS_xO_{1-x}$ | Present work (GGA-WC) | | Other calculations (GGA-WC) | | Experiment | |
|---|---|---|---|---|---|---|
| | *a*(Å) | B(GPa) | *a*(Å) | B(GPa) | *a*(Å) | B(GPa) |
| MgO | 4.2206 | 154.8660 | 4.257 [3] | | 4.203 [2] | |
| $MgS0_{0.125}O_{0.875}$ | 4,39375 | 133.8321 | | | | |
| $MgS_{0.250}O_{0.850}$ | 4,54635 | 118.7816 | | | | |
| $MgS_{0.375}O_{0.750}$ | 4,6821 | 103.625 | | | | |
| $MgS0_{0.500}O_{0.500}$ | 4,8042 | 97.6942 | | | | |
| $MgS0_{0.625}O_{0.375}$ | 4,9133 | 91.7239 | | | | |
| $MgS0_{0.750}O_{0.250}$ | 5,01295 | 85.2068 | | | | |
| $MgS0_{0.875}O_{0.125}$ | 5,10435 | 78.6503 | | | | |
| SO | 5.1889 | 77.5503 | | | 5.203 [2] | |

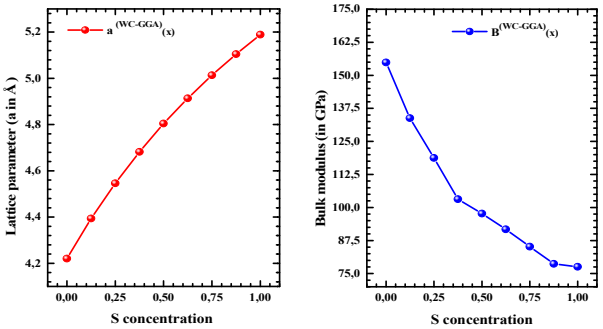


**Fig.1**. calculated lattice parameter (a) and bulk modulus (B) for $MgS_xO_{1-x}$ in rock Salt structure

**Table2**. Band gap values (Eg) of $MgS_xO_{1-x}$ in rock Salt structure , according to GGA-WC approach

| $MgS_xO_{1-x}$ | Present work | | Other calculations | | Exp. |
|---|---|---|---|---|---|
| | (WC-GGA) | (TB-mBJ) | (WC-GGA) | (TB-mBJ) | (WC-GGA) |
| MgO | 4.612 | 7.153 | - | - | 7.8 [2] |
| $MgS_{0.125}O_{0.875}$ | 3.875 | 6.285 | - | - | - |
| $MgS_{0.250}O_{0.850}$ | 3.282 | 5.480 | - | - | - |
| $MgS_{0.375}O_{0.750}$ | 2.989 | 4.838 | - | - | - |
| $MgS_{0.500}O_{0.500}$ | 2.620 | 4.262 | - | - | - |
| $MgS_{0.625}O_{0.375}$ | 2.685 | 4.299 | - | - | - |
| $MgS_{0.750}O_{0.250}$ | 2.642 | 4.180 | - | - | - |
| $MgS_{0.875}O_{0.125}$ | 2.417 | 3.679 | - | - | - |
| MgS | 2.757 | 4.013 | - | - | - |

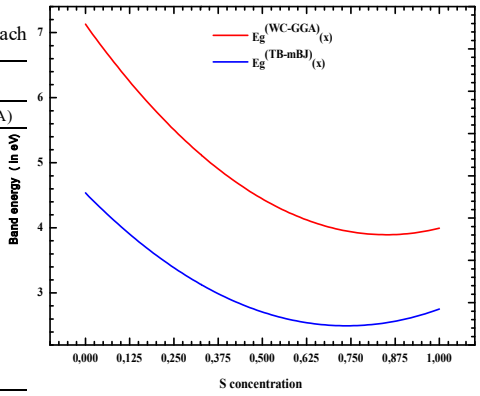


**Fig.2**. band gap as function of S concentration

## Conclusion

we calculated and analyzed in detail the opticelectronic properties of $MgS_xO_{1-x}$ ternary alloys. Our obtained results are in excellent agreement with the existing data in literature. The calculation endorses that the $MgS_xO_{1-x}$ ternary alloys is a promising candidate for photovoltaic application

## References

[1] D. Koelling, B. Harmon, Journal of Physics C: Solid State Physics, 10 (1977) 3107.
[2] W. Kohn, L.J. Sham, Physical review, 140 (1965) A1133.
[3] Z. Wu, R.E. Cohen, Physical Review B, 73 (2006) 235116.
[4] M.H. Hachemi, M. Benchehima, K. Bencherif, H. Abid, Optik, (2022) 169282
[5] R. Swalin, Wiley-Interscience, New York. 1972, 387, (1972).
[7] D. Bouragba, M. Benchehima, H. Abid, A. Djili, Optik, 222 (2020) 165472.
[8] F. Tran, P. Blaha, Physical review letters, 102 (2009) 226401.

# Ab-initio investigation of optoelectronic properties of AlGaInAs quaternary alloys

**Hakim SLIMANI[1], Miloud BENCHEHIMA [*,1,2] , Hamza ABID[1]Abdelhadi LACHABI[1]**

[1]*Applied Materials Laboratory, Research Center (CFTE), Sidi Bel Abbès Djillali Liabes University, 22000, Algeria*
[2]*Electronic Department University of Sciences and Technology of Oran, Mohamed Boudiaf (USTO), El M'nouar BP 1505, Oran, Algeria*

Email: slimanihakim32@yahoo.fr

**ABSTRACT**

Optoelectronic properties of AlGa InAs quaternary alloys have been calculated using the first-principles calculations based on the density functional theory. Both (LDA) and (GGA-WC) approximations have been used to calculate the structural properties of $Al_xGa_yIn_{1-x-y}As$ for ($x$, $y$) = (0.375, 1.25), (0.250, 0.250) and (0.375, 0.125) and their binaries. In adding to the (WC-GGA) approach, the PBEsol-GGA), the (EV-GGA) and the recently (TB-m BJ) approaches have been used to calculate the electronic properties. It has been found that the lattice constant of the $Al_xGa_yIn_{1-x-y}As$ can be controlled by indium concentration while the band gap can be adjusted by aluminum concentration. We have calculated the optical parameters (dielectric functions, loss function, reflectivity, absorption, refractive index and extinction coefficient). The composition dependence of the refractive index was studied by Ravindra et al. and Moss model. The obtained results have been compared with other theoretical results and experimental data.

**Keywords**: Binary compounds; $Al_xGa_{1-x}$ $In_{1-x-y}As_zSb_{1-z}$ quinary alloys; optoelectronic properties; Wien2k program; (TB-mBJ) approach;

## Results and discution

### Structural propertiees

Firstly, we study the structural properties of the binary compounds AlAs, GaAs and InAs and the quaternary $Al_xGa_yIn_{1-x-y}As$ in the zinc blende structure. Then the quaternary alloy was modeled at selected compositions ($x$=0.125, $y$=0.375), ($x$=0.250, $y$=0.250) and ($x$=0.375, $y$=0.125) by applying special quasi-random scheme proposed by Zunger et al. [1]. The lattice constant and bulk modulus for $Al_xGa_yIn_{1-x-y}As$ for different values of x and y were calculated and are listed in Table 2. To our knowledge, there are no experimental and no theoretical data for the structural properties of $Al_xGa_yIn_{1-x-y}As$ alloys for these concentrations ($x$=0.125, $y$=0.375), ($x$=0.250, $y$=0.250) and ($x$=0.375, $y$=0.125).

### Optoelectronic properties

The electronic properties of the quinaries and their end binaries have been calculated by utilizing our optimized lattice parameters (a $^{(WC\text{-}GGA)}$) within (GGA-WC) and Tran Blaha modified Becke–Johnson (TB-mBJ) [23] schemes. Table 1 summarizes the calculated band gap values of binaries and quinary alloys.
Table 1 presents the calculated lattice constants and bulk modulus of AlAs, GaAs, InAs and $Al_xGa_yIn_{1-x-y}As$ with LDA and WC-GGA compared with experimental and other theoretical calculation. Table 2 shows our results for the band gap energy deduced using different approximations compared to other theoretical studies and experimental values.

**Table 1.** Calculated lattice constants and bulk modulus $Al_xGa_yIn_{1-x-y}As$ with LDA and WC-GGA compared with experimental and other theoretical calculation.

| Compound | Lattice constants (a (Å)) | | | | Bulk modulus (B (GPa)) | | | |
|---|---|---|---|---|---|---|---|---|
| | LDA | WC-GGA | Other studies | Exp. | LDA | WC-GGA | Other studies | Exp. |
| **AlAs** | 5.633 | 5.677 | 5.734 [2]<br>5.644 [3] | 5.661 [4] | 75.15 | 72.18 | 66.50 [2]<br>75.40 [3] | 77.30 [5] |
| **GaAs** | 5.610 | 5.668 | 5.666 [6]<br>5.750 [7] | 5.653[8],<br>5.654 [9] | 74.02 | 68.50 | 69.60 [6]<br>61.32 [7] | 75.50 [8] |
| **InAs** | 6.036 | 6.099 | 6.030 [2]<br>5.921 [10] | 6.036 [9]<br>6.058 [11] | 60.85 | 56.33 | 60.90 [2]<br>61.70 [10] | 58.00 [12] |
| $Al_{0.125}Ga_{0.375}In_{0.500}As$ | 5.852 | 5.909 | 5.856[a] | _ | 65.73 | 60.51 | 66.97[b] | _ |
| $Al_{0.250}Ga_{0.250}In_{0.500}As$ | 5.852 | 5.910 | 5.857[a] | _ | 66.26 | 61.28 | 67.20[b] | _ |
| $Al_{0.375}Ga_{0.125}In_{0.500}As$ | 5.853 | 5.911 | 5.858[a] | _ | 66.83 | 62.20 | 67.42[b] | _ |

**Table 2.** Calculated band gap $E_g$ of $Al_xGa_yIn_{1-x-y}As$ with (PBEsol-GGA), (EV-GGA) and (TB- mBJ) compared to experimental and other theoretical studies.

| Compounds | This work | | | | Other work | |
|---|---|---|---|---|---|---|
| | WC-GGA | PBEsol-GGA | EV-GGA | TB- mBJ | Theoretical studies | Exp. |
| **AlAs** | 1.341 | 1.347 | 2.315 | 2.162 | 1.310[2],1.40[2],2.250[2] | 2.24 [13] |
| **GaAs** | 0.328 | 0.380 | 0.957 | 1.560 | 0.336[6]],0.966[6],1.03[2] | 1.52 [14] |
| **InAs** | 0.000 | 0.00013 | 0.209 | 0.586 | 0.00[2], 0.400[2] | 0.42[13] |
| $Al_{0.125}Ga_{0.375}In_{0.500}As$ | 0.000 | 0.00002 | 0.548 | 1.003 | 0.99125[b] | _ |
| $Al_{0.250}Ga_{0.250}In_{0.500}As$ | 0.090 | 0.131 | 0.741 | 1.165 | 1.1725[b] | _ |
| $Al_{0.375}Ga_{0.125}In_{0.500}As$ | 0.298 | 0.336 | 0.984 | 1.381 | 1.3537[b] | _ |

**References**

[1] A. Zunger, S.-H. Wei, L. Ferreira, J.E. Bernard, Physical review letters, 65 (1990) 353.
[2] R. Ahmed, S.J. Hashemifar, H. Akbarzadeh, M. Ahmed, Computational materials science, 39 (2007)
[3] S.-H. Wei, A. Zunger, Physical Review B, 60 (1999) 5404
[5] I. Vurgaftman, J. Meyer, L. Ram-Mohan, Journal of applied physics, 89 (2001) 5815-5875.
[6] F.E.H. Hassan, A. Postnikov, O. Pagès, Journal of Alloys and Compounds, 504 (2010) 559-565.
[7] B.H. Reshak, Y. Al-Douri, Appl. Phys. A, 106 (2012) 687-696.
[8] S. Adachi, Journal of applied physics, 61 (1987) 4869-4876.

# Implementation of the new algorithm Rao1 as an MPPT controller in photovoltaic systems

**Berrabah Zouaoui , Khadraoui Mohamed, Nekrela Abdelkader, Sahraoui Kamel, Medles Mourad**

*Laboratory for the Elaboration and Characterization of Materials(L.E.C.M), Faculty of Electrical Engineering, DjillaliLiabès University, BP89, Sidi Bel-Abbès, 22000, Algeria*
*Contact: berrabahzo70@gmail.com*

## ABSTRACT

The ability of the Maximum Power Point Tracking (MPPT) technology to prevent losses by stabilizing power fluctuations during severe weather conditions is critical in improving photovoltaic power generation systems. Overall system stability is improved by carefully tracing the maximum power point (MPP). This research focuses on improving MPPT performance in solar systems by employing the "Rao1" control method. The simulation, which is run in MATLAB/Simulink, includes a detailed model of the entire system. The primary circuit is designed with a DC-DC Boost architecture and a single MOSFET transistor [1] [2].

Rao1 is a metaphor-less optimization algorithm developed by Ravipudi Venkata Rao in 2019 [3] [4] . It is an effective metaheuristic algorithm, one of three sub-algorithms called Rao-1, Rao-2, and Rao-3, designed to solve both unconstrained and constrained optimization problems. The structure of Rao-1 is simple and has fast convergence, so the Rao-1 algorithm has attracted much attention. This algorithm utilizes the best and worst solutions found during optimization and involves random interactions among candidate solutions. In this work research, Rao1's algorithm was implemented via Matlab Simulink to control the Boost converter by adjusting the duty cycle. This new algorithm was compared to two others, namely P&O [5] and PSO [6]. The results were analyzed, and differences were identified through the results and graphs generated by the simulation, given in figure 1.

**Keywords**: DC converter, MPPT, Méta-heuristique; RaoA algorithm

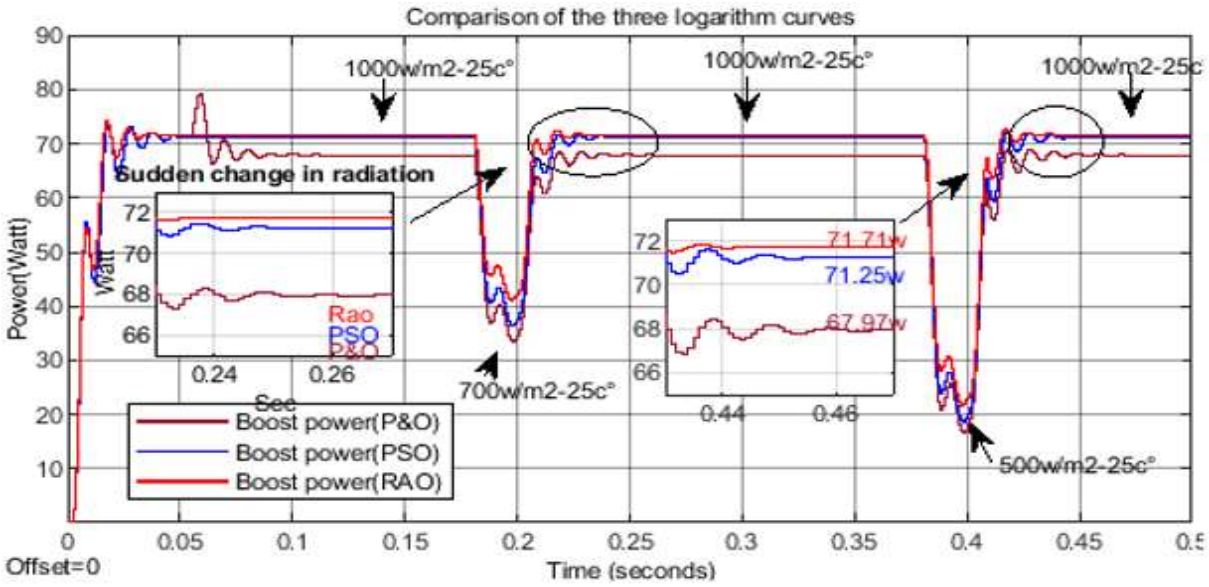


Fig. 1: Comparative Results of the Three Methods

## References

[1] P.Thakor, A.Chavada,B.Patel,Comparative analysis of different MPPT techniques for solar pv system , 3 (2016)

[2] M. Elshaer, A. Mohamed,O. Mohammed, Smart optimal control of DC-DC boost converter in PV systems,10(2010)

[3] R. V. Rao, Rao algorithms: Three metaphor-less simple algorithms for solving optimization problem,2(2009)

[4] X. Jian and Y. Zhu, 'Parameters identification of photovoltaic models using modified Rao-1 optimization algorithm,231(2021).

[3] M. A. G. De Brito, L. Galotto, L. P. Sampaio, G. D. A. E Melo, and C. A. Canesin, Evaluation of the Main MPPT Techniques for Photovoltaic Applications,60(2013).

[6] J. Shi, W. Zhang, Y. Zhang, F. Xue, and T. Yang, 'MPPT for PV systems based on a dormant PSO algorithm,123(2015)

[5] R. V. Rao, Rao algorithms: Three metaphor-less simple algorithms for solving optimization problem,2(2009)

[6] X. Jian and Y. Zhu, 'Parameters identification of photovoltaic models using modified Rao-1 optimization algorithm,231(2021).

# Mixed phase formation of ZnS-ZnO on air-annealed thermally ZnS thin films

**M. Hambi, M. Khadraoui, R. Miloua, A. Bouzidi, A. Nakrela**

[1]*Laboratory 1Materials Development and Characterization Laboratory, Department of Electronics, Djillali Liabes University, BP89, Sidi Bel Abbes 22000, Algeria*
meriemhambi@gmail.com

## ABSTRACT

ZnS thin films have been effectively prepared with varying thicknesses using the spray pyrolysis method at 350°C on glass substrates**[1, 2, 3]**. The impact of the annealing process on the physical properties of our thin films is reported in this work. The structural characterization was performed at room temperature using a Bruker X-ray diffractometer model D2 Phaser with CuKα radiation (λ =1.5406 Å), in the results, the XRD shows the phase transition from ZnS to ZnS ZnO and the grain size increases from 3 until 31nm with increases times annealing.SEM (Scanning Electron Microscopy) was used to examine the morphological qualities.Transmittance measurements in the wavelength range [200-2500 nm] were used to determine the optical characteristics of ZnS treated films Using a UV (Ultra-Violet) Visible JASCO type V-570 double beam spectrophotometer, the grown films exhibit transparency above 40-75% in the visible range and 75-98% in the infrared region of 75-98%. The angle contact measurements show a change in the surface Wettability from hydrophilic to hydrophobic during times annealing which is required for self-cleaning in solar cell applications**[4, 5]**.

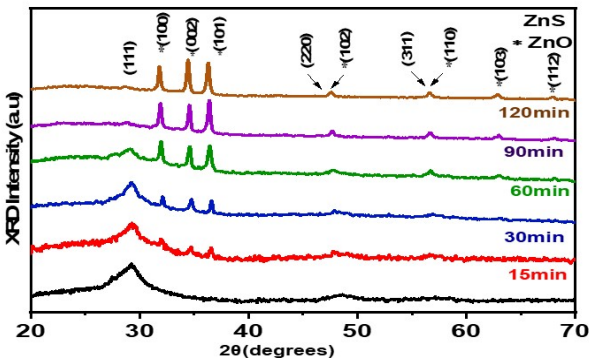


**Fig.1.**. XRD profiles of ZnS thin films annealed at 450°C under the air with various duration thermaltreatments

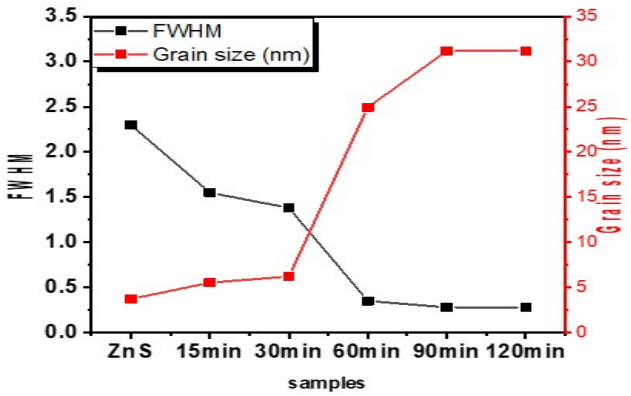


**Fig.2.** Structural parameters evolution of ZnS thin films annealed under the air withvarious duration thermal treatments

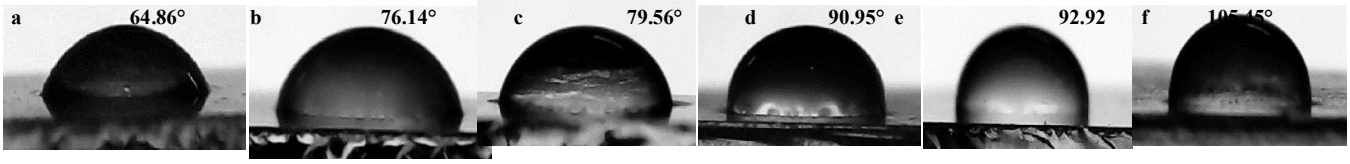


**Fig.3 .**The contact angle of ZnS thin films annealed under the air with various durations thermal treatments

**Keywords:** ZnS thin films; Spray pyrolysis; X-ray diffraction; scanningelectron microscopy (SEM)

## References

[1]Xiao, Jingkun, et al. "Preparation and gas sensing properties of hollow ZnS microspheres." *Journal of Nanoscience and Nanotechnology* 16.3 (2016): 3026-3029.

[2] Xu, Xiaojie, et al. "Design principles and material engineering of ZnS for optoelectronic devices and catalysis." *Advanced Functional Materials* 28.36 (2018): 1802029.

[3] Ummartyotin, Sarute, and YingyotInfahsaeng. "A comprehensive review on ZnS: From synthesis to an approach on solar cell." *Renewable and Sustainable Energy Reviews* 55 (2016): 17-24.

[4] Lin, Yibing, et al. "CdS quantum dots sensitized ZnO spheres via ZnS overlayer to improve efficiency for quantum dots sensitized solar cells." *Ceramics International* 40.6 (2014): 8157-8163.

[5] Ali, Hassan, et al. "Richardson-Schottky transport mechanism in ZnS nanoparticles." *AIP Advances* 6.5 (2016)

# Simulation and optimization of transmittance and UV blocking of $SiO_2/TiO_2$ multilayer structures

**A. Lacidi[1], R. Miloua[1,2], M. Khadraoui[1], Z. Amara[1,3]**

[1] *Materials Development and Characterization Laboratory, Djillali Liabes University, 22000 Sidi Bel-Abbes, Algeria*
[2]*Faculty of Natural and life Sciences, Ibn Khaldoun University of Tiaret, 14000, Tiaret, Algeria*
[3]*Institute of technologies, University center Salhi Ahmed,45000, Naama, Algeria*
*Contact: lacidiamel45@gmail.com*

**ABSTRACT**

Light management is of crucial importance in photovoltaics; especially in thin film solar cells it is advantageous to extend the pathway of incident solar radiation in the absorber material. Unfortunately, UV radiation can have a detrimental effect on both absorber and encapsulant material in PV modules [1].

In order to optimize both the UV blocking and the visible light transmittance under the AM1.5G spectrum, we simulated ten different structure (i.e. monolayers, bilayers and multilayers) based on $SiO_2$ and $TiO_2$ materials. We also considered the addition of porous $SiO_2$ in the multilayer structures. The results showed that the increase in UV blocking strongly depends on the thickness of $TiO_2$ layers. In addition, we identified the best thickness values that could lead to the improvement of effective transmittance of the structures. We demonsrated that, under certain conditions, some multilayer structures achieved good UV blocking and antireflection behaviour at the same time [2-4].

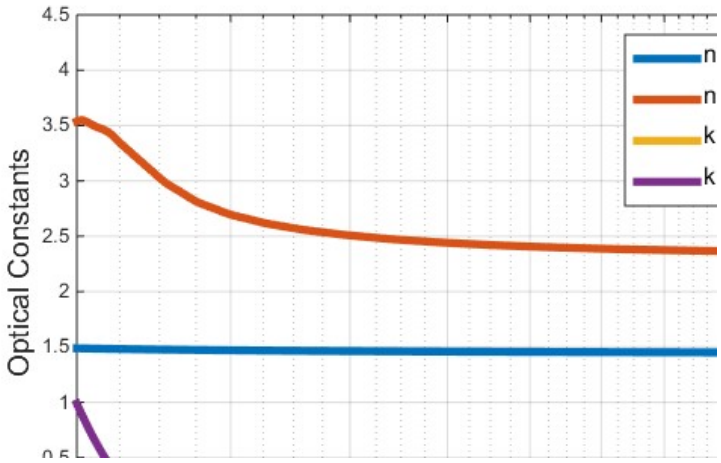


*Figure 1: Optical constants of $SiO_2$ (fused silica) and $TiO_2$ (anatase).*

The variation of n and k with wavelength is represented in Figure 1. As can be seen in this figure, the refractive index of $TiO_2$ and $SiO_2$ were varied between 3.5 – 2.4 and 1.5 in the range 300nm - 1200nm, respectively. Also, it is noted that the extinction coefficient varies between 1.5-0 for $TiO_2$ and is almost equal 0 for SiO2 the region. The extinction coefficient is related to the absorption coefficient $\alpha = 4\pi k/\lambda$.

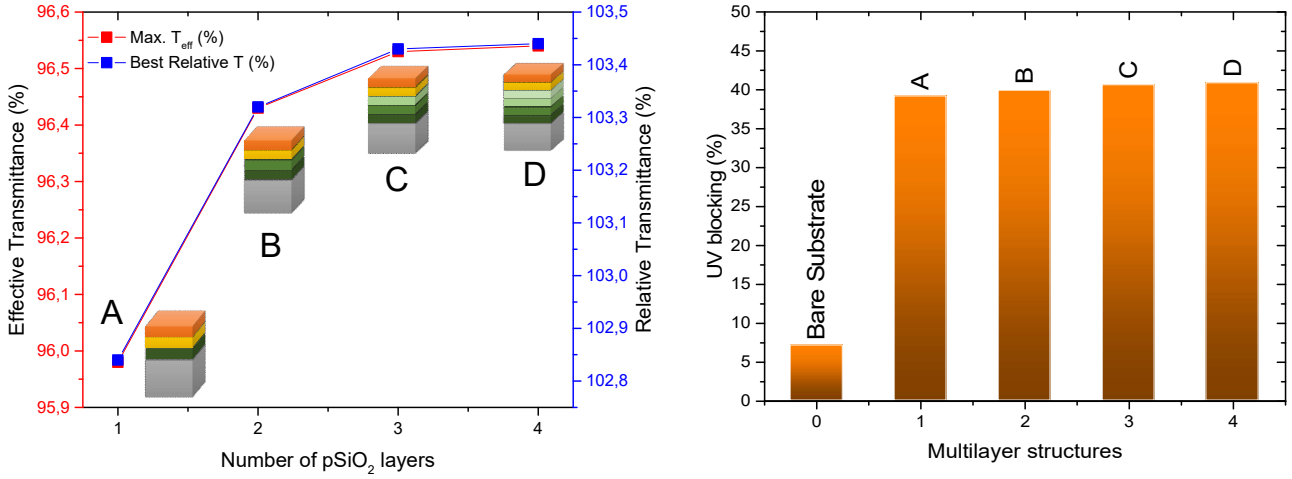


*Figure 2: Left : maximum effective (and relative) visible transmittances of A, B, C and D multilayer structures. Right : UV blocking of A, B, C and D multilayer structures.*

For the multilayer structures (Figure 2), firstly, the simplest structure (named "A") is fundamentally composed of $TiO_2/SiO_2$ and a single layer of porous $SiO_2$. The structure A achieved transmittance of 96.46 % which constitutes a good enhancement in comparison o bare substrate transmittance (93.33%). Subsequently, when we added additional layers of porous $SiO_2$ (structures B, C, D), we achieved transmittance enhancement of 96.54% (Figure 2, Left panel). Simultaneously, a good UV blocking better than 40% is reached (Figure 2, Right panel).

**Keywords:** Transmittance; UV blocking; $SiO_2$; $TiO_2$.

## References

[1] N. Pinochet, R. Couderc, S. Therias. Progress in Photovoltaics: Research and Applications Prog. Photovolt. Res. 31 (2023) 1091.

[2] Jindi Wanga, Juanjuan Gea, Haigang Houa, Mingsong Wanga, Guiwu Liua, Guanjun Qiaoa, Yongsheng Wang. Applied Surface Science 422 (2017) 970.

[3] D. Karthik, S. Pendse, S. Sakthivel, E. Ramasamy, S.V. Joshi, Sol. Energy Mater. Sol. Cells 159 (2017) 204.

[4] S.M. Kang, S. Jang, J.-K. Lee, J. Yoon, D.-E. Yoo, J.-W. Lee, M. Choi, N.-G. Park, Small 12 (2016) 2443.

# Comparative Study Between Conventional and Metaheuristic MPPT Algorithms under Variating Irradiance Conditions

**A. Mederbel[1], M. Khadraoui[1], K. Sahraoui[1]**

[1]1Laboratoire d'Elaboration et Caracterisation des Materiaux LECM, Electronics Department, Electrical Engineering Faculty, University of DjilaliLiabes, Sidi Bel Abbes 22000, Algeria
Email : mederbel96@gmail.com

## ABSTRACT

This paper explores how Maximum Power Point Tracking (MPPT) controllers enhance the output of photovoltaic (PV) arrays, especially under varying irradiance conditions. The clean and limitless nature of PV energy has sparked considerable interest, but optimizing PV array performance using various MPPT methods, from simple conventional techniques to advanced metaheuristic algorithms, requires addressing output variations. We highlight their strengths and weaknesses under varying irradiance conditions.

**Keywords:** Boost; CSA; DC-DC; MPPT; P&O; PSO; PV.

## INTRODUCTION

PV energy has become increasingly popular in recent years due to its sustainability, affordability, and scalability. However, the output of photovoltaic (PV) arrays is subject to variations due to changing irradiance conditions. To maximize the efficiency of PV arrays under these varying conditions, Maximum Power Point Tracking (MPPT) controllers are essential. This paper reviews a variety of MPPT methods, from traditional techniques to advanced metaheuristic algorithms, and compares their strengths, weaknesses, and performance in real-world applications

## MATERIALS AND METHODS

This study employed a DC-DC boost converter, where the MOSFET's commutation is managed by the MPPT controller, which adjusts the duty cycle to track the maximum power point of the PV array. By doing so, the MPPT controller ensures that the PV array operates at its maximum efficiency.

Various MPPT methods have been proposed to maximize the output of a PV array. These methods can be broadly classified into two categories: conventional methods and intelligent algorithms.

1. Perturb and Observe (P&O): chosen as a baseline to our comparison, P&O is a conventional MPPT method that operates by incrementally adjusting the PV module's voltage and monitoring the resulting change in output power. It continuously perturbs the operating point and observes whether the power increases or decreases, thus tracking the MPP[2].
2. Particle Swarm Optimization (PSO): chosen due to its popularity in optimization problems, PSO is based on the population-based stochastic optimization algorithm inspired from swarms. Mimicking the performance gained by interaction between the different individuals or particles. The particles mouvement is defined as follows: [2]

$$X_i^{k+1} = X_i^k + V_i^{k+1} \quad (1)$$

$$V_i^{k+1} = wV_i^k + c_1 r_1 \left(Pbest_i - X_i^k\right) + c_2 r_2 (Gbest_i - X_i^k) \quad (2)$$

where $X$ is the position of the particle; $i$the particle number, $k$ the number of iteration; $V$ the velocity; w the inertial weight; $c_1$ and$c_2$ the particle acceleration coefficients; *Pbest* and *Gbest* are the best local position and the best global position respectively; $r_1$,$r_2 \in [0.1]$ are uniformly distributed random coefficients.

3. Cuckoo Search Algorithm (CSA): which imitates the behaviors of the cuckoo birds and relies on the Lévy flight search to find a suitable host nest to lay its egg on, the MPP in our case. [3]

$$X^{(t+1)} = X_i^t + \alpha \oplus Lévy(\lambda) \text{where} \alpha = \alpha_0(x_{best} + x_i) \text{and} Lévy(\lambda) \approx u = l^{-\lambda}, \ (1 < \lambda < 3)(3)(4)(5)$$

$X_i^t$ is samples/eggs, $i$ is the sample number, $t$ is the number of iteration and $\alpha > 0$ is the step size $l$ is the flight length and $\lambda$ is the variance. Since $1 < \lambda < 3$, thus $u$ has an infinite variance.

## RESULTS AND DISCUSSION

As shown in Table 1, the CSA exhibited the fastest convergence time, taking only 0.027s to reach the maximum power point. It had a settling time of 0.17s, a high efficiency of 99.4%, and a low error rate of 0.6%.The PSO had a slightly longer convergence time of 0.083s, but it was still relatively fast. It had a settling time of 0.22s, high efficiency at 99.6%, and a low error of 0.4%.The P&O, while achieving a high efficiency of 97.6%, had the slowest convergence time at 0.422s and a relatively longer settling time of 0.53s, along with a higher error rate of 2.4%.

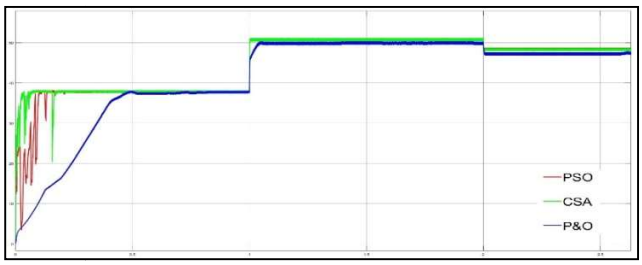


*Fig 1 Comparison of PSO, CSA and P&O power outputs at 0.5kw/m2, 1kw/m2 and 0.8kw/m2*

*Table 1 Result of the comparison between PSO, CSA and P&O*

| Algorithm | Convergence time (s) | Settling time (s) | Efficiency (%) | Error (%) |
|---|---|---|---|---|
| P&O | 0.422 | 0.53 | 97.6 | 2.4 |
| PSO | 0.083 | 0.22 | 99.6 | 0.4 |
| CSA | 0.027 | 0.17 | 99.4 | 0.6 |

## CONCLUSION

In summary, the comparative analysis of the MPPT algorithms indicates that metaheuristic algorithms like PSO and CSA outperform conventional methods like P&O in variable irradiance conditions. Both PSO and CSA demonstrate faster convergence times, higher efficiency, and lower error rates, making them more suitable for optimizing the energy conversion process in challenging and changing solar irradiance conditions.

## References

[1] Salman, S., AI, X. & WU, Z. Prot Control Mod Power Syst. Volume 3, 25 (2018).

[2] F. M. Oliveira, S. A. O. da Silva, F. R. Durand and L. P. Sampaio, 2015 IEEE 13th Brazilian Power Electronics Conference and 1st Southern Power Electronics Conference (COBEP/SPEC), 2015, pp. 1-6.

[3] Hussaian Basha, C., Bansal, V., Rani, C., Brisilla, R.M., Odofin, S. Soft Computing for Problem Solving. Volume 1048. pp 727–736 (2019).

# Synthesis and Characterization Of $SnO_2$ Thin Films : A Simple and Inexpensive Wet Chemical Route

**A. Tioursi[1,*], R. Miloua[1,2], A. Nakrela[1], W. Azzaoui[1], A.H. Yahi[1], A. Bouzidi[1], M. Medles[1], M. Khadraoui[1]**

[1] *Laboratoire d'Elaboration et de Caractérisation des Matériaux, Faculté de Génie Electrique, Université DjillaliLiabès, Sidi Bel Abbès, Algeria*
[2] *Faculté des Sciences de la Nature et de la Vie, Université Ibn Khaldoun, Tiaret, Algeria*
** Email:amina_tioursi@outlook.com*

## ABSTRACT

Tin dioxide ($SnO_2$) is a material belonging to the transparent conductive oxide (TCO) family. Its nontoxic and abundant composition on Earth makes it an ideal candidate for transparent electrical contacts for electronic, optical, and catalytic applications. $SnO_2$ exhibits a good compromise between transparency in the visible range and high electrical conductivity [1, 2].

In the present work, we propose a straightforward chemical method for the preparation of $SnO_2$ thin films. The method has many advantages:

- It is based on a well-documented chemical basis (i.e. Sol-Gel method)
- Affordable precursors and solvents are used,
- A homemade deposition technique (namely, spin coating) is employed to deposit $SnO_2$ thin films at room temperature (RT).
- Oxide materials of various structures (monolithic, thin layer, fiber, powder) can be obtained.

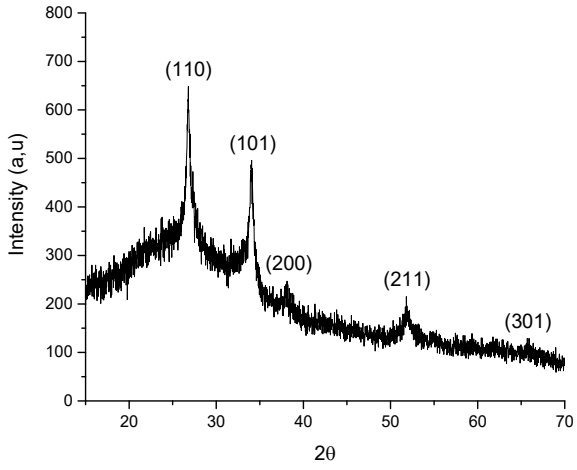


***Fig 1.*** *X-ray diffraction diagram of $SnO_2$ thin film.*

In Figure.1, we depicted the X-ray diffraction pattern of $SnO_2$ sample. As observed from the XRD pattern, four diffraction peaks could be identified at positions of 26.794, 34.057, 38.12, 51.82, and 65.90 degrees according to (110), (101), (200), (211), and (301) planes, respectively. The diffraction lines at these planes

are well matched to the tetragonal rutile phase of $SnO_2$ according to JCPDS card No. 72–1147. As observed from the XRD patterns for the deposited thin films, there are no diffraction peaks consistent with other phases of tin oxide.

From Figure.2 (left panel), $SnO_2$ exhibits strong absorption in the ultraviolet range. However, across the entire visible and near-infrared spectral ranges, the $SnO_2$ thin film exhibits high transmission with interference fringes. The investigation of the transmission curve in the UV-Visible leads to the definition of three important parameters: the optical constants (refractive index and extinction coefficient), the thickness of the film, and the band gap energy [2].

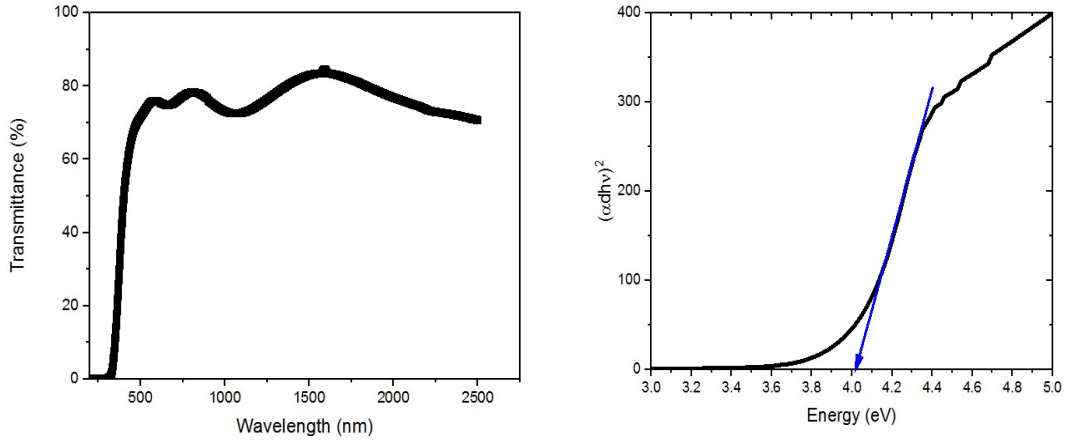


***Fig 2.*** *Left panel: Measured transmittance vs. wavelength of $SnO_2$ sample. Right panel: $(\alpha h\nu)^2$ as a function of photon energy (hν).*

The band gap energy can be deduced by plotting $(\alpha h\nu)^2$ as a function of photon energy (hν), as indicated in Figure.2 (right panel). The $E_g$ value is determined at the point of intersection of the tangent line with the abscissa axis (energy). For our sample, we obtained $E_g$ = 4 eV which is in excellent agreement with the literature [1, 2].

**Keywords:** $SnO_2$; Spin coating; Sol-Gel; Thin films.

**References**

[1] A. ElhamHalvani, et al. Energy&Environmental Science, 9.10 (2016) 3128.
[2] A. H. Yahi, et al. Optik, 196(2019)163198.

# Performance evaluation of binary descriptors on remote sensing imagery

**N. M. Belmessaoud[1], Y. Bentoutou[2], M. Chikr El Mezouar[1]**

[1]*RCAM Laboratory, Department of Electronics, DjillaliLiabes university, SidiBel Abbes, 22084, SidiBel Abbes, Algeria*
[2]*Satellite Development Center, Algerian Space Agency, Bir El Djir, 31130, Oran, Algeria*
*Email : bmnadir2@gmail.com*

## ABSTRACT

The emergence of binary feature descriptors as viable alternatives to the already established detectors has garnered considerable interest from various subdisciplines of the broader computer vision community. This includes, but is not limited to, topics such as object recognition [1], image retrieval [2], and visual simultaneous localization and mapping [3]. However, this interest did not extend to remote sensing, a field that could stand to benefit immensely from the computational advantages offered by these descriptors. This holds especially true in areas where the precise and timely extraction and matching of feature points is critical. But before these techniques can be reliably applied to remotely sensed imagery, a quantitative assessment of their effectiveness needs to be conducted. This work aims to address this need by evaluating the performance of prominent binary descriptors, namely: BRIEF [4], ORB [5], BRISK [6], and FREAK [7], on a dataset that comprises multi-temporal, multi-view, and multi-modal image pairs. The efficacy of each of these descriptors is compared with SIFT [8] features, which serve as a reference and are employed to derive the transformation function in each test case. The results, which are depicted in Table 1, demonstate that SIFT outperformed the binary descriptors across all tested cases; nevertheless, it exhibits two primary drawbacks. Firstly, it detects significantly fewer features compared to the other techniques, and secondly, it is considerably slower, rendering it impractical for applications with stringent time constraints. In contrast, ORB achieved a favorable balance between performance and runtime efficiency on the multi-temporal and multi-view images, second only to SIFT. However, and like all other binary descriptors, it failed in the multi-modal case to achieve sufficient matches to derive the transformation.

**Keywords:**Remote sensing; Local features; Binary descriptors; Performance comparison .

| Test case | Algorithm | Number of matches | Number of inliers | Precision | Runtime (ms) |
|---|---|---|---|---|---|
| Multi-temporal | SIFT | 54 | 49 | 90.7% | 1340 |
| | ORB | 100 | 26 | 26% | 225 |
| | BRISK | 508 | 122 | 24% | 364 |
| | FREAK | 188 | 31 | 16.5% | 90 |
| | BRIEF | 232 | 60 | 25.9% | 30.4 |
| Multi-view | SIFT | 17 | 17 | 100% | 5930 |
| | ORB | 586 | 67 | 11.4% | 506 |
| | BRISK | 677 | 61 | 9% | 3150 |
| | FREAK | 381 | 16 | 4.2% | 144 |
| | BRIEF | 353 | 40 | 11.3% | 81.3 |
| Multi-modal | SIFT | 16 | 8 | 50% | 1840 |
| | ORB | 390 | 1 | 0.3% | 349 |
| | BRISK | 398 | 0 | 0% | 650 |
| | FREAK | 259 | 0 | 0% | 84.6 |
| | BRIEF | 265 | 0 | 0% | 41.9 |

*Table 1: The results obtained by the different algorithms on the three test cases*

**References**

[1] A. Kulkarni, J. Jagtap, and V. Harpale, "Object recognition with orb and its implementation on fpga," International Journal of Advanced Computer Research, vol. 3, no. 3, p. 164, 2013.

[2] M. Kumar, P. Chhabra, and N. Garg, "Content-based image retrieval system using orb and sift features," Neural Computing and Applications, vol. 32, 04 2020.

[3] R. Mur-Artal, J. M. M. Montiel, and J. D. Tardos, "ORB-SLAM: a versatile and accurate monocular SLAM system,"CoRR, vol. abs/1502.00956, 2015.

[4] M. Calonder, V. Lepetit, C. Strecha, and P. Fua, "Brief: Binary robust independent elementary features," in Computer Vision – ECCV 2010 (K. Daniilidis, P. Maragos, and N. Paragios, eds.), (Berlin, Heidelberg), pp. 778–792, Springer Berlin Heidelberg, 2010.

[5] E. Rublee, V. Rabaud, K. Konolige, and G. Bradski, "Orb: An efficient alternative to sift or surf," in 2011 International Conference on Computer Vision, pp. 2564–2571, 2011.

[6] S. Leutenegger, M. Chli, and R. Y. Siegwart, "Brisk: Binary robust invariant scalable keypoints," in 2011 International Conference on Computer Vision, pp. 2548–2555, 2011.

[7] A. Alahi, R. Ortiz, and P. Vandergheynst, "Freak: Fast retina keypoint," in 2012 IEEE Conference on Computer Vision and Pattern Recognition, pp. 510–517, 2012.

[8] D. G. Lowe, "Distinctive image features from scale-invariant keypoints," Int. J. Comput. Vision, vol. 60, pp. 91–110, Nov. 2004.

# Various GPU-Based Implementations of MRF-Based Deformable Image Registration Algorithm

**Miloud Chemam, Chakib Mustapha Anouar ZOUAOUI, Nasreddine TALEB**

*RCAM Laboratory, Djillali Liabes University, Sidi Bel Abbes, 22000, Algeria*
*Email : mchemam504@gmail.com*

**ABSTRACT**

Deformable Image Registration plays a crucial role in medical image analysis. However, some algorithms can be time-consuming. To address this issue, we have introduced many core processors, specifically GPUs (Graphical Processing Units), to expedite the image registration process. GPU is an excellent platform for accelerating compute-intensive algorithms, like image registration, because it excels at performing a multitude of arithmetic operations in parallel.

Our GPU implementations leverage NVIDIA's CUDA (Compute Unified Device Architecture), a parallel computing interface that provides software developers with C programming language extensions. Algorithms designed with CUDA can be executed on NVIDIA GPUs, such as GTX 1070ti, which included 2430 CUDA cores.

To evaluate the impact of this approach, we have conducted various implementations and comparisons between GPU,

CPU Serial, CPU OpenMp, and GPU/CPU combinations; primarily focusing on time efficiency. This research aims to determine the best suitable CPU, GPU or Both for acceleration in deformable image registration, and assess the potential for improving the speed and efficiency of these critical medical image analysis tasks.

The implementations are built upon the CPU implementation of MRF (Markov Random Field)-based deformable image registration. This approach involves adapting and enhancing the existing CPU-based MRF registration algorithm to harness the computational power of GPUs. By doing so, we aim to significantly improve the performance and reduce the processing time of deformable image registration, making it a more efficient and practical tool for medical image analysis. Our goal is to demonstrate the advantages of GPU acceleration in comparison to traditional CPU implementations, with a focus on speed and efficiency gains.

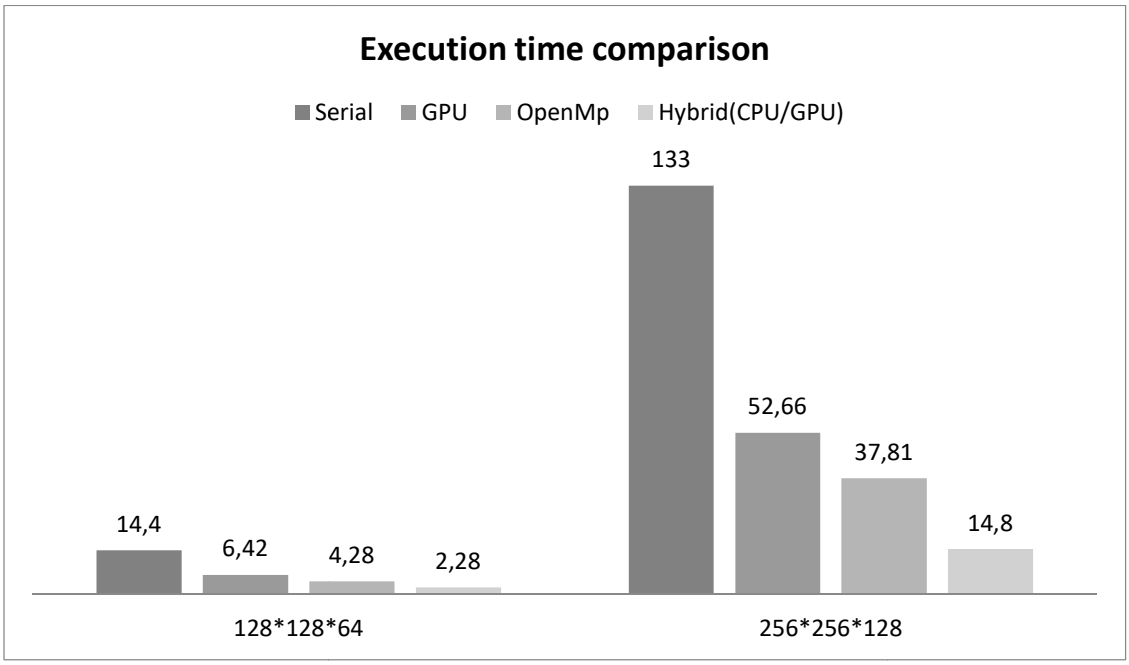


**Keywords:** CUDA, Image Registration, GPU, OpenMp.

**References**

[1] M. P. Heinrich, M. Jenkinson, M. Brady and J. A. Schnabel, "MRF-Based Deformable Registration and Ventilation Estimation of Lung CT," in *IEEE Transactions on Medical Imaging*, vol. 32, no. 7, pp. 1239-1248, July 2013.

[2] M. P. Heinrich M. Jenkinson S. M. Brady J. A. Schnabel "Globally optimal registration on a minimum spanning tree using dense displacement sampling" in Medical Image Computing and Computer-Assisted Intervention MICCAI 2012 Germany Berlin:Springer 2012.

[3] Ben Glocker, Nikos Komodakis, Georgios Tziritas, Nassir Navab, Nikos Paragios,Dense image registration through MRFs and efficient linear programming, Medical Image Analysis, Volume 12, Issue 6,2008,Pages 731-741,ISSN 1361-8415

[4] NVidia CUDA [http://developer.NVidia.com/object/cuda.html]

# A Comparative study between two unsupervised remote sensing change detection methods :PCA K-Means and PCACVA

**A. I. Goffa[1], Y. Bentoutou[2,1], N. Taleb[1]**

[1]*RCAM Laboratory (Communication Networks, Architecture, and Multimedia) ,Department of Electronics, Djillali Liabes University, ,Sidi Bel Abbes, BP 89, 22000 Algeria*
[2]*Satellite Development Center, POS 50, ILOT T12 Bir El Djir ORAN, 31130 Algeria*
*Email: adelgof18@gmail.com*

## ABSTRACT

In this paper, we present a comparative study of two unsupervised change detection methods, Principal Component Analysis combined with K-means clustering (PCAK-means) and a proposed method utilizing PCA combined with Change Vector Analysis (PCACVA), applied to satellite imagery. The aim is to assess the effectiveness of these methods in detecting significant land cover changes.This is achieved by analyzing the difference image derived from two satellite images representing the same geographical area and taken at two distinct time points. We extract eigenvectors from non-overlapping 5×5 blocks within the difference image using Principal Component Analysis (PCA). Subsequently, we create a feature vector for every pixel within the difference image by projecting the data from 3×3 neighborhood onto the eigenvector space.The primary difference between the methods lies in the clustering approach. In the first method, PCAK-means, the feature vector space is partitioned into K=2 (Number of clusters) clusters using the K-means algorithm. Each cluster is represented by a mean feature vector. The second method, CVA, extracts feature vectors for each pixel's neighborhood data and categorizes changes based on a user-defined threshold β=0.9.Finally, the change detection process,as shown in fig. 1, is achieved by assigning each pixel within the difference image to one of the clusters based on the minimum Euclidean distance between its feature vector and the mean feature vector.

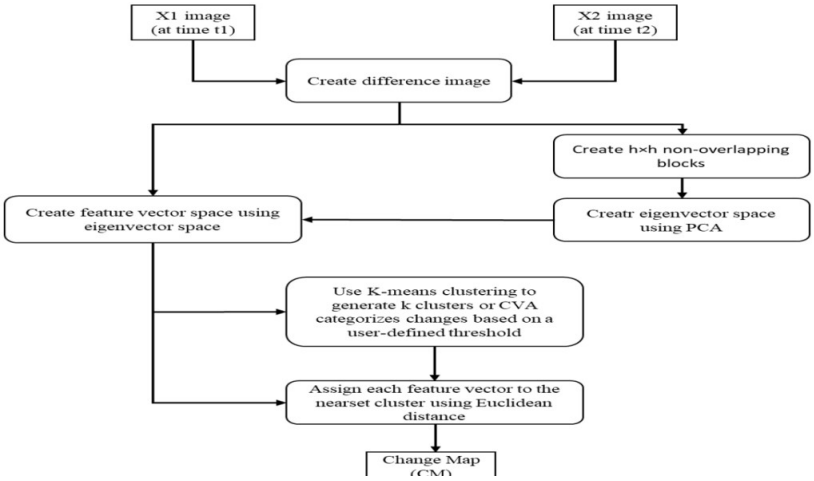


**Fig. 1.**General scheme of the proposed approach

To evaluate the performance of the two approaches, we utilized real dataset images (see **Fig.2** and **Fig.3**). Our evaluation involved conducting comprehensive qualitative and quantitative comparisons against the methodologies outlined in the existing literature. The result is a binary change map, with 255 indicating areas of change and 0 indicating no change. This map is subsequently cleaned for finer detail.

(a) (b) (c) (d) (e)

**Fig.2.** Change detection results for the two approaches on Natural Disasters images (a) Input image X1. (b) Input image X2. (c) Ground truth change map. (d) PCAK-means change map. (e) PCACVA change map.

**TABLE.I.** COMPARISON OF DETECTION RESULTS ON THE ARCADIALAKE DATA SET

| Dataset | Methods | Kappa | F1-Score | Precision | PCC | IOU | OA | Time(s) |
|---|---|---|---|---|---|---|---|---|
| ArcadiaLake | PCAKmeans | 0.20 | 0.95 | 0.98 | 0.46 | 0.15 | 0.92 | 25.52 |
| | PCACVA | 0.27 | 0.96 | 0.98 | 0.57 | 0.21 | 0.95 | 5.52 |

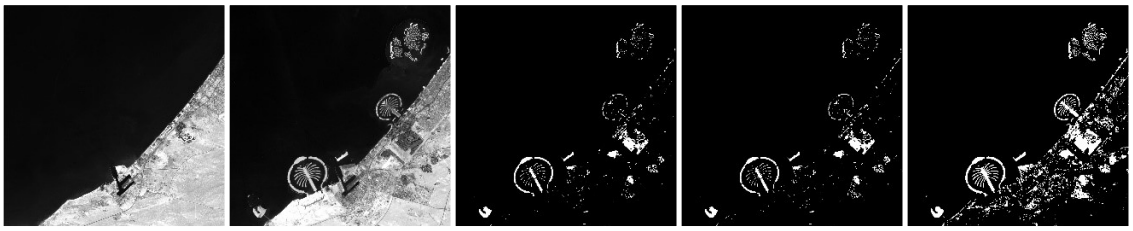

(a) (b) (c) (d) (e)

**Fig.3.** Change detection results for the two approaches on Urban Development images (a) Input image X1. (b) Input image X2. (c) Ground truth change map. (d) PCAK-means change map. (e) PCACVA change map.

**TABLE.II.** COMPARISON OF DETECTION RESULTS ON THE DUBAI DATA SET

| Dataset | | Methods | Kappa | F1-Score | Precision | PCC | IOU | OA | Time(s) |
|---|---|---|---|---|---|---|---|---|---|
| Dubai | | PCAKmeans | 0.49 | 0.95 | 0.95 | 0.94 | 0.56 | 0.95 | 13.77 |
| | | PCACVA | 0.32 | 0.92 | 0.95 | 0.58 | 0.34 | 0.90 | 5.20 |

As a conclusion , the choice between these methods may depend on the specific characteristics of the problem at hand. The PCAK-means method may be more suitable for cases where changes are complex and don't conform to a simple threshold. On the other hand, the PCACVA method with a threshold is more straightforward to set up but may require a carefully chosen threshold for optimal results.

**Keywords:** Remotesensing; Changedetection;K-meansclustering; CVAthreshold;Principal component analysis(PCA).

**References**

[1]Turgay Celik. (2009). Unsupervised Change Detection in Satellite Images Using Principal Component Analysis and k-Means Clustering. IEEE Geoscience and Remote Sensing Letters, 6(4), 772–776.
[2]Chughtai, A. H., Abbasi, H., & Karas, I. R. (2021). A review on change detection method and accuracy assessment for land use land cover. Remote Sensing Applications: Society and Environment, 22, 100482.

# Benchmarking Memory Allocation Performance in Windows: a Comparative Analysis of Malloc across Different Compilers

**Yacine HADJADJ, Chakib Mustapha Anouar ZOUAOUI, Nasreddine TALEB**

*RCAM Laboratory, Djillali Liabes University, Sidi Bel Abbes, 22000, Algeria*
*Email: mail@ycinhdj.com*

## ABSTRACT

This research delves into the critical domain of memory allocation in software development and its profound impact on performance and efficiency. The study conducts a comprehensive evaluation of memory allocation performance in four major compilers within the Windows environment, namely GCC (MSYS2)[1], MSVC[2], Clang[3], and WSL2[4]. Rigorous benchmarking procedures were implemented under full optimization settings to scrutinize memory allocation, reallocation, and deallocation operations facilitated by the Malloc allocator. The investigation predominantly focuses on the time efficiency of these operations, uncovering pivotal performance distinctions among the compilers.

Memory allocation is pivotal in programming, encompassing the allocation and release of memory blocks, and this study scrutinizes how various compilers handle these operations under full optimization settings. The research approach is systematically outlined, encompassing compiler selection, optimization settings, benchmarking operations, replicability, and data collection. The experimental configuration includes detailed information on the hardware and software environment, providing insight into the processor, memory, operating system, compiler versions, and test cases.

The evaluation results highlight the efficiency disparities among the compilers in memory allocation, reallocation, and deallocation operations. These variations open avenues for software developers to optimize their code and choose the compiler that best aligns with their performance goals. The conclusion unveils a performance hierarchy among the studied compilers, with Clang and MSVC emerging as the top performers, followed by WSL2, and MSYS2. The findings provide valuable guidance for developers seeking efficient memory management solutions in a Windows context, with Clang and MSVC as compelling options for high-performance projects and WSL2 as a commendable, versatile choice offering improved performance compared to MSYS2.

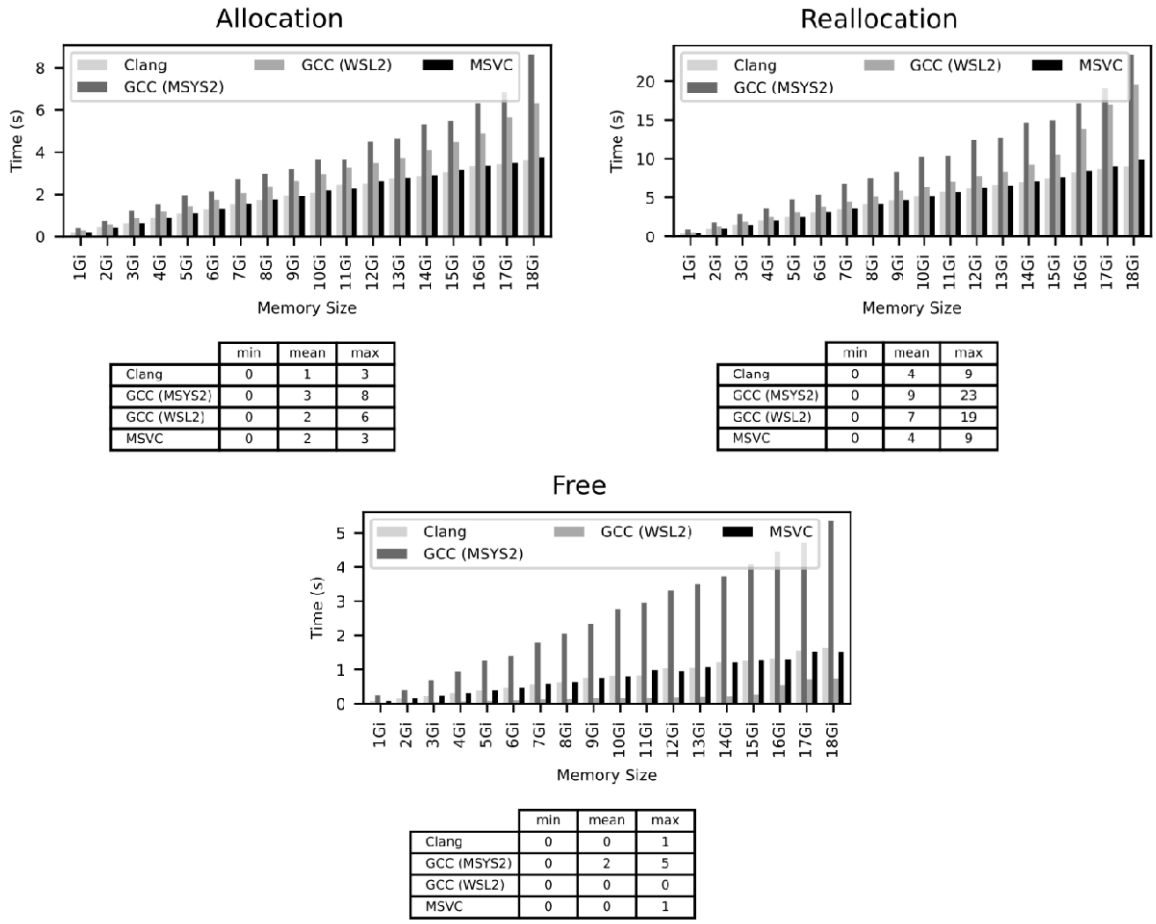


| | min | mean | max |
|---|---|---|---|
| Clang | 0 | 1 | 3 |
| GCC (MSYS2) | 0 | 3 | 8 |
| GCC (WSL2) | 0 | 2 | 6 |
| MSVC | 0 | 2 | 3 |




| | min | mean | max |
|---|---|---|---|
| Clang | 0 | 4 | 9 |
| GCC (MSYS2) | 0 | 9 | 23 |
| GCC (WSL2) | 0 | 7 | 19 |
| MSVC | 0 | 4 | 9 |




| | min | mean | max |
|---|---|---|---|
| Clang | 0 | 0 | 1 |
| GCC (MSYS2) | 0 | 2 | 5 |
| GCC (WSL2) | 0 | 0 | 0 |
| MSVC | 0 | 0 | 1 |

**Keywords:** Memory Allocation, Compilers, Windows Development, GCC, Clang, MSVC.

**References**

[1] "MSYS2." Accessed: Nov. 02, 2023. [Online]. Available: https://www.msys2.org/

[2] "Visual Studio C/C++ IDE and Compiler for Windows," Visual Studio. Accessed: Nov. 02, 2023. [Online]. Available: https://visualstudio.microsoft.com/vs/features/cplusplus/

[3] TylerMSFT, "Clang/LLVM support in Visual Studio projects." Accessed: Nov. 02, 2023. [Online]. Available: https://learn.microsoft.com/en-us/cpp/build/clang-support-msbuild?view=msvc-170

[4] craigloewen-msft, "Windows Subsystem for Linux Documentation." Accessed: Nov. 02, 2023. [Online]. Available: https://learn.microsoft.com/en-us/windows/wsl/

# Efficiency and Memory Utilization Benchmarking of C++ Multidimensional Array Libraries : a Comparative Study

**[1]Yacine HADJADJ, [1]Chakib Mustapha Anouar ZOUAOUI, [1]Nasreddine TALEB**

*[1]RCAM Laboratory, Djillali Liabes University, Sidi Bel Abbes, 22000, Algeria*
*Email: mail@ycinhdj.com*

## ABSTRACT

This research addresses the fundamental challenge of selecting an optimal C++ multidimensional array library to enhance computational efficiency in scientific and engineering applications. The problem at hand revolves around the critical decision faced by C++ programmers and researchers when choosing a library for multidimensional array manipulation, as this choice can significantly impact both performance and memory utilization. To tackle this challenge, we conducted a benchmarking study encompassing four prominent C++ multidimensional array libraries: the Standard Template Library (STL)[1], Armadillo[2], Eigen[3], and Boost MultiArray[4].

Our primary objective was to assess the performance and memory utilization of these libraries across key array operations, which include array creation, element access, array resizing, and access after resizing. To ensure the study's comprehensiveness, we examined square arrays of varying sizes, ranging from 1K to 10K elements per dimension.

The major results obtained from our benchmarking efforts unveiled intriguing insights. Notably, the Standard Template Library (STL) emerged as the top performer in terms of computational speed across all assessed operations. Armadillo, recognized for its prowess in linear algebra and numerical computing, closely followed as the second-best library. In contrast, Eigen and Boost MultiArray displayed comparatively slower performance, concerning element access and resizing operations.

Surprisingly, we observed nearly identical memory consumption during array creation and resizing operations across the tested libraries. This finding suggests that the choice of library has a more significant impact on computational speed than on memory overhead, allowing C++ programmers to prioritize performance considerations without substantial concerns about memory usage disparities.

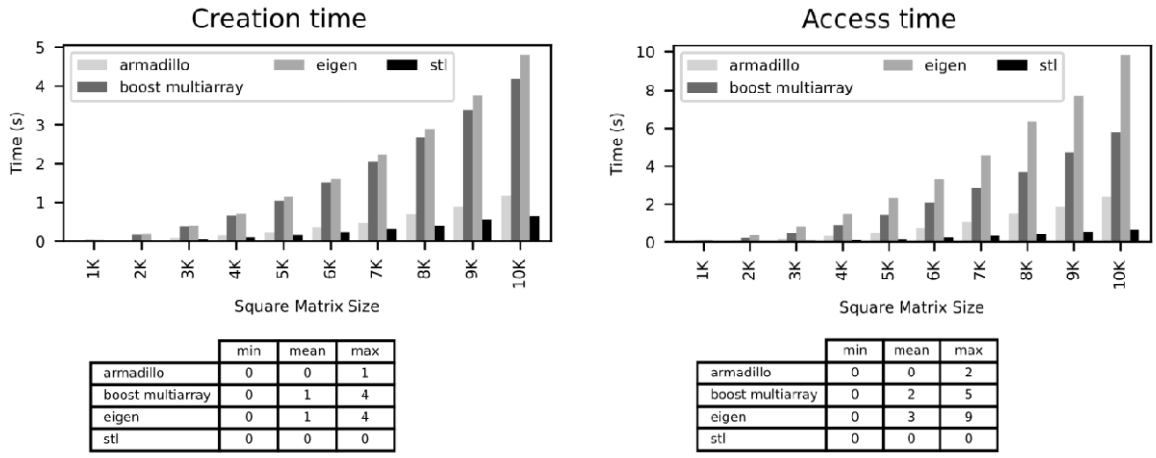


| | min | mean | max |
|---|---|---|---|
| armadillo | 0 | 0 | 1 |
| boost multiarray | 0 | 1 | 4 |
| eigen | 0 | 1 | 4 |
| stl | 0 | 0 | 0 |




| | min | mean | max |
|---|---|---|---|
| armadillo | 0 | 0 | 2 |
| boost multiarray | 0 | 2 | 5 |
| eigen | 0 | 3 | 9 |
| stl | 0 | 0 | 0 |

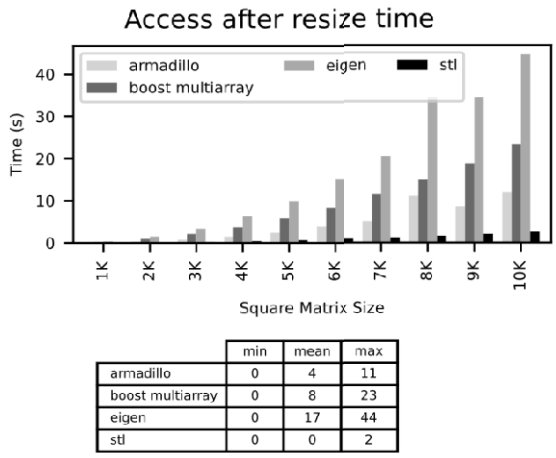


| | min | mean | max |
|---|---|---|---|
| armadillo | 0 | 4 | 11 |
| boost multiarray | 0 | 8 | 23 |
| eigen | 0 | 17 | 44 |
| stl | 0 | 0 | 2 |

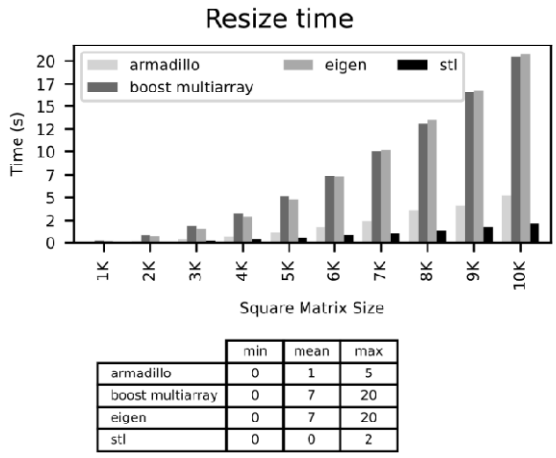


| | min | mean | max |
|---|---|---|---|
| armadillo | 0 | 1 | 5 |
| boost multiarray | 0 | 7 | 20 |
| eigen | 0 | 7 | 20 |
| stl | 0 | 0 | 2 |

**Keywords:**Multidimensional Arrays, C++ Libraries, Benchmarking, Performance Evaluation, Memory Usage, Array Resizing.

**References**

[1] "std::vector - cppreference.com." Accessed: Nov. 05, 2023. [Online]. Available: https://en.cppreference.com/w/cpp/container/vector

[2] C. Sanderson, "Armadillo: An open source C++ linear algebra library for fast prototyping and computationally intensive experiments," 2010.

[3] G. Guennebaud and B. Jacob, "Eigen: a c++ linear algebra library," *URL HttpeigenTuxfamily Org Accessed*, vol. 22, 2014.

[4] R. Garcia and A. Lumsdaine, "MultiArray: a C++ library for generic programming with arrays," *Softw. Pract. Exp.*, vol. 35, no. 2, pp. 159–188, 2005.

# Détection et classification de la maladie broncho-pneumopathie chronique obstructive à travers l'apprentissage automatique et le nez électronique

**N. KAZITANI[1], M. CHIKR-EL-MEZOUAR[1] et E. BOUTELLAA[2]**

[1]*Laboratoire Réseaux de Communication, Architecture et Multimédia, Département d'Electronique, Université DjillaliLiabès, BP89,Sidi-Bel-Abbès 22000, Algérie*
[2]*Institut de Génie Electrique et Electronique, Boulevard de l'Independence, 35000, Boumerdes, Algérie.*
*Contact : kazitaninoreddine@gmail.com*

**RESUME**

Le cancer du poumon constitue une menace très graveà la vie d'une personne s'il n'est pas prise en charge à temps, comme le nombre de personnes atteint parce cancer augmente sans cessedepuis ces 15 dernières années, la détection de BCPO(broncho-pneumopathie chronique obstructive) qui est une maladie chronique liée généralement au tabagisme, permet à la détection du cancer du poumon dans des stages précoces et encore guérissable. Notre étude consiste à la détection de BCPO avec un nez électronique et en utilisant l'apprentissage automatique connu sous le nom de "machine learning". Pour cela on a utilisé une base de données proposé par Acevedo et al. Cette base de données utilise 8 capteurs en mesurant le taux de COV (composés organiques volatile) présent dans l'air expiré par le patient. En utilisant k-voisins les plus proches comme d'apprentissage automatique, on a fait la classification entre les échantillons de l'air expiré par les malades atteint de BCPO, les personnes fumeurs non atteintes par cette maladie, les personnes saines et en bonne santé et des échantillons d'air, les résultats obtenus sont : 92.13% deprécision,90% de f1-score et 93.93% de spécificité.

**Mots clés :** BCPO ;nez-électronique ;apprentissage automatique; KNN; COV.

## INTRODUCTION

Le nez électronique(e-nose) est un dispositif qui simule le nez biologique,celui-ciregroupe un ou plusieurs capteurs dans le but de mesurer les COVs (composés organiques volatiles) contenus dans des échantillons gazeuses, une étude a révélé que l'air expiré par une personne en bonne santé contient 1259 COVs différentes [1] .Le nez électronique est principalement utilisé pour détecter les maladies de nature respiratoire, pour cela on a mis en œuvre une étude permettant la détection de BCPO (broncho-pneumopathie chronique obstructive) cette maladie permet deprévenirle cancer du poumon. BCPO peut être mortel si elle n'est pas diagnostiquée et traitée.Une recherche a été faite par Al Wachami et al. nous informe que le BCPO cause 4.2 millions de morts chaque année[2].

Plusieurs recherches ont été faites pour la détection de BCPO, un algorithme du nom de XGboost associé avec KPCA (kernel principal component analysis) avec la méthode k-fold pour la validation croisée, le résultat été de 90.68% pour la précision[3], dans une autre expérience 5 différents algorithmes ont été utilisés sur une base de données contenant 2 classes,(cancer du poumon et BCPO), combiné avec un filtrage des données comme prétraitement ,une réduction de caractéristiques avec la méthode PCA (principal component analysis) et une validation croisée k-fold, le model avec les meilleurs résultats a été SVM (support vector machine) avec 92.3% de précision , 84.2% de sensitivité et 95.8% de spécificité ont été obtenu comme résultat.

Dans notre étude à travers une base de données proposé par Acevedo et al[4] qui contient 4 classes dont les échantillons de la maladie BCPO. On a utilisé un système contenant un algorithme de l'apprentissage automatique nommé KNN (k-neighbors classifier)comme algorithme de l'apprentissage automatique associé avec une normalisation

des données comme prétraitement et un algorithme nommé foret aléatoire (random forrest classifier) pour la sélection des caractéristiques, on a obtenu 92.13% de précision,90% de f1-score et 93.93% de spécificité comme résultats.

## METHODES

Le nez électronique est composé de 8 capteurs (SP3, MQ-3, TGS 822, MQ-138, MQ-137, TGS 813, TGS-800, MQ-135). Pour la mesure des échantillons pour la base de données cité auparavant, les participants doivent être à jeun pour ne pas que les COVs produits par la nourriture interfère avec les autres COVs produit par le corps humain qui sont au niveau de la bouche.2 échantillons ont été prise de chaque participant. Au total 10 échantillons d'air,40 échantillons de personnes atteint par la BCPO,8 échantillons de personnes fumeurs et 20 échantillons de personnes en bonne santé.

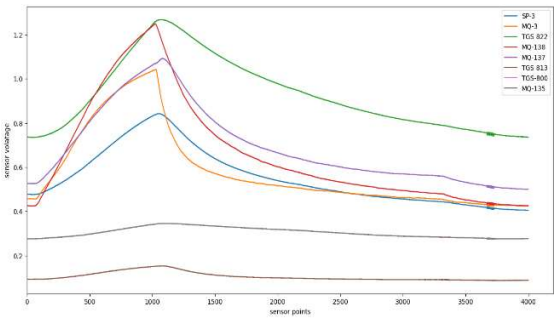


*Fig.1 : réponses des capteursà un échantillon de BCPO*

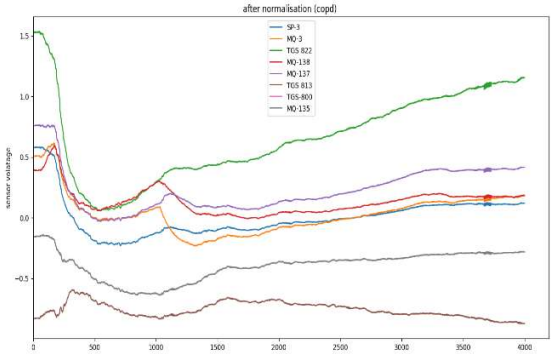


*Fig.2 : résultat dela normalisation*

## CONLUSION

On peut conclure le nez électronique est un outil efficace pour la détection du BCPO qui a son tour prévient le cancer de poumon, dans notre étude on a réalisé un système qui permet à une détection rapide du BCPO en termes de temps d'exécution et efficace en termes de performance.

## REFERENCES

[1] M. Phillips, Method for the Collection and Assay of Volatile Organic Compounds in Breath, 2(1997)272-278.

[2] N. Al Wachami, M. Louerdi, Y. Iderdar, K. Boumendil, M. Chahboune, Chronic obstructive pulmonary disease (COPD) and air pollution: The case of Morocco,72(2023)3738-3748.

[3] B.V.A., M. Subramoniam, L. Mathew, Detection of COPD and Lung Cancer with electronic nose using ensemble learning methods, 523(2021)231-238.

[4] C. M. Durán Acevedo, C. A. Cuastumal Vasquez, et J. K. Carrillo Gómez, Electronic nose dataset for COPD detection from smokers and healthy people through exhaled breath analysis, 35(2021)106767.

# Review of remote sensing pansharpening techniques

**Farid Talbi[1,2], Miloud Chikr Elmezouar[1], ElhocineBoutellaa[3], Fatiha Alim[2]**

[1]*Communication Networks, Architecture and Multimedia Laboratory, Department of Electronics, Djillali Liabès University, Sidi Bel Abbes, Algeria;*
[2]*Division architecture et système multimédia, Centre de Développement des Technologies Avancées, Algiers, Algeria;*
[3]*Institut de Génie Electrique et Electronique Université M'Hamed BOUGARA, Boumerdès, Algeria*
[*]*Corresponding author: ftalbi@cdta.dz; farid.talbi@univ-sba.dz*

## ABSTRACT

Our work consists of fusing a multispectral image with a panchromatic image to produce an image with high spatial and spectral resolution. We present a review for image fusion methods in remote sensing applications to fuse the spectral content of MS (multispectral) image data with the spatial content of PAN (panchromatic) image data. The effectiveness of the fusion is often judged by the quality of the fused image result, which is useful both for visual interpretation and as a preliminary step for higher-level processing.

**Keywords:** Images, Multispectral, Panchromatic, Pansharpening, fusion

## 1. Introduction

Remote sensing image fusion techniques aim to obtain an image with simultaneously high spectral and spatial resolution[1]. This objective can be achieved by improving the equipment to resolve many more details in the spatial and frequency domains. But this improvement is proving to be a difficult task because of the strict constraints on the signal-to-noise ratio of satellite products[2]. One way around this problem is to combine several images with complementary characteristics to obtain high-quality products using signal processing[3]. Several Pansharpening techniques have been proposed, generally classified into four families[4]: COMPONENT SUBSTITUTION (CS), MULTI-RESOLUTION ANALYSIS (MRA),The VARIATIONAL OPTIMIZATION (VO) And The DEEP Learing (DL)

## 2. Reduced resolution assessment (RR) :


Fig. 2 Fusion result for each method (reduced resolution)

Tableau1 : les performances (ERGAS, Qm,SAM,SccGT,Qavg,Time) calculées pour des données à résolution réduite (RR)

| | | | ERGAS | Q | Q-avg | SAM | SCC-GT | Time (s) |
|---|---|---|---|---|---|---|---|---|
| CS | EXP | | 3,8347 | 0,4641 | 0,4572 | 4,331 | 0,6718 | |
| | BT-H | | 2,3447 | 0,8059 | 0,7768 | 3,9887 | 0,9224 | 0,125 |
| | BDSD | | 2,1781 | 0,8445 | 0,8298 | 3,8711 | 0,9404 | 0,1629 |
| | C-BDSD | | 2,3656 | 0,8417 | 0,8288 | 3,9302 | 0,9265 | 0,8224 |
| | BDSD-PC | | 2,1798 | 0,8444 | 0,8296 | 3,8702 | 0,9403 | 0,2836 |
| | GS | | 2,8493 | 0,6962 | 0,6758 | 4,1863 | 0,8973 | 0,0633 |
| | GSA | | 2,2127 | 0,8273 | 0,8099 | 3,9383 | 0,9372 | 0,1063 |
| | C-GSA | | 2,2402 | 0,8201 | 0,8012 | 3,8881 | 0,9304 | 0,3191 |
| | PRACS | | 2,5646 | 0,7529 | 0,7324 | 3,9821 | 0,9084 | |
| MRA | AWLP | | 2,2028 | 0,8375 | 0,8218 | 3,9476 | 0,9367 | 0,1527 |
| | MTF-GLP | | 2,2386 | 0,8423 | 0,8273 | 3,9453 | 0,9389 | 0,2068 |
| | MTF-GLP-FS | | 2,2012 | 0,8318 | 0,8146 | 3,936 | 0,938 | 0,1227 |
| | MTF-GLP-HPM | | 2,2341 | 0,8428 | 0,8281 | 3,9555 | 0,9396 | 0,1959 |
| | MTF-GLP-HPM-H | | 2,3177 | 0,8135 | 0,7838 | 3,9872 | 0,9238 | 0,1571 |
| | MTF-GLP-HPM-R | | 2,1947 | 0,8335 | 0,8164 | 3,9555 | 0,9382 | 0,1466 |
| | MTF-GLP-CBD | | 2,2019 | 0,8318 | 0,8144 | 3,9393 | 0,9379 | 0,114 |
| | C-MTF-GLP-CBD | | 2,2314 | 0,8241 | 0,805 | 3,8886 | 0,9314 | 0,4042 |
| | MF | | 2,407 | 0,7955 | 0,7781 | 4,0275 | 0,9249 | 0,1959 |
| VO | FE-HPM | | 2,3515 | 0,7996 | 0,7824 | 4,0227 | 0,9396 | 0,4286 |
| | SR-D | | 2,3078 | 0,813 | 0,203 | 3,8657 | 0,929 | 1,7067 |
| | PWMBF | | 2,6018 | 0,7433 | 0,7238 | 4,3377 | 0,914 | 0,4702 |
| | TV | | 3,113 | 0,6673 | 0,6441 | 4,2437 | 0,8611 | 2,3722 |
| | RR | | 6,0763 | 0,5584 | 0,203 | 8,9589 | 0,7883 | 5,0943 |
| DL | PNN | | 2,5692 | 0,8086 | 0,7924 | 4,0241 | 0,9077 | 4,9857 |
| | PNN-IDX | | 2,4795 | 0,8164 | 0,7908 | 4,0816 | 0,9229 | 0,9934 |
| | A-PNN | | 2,4903 | 0,8136 | 0,791 | 3,7564 | 0,9217 | 0,8626 |
| | PAN-GAN | | 2,3071 | 0,8218 | 0,813 | 3,4877 | 0,9333 | 7,9332 |
| | | | | | | | | |
| | | | | | | | | |
| | GT | | 0 | 1 | 1 | 0 | 1 | 0 |

## 3. Conclusion

Les images produites par ces modèles présentent de bonne performances et les propriétés spectrales sont également préservées à un niveau acceptable et peuvent être utilisé efficacement dans des applications d'ingénierie pour la télédétection, où une qualité spatiale élevée et une géométrie d'objet précise est requise. Nous avons aussi fait l'implémentation de la méthode de fusion PanColorGAN qui est un réseau de haute qualité du GAN pour l'amélioration de la netteté des images de télédétection. Le résultat obtenu des images lors de la phase de test confirme l`efficacité de cette méthode.

## References

[1] Y. Liu, X. Chen, Z. Wang, Z. J. Wang, R. K. Ward, et X. Wang, « Deep learning for pixel-level image fusion: Recent advances and future prospects », Information Fusion, vol. 42, p. 158‑173, juil. 2018, doi: 10.1016/j.inffus.2017.10.007.

[2] X. Meng, H. Shen, H. Li, L. Zhang, et R. Fu, « Review of the pansharpening methods for remote sensing images based on the idea of meta-analysis: Practical discussion and challenges », Information Fusion, vol. 46, p. 102‑113, mars 2019, doi: 10.1016/j.inffus.2018.05.006.

[3] A. Arienzo, G. Vivone, A. Garzelli, L. Alparone, et J. Chanussot, « Full-Resolution Quality Assessment of Pansharpening: Theoretical and hands-on approaches », IEEE Geoscience and Remote Sensing Magazine, vol. 10, no 3, p. 168‑201, sept. 2022, doi: 10.1109/MGRS.2022.3170092.

[4] F. Ozcelik, U. Alganci, E. Sertel, et G. Unal, « Rethinking CNN-Based Pansharpening: Guided Colorization of Panchromatic Images via GANs », IEEE Trans. Geosci. Remote Sensing, vol. 59, no 4, p. 3486‑3501, avr. 2021, doi: 10.1109/TGRS.2020.3010441.

# Depth map completion through mode filtering: arobust approach for kitti dataset

**M. Chaouki Ziara, M. Elbahri, N. Taleb**

*R. C. A. M. Laboratory, Djilali Liabes University, Sidi Bel Abbes*
*Email: chaouki.ziara@univ-sba.dz*

**ABSTRACT**

This study addresses the challenge of depth map completion in scenarios where the original depth map is characterized by a substantial number of zero values, a situation particularly pronounced in the Kitti dataset, where nearly 80% of the depth map consists of zero values. This high prevalence of zero values significantly hampers the training of deep learning models for depth estimation based on RGB images. Leveraging the Kitti dataset, we introduce an innovative approach to enhance the quality and completeness of initial depth maps. Our methodology begins with the application of bilateral filtering, a technique renowned for its ability to smooth images while preserving edges, We then apply conditional mode filtering, tailored to zero-depth pixels, enabling effective inference of missing depth information in these regions.The results of our method were measured by comparing the histograms of the original depth map with those of the processed map, using metrics such as Correlation (0.98), Chi-Square Distance (0.71), Intersection Distance (0.65), and KL Divergence (0.29). The best values for each metric are indicated in parentheses, showcasing the capacity of our approach to significantly enhance depth map quality and depth intensity distribution preservation. This substantial improvement increases the percentage of non-zero values from the Kitti dataset's initial 20% to 48%, making it a valuable tool for training deep learning models in depth estimation tasks based on RGB images.

**Keywords:** Depth completion; Deep learning; Kitti dataset; Image processing.

## BILATERAL FILTERING

The bilateral filter converts any input image (B)to a smoothed version (A). It removes most texture, noise, and fine details,but preserves large sharp edges withoutblurring following the according formula :

$$B(x) = \frac{1}{Wp} \sum_{x_i \in \delta} A(x) f_r(\|I(x_i) - I(x)\|)\, g_m(\|x_i - x\|)$$

Where :

- $x$are the coordinates of the current pixel to be filtered;
- $\delta$ is the window centred on the pixel we need to apply the filtering around (i.e$x$);
- $f_r$ and $g_m$are functions for Gaussian smoothing in intenceties and coordenatesaccordingly;

**WORKFLOW DIAGRAMAND RESULTS**

The following diagram illustrates the key steps and processes involved in our depth map completion approach using bilateral filtering and conditional mode filtering.

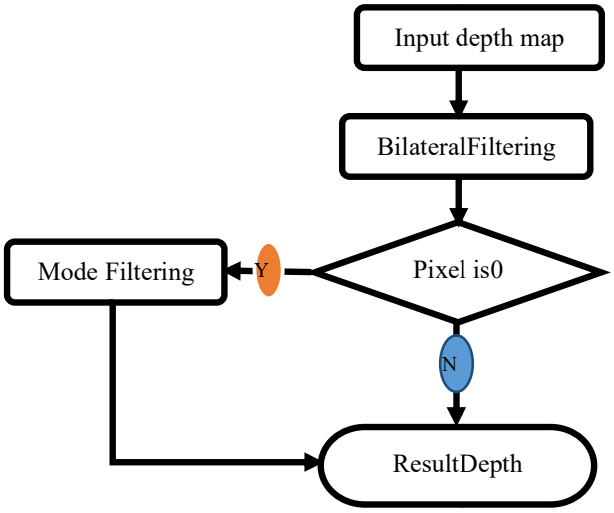


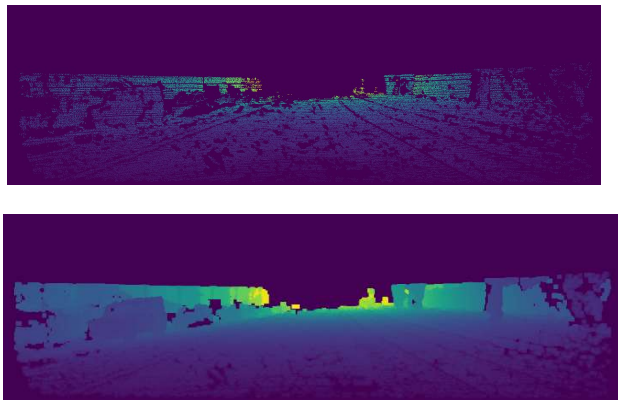

A visual comparison of the original image, the original depth map, and the resulting depth map.

**References**

[1] Lewis D. Griffin, "Mean, median and mode filtering of images," Dec. 2000, Proc. R. Soc. Lond. A.4562995–3004, doi: 10.1098/rspa.2000.0650

[2] C. Tomasi and R. Manduchi, "Bilateral filtering for gray and color images," Sixth International Conference on Computer Vision (IEEE Cat. No.98CH36271), Bombay, India, 1998, pp. 839-846, doi: 10.1109/ICCV.1998.710815.

[3] Fredo Durand, Julie Dorsey "Fast Bilateral Filtering for the Display of High-Dynamic-Range Images,"Laboratory for Computer Science, Massachusetts Institute of Technology.

[4] Y. Gong, "Imposing Total Variation Prior Into Guided Filter," Oct. 2023, doi: 10.1109/icip49359.2023.10222506.

[5] Y. Li and C. Jung, "Deep Sparse Depth Completion Using Joint Depth and Normal Estimation," 2023 IEEE International Symposium on Circuits and Systems (ISCAS), Monterey, CA, USA, 2023, pp. 1-5, doi:10.1109/ISCAS46773.2023.10181618.

# Multi-Segmentation Method for Tumor Detection in MRI Images using Constrained kmeans-Iterated Conditional Mode Method and Region Growing-Quasi Monte Carlo Method

**A. BAGDAOUI [1], S. A. BOUCENNA[1], Z. CHAMA[1] and H. BELKACEM [2]**

*1:LEPO Laboratory, Department of Electronics, Faculty of Electrical Engineering*
*Djillali Liabes University, Sidi Bel-Abbes, Algeria*
*2: CDTA, Centre de Developpement des Techniques Avancees, Algiers, Algeria*
*Email : bagdaoui.amina@outlook.fr (Corresponding author's email)*

**ABSTRACT**
Magnetic Resonance Imaging (MRI) has become an indispensable tool in the medical field, enabling the detection of critical abnormalities affecting various organs within the human body. Despite its inherent complexity, the development of automated or semi-automated detection and recognition techniques has made significant strides. In this paper, we present an innovative approach for the automatic multi and full segmentation of tumor regions within MRI scans. An enhanced region-growing method founded on the Quasi-Monte Carlo sampling and constrained k-means algorithm is presented in this paper, we define distinct classes to facilitate precise segmentation. The efficacy of our technique is evaluated through a range of metrics, demonstrating its robust performance. The proposed fully automated multi-segmentation method showcases superior results and holds potential to supplant conventional techniques for tumor detection in MRI images.

**Keywords:** Brain tumor, Multi Segmentation, Region growing, constrained k-means, Quasi Monte carlo, naive Bayes.

Magnetic Resonance Imaging (MRI) has revolutionized medical diagnosis and treatment by enabling non-invasive visualization of internal structures. Detecting abnormalities in organs is crucial for timely medical interventions. Automation of this process has gained prominence due to the sheer volume and complexity of MRI data. This paper introduces an automatic method for the multi-segmentation of tumor regions in MRI scans, leveraging an innovative combination of the quasi-Monte Carlo method and the Expectation Maximization algorithm. MRI segmentation can be done using three different methods, such as manual, semi-automatic and full automatic techniques. For manual MRI segmentation, which is the most common technique, the segmentation is done by a doctor or an expert, and its accuracy depend on the performance and the knowledge of the doctor. Full automatic segmentation technique is an autonomous process and which need evolved algorithms for calculation and recognition. Medical image processing methods, used for full automatic segmentation, are classified into four main categories: Threshold based techniques, such as otsu and kapur thresholding, and adaptive thresholding. The second category is the region based technique, such as region growing and watershed. Third, the classification techniques that need a training phase, such as SVM and KNN, and clustering methods, such as K-means and EM mixture. The last category is contour detection, such as ACM, GVF, VFC and level set.
Many researchers have presented full automatic and hybridized MRI image segmentation model. Lu et al. used an improved region growing algorithm initialized by the QMC method for liver segmentation. In their turn, W. Y. Zhanfang, and Hongbiao used an improved PCNN method to perform automatic segmentation. However, their method was not applied for the segmented more complex areas. Kuwazuru et al. used hybrid method by combining ANN with the level-set method for segmentation of multiple sclerosis lesion (MS) of the brain. Their method is based on a concatenation of ANN and level set, but their method was unable to detect small areas. D. Veloz, and Allende used modified EM to segment MRI images.

In this paper, we employed enhancement and denoising filters to preprocess the image. Subsequently, we used the Kapur thresholding method to locate the region of interest (ROI). Then, we applied the quasi Monte Carlo method to generate a large number of seeds (Quasi Random Sampling). These seeds were grouped into k classes using an improved version of the K-means method, referred to as constrained K-means, where the spatial dependency of the samples is taken into account. The classification is established within a Naive Bayesian framework. After selecting the optimal seed for each cluster, we initialize our improved region-growing approach.
Our approach is structured around three primary stages: preprocessing, localization, and segmentation and recognition. Initially, we employed the deformable model proposed by Rifai et al. to remove the kull. Subsequently, we applied contrast enhancement to accentuate high-frequency regions using sigmoid filtering, as outlined in the work by Lu et al.
Subsequently, we employed the thresholding method based on the Kapur algorithm [3] to isolate the tumor region, which stands out due to its enhanced color. We computed the entropies of the object HROI and the background HBg. Next, we applied morphological processing to decrease the number of connected regions. Afterward, we labeled regions consisting of connected pixels and identified the region with the highest pixel count as the Region of Interest (ROI).
We introduce a new segmentation approach comprised of three pivotal steps, which is an improved iteration of the method proposed before. The initial step involves seed generation, followed by seed clustering into k-classes in the subsequent step. Ultimately, the multi-segmentation is executed after the optimal seeds are selected. The strength of the constrained k-means method lies in its capacity to consider neighboring pixels during the classification process, in contrast to the EM algorithm. This characteristic contributes to a more homogeneous classification.
The objective of the Quasi Monte Carlo method is to generate a discrepancy sequence of pixels L in our Region (ROI). To ensure the good coverage of the ROI, we generated the sequence in a rectangle (referenced as RECT) that covers the area.
We employed a statistical method to partition the subset S l into k classes denoted as Ci, where i = 1, . . . , k. This clustering process enabled the creation of pixel subsets corresponding to distinct regions within our Region of Interest (ROI). To achieve this, we utilized the constrained k-means algorithm within a naive Bayesian framework. Notably, this algorithm excels in providing optimal classification by incorporating neighboring pixel information. To further enhance the effectiveness of these classes, the constrained k-means algorithm initializes the parameter vector with the state n, and subsequently, we maximize the `a posteriori probability to estimate the new state class parameters (n + 1).
For multi-segmentation, we employed an innovative approach by initializing the region-growing method with a hybrid technique combining K-means clustering with a Naive Bayesian approach. To further refine our results, we maximized the a posteriori probability through an Iterated Conditional Mode approach, and improved the region growing process by incorporating a Quasi Monte Carlo sampling method.
The outcomes of our study have demonstrated impressive performance, suggesting that our approach has the potential to replace conventional techniques for brain tumor detection. The combination of image enhancement, advanced segmentation, and probability maximization contributes to the robustness and accuracy of our method, making it a promising advancement in the field of medical image analysis.

**References**

[1] B. Hachemi, Z. Chama, Fully automatic multisegmentation approach for magnetic resonance imaging brain tumor detection using improved region-growing and quasi-monte carlo-expectation maximization algorithm., *Int. J. Imaging Syst. Technol, Wiley*. 30 (1) (2020) 104–111.
[2] Z. Muda, M. Warusia, S. md, nasir, U. Nur, Izura, K-means clustering and naive bayes classification for intrusion detection., *Journal of IT in Asia* 4 (1) (2016) 13–25.
[3] MICCAI BraTS Database 2015, http://braintumorsegmentation.org/, [Online; accessed 29-November-2016] (2015).
[4] B. H. Menze, A. Jakab, S. Bauer, J. Kalpathy-Cramer, K. Farahani, J. Kirby, Y. Burren, N. Porz, J. Slotboom, R. Wiest, et al., The multimodal brain tumor image segmentation benchmark (brats), *IEEE transactions on medical imaging* 34 (10) (2015) 1993–2024.

# Phase Less Image Reconstruction

**BAGDAOUI Amina[1], BENDAOUDI Amina[1] and Ali Djafari [2]**

*1: LEPO Laboratory, Department of Electronics, Faculty of Electrical Engineering*
*Djillali Liabes University, Sidi Bel-Abbes, Algeria*
*2: CNRS, SUPELEC, Paris, France*
*Email : bagdaoui.amina@outlook.fr (Corresponding author's email)*

**ABSTRACT**
The phase retrieval problem is a challenging issue in image processing, which aims to reconstruct an object from magnitude-only measurements in the Fourier domain. Most methods for phase retrieval are deterministic frameworks, and their results are often unsatisfactory when the available measured spectrum magnitude is corrupted by additive noise. The a priori knowledge characterizing the object is the finite number of homogeneous materials that compose it. This knowledge is represented by a Gauss-Markov prior. Iterative joint reconstruction and classification techniques are used to calculate a satisfactory reconstruction. The reconstructed image is obtained by first specifying the a posteriori distributions of all the unknowns, followed by the application of the Gibbs sampling algorithm to estimate the posterior mean of the unknowns. Simulation results are presented to demonstrate the accuracy of the proposed prior compared to the case where only the Potts-Markov prior is used.

**Keywords:** Phase retrieval, Fourier Synthesis (FS), Inverse Problems, Bayesian estimation, Hidden Markov

For many years, the phase retrieval problem, which involves reconstructing an object solely from its spectral magnitude in the Fourier domain, has been a significant and long-standing challenge. Several optical detection techniques, including coherent diffraction imaging (CDI), face the challenge of not being able to directly measure the phase of a light wave. The sensors used in these techniques only record the magnitude of diffracted rays while losing the phase information. However, the phase is essential for inverting the 2D Fourier transform and reconstructing the image accurately. This problem arises in various applications including X-ray crystallography, diffraction imaging, acoustics, optics, astronomy, and quantum mechanics. The primary objective of this task is to determine a method for retrieving the missing phase information from the measurements, which is challenging to obtain. The ultimate goal is to recover the unknown object using only the intensity of the measurements (spectrum magnitude). In this paper the aim of the image reconstruction task is to recover the original image denoted as f(r), where $r \in R^2$ from the noisy magnitude of its Fourier transform represented as g(ω), where $\omega \in R^2$. The reconstruction process relies on the known a priori information about the image.
we employ a Bayesian approach to quantitatively reconstruct homogeneous multi-material image from their spectral magnitude measurements in the Fourier domain, even in the presence of incomplete data. The proposed method in our study utilizes a non-linear frequency domain observation model. Specifically, we employ a Bayesian approach with a stochastic framework. It is important to note that if we assume an image with r pixels in the spatial domain belongs to a finite lattice R, the lattice will consist of n pixels. We consider a discrete lattice with a length of N. In the subsequent equations, vector notation will be employed. The approach introduce a Bayesian framework to handle a priori models for the pixel distribution of the desired image results. It is founded on the assumption that the reconstructed image consists of homogeneous materials. Consequently, the a priori probability distribution of the pixels is modeled using a Finite Mixture Model (FMM), enabling classification into a finite number of classes through a Potts Markov Model (PMM)

for labels. The Potts Markov Random Field (MRF) is utilized to model the spatial relationships and dependencies between neighboring pixels. It promotes smoothness and encourages similarity between adjacent pixels within the same class.
Additionally, a new Gauss-Markov a priori model is introduced to capture pixel dependencies within each class specifically. This model assumes that the pixel values within a class follow a Gaussian distribution, and the dependencies between pixels within the same class are described by a Markov property. This enables the model to capture fine-grained details and dependencies within individual classes while maintaining the global spatial coherence imposed by the Potts MRF. The combination of the FMM, Potts MRF, and Gauss-Markov a priori model provides a comprehensive framework for capturing both global and local characteristics of the image, allowing for more accurate and realistic pixel distributions and dependencies within the image. The effectiveness and accuracy of the proposed framework can be demonstrated, showing its ability to achieve high-quality reconstructions and preserve the characteristics of the original image.
This technique is used in microwave imaging, x-ray tomography, .....

**References**

[1] Romain Arnal. Aspects of Phase Retrieval in X-ray Crystallography, *Thesis, University of Canterbury, Christchurch, New Zealand*, 2019.
[2] Tatiana Latychevskaia. Iterative phase retrieval in coherent diffractive imaging: practical issues, Applied Optics 57(25), 7187 - 7197, 2018.
[3] Hui-ping Li, Song Li. Phase retrieval with PhaseLift algorithm, *Applied Mathematics*, 35, 4: 479-502, 2020.
[4] Jian-Wei, LiuZhi-Juan, CaoJing LiuShow, Long-Chuan Guo. Phase Retrieval via Wirtinger Flow Algorithm and Its Variants, *Conference: 2019 International Conference on Machine Learning and Cybernetics (ICMLC)*, July 2019.
[4] Praneeth Netrapalli, Prateek P JainPrateek P Jain, Sujay Sanghavi. Phase Retrieval Using Alternating Minimization, *IEEE Transactions on Signal Processing*, 63, 18, 2013.

# Quasi Random Sampling sequences and Improved Region Growing for the Classification of Tumor in MRI image

**BOUCENNA Sidahmed[a], BAGDAOUI Amina[a], HACHEMI Belkacem[b] and CHAMA Zouaoui[a]**
*a Optronic and Photonics Laboratory University of Djillali Liabes, Sidi Bel Abbes, Algeria*
*b CDTA, Centre de Developpement des Techniques Avancées, Algiers, Algeria*
*Contact : sidahmedboucenna97@gmail.com*

## ABSTRACT

In order to improve the accuracy of the medical image segmentation and reduce the effect of selecting seed points using region growing algorithm, A comparison of 03 quasi-Random sampling methods is presented in this paper for generating low-dispersion sequences points in the region of interest and the optical seed points are selected by computing these points in the goal to improved the region growing method. The aim of this article is to make a comparative study in terms of quality of tumor detection and classification in MRI image between 03 quasi random sampling to obtain numerical sequences (Halton, Sobol and Hammersley) coupling with the region growing method to achieve quasi-random numbers with a low discrepancy instead of the pseudorandom sequence of Monte Carlo. Somme performances results of these three methods are presentedin the way to choose the best one in the detection and classification procedure.

**Keywords:** Halton sequence, Sobol sequence, Hammersley sequence, Quasi-Monte Carlo, region growing.

## I. INTRODUCTION

the Monte-Carlo method aims to speed up the rate of convergence by decreasing the constant using pseudo-random sequences [2]. An alternative approach is to change the sequences into quasi-random numbers. These numbers are correlated to intentionally make them more uniform than "pure" random sequences. The d-dimensional Halton sequence is a low-discrepancy sequence obtained from the 1-dimensional Van Der Corput sequence, The Halton and Hammersley sequences are two closely related sets of low-discrepancy points, both are based on a construction called the radical inverse. In opposition to Halton and Hammersley, each dimension of the Sobol sequence consists of a radial inversion of base 2. The comparison between these three methods has been established According to many criteria. The region of interest (tumor) will be filled by theses 3 sequences after the region growing is started [1] until the classification is achieved. see figure.1.(MRI of a human head with tumor).

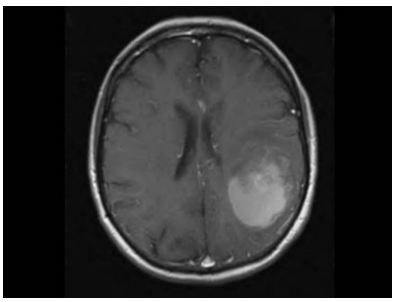

*Fig. 1. MRI image of a human head with tumor*

## II. COMPARISON:

### A. Comparison of results by exclusion time:

According to the following vertical chevron list, it can be seen that the execution time of the Sobol sequence is smaller than the execution time of Halton and Hammersley, because the number of computations in the Sobol sequence is minimal compared to the number

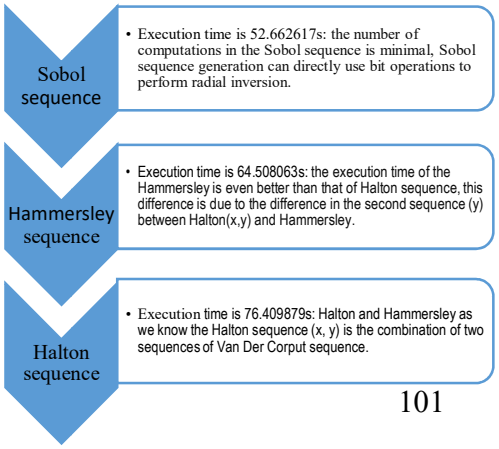

of computations, sobol sequence generation can directly use bit operations to perform radial inversion, which is very efficient. We notice that the execution time of the Hammersley is even better than that of Halton sequence, this difference is due to the difference in the second sequence ($y$) between Halton and Hammersley as we know the Halton sequence ($x$, $y$) is the combination of two sequences of Van Der Corput sequence; one a coordinates ($x$) and the second coordinates (y), the hammersley sequence is identical with halton sequence except in the second coordinates we attribute $n/N$, for: $n$ = 1, 2, .. and $N$ is a different number of samples.

### B. Comparison of results by convergence graph:

The three graphs represent the convergence of the logarithmic probability of the existence of a pixel variation as a function of the number of iterations The first curve using Halton sequence is convex and starts with 0.117 and increases rapidly between [0 3.50] to 0.125 then it grows uniformly between [3.50 90] to the value 0.137 then it increases slowly to its convergence point 0.1390 where it stabilizes.

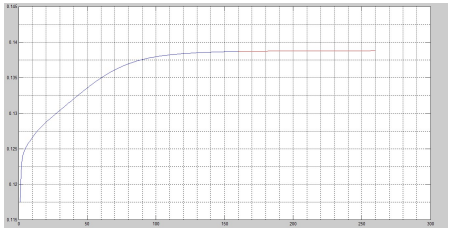

*Fig. 2. Convergence graph using Halton sequence*

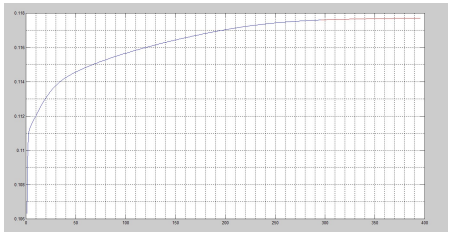

*Fig.3. Convergence graph using Hammersley sequences*

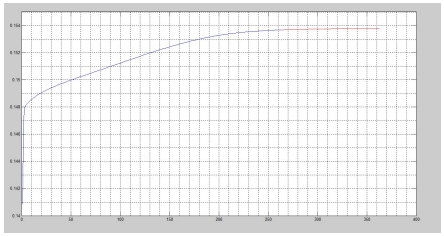

*Fig. 4. Convergence graph using Sobol sequence*

### C. Comparison of results by distribution of points:

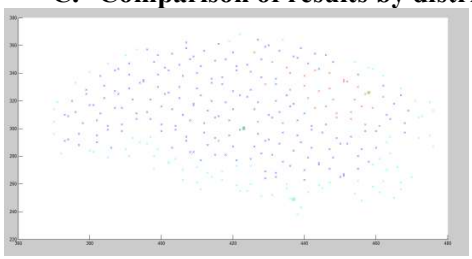

With Sobol sequence, the points are distributed in the in the region of interest (tumor region) with a minimal time compared to the two other sequences.

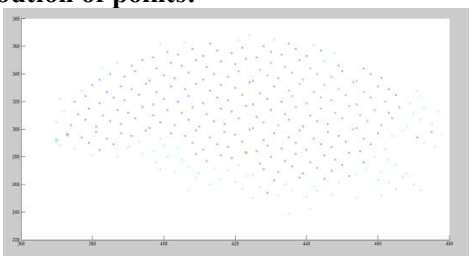

With Hammersley sequence,the distribution of points with this sequence is uniformly distributed compared to Halton and Sobol sequences.

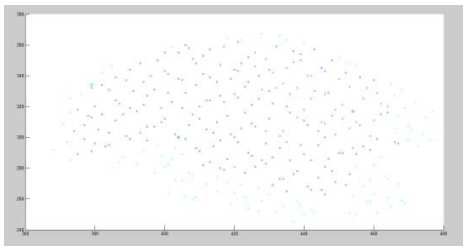

With Halton sequence, the distribution are in accordance with the expected results better then the two others so the distinction of the brain tumor is very clear.

## III. CONCLUSION:

The results presented that the sequences achieved from three quasi random sampling methods are very representative and each from them is characterized by an advantage; for the execution time of the program with the sequence of Sobol is the least, the sequence of Hammersley is characterized by its uniform points, while for the sequence of Halton has the most reliable results compared to the other sequences. In the future we will improved region growing algorithm for segmenting and detecting tumor in MRI image by using three Quasi random sampling sequence and compared with the traditional region growing method.

## IV. REFERENCES:

[1] B. Hachemi, Z. Chama, International Journal of Imaging Systems and Technology,(2020).
[2] B.MANGA, an intermediary between deterministic and Monte-Carlo methods,(2021).

# Gas Detection System: Combining Sensor Technology and Machine Learning for Precise Gas Classification

**B. ERROUANE[1], Z. MAHDJOUB[1], M. CHIKR EL MEZOUAR[2]**
[1]*Laboratory of Electromagnetism, Photonics, and Optoelectronics, Djillali Liabes University, Sidi Bel-Abbes, 22000, Algeria*
[2]*Communication Networks, Architectures and Multimedia (RCAM)Laboratory, Djillali Liabes University, Sidi Bel-Abbes, 22000, Algeria*
*Email: errouanebadiaa@gmail.com*

## ABSTRACT

This study explores the application of electronic sensors and machine learning algorithms in the development of a reliable and accurate gas detection system. The results demonstrate the differentiated sensitivity of certain sensors to specific types of gases. The MQ9 and MQ4 sensors showed the best performance in detecting ethanol, acetone, and alcohol. Moreover, the Random Forest model proved to be the most effective in classifying different types of gases. This research has significant implications for improving industrial safety, monitoring air quality, and reducing risks associated with the emission of harmful gases in various environments such as perfumery, industry, healthcare facilities, etc.

**Keywords:** Electronic sensors ; Machine learning; Detection system; Sensitivity; Performance; Random Forest.

## INTRODUCTION

Ethanol, alcohol, and acetone represent flammable and toxic substances that can be present in various contexts. Their emission can come from medical equipment, cleaning products, chemical substances, etc. Prolonged exposure to these gases can cause health problems for workers, such as eye, skin, and respiratory irritation, as well as central nervous system alterations. Therefore, carefully monitoring the concentration of these gases in these environments is crucial for preventing health risks. The detection of gases is essential in numerous fields, including industrial safety and air quality monitoring, especially in healthcare facilities. The goal of this research was to develop a reliable and accurate gas detection system by combining electronic sensors with machine learning techniques.

## MATERIALS AND METHODS

The sensors MQ2, MQ4, MQ9, and MQ135 were used to evaluate their response towards three distinct gas sources: ethanol, acetone, and alcohol. The primary objective was to classify these different types of gases using machine learning algorithms and determine the most performing sensor for each gas. To conduct these experiments, we carried them out in our laboratory, where no gas source was present. We set up an electronic circuit consisting of five sensors (MQ2, MQ4, MQ9, MQ135, and DHT11) connected to an Arduino Mega board. These sensors were exposed to the three gas sources and ambient air, with variations in distance between the sensors and the gas sources ranging from 0 to 60 centimeters in 5-centimeter increments. Prior to data collection, a 30-minute stabilization period in ambient air was conducted to ensure a stable base. In total, 12,743 data points were collected (air: 1,026, alcohol: 3,956, ethanol: 3,883, acetone: 3,878) and recorded in a CSV file. These data were used to train three machine learning models (Random Forest, Support Vector Machine, and k-Nearest Neighbors), taking into account the specific responses of each sensor.

### Results

The results obtained showed a differentiated sensitivity of the sensors to specific types of gases. As shown in Figure 1, for ethanol, the MQ9 sensor showed the greatest reactivity, followed by MQ4 and MQ135. Regarding alcohol, the MQ4 and MQ9 sensors were the most suitable, while for acetone, the MQ9 sensor demonstrated the highest reactivity,

followed by MQ4 and MQ135. Table 1 summarizes the accuracy of each machine learning model used in this study, highlighting that the Random Forest model showed the best precision (99.99%) for gas classification.

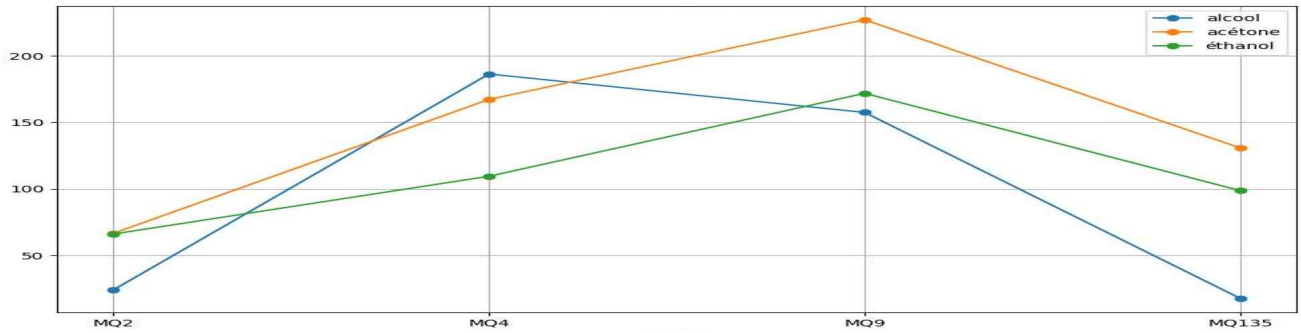


*Figure 1 Reactivity of Sensors to Different Gases*

| Algorithms | k-Nearest Neighbors | Random Forest | Support Vector Machine |
|---|---|---|---|
| Average accuracy (%) | 97.41 | 99.99 | 82.83 |
| Accuracy on the test set (%) | 97.21 | 100 | 82.34 |

*Table 1 Accuracy of Machine Learning Models for Gas Classification*

## CONLUSION

This study successfully achieved the selection of sensors specifically designed for the detection of various gases, highlighting their unique reactivity towards different types of gases. Moreover, the Random Forest model emerged as the best option for classifying these diverse gases. The implications of this research are numerous, including the improvement of industrial safety, monitoring of air quality in various environments where these gases may be present, and reducing risks associated with the emission of these three hazardous gases. This study also contributes to the advancement of gas detection technologies, opening up new perspectives for more accurate and reliable applications.

## REFERENCES

[1] S. Feng, F. Farha, Q. Li, Y. Wan, Y. Xu, T. Zhang, H. Ning, Review on smart gas sensing technology,19 (2019)3760.

[2] S. Chen, J. Ren, Y. Yan, M. Sun, F. Hu, H. Zhao, Multi-Sourced sensing and support vector machine classification for effective detection of fire hazard in early stage, 101 (2022) 108046.

[3] D. Sales-Lérida, A.J. Bello, A. Sánchez-Alzola, P.M. Martínez-Jiménez, An approximation for Metal-Oxide sensor calibration for air quality monitoring using multivariable statistical analysis, 21 ( 2021) 4781.

[4] J.A. Cavalcante, G.I. Gadotti, A.H.M. da Silva, Á.S. Araújo, R.C.M. Monteiro, D.M. de Moraes, Development of an ethylometer with an MQ-3 sensor for measuring ethanol in soybean seeds, 26 (2022) 374-380.

# A new approach for MRI Brain Tumor Segmentation based on Generalized Gaussian Mixture Model and EM algorithm

**Khalil Ibrahim LAIREDJ*[1], Amina BAGDAOUI [1], Sid Ahmed BOUCENNA [2] and Zouaoui CHAMA[1]**
[1]*LEPO Laboratory, Electronic Department , University of DJillali Liabes, S.B.A., Algeria.*
*Email: lairedjkh@gmail.com*

**ABSTRACT**

Image segmentation plays a crucial role in the domain of medical science, as it facilitates the extraction, analysis, and interpretation of distinctive features. Particularly, the segmentation of brain tumors poses significant challenges, prompting prior researchers to propose both semi automatic and fully automatic methodologies for this purpose. In the current study, we introduce a novel automatic approach that combines the utilization of thresholding and the generalized Gaussian mixture model, employing the EM algorithm, to effectively carry out brain tumor seg mentation using MRI histogram data. Our proposed method effectively separates the tumor area using a thresholding technique, followed by applying the generalized Gaussian mixture model to classify the different regions of the tumor. To assess the performance of our approach, we carried out a thorough analysis using ground truth pre-segmented images as a reference. The results re vealed that our method exhibits exceptional performance in terms of tumor region detection, as indicated by high values for various metrics such as Dice coefficient, sensitivity, accuracy, speci ficity, and precision. To validate our methodology, we utilized a dataset comprising of five distinct patient MRIs, which were randomly selected. The Flair MRI modality was utilized for threshold ing, while the T1ce MRI modality was employed for segmentation. The obtained results exhibit promising outcomes, signifying successful tumor region detection and segmentation..

**Keywords:** Brain tumor ; MRI ; EM algorithm ; GGMM ; Segmentation.

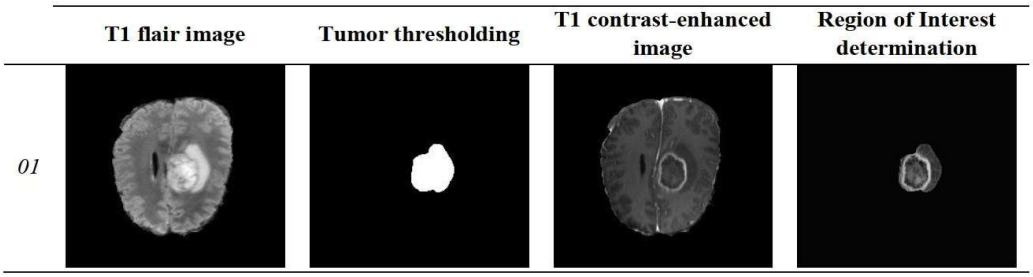


*Figure 1 : Results of the preprocessing step for the first image*

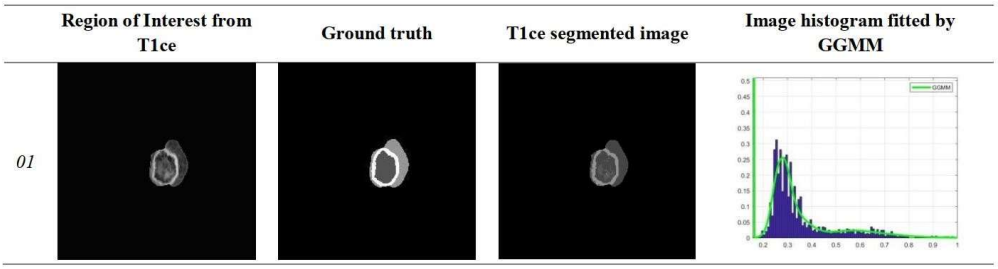


*Figure 2 : Results of the processing step for the first image*

**References**

[1] T.O. Seeyou, N.X. May, I.N. Kyoto, Hope. For. Success, 5 (2016) 22.

[1] N. Gordillo, E. Montseny, and P. Sobrevilla, Oct. 2013.State of the art survey on MRI brain tumor segmentation, Magnetic Resonance Imaging, vol. 31, no. 8. (pp. 1426–1438), Oct. 2013.

[2] [E. Abdel-Maksoud, M. Elmogy, and R. Al-Awadi, 2015, Mar.Brain tumor segmentation based on a hybrid clustering technique, Egypt. Informatics J., vol. 16, no. 1, (pp. 71–81),

[3] S. Bakas et al., 2017, Sep. .Advancing The Cancer Genome Atlas glioma MRI collections with expert segmentation labels and radiomic features, Sci. Data, vol. 4,

[4] B. Hachemi et al., 2020, Mar. .Fully automatic multi-segmentation approach for magnetic resonance imaging brain tumor detection using improved region-growing and quasi-Monte Carlo-expectation maximization algorithm, Int. J. Imaging Syst. Technol., vol. 30, no. 1, (pp. 104–111),

[5] M. Havaei et al., 2017, Jan. .Brain tumor segmentation with Deep Neural Networks, Med. Image Anal., vol. 35, (pp. 18–31),

[6] N. Nacereddine et al., 2009, .L'algorithme EM et le Modèle de Mélanges de Gaussiennes Généralisées pour la Segmentation d'images. Application au contrôle des joints soudés par radiographie, 2009, .

[7] O. M. M. Mohamed and M. Jaïdane-Saïdane, Aug. 2009.Generalized Gaussian mixture model, in 2009 17th European Signal Processing Conference, Aug. 2009, (pp. 2273–2277).

[8] T. M. Nguyen, Q. M. Jonathan Wu, and H. Zhang, 2014, Bounded generalized Gaussian mixture model, Pattern Recognit., vol. 47, no. 9, (pp. 3132–3142),

[9] N. Nacereddine, S. Tabbone, D. Ziou, and L. Hamami, 2010.Asymmetric generalized Gaussian mixture models and EM algorithm for image segmentation, in Proceedings - International Conference on Pattern Recognition, 2010, (pp. 4557–4560).

[10] T. M. Nguyen, Q. M. J. Wu, D. Mukherjee, and H. Zhang, 2014, .A Bayesian bounded asymmetric mixture model with segmentation application, IEEE J. Biomed. Heal. Informatics, vol. 18, no. 1, (pp. 109–119),

[11] U. Baid et al., 2021, Jul. .The RSNA-ASNR-MICCAI BraTS 2021 Benchmark on Brain Tumor Segmentation and Radiogenomic Classification,

[12] B. H. Menze et al., 2015, Oct. .The Multimodal Brain Tumor Image Segmentation Benchmark (BRATS), IEEE Trans. Med. Imaging, vol. 34, no. 10, (pp. 1993–2024),

[13] A. Tiwari, S. Srivastava, and M. Pant, 2020, Mar. .Brain tumor segmentation and classification from magnetic resonance images: Review of selected methods from 2014 to 2019, Pattern Recognit. Lett., vol. 131, (pp. 244–260),

[14] J. K. Ruffle, S. Mohinta, R. Gray, H. Hyare, and P. Nachev, 2023, Mar.Brain tumor segmentation with incomplete imaging data, Brain Commun., vol. 5, no. 2,

[15] K. C. Patra, M. Panigrahi, S. K. Mahapatra, and M. Samantaray, Aug. 2016.An Enhanced BE-GGMM-EI Algorithm for Medical Image Denoising, in Proceedings - International Conference on Computational Intelligence and Networks, Institute of Electrical and Electronics Engineers Inc., Aug. 2016, (pp. 57–62).

[16] K. H. Zou et al., 2004, Feb. .Statistical validation of image segmentation quality based on a spatial overlap index1, Acad. Radiol., vol. 11, no. 2, (pp. 178–189)

# New approaches to miniaturizing microwave filters inspired by ordinary and complementary metamaterial resonators in taper

**Ahmed Yacine Rouabhi[1], Mohammed. Berka[2], Zoubir. Mahdjoub[1]**

*[1] Electronic Department, Sidi Bel Abbes University, University Compus 3000 Teaching Places, Sidi Bel Abbes, 22000 Algeria*
*[2]Electrical Engineering Department, Mustapha Stambouli University , Science and Technology Faculty, Mascara, 29000 Algeria*
*Email : rouabhi.yacine95@gmail.com*

**ABSTRACT**

The filter function is very much needed in the microwave domain (3-300 GHz), and was first used in the early 1950s by a group of researchers at Stanford University [1]. This filter function is of great value for improving microwave applications such as radar systems, modern telecommunication systems and medical systems. Because of its interest and multifunctional use in most of these systems, research is progressing and the common objective of this work is to optimize the electrical qualities of microwave filters. Nowadays, the problem of filter size and volume remains the major constraint. In practice, when a microwave filter is built, the loss-increasing factor will always appear as the major threat, especially for the miniaturization procedure. After 15 years of using microwave filters, and with the proposed solutions for minimizing losses, physicist Victor Veselago first developed the concept of a much-needed material called metamaterials [2].
One of the most widely used methods for miniaturizing microwave filters is the use of ordinary and complementary tapered metamaterial resonators (SRR).
In our work, we use the 3D Modeler of the high-frequency structure simulator ( HFSS) to design a bandpass filter inspired by symmetric tapred split ring resonator.
The diagram of the prospective structure is shown in figure 1 and Figure 2 shows the filter response obtained after simulation of our structure.

**KEYWORDS :** microwave filter; metamaterial; SRR; taper; HFSS

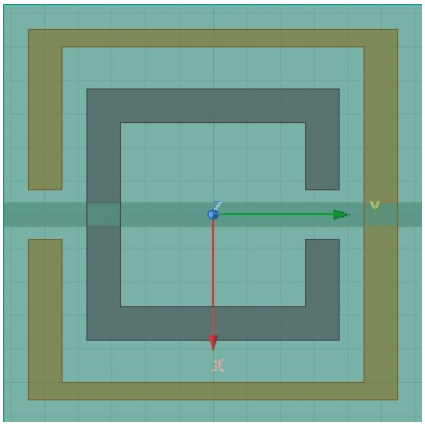

*Figure 1. Representation in ring of the proposed sysmmetric tapred split ring resonator*

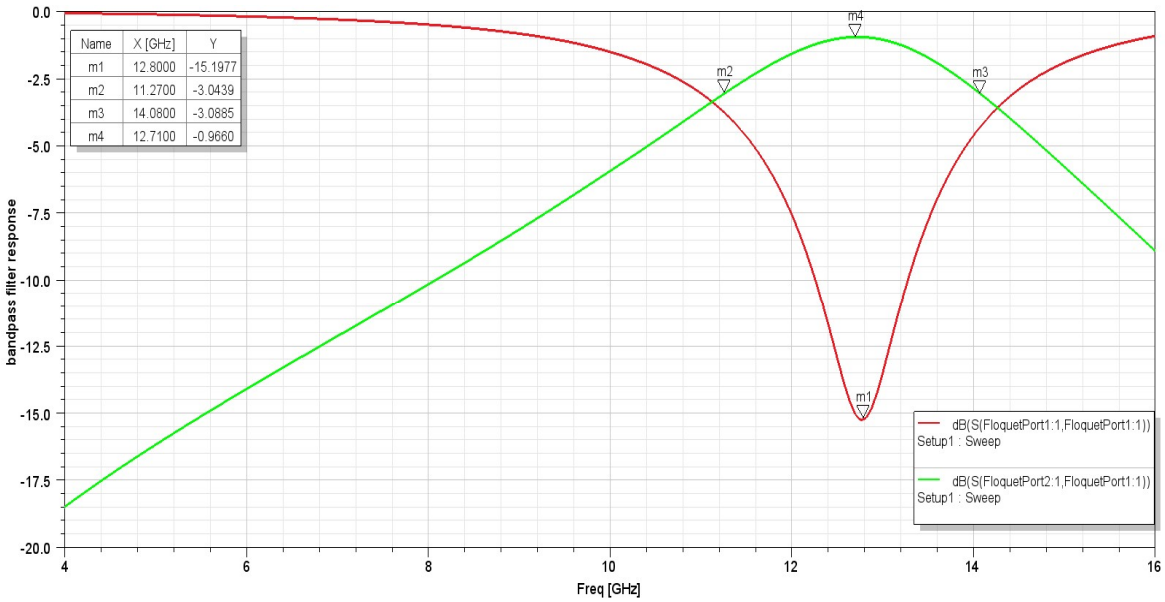


*Figure 2. bandpass filter response*

**References**

[1] *Pozar, David M. Microwave Engineering. Hoboken, NJ :Wiley, 2012.*
[2] Veselago V G 1968 Sov. Phys. Uspekhi. 10 509.

# A NEW Design of BSF Using Complementary Split Ring Resonator For spatial application

**Abdelkader Serhane[1], Dr. Mohammed Berka[2], Dr. Zoubir Mahdjoub[3]**

[1] *phD, Networks and telecommunications University of Mascara, Algeria*
[2] *Professor, Department of electrical engineering, University of Mascara,. Algeria*
[3] *Professor , Laboratory E.P.O, University of Sidi-Bel-Abbes, Algeria*
*Contact: abdelkader.serhane@univ-mascara.dz*

**ABSTRACT**

.

In recent years, new materials called (meta-materials) have features that allow developing new microwave components for new applications. In the literature, various types of reconfigurable band stop filters were proposed .

This article proposes a new Design of microwave band-stop filter use of complementary split ring resonator CSRRs. The structure is composed of a modified micro-strip line in the center and two unit cells The CSRRs modified are etched on the ground plane symmetrically in the center.

This work is a contribution that can subsequently design a new class of sensors which are miniaturized microwave biosensors capable of. detecting and characterization of unknown physical properties .

The simulation was performed using Ansoft HFSS (High Frequency Structure Simulator).

**Keywords:**Single; band-stop-filter,Micro-strip,Metamaterial, Complementary split ring resonator (CSRR),HFSS

**References**

[1] Lee, K., T.-H. Lee, et al., "Reconfigurable dual-stopband filters with reduced number of couplings between a transmission line and resonators" , IEEE MWCL , Vol. 25, No. 2, 106–108, 2015.

[2] Lee, K., T.-H. Lee, et al., "Reconfigurable dual-stopband filters with reduced number of couplings between a transmission line and resonators" , IEEE MWCL , Vol. 25, No. 2, 106–108, 2015.

[3] Khelil Fertas "Design and Development of Compact Reconfigurable Tri-Stopband Bandstop Filter Using Hexagonal Metamaterial Cells for Wireless Application ", Journal of Progress In Electromagnetics Research M, Vol. 80, 93–102, 2019.

[4] Becharef Kada "Design of Band-Stop Filter Composed of Array Rectangular Split Ring Resonators", Journal of Nano- and Electronic Physics · January 2018.

[5] Badr Nasiri "Microstrip band-stop filter based on double negative metamaterial", International Journal of Electrical and Computer Engineering(IJECE)Vol.12,No.2,DOI:10.11591/ijece.v12i2.pp1579-1584, April2022.

[6] Mustafa K. Taher Al-Nuaimi "Compact microstrip band stop filter using SRR and CSSR: Design, simulation and results ,"Conference paper , may 2010

[7] Badr Nasiri " A Miniature Microstrip BSF Using Complementary SplitRing Resonator", International Journal of engineering intelligent systems January 10, 2018.

[8] Michel A. Abaga Abessolo" Application d'une structure métamatériau sous forme triangulaire pour la réalisation de Filtres Coupe Bande ", Mediterranean Telecommunication Journal vol. 3, n°2, july 2013 .

[9] Michel Le Coq " Miniaturisation de filtres hyperfréquences par l'utilisation de substrats à forte permittivité", 17èmes Journées Nationales Microondes , BREST ,18-19-20 Mai 2011.

# Biosensors Using Electromagnetic Coupling of Band Stop Filter and CSRRs for Applications in Medical

**Abdelkader Serhane[1], Mohammed Berka[2], Zoubir Mahdjoub[3]**

[1] *phD, Networks and telecommunications University of Mascara, Algeria*
[2] *Professor, Department of electrical engineering, University of Mascara,. Algeria*
[3] *Professor , Laboratory E.P.O, University of Sidi-Bel-Abbes, Algeria*
*Contact: abdelkader.serhane@univ-mascara.dz*

**ABSTRACT**

In this work, we will propose a new class of sensors which are the miniaturized microwave biosensors capable of detecting solids and liquids of unknown physical properties.

This genre of sensor (effective in the field of medicine) is based on the effect of electromagnetic coupling between microwave filters band stops and metamaterial resonators (with the exception of (CSRRs)). The band-stop filters thus constituting the biosensors proposed make it possible to eliminate unwanted harmonics.

Once that we will be able to determine the overall shape of each biosensor (Filter+ (CSRRs)), we will place the materials under test in the place of the biosensor where the electric field (mode fundamental at resonance) will be maximum. This step will help us apply the technique of resonant disturbance which allows us then to detect the value of the permittivity of each material.

Desired results can subsequently offer factors of qualities and also high sensitivities for our biosensors, which makes them very effective for disease detection. For justify our results, we will do simulations using the software Commercial Ansoft HFSS..

**Keywords:** Band-Stop-Filte, Biosensor, Complementary split ring resonator (CSRR), Metamaterial.

**References**

[1] Tao Chen, Suyan Li ; Hui Sun. "Metamaterials Application in Sensing", Sensors Journal , 2012.
[2] KUMAR, D. Shashi; SUGANTHI, S. "Miniaturization of Microstrip Antenna with Enhanced Gain Using Defected Ground Structures. " International Conference on Data Science and Communication (IconDSC). IEEE, p. 1-5 , 2019.

[3] RAMBE, Ali Hanafiah, et al. " Miniaturization of rectangular patch microstrip antenna by using complementary

split ring resonator. In: IOP Conference Series: Materials Science and Engineering. IOP Publishing,. p. 012132, 2018.
[4] Salim, A; Lim, S. "Review of Recent Metamaterial Microfluidic Sensors". Sensors, 2018.
[5] Pozar, D.M. " Microwave Engineering; John Wiley & Sons, Inc.: Hoboken, NJ, USA; ISBN 97898965408213, 2012.
[6] Ebrahimi, A.; Scott, J.; Ghorbani, K. "Ultrahigh-Sensitivity Microwave Sensor for Microfluidic Complex Permittivity Measurement" . IEEE Trans. Microw. Theory Tech., 67, 4269–4277 , 2019.
[7] Ebrahimi, A.;Withayachumnankul,W.; Al-Sarawi, S.; Aboott, D. "High-Sensitivity Metamaterial-Inspired Sensor". IEEE Sens. J. 2014, 14, 1345–1351 , 2014 .[CrossRef]

[8] Rowe, D.J.; Abduljabar, A.A.; Porch, A.; Barrow, D.A.; Allender, C.J. "Improved Split-Ring Resonator for Micro Fluidic Sensing". IEEE Trans. Microw. Theory Tech., 62, 689–700 , 2014 .

[9] Abdolrazzaghi, M.; Daneshmand, M.; Iyer, A.K. Strongly Enhanced Sensitivity in Planar Microwave Sensors Based on Metamaterial Coupling". IEEE Trans. Microw. Theory Tech., 66, 1843–1855 , 2018.
[10] Galindo-Romera, G.; Javier Herraiz-Martínez, F.; Gil, M.; Martínez-Martínez, J.J.; Segovia-Vargas, D. "Submersible Printed Split-Ring Resonator-Based Sensor for Thin-Film Detection and Permittivity Characterization". IEEE Sens. J, 16, 3587–3596, 2016 .
[11] Su, L.; Mata-Contreras, J.; Vélez, P.; Fernández-Prieto, A.; Martín, F. "Analytical method to estimate the complex permittivity of oil samples". Sensors, 18, 984. 2018.
[12] Tanveerul Haq; Cunjun Ruan; Xingyun Zhang; Shahid Ullah. "Extremely Sensitive Microwave Sensor for Evaluation
of Dielectric Characteristics of Low-Permittivity Materials". Journal Sensors ; doi:10.3390/s20071916.2020.
[13] Ankit Singh,"Split ring resonator biosensor-an innovative design and analysis" , IEEE 8th International Conference on Photonics (ICP) , 2020.
[14] Tanveerul Haq," Rapid Design Optimization and Calibration of Microwave Sensors Based on Equivalent Complementary Resonators for High Sensitivity and Low Fabrication Tolerance" Journal Sensors ;doi:10.3390/s s23021044.20 23.
[15] Rammah Ali Alahnomi," Review of Recent Microwave Planar Resonator-Based Sensors: Techniques of Complex Permittivity Extraction, Applications, Open Challenges and Future Research Directions" Journal Sensors ;doi:10.3390/s s21072267.20 21.
[16] Ali Mohammed Albishi," Ultrasensitive Microwave Near-Field
Sensors For Detection, Imaging, and Material Characterization" thesis Doctor in Electrical and Computer Engineering;.20 18 .
[17] Ali Mohammed Albishi," A Novel Coupling Mechanism for CSRRs as Near-Field Dielectric Sensors" ;Journal Sensors ;doi :103.390 /s/s22093313.20 22.
[18] A. Zaheetha Banu ,"cancer detection using metamaterial biosensor in the terahertz regime" .Review Of Research UGC Approved Journal; No. 48514 ISSN: 2249-894X.2018.
[19] D.M. Pozar," Microwave Engineering" ;John wiley & sons Journal; 2011.
[20] ChandraR, ZhouH, Ba BalasinghamI," On the opportunities and challenges in microwave medical sensing and imaging" ; IEEE Trans Biomed Eng;62(7):1667–982; 2015.
[21] K.Abdesselama, C.Hannachia," A Non-Invasive Honey-Cell CSRR Glucose Sensor: Design Considerations and Modelling" ; Published by Elsevier Masson;doi.org/10.1016/j.irbm.2022.
[22] Ankit Singh , Alok RajK ," Split ring resonator biosensor-an innovative design and analysis" ; 2020 IEEE 8th International Conference on Photonics (ICP).2020.

# Reinforcement learning control for simple urban traffic isolated intersection

**Y. HASSANI and B. TOLBI**

*Department of Automatic, faculty of electrical engineering, University Djillali Liabes of Sidi Bel Abbes, Algeria*
*Email : youmvs98@gmail.com*

**ABSTRACT**

Machine Machine learning focuses on developing algorithms and models that allow computers to learn from data and make predictions or decisions without explicit programming [9], there are largely three broad recognized categories: supervised learning, unsupervised learning, semi-supervised learning, and reinforcement learning. In supervised learning, the machine receives the answer key and learns by finding correlations between all correct results. The reinforcement learning model does not include an answer key, but rather a set of allowed actions, rules, and potential end states. Reinforcement learning (RL) has received considerable contributions due to its successful application in several fields, including operations research, combinatorial optimization, information theory, simulation-based optimization, control theory and statistics.

**Keywords:** artificial intelligence; optimization; vehicle flow; urban traffic control.

In this work, the important model strengthening tools will be explained with the following steps: Firstly, we start with the hyper parameters, that is to say what are the important parameters which affect the change of model, next we explain the different types of reinforcement learning models with its algorithm, i.e. how to build these models. Finally, we will select and study a simple environment (isolated intersection) and analyze with the mentioned methods. After explanation, the results of a comparison study are presented.

In the first step of our work, a classical reinforcement-free method is used to learn how the time cycle affects traffic lights on a single isolated intersection (Figure.1). So we will set t = 35s to move vehicles from lane 1 and lane 3; then we set t = 45s to move vehicles from lane 2 and lane 4.

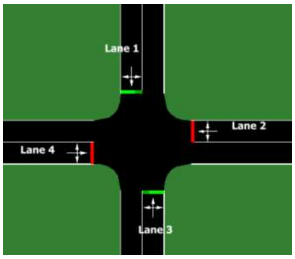


Fig.1. Four Lanes storages in isolated intersection.

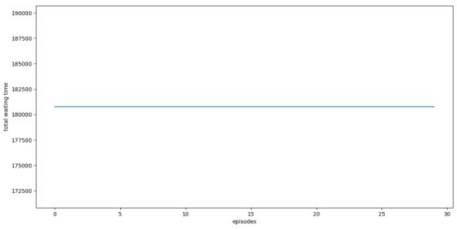

Fig.2. total waiting time per episode with traffic light classic method

So with this classic method there is a constant total waiting time which clearly means that we are using our environment with the same vehicles and the same traffic light actions for each episode.

Firstly, we define the number of vehicles for each lane, so in our simple environment (isolated intersection) we have 4 states. Secondly, we use all actions, so we have two actions (action 1 to move vehicles from lane 1 and lane 3), (action 2 to move vehicles from lane 2 and lane 4). Thirdly, we know the effect of Q learning on these hyper parameters (learning rate, Epsilon, discount factor and Q algorithm). We use our training with our parameters (Epsilon = 0.1; learning rate = 0.1; and discount factor = 0.98). After training our model with Q learning, figure 3 shows the total

waiting time for each episode, after that, a deep Q networks method is used by combining the Q target of the Bellman equation and neural networks using the same parameters as shown in figure 4.

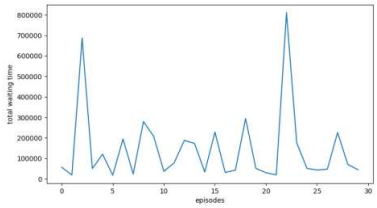


Fig.3. Total waiting time per episode with Q learning method.

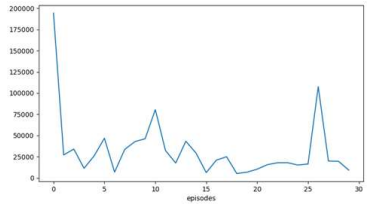


Fig.4. Total waiting time per episode with DQN method.

In the second part of this work, we have defined the same parameters as the previous section (DQN) and we applied a new DDQN algorithm as shown in figure 5. The results of comparative study of the developed agent using classical method, Q learning, DQN and DDQN are shonw in figure.6

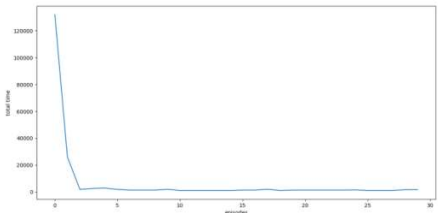

Fig.5. total waiting time per episode with DDQN method.

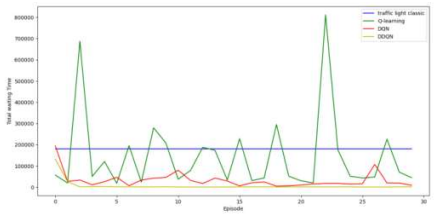


Fig.6. Comparison between traffic light classic, Q learning, DQN and DDQN.

Through innovations like experience replay, target networks, and loss functions, DQN has addressed longstanding challenges in RL, double DQN appears more robust to this more challenging evaluation, suggesting that appropriate generalizations occur and that the found solutions do not exploit the determinism of the environments.

The results show that the DDQN method is a more efficient agent for reducing urban traffic congestion for the selected environment (single isolated intersection).

**References**

[1] MyeongSeop Kim, Myoung-Su Choi, and Jae-Han Park, "Sensors | Free Full-Text | Adaptive Discount Factor for Deep Reinforcement Learning in Continuing Tasks with Uncertainty."
[2] Grokking Deep, "discount-factor in reinforcement-learning."
[3] baeldung, "Epsilon-Greedy Q-learning | Baeldung on Computer Science," Dec. 18, 2020.
[4] J. Brownlee, "Understand the Impact of Learning Rate on Neural Network Performance," *MachineLearningMastery.com*, Jan. 24, 2019.
[5] Q. T. Luu, "Q-Learning vs. Deep Q-Learning vs. Deep Q-Network | Baeldung on Computer Science," Apr. 10, 2023.
[6] Sammoud, Bassem. "Contribution à la modélisation et à la commande des feux de signalisation par réseaux de Petri hybrides," n.d.
[7] Yan, Fei. "Contribution of modelling and traffic control at intersections : Integration with the communication Vehicles-Infrastructure." Phdthesis, Université de Technologie de Belfort-Montbeliard, 2012.
[8] "Neural Network: Introduction to Learning Rate – Study Machine Learning."
[9] Nikita Duggal, "What is Artificial Intelligence? Types, History, and Future [2023 Edition] | Simplilearn," *Simplilearn.com*, Oct. 11, 2023.
[10] Mayank Banoula, "What is Q-Learning: Everything you Need to Know | Simplilearn," *Simplilearn.com*, Feb. 22, 2023.
[11] Thomas Simonini, "Improvements in Deep Q Learning: Dueling Double DQN, Prioritized Experience Replay, and fixed…," *freeCodeCamp.org*, Jul. 06, 2018.
[12] Everton Gomede, PhD, "Deep Q-Networks (DQN): Bridging the Gap between Deep Learning and Reinforcement Learning | by Everton Gomede, PhD | Sep, 2023 | Medium," Sep. 11, 2023.

# Effect of metallic contacts on Metal/InGaN Schottky Barrier Diodes

**Arbi Kada Benchiha[1], Ahmed Hichem Yahi [2], Arslane Hatem Kacha [3] and Macho Anani[1]**

*[1]Djillali Liabes University of Sidi Bel Abbes. 22000. Sidi Bel Abbes. Algeria.*
*[2]Materials Elaboration and Characterization Laboratory, Djillali Liabes University of Sidi Bel Abbes. 22000. Sidi Bel Abbes. Algeria.*
*[3]Applied MicroElectronics Laboratory. AMEL. Djillali Liabes University of Sidi Bel Abbes. 22000. Sidi Bel Abbes. Algeria.*

**ABSTRACT**

Metal/InGaN Schottky Barrier Diodes (SBDs) were designed by $N_2$ plasma nitridation of n-GaN (100) surface yielding to the formation of InGaN semiconductor device where the anode was made by a metal as different as gold, platinum, chromium, Aluminum, Silver, Cupper, Iron and Nickel, to give Schottky contacts on InGaN substrate.

Choice of these metals was in order to study the effect of work function on the Schottky contacts. The thickness was the same for all samples at an ambient temperature of 300K. The Metal/InGaN Schottky Barrier Diodes were electrically tested by Current–Voltage measurements in dark and room temperature.

Results show a strong dependence of electrical parameters and device performances on the chemical composition of the semiconductor surface and the quality of the Metal/Semiconductor interface. Changing the metal gave different threshold voltages. Electrical parameters gave different ideality factors "n", around 1.2, depending on the metal used. In another hand, electrical parameters do not varied remarkably with the increase of work function even in the case of a better fabrication process. Also, one factor, greatly depending on the work functions of different metals were Schottky Barrier Heights, and there, differences were really significant from one structure to another

**Keywords:**Nitride materials, Work function, Schottky Barrier Diode (SBD), Schottky Barrier Height (SBH).

**Main results.**

**Pt: WF = 5.3 eV**

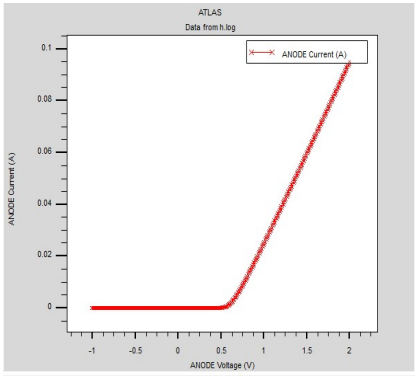


**Au: WF = 4.8 eV**

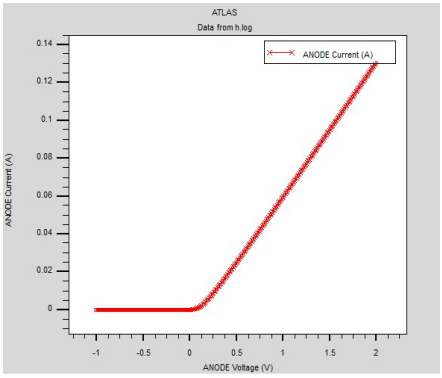


**Cr: WF = 4.6 eV**

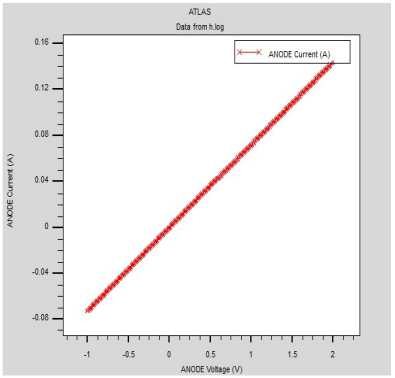


**Cu, Fe, Ni: WF = 4.4 eV**

**I(V) Characteristics**

**Al, Ag: WF = 4.8 eV**

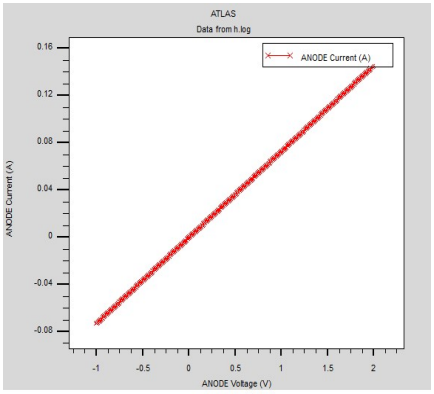


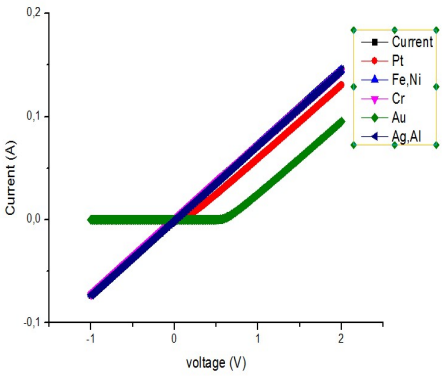


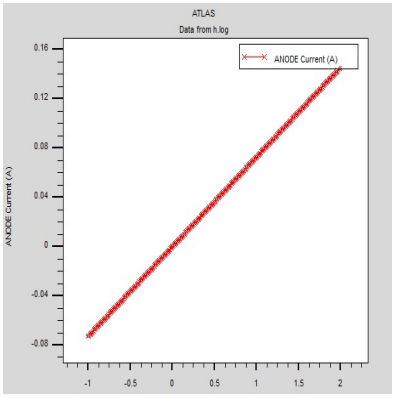


**Ln(I)-V Characteristic for Pt** **Ln(I)-V Characteristic for Au** **Ln(I)-V Characteristic for Cr**

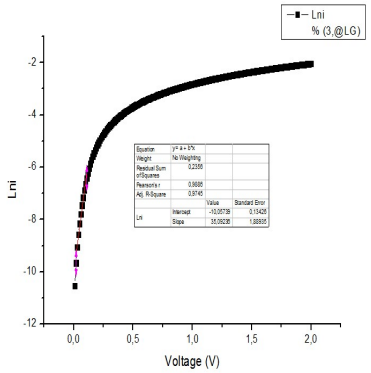


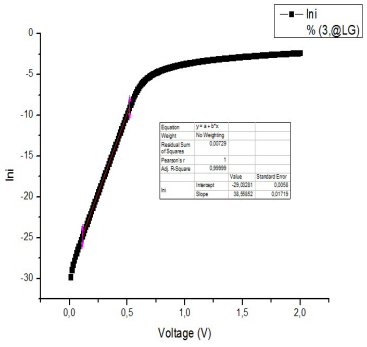


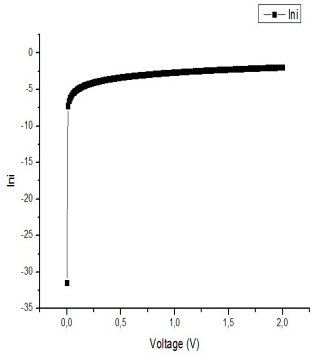


**Ln(I)-V Characteristic for Fe, Ni, Cu** **Ln(I)-V Characteristic for Al, Ag**

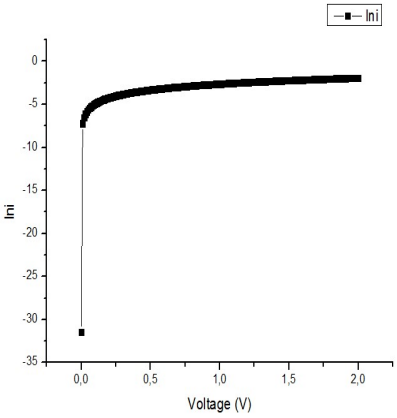


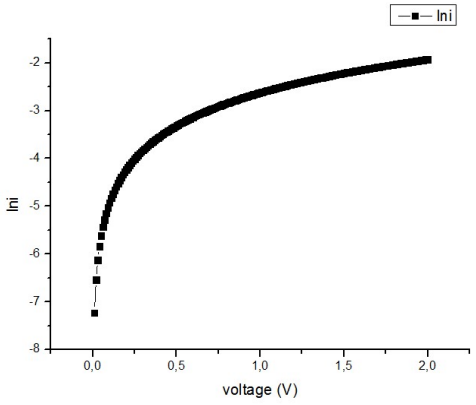


**References**

[1] Journal of Nanoelectronics and Optoelectronics, 14 (8) 1126-1132 (2019)

[2] J. Mater. Sci. Mater. Electron., 30 (8) 17032-17039 (2019) and 31 (2020)8033-8042.

[3] Physica B 576 (2020) 411733.

[4] Journal of Physics and Chemistry of Solids 148 (2021) 109758.

[5] Journal of Electronic Materials, https://doi.org/10.1007/s11664-020-08473-4.

# Station de Traitement d'Eau à l'ozone pour les Zones Isolées

**M. Belabed[1], S. Bechekir[1], M. N. Brahami[1], M. Jbilou[1], Y. Bouroumeid[1], Khelifi El Mabrouk[1], S. Nemmiche[2], M. Brahami[1]**

*[1]Laboratory: Intelligent Control and Electrical Power System ICEPS Djilali Liabes University of Sidi Bel Abbes, Algeria*
*[2]Applications of Plasma, Electrostatics and Electromagnetic Compatibility, APELEC, Djillali Liabes University of Sidi Bel Abbès, Algeria*
*Email: mbrahami@yahoo.fr*

**ABSTRACT**

Ce résumé présente les résultats d'une étude approfondie sur la conception et la réalisation d'une station de traitement d'eau par l'ozone, alimentée par un système photovoltaique, spécifiquement conçue pour les zones isolées. L'objectif principal de cette recherche est d'optimiser le processus de pompage et de traitement afin d'augmenter la quantité d'eau pompée, d'améliorer l'efficacité du traitement tout en minimisant la consommation d'énergie. Les chercheurs ont mené des études expérimentales approfondies sur divers paramètres impactant les performances du système.

Les résultats obtenus, soigneusement expliqués et discutés, apportent une contribution significative à l'avancement des technologies respectueuses de l'environnement dans le domaine du traitement de l'eau. Cette recherche propose des solutions spécialement adaptées aux défis uniques rencontrés dans les zones isolées, offrant ainsi une réponse précieuse aux besoins en eau potable de ces régions. Mettant l'accent sur la durabilité et l'efficacité énergétique, ces découvertes offrent des perspectives prometteuses pour les communautés vivant les endroits éloignés et difficilement accessibles.

Ce travail porte sur la conception d'un système de pompage d'eau photovoltaïque autonome et efficace pour répondre aux besoins en eau potable dans les zones désertiques. L'étude met en évidence le défi posé par les températures élevées, favorisant la croissance de micro-organismes dans l'eau, nécessitant ainsi un traitement d'eau plus complet. Contrairement aux désinfectants traditionnels comme le chlore et le brome, l'ozone est présenté comme une solution écologique et puissante pour le traitement de l'eau.

L'objectif principal était de développer un système autonome de pompage d'eau photovoltaïque intégrant l'ozone dans le processus de traitement. Les résultats des essais ont révélé que la température élevée impacte négativement l'efficacité du traitement de l'eau, soulignant ainsi la nécessité d'ajouter des systèmes de refroidissement au générateur d'ozone et à l'eau à traiter. De plus, la puissance consommée par le système dépend du débit d'eau à traiter, ce qui implique l'ajustement de la section de passage de l'eau par vannage pour maintenir une consommation d'énergie acceptable par le générateur photovoltaïque.

En conclusion, ce procédé de traitement de l'eau est efficace sous certaines conditions, à savoir une température ambiante modérée et un débit d'eau optimal. Cependant, des ajustements techniques, tels que l'ajout de systèmes de refroidissement et l'optimisation du débit d'eau, sont nécessaires pour assurer un fonctionnement continu et efficace du système dans les zones désertiques, offrant ainsi une solution prometteuse pour l'approvisionnement en eau potable dans ces régions reculées.

**Keywords:** Ozone, Générateur photovoltaique, Traitement de l'eau, Zones isolées.

**Fig 1:** Photographie du montage expérimental

**Références**

[1] **NEMMICH Saïd** « Modélisation expérimentale et optimisation du procédé de génération d'ozone par décharge à barrière diélectrique pour traitement de l'eau » Thèse Doctorat en Électrotechnique, Université Djilali Liabes De Sidi-Bel-Abbes 2015.

[2] **BECHEKIR Seyf Eddine** « étude et réalisation d'un onduleur à commande MLI pour système photovoltaïque muni de protection : application à la production d'ozone » Doctorat en Électrotechnique Systèmes d'Energie Electrique Université Djillali Liabes De Sidi-Bel-Abbes 2021.

[3] **NASSOUR Kamel** « Optimisation du procédé de génération d'ozone par décharge à barrière diélectrique mixte surfacique-volumique » pour le traitement d'eau » Doctorat en sciences université Djilali liabes SBA Décembre 2016.

[4] **BECHEKIR, S., BRAHAMI, M., OULD ABDESLAM, D., *et al.*** Development of a Low-Cost Ozone Generator Supply-Optimization Using Response Surface Modeling. *International Journal of Plasma Environmental Science and Technology*, 2019, vol. 13, no 1, p. 7-13.

[5] **JBILOU, M., NEMMICH, S., NASSOUR, K., *et al.*** Ozonation of river water for irrigation powered by a photovoltaic/diesel hybrid system. 2022.

# Enhancing Energy Efficiency in Public Lighting with Intelligent System

**R. Belhabri [1], S. A. Zidi [1], S. Hadjeri [1], H. Boubekeur [1]**

[1] *Electrical Engineering Department Intelligent Control & Electrical Power Systems Laboratory (ICEPS), Djillali Liabes University Sidi Bel-Abbes,22000, Algeria*
*Contact: ri123hab@gmail.com*

**ABSTRACT**

street lighting it is a very important and energy-intensive element of infrastructure in modern cities , energy use for street lighting makes up over 40% of total city consumption, in particular in Oran, Algeria. This puts a lot of pressure on the electric energy supply and impacts the environmental protection , the great consumption rate is mainly due to the primitive form the streetlight systems take , the tend to have a single controlling sources, on and off with a single light intensity when turned on , and are left fully on all through th night ,these features do not give room for flexiblity of control leading to great energie waste This is why it is crucial and advantageous to suggest technical solutions for monitoring and controlling lighting ,reduce energy consumption and improve energy efficiency of the street lighting systems;our study was based on a two-phase methodology, The first phase consists of an in-depth diagnosis of the existing lighting in the residential area known as "Quartier résidentiel TIZI OUAZO" in Oran, using Dialux Evo to optimize lighting management parameters such as brightness, luminaire distribution, identifying lighting inefficiencies and collecting essential data. Lighting simulation is used to adjust parameters, We replaced the 250W sodium SHP lamps from the Ibiza brand with 72W Philips LED luminaires,The second phase focuses on an intelligent lighting management system with motion and brightness sensors ,The foundation of this system is the concept of a "gradator," which lets you regulate how much power is sent to lights that are connected to an electrical network. Triac-based devices offer a very accurate setting for public lighting by automatically controlling the illumination intensity on a range of 0% to 100%, the main server to control LED street light which has illuminance level calculated by DIALux. When autonomously controlling street lighting system, the server system decides which street light should be dimmed according to motion sensors. If no vehicle passes the area for adjusted amount of time, the street light will dim. If any of the vehicle passes the area, the closest street to that area will raise the illumination level to normal level;The results of our simulation in DIALux Evo is represented in Figure 01 and Figure 02 verify that the neighborhood has uniform, well-lit lighting that meets all requirements. Our method has successfully improved lighting quality while consuming less energy for public lighting. Furthermore , The implementation of an intelligent lighting management system is represented in Figure 03 shows that the integrated system effectively maintains a balance between safety and energy efficiency by dynamically adjusting illumination levels based on real-time conditions. By integrating motion detection and brightness sensors, we have successfully achieved a more sustainable and cost-effective solution for public lighting;This study emphasizes how crucial it is to combine technical solutions like sensor integration, lighting management, and Dialux to optimize public lighting in the city of Oran. These strategies have a great deal of promise to lower energy usage, save expenses, and create a smarter, more sustainable city. These methods are not only workable but also a step toward the direction that contemporary urban management is taking.

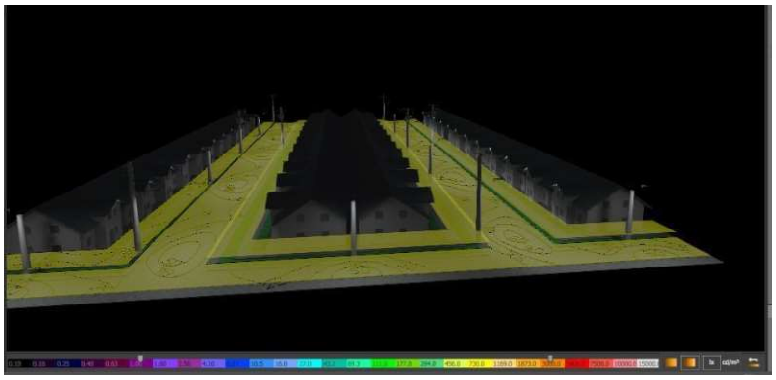

***Fig 1:*** *3D representation of the distribution of light from 'TIZI OUAZO' in the city of Oran*

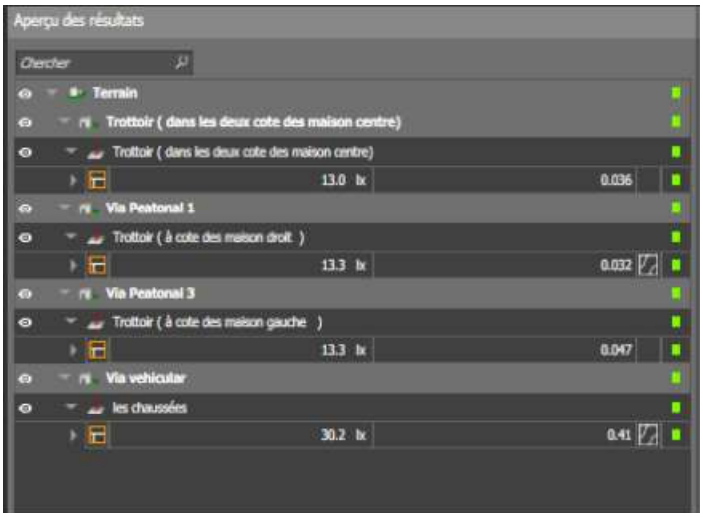


***Fig 2****: Result of calculation after simulation with dialux evo*

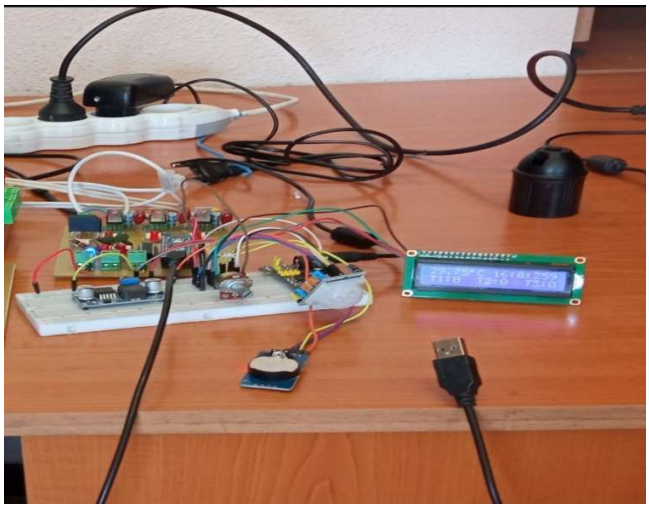

***Fig 3****: Electronic Circuit with Arduino*

**Keywords:** street lighting, energy efficiency, intelligent control system, dialux evo , motion detectionn

## References

[1] B. Rihab et A. Djihane, « DIAGNOSTIC ET OPTIMISATION DE L'ÉCLAIRAGE PUBLIC DE LA VILLE D'Oran » École Supérieure en Génie Électrique et Énergétique d'Oran (ESGEE)2021

[2] N. Sukhathai et T. Tayjasanant, « Smart Street Lighting System with Networking Communication », in *2019 IEEE Innovative Smart Grid Technologies - Asia (ISGT Asia)*, Chengdu, China: IEEE, mai 2019, p. 2826-2831. doi: 10.1109/ISGT-Asia.2019.8881684.

[3] A. Ozadowicz et J. Grela, « The street lighting integrated system case study, control scenarios, energy efficiency », in *Proceedings of the 2014 IEEE Emerging Technology and Factory Automation (ETFA)*, Barcelona, Spain: IEEE, sept. 2014, p. 1-4. doi: 10.1109/ETFA.2014.7005345.

[4] Benmebrouk Amira, « L'éclairage public à Djamaa. État des lieux », Université Mohamed Khider de Biskran 2020

# Navigation automnome d'un robot par l'approche champs de potentiels artificiels (APF)

**N. BENALI, H. CHEBI**
*Laboratory Intelligent Control and Electric Power System*
*Faculty of Electrical Engineering, Djillali Liabes University of Sidi Bel Abbes.*
*e-mail: chebi.hocine@yahoo.fr, hocine.chebi@univ-sba.dz*

**ABSTRACT**

La navigation autonome des robots est d'une importance cruciale, notamment dans l'agriculture. Les champs de potentiels artificiels, une méthode couramment utilisée pour orienter les robots en contournant les obstacles et les conduisant à leurs destinations, jouent un rôle central dans ce contexte. Cet article présente un nouvel algorithme basé sur les champs de potentiels artificiels (APF) qui surmonte les difficultés inhérentes aux minima locaux tout en optimisant les trajectoires des robots, en mettant particulièrement l'accent sur les robots agricoles. Les résultats obtenus attestent de son efficacité, se traduisant par des trajectoires optimales et une capacité à éviter les obstacles

**Keywords:**Navigation autonome ; Champs de potentiels artificiels ;Robotique ;Agriculture durable ; Obstacles.

La navigation autonome occupe une place cruciale dans l'autonomie des robots, leur permettant de se déplacer de manière efficiente à travers divers environnements, contournant les obstacles et atteignant leurs destinations. Elle revêt une importance particulièrement élevée dans des secteurs tels que l'agriculture, où l'automatisation joue un rôle essentiel dans l'amélioration de la productivité, de la rentabilité, de la durabilité et de la robustesse.

Dans cet article, la principale contribution réside dans la proposition d'un nouvel algorithme APF, qui représente une modification de la méthode APF standard. Ce nouvel algorithme vise à aider les robots à échapper aux minima locaux. Une analyse détaillée de cet algorithme est effectuée en utilisant la planification de trajectoire d'un robot agricole, évoluant dans un environnement composé d'obstacles polygonaux, qu'ils soient convexes ou non-convexes. Bien que, dans ce travail, le problème soit simplifié pour faciliter l'étude des paramètres de recuit, il convient de noter que cette méthode peut être étendue pour être appliquée à des environnements plus complexes.

## APPROCHE DU CHAMP DE POTENTIEL ARTIFICIEL

La méthode des champs de potentiel classiques a été développée principalement et indépendamment par (Khatib, 1986), c'est une approche de navigation et d'évitement d'obstacles dans laquelle un champ de potentiel artificiel est généré dans un environnement donné. Ce champ de potentiel comporte deux composantes principales : une composante attractive qui attire les agents vers leur destination souhaitée, et une composante répulsive qui repousse les agents des obstacles.
Cet algorithme représente le processus de navigation d'un robot en utilisant des champs de potentiel attractifs et répulsifs pour atteindre sa destination tout en évitant les obstacles. Il commence par initialiser les paramètres, les positions du robot et de la destination, ainsi que la liste des obstacles. Ensuite, il entre dans une boucle de contrôle du robot où la vitesse de référence est calculée en fonction des champs de potentiel attractifs et répulsifs. Enfin, la position du robot est mise à jour en fonction de la vitesse de référence jusqu'à ce que le robot atteigne sa destination.

- *ALGORITHME Champs_Potentiel*
- *// Déclarer les paramètres, les positions et les obstacles, $U_d$ : Le Champ de potentiel attractif, $q$ : La position du robot dans l'espace cartésien bidimensionnel, où $q = (x, y)$, $k_p$ : Le gain potentiel attractif, $q_d$ : Les coordonnées de la position cible, où $q_d = (x_d , y_d )$, $U_o$ : Le champ de potentiel répulsif, $\eta$ : Le gain potentiel répulsif, $\rho$ : La distance minimale entre le robot et l'obstacle, $\rho_0$ : La distance la plus courte à l'obstacle, $v_d$ : La vitesse d'attraction provoquée par la cible, $v_o$ : La vitesse de répulsion provoquée par l'obstacle, $v_{do}$ : La vitesse de référence à imposer au robot, $\nabla U_d$: Le gradient du champ de potentiel attractif, $\nabla U_o$:Le gradient du champ de potentielrépulsif, $\nabla U_{do}$ :Le gradient du champ de potentiel total.*
- *// Initialiser les paramètres, les positions et l'obstacle avec des valeurs données*
- *// Calculer le champ de potentiel attractif* $U_d U_d(q) = \frac{1}{2} k_p (q - q_d)^2$
- *// Calculer le champ de potentiel répulsif* $U_o, \rho = \sqrt{(q - q_d)^2}$ *//La distance entre le robot et l'obstacle.*
- *SI* $\rho \leq \rho_0$ *Alors*
- $U_o(q) = \frac{1}{2} \eta \left(\frac{1}{\rho} - \frac{1}{\rho_0}\right)^2$
- *SINON*
- $U_o(q) = 0$
- *FIN SI*
- *// Calculer le gradient du champ de potentiel total* $\nabla U_{do}$
- *SI* $\rho \leq \rho_0$ *ALORS*

- $\nabla U_{do}(q) = \nabla U_d(q) + \nabla U_o(q) = k_p(q - q_d) + \eta\left(\frac{1}{\rho} - \frac{1}{\rho_0}\right)\frac{(q-q_d)}{\rho^3}$
- *SINON*
- $\nabla U_{do}(q) = \nabla U_d(q) = k_p(q - q_d)$
- *FIN SI*
- *// Calculer la vitesse de référence* $v_{do}$ *comme l'opposé du gradient,* $v_{do}(q) = -\nabla U_d(q) - \nabla U_o(q)$
- *// Afficher la vitesse de référence du robot*
- *Ecrire("La vitesse de référence du robot est ",* $v_{do}(q)$*);*

**RESULTATS**

Cette section présente plusieurs expérimentations réalisées dans le but de démontrer l'efficacité de la méthode que nous avons proposée. Les expériences comparatives visent à mettre en évidence le bon fonctionnement de l'algorithme que nous avons développé dans divers contextes spécifiques. Les résultats issus de la simulation et des expériences comparatives confirment la capacité de l'algorithme que nous avons présenté à résoudre des problèmes de planification de trajectoire dans une variété d'environnements. Notre algorithme se montre particulièrement adapté aux environnements complexes caractérisés par la présence d'obstacles polygonaux, qu'ils soient convexes ou non convexes voir la figure 1, et 2. Le Schéma de la figure 1 représente l'obstacle sous forme d'un ellipsoïde avec n=1 ; n=2 ; n=4 ; n=20 qui est parallélépipède:

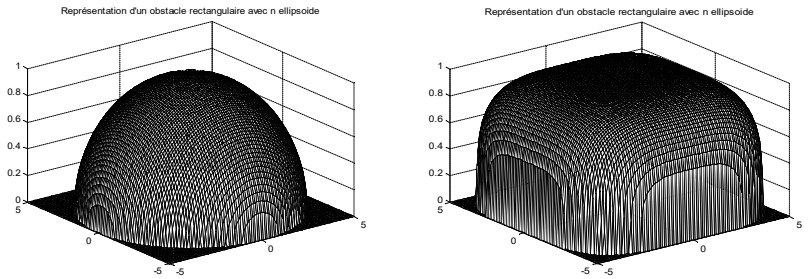


*Figure 1: obstacle avec n=1.*

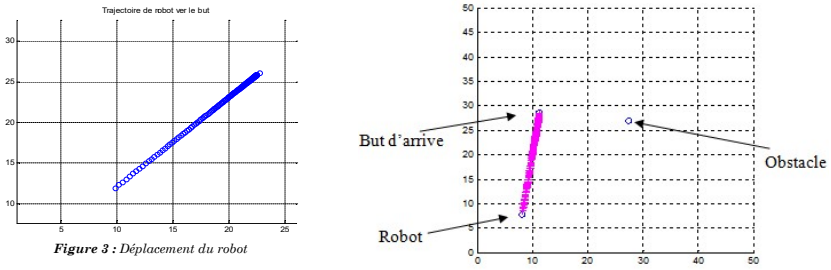


***Figure 3 :*** *Déplacement du robot*

*Figure 2: Plan d'evitement d'obstacle avec n=1*

**CONCLUSION**

L'étude a présenté une analyse expérimentale d'une technique de navigation de robot mobile qui utilise un champ de potentiel artificiel amélioré. Les tests ont confirmé la validité de cette méthode, où le robot se déplaçait sous l'influence du champ de potentiel amélioré en utilisant le suivi du gradient pour suivre les lignes de gradient. Cet article décrit un algorithme amélioré par rapport à l'APF standard pour la planification de trajectoires de robots dans des environnements avec des obstacles. Notre méthode introduit un paramètre visant à aider le robot à éviter les minima locaux en utilisant la stratégie décrite dans l'article. De plus, elle permet d'obtenir le minimum global de la fonction de champ de potentiel amélioré pour optimiser la sélection du chemin initial. Les résultats de la simulation confirment l'efficacité de cette méthode pour la planification de trajectoires dans des environnements complexes, y compris l'environnement agricole, en assurant des trajectoires optimales avec une bonne fluidité et des distances de sécurité constantes. Pour nos futurs travaux, nous explorerons en détail la planification de trajectoire en temps réel en combinant cette technique avec d'autres méthodes de navigation dans le but d'obtenir les meilleurs résultats possibles.

**REFERENCES**

[1] Khatib, O. (1986). Real-time obstacle avoidance for manipulators and mobile robots. The international journal of robotics research, 5(1), 90-98.

[2] Ren, J., McIsaac, K. A., & Patel, R. V. (2006). Modified Newton's method applied to potential field-based navigation for mobile robots. IEEE transactions on robotics, 22(2), 384-391.

[3] Ge, S. S., & Cui, Y. J. (2000). New potential functions for mobile robot path planning. IEEE Transactions on robotics and automation, 16(5), 615-620.

[4] Moreau, J., Melchior, P., Victor, S., Moze, M., Aioun, F., & Guillemard, F. (2018). Planification de trajectoire par champs de potentiel fractionnaires appliquée au véhicule autonome. Open Science Automatique, 2.

# Etude technico-économique d'un système hybride dans un site isolé de la willaya de Sidi Bel-Abbes

**H. Boubekeur[1], S. Hadjeri[1] , S.A. Zidi[1] , M. Jbilou[1] , R. Belhabri[1]**

[1] *Laboratoire ICEPS, Université Djilali Liabes, Sidi Bel-Abbes , 22000 , Algérie*
*Contact: boubekeur97sba@gmail.com*

**ABSTRACT**

La difficulté et les coûts importants du raccordement au réseau central de distribution d'un site isolé dans le territoire sud de la willaya de Sidi Bel-Abbes ( la région de Sidi Chaib ) , posent des contraintes pour l'allimentation d'électricité . Au premier temps est de répondre au besoins énergétiques de cette région et au moindre coût . Le but de cet article est de faire une étude technico-économique du système hybride (Photovoltaïque-Groupe diesel-Batterie) et (Photovoltaïque-Eolien-Batterie) avec l'utilisation du logiciel HOMER , et de faire une comparaison pour obtenir un coût , fiabilité et performance optimal de ces deux configurations . Le modèle de chaque configuration introduit dans le logiciel HOMER; avec les options de disponibilité technologique des resources et les coûts des composants . Afin d'analyser les résultats de simulation pour les deux configurations ; (Photovoltaïque-Groupe diesel-Baterrie) et (Photovoltaïque-Eolien-Batterie) cela permet de trouver que le système hybride représente un choix stratégique sur les plans économique et environnemental. A titre de comparaison , la meilleure installation énergtique pour la region de Sidi Chaib est celle d'un systeme hybride (Photovoltaïque-Eolien-Batterie) , grâce à son emplacement stratégique et les énergies auxiliaires renouvelables (vent , soleil) et leur exploitation .

**Mots clés :** Photovoltaïque ; Eolien ; Groupe diesel ; Homer .

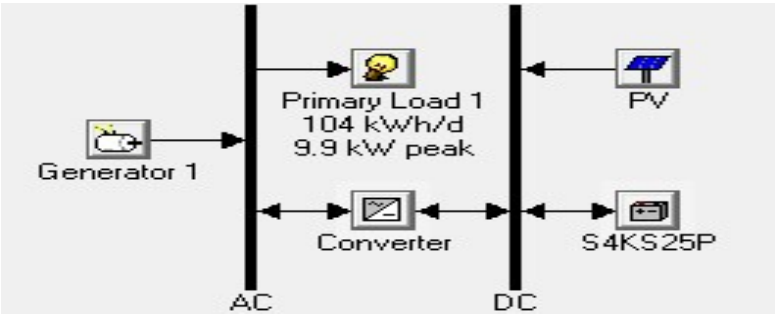


*Fig.1. Schéma de l'installation hybride Photovoltaïque-Diesel-Batterie.*

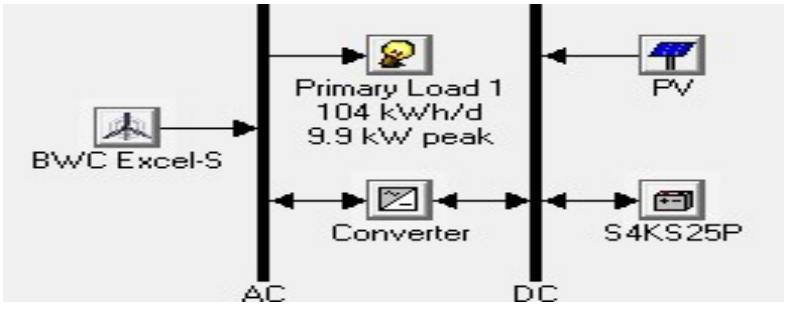


*Fig.2. Schéma de l'installation hybride Photovoltaïque-Eolien-Batterie.*

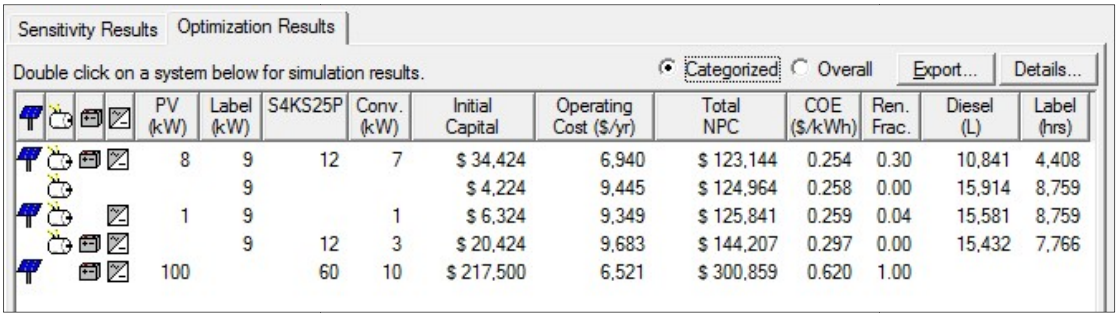

Sensitivity Results | Optimization Results

Double click on a system below for simulation results. Categorized Overall Export... Details...

| PV (kW) | Label (kW) | S4KS25P | Conv. (kW) | Initial Capital | Operating Cost ($/yr) | Total NPC | COE ($/kWh) | Ren. Frac. | Diesel (L) | Label (hrs) |
|---|---|---|---|---|---|---|---|---|---|---|
| 8 | 9 | 12 | 7 | $ 34,424 | 6,940 | $ 123,144 | 0.254 | 0.30 | 10,841 | 4,408 |
| | 9 | | | $ 4,224 | 9,445 | $ 124,964 | 0.258 | 0.00 | 15,914 | 8,759 |
| 1 | 9 | | 1 | $ 6,324 | 9,349 | $ 125,841 | 0.259 | 0.04 | 15,581 | 8,759 |
| | 9 | 12 | 3 | $ 20,424 | 9,683 | $ 144,207 | 0.297 | 0.00 | 15,432 | 7,766 |
| 100 | | 60 | 10 | $ 217,500 | 6,521 | $ 300,859 | 0.620 | 1.00 | | |

*Fig.3. Résultats obtenus après la première simulation : Photovoltaïque-Diesel-Batterie.*

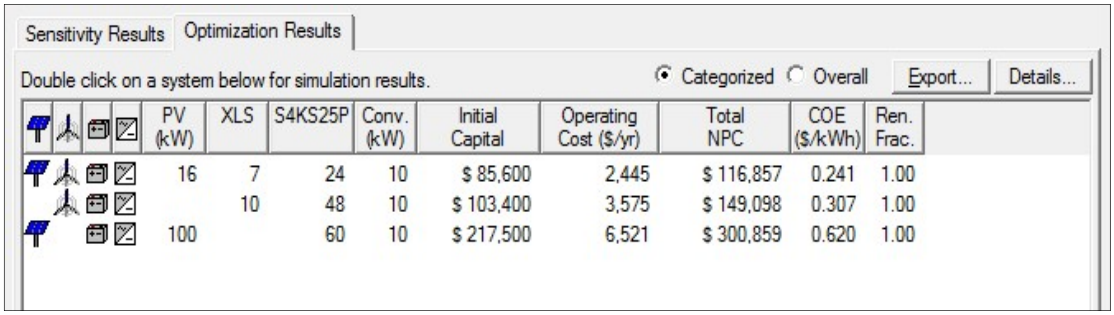

Sensitivity Results | Optimization Results

Double click on a system below for simulation results. Categorized Overall Export... Details...

| PV (kW) | XLS | S4KS25P | Conv. (kW) | Initial Capital | Operating Cost ($/yr) | Total NPC | COE ($/kWh) | Ren. Frac. |
|---|---|---|---|---|---|---|---|---|
| 16 | 7 | 24 | 10 | $ 85,600 | 2,445 | $ 116,857 | 0.241 | 1.00 |
| | 10 | 48 | 10 | $ 103,400 | 3,575 | $ 149,098 | 0.307 | 1.00 |
| 100 | | 60 | 10 | $ 217,500 | 6,521 | $ 300,859 | 0.620 | 1.00 |

*Fig.4. Résultats obtenus après la première simulation : Photovoltaïque-Eolien-Batterie.*

**Références**

[1] BOUBEKEUR Halima, AOUS Saadia Amina . "opportunite de l'utilisation des systemes de production d'electricite hybrides dans le haut plateau de la wilaya de sidi bel Abbes". Université Djillali Liabes. Sidi Bel Abbes , Mémoire de Master, 2020.

[2] BAGHDADI ,Fazia. "Modélisation et simulation des performances d'une installation hybride de conversion d'énergies renouvelables". Université Mouloud Mammeri . Tizi-Ouzou Mémoire de Magister, 26/06/2011.

[3] REGUIEG Elhadi Mohamed et Elsaid, YAHIAOUI Amara Mohamed. "Etude de l'utilisation de l'énergie hybride photovoltaïque-groupe électrogène dans les fermes agricoles et leurs contributions dans le développement durable dans la région sud de Sidi Bel Abbes". Université Djillali Liabes. Sidi Bel Abbes , Mémoire de Master, 2019 .

[4] KARA Abdelfattah "Dimensionnement et analyse du coût d'un système hybride de production d'énergie renouvelable pour des sites isolés en Algérie". Université Farhat Abbas. Setif , Mémoire de Master , 24/06/2014.

[5] KHENFOUS S., KAABECHE A. et Diaf.S "Optimisation du dimensionnement d'un système hybride photovoltaïque/éolien par des méthodes méta heuristiques" Vol. 20,pp. 267-284, 2017.

# Dimensioning of a photovoltaic pumping system for a drip irrigation system aimed at minimizing energy losses

**Y. Bouroumeid[1], M. Jbilou[1], S. Bechekir[1], M. Brahami[1], S. Nemmich[2], M. Belabed [1], BEL. Oulad Naoui [2,] O. Ghaitaoui [1]**

[1 1]*Laboratory: Intelligent Control and Electrical Power System ICEPS Djilali Liabes University of Sidi Bel Abbes, Algeria*
[2]*Laboratory: Applications of Plasmas, Electrostatics and Electromagnetic Compatibility APELEC Djilali Liabes*
*Bouroumeid.yassine@yahoo.com*

## ABSTRACT

The water crisis, exacerbated in Algeria's arid regions, calls for innovative solutions. This study focuses on the critical importance of irrigation in these areas, highlighting the need for affordable systems to support small farms. The objective of this work is to supply a water reservoir through photovoltaic pumping, thus feeding a gravity drip irrigation system adapted to the dimensions of small farms of 2500 plants, each consuming 1 L/h. To meet these needs, a flow rate of approximately 0.8 liters per second at the outlet of the tank is required. Thus, it is necessary to calculate the height of the reservoir to obtain this flow rate, which is equivalent to 2.1 meters. This precise height determination allows for the implementation of a night-time irrigation system that operates without the use of pumps, thus promoting an energy-efficient and efficient approach in the agricultural context. This height must be taken into account when sizing the pumping with the PVsyst software. In addition, we plan to carry out a techno-economic study of this system using the Homer software. This approach is effective in minimizing energy and water losses while maximizing the agricultural productivity of small farms. This significant contribution promises to improve food and energy security in vulnerable regions, paving the way for sustainable and resilient practices.

**Keywords:** PVsyst; Irrigation; Renewable energy; Energy efficiency, Homer.

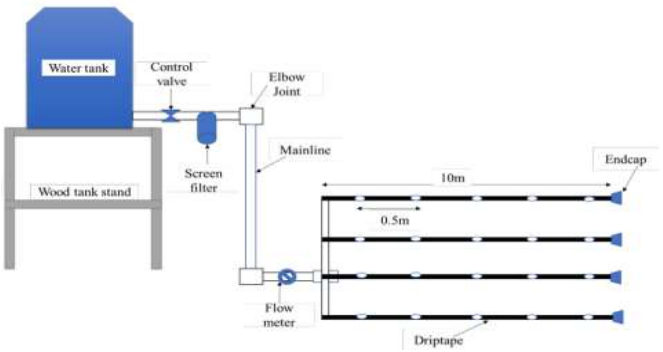


*Figure 1 Schematic layout of small gravity drip irrigation system.*

- Water requirements fluctuate with the seasons, and Figure 2 depicts the amount of energy consumed by the pump to meet these monthly needs, ensuring an annual total demand of 1553 cubic meters of water.
- The annual average performance ratio stands at 73%, as depicted in Figure 3.
- Figure 4 provides a techno-economic analysis of this system over a 25-year period, encompassing the initial investment, replacements, operational costs, and residual value.

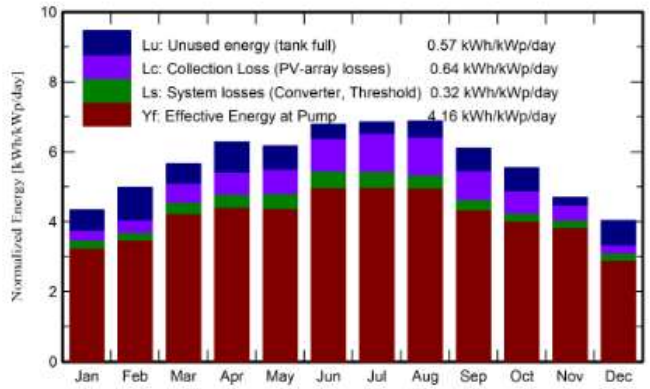


*Figure 2 Normalized productions (per installed kWp)*

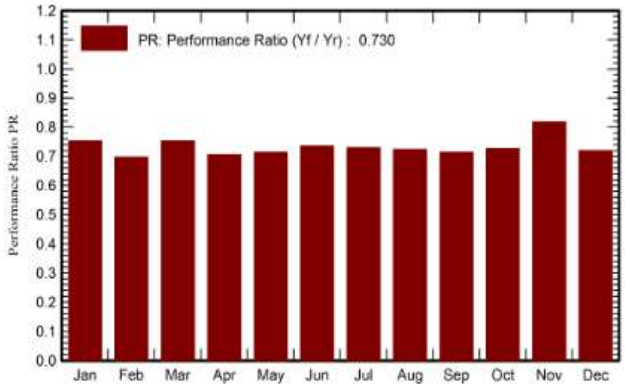


*Figure 3 Performance Ratio PR*

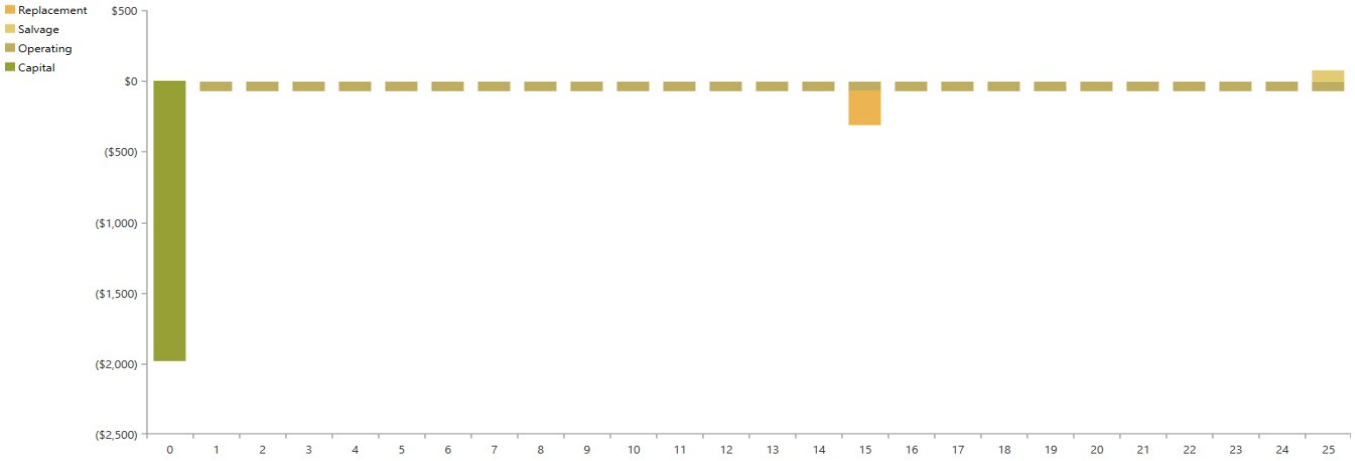


*Figure 4 Economic and Technical Analysis of Systems Using Homer Software.*

[1] R. Saefuddin and Z. Sirajuddin 2023 IOP Conf. Ser.: Earth Environ. Sci. 1230 012139
[2] M. Jbilou, M.N. Brahami, S. Nemmich, M. Brahami, & A. Tilmatine. (2018). Ozone food storage supplied by photovoltaic energy. Carpathian Journal of Food Science & Technology, 10(4).
[3] D. Goldberg, B. Gornat, & D. Rimon,(1976). Drip irrigation. Principles, design and agricultural practices. Drip irrigation. Principles, design and agricultural practices.
[4] B. Ben Saada, M. Chahbounia, D. Hassani, & A. Ferrai, (2022). Dimensionnement d'un syseme de pompage photovoltaique destine a'l'irrigation agricole.
[5] F. Antonio Barrozo Budes, G. Valencia Ochoa, L.G. Obregon, A .Arango-Manrique, & J. Ricardo Núñez Álvarez, (2020). Energy, economic, and environmental evaluation of a proposed solar-wind power on-grid system using HOMER Pro: A case study in Colombia. Energies, 13(7), 1662.

# Analyse technico-économique d'un système d'énergie hybride hors réseau à Sidi Bel-Abbès

**Y. Bouroumeid[1], M. Jbilou[1], S. Bechekir[1], M. Brahami[1], S. Nemmich[2], M. Belabed [1], BEL. Oulad Naoui [2,] O. Ghaitaoui [1]**

[1 1]*Laboratory: Intelligent Control and Electrical Power System ICEPS Djilali Liabes University of Sidi Bel Abbes, Algeria*
[2]*Laboratory: Applications of Plasmas, Electrostatics and Electromagnetic Compatibility APELEC Djilali Liabes*
*Bouroumeid.yassine@yahoo.com*

## ABSTRACT

En Algerie comme tout autre pays du monde ,cetain foyers ne sont pas raccordés au réseaux électriques conventionnels. Les énergies renouvelables s'imposent comme les candidats privilégiés, bien que leur production puisse être intermittente. L'objectif de ce projet est d'évaluer la rentabilité et la faisabilité d'un système autonome de production d'électricité. Ce système associe des panneaux solaires, des éolienne, un générateur diesel et un système de stockage basé sur des batteries pour répondre aux besoins énergétiques d'un village rural dans la région de Sidi Bel Abbess. Ce village affiche une consommation électrique moyenne de 116 kWh par jour, avec un pic de 14,48 kW. Pour mener à bien cette étude, de nombreuses simulations numériques ont été réalisées à l'aide du logiciel HOMER, en utilisant des données techniques et météorologiques spécifiques à la région de Sidi Bel Abbess. Les résultats démontrent que cette combinaison hybride est économiquement plus avantageuse, avec un investissement initial réduit. Le système présente un coût total net (CTN) de 91 784 $, un coût opérationnel annuel de 3 142 $, et un coût de production d'énergie (CEP) de 0,168 $ par kilowattheure. Ces résultats mettent en évidence une optimisation supérieure de l'utilisation du système d'énergie hybride, répondant ainsi à la demande énergétique et contribuant à la préservation de l'environnement pour lutter contre le changement climatique.

**Keywords:** Homer; Energie hybride; Energies renouvelables; efficacité énergétique; système autonome.

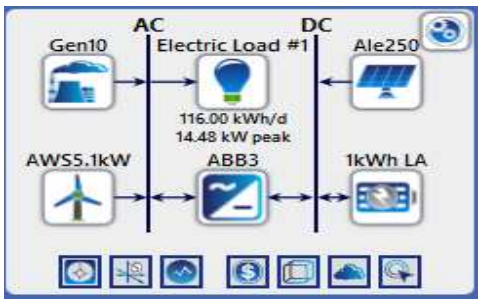


Fig.1. Schéma synoptique du système hybride étudié.

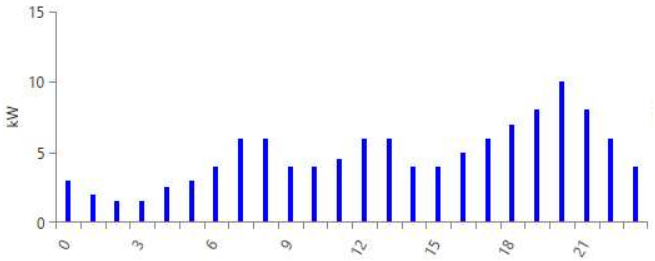


Fig.2. Profil de la demande tout au long de la journée.

La Figure 2 révèle que tôt le matin, la demande en électricité atteint son point culminant entre 6h00 et 7h00, atteignant une charge estimée de 6 kW. Le pic le plus élevé se produit en fin de journée, entre 20h00 et 21h00. Ces pics correspondent aux moments où les résidents ont tendance à consommer davantage d'électricité pour répondre à leurs besoins quotidiens.

| Ale250 (kW) | AWS5.1kW | Gen10 (kW) | 1kWh LA | ABB3 (kW) | Dispatch | NPC ($) | COE ($) | Operating cost ($/yr) | Initial capital ($) | Ren Frac (%) | Total Fuel (L/yr) |
|---|---|---|---|---|---|---|---|---|---|---|---|
| 20.0 | 5 | 10.0 | 30 | 12.0 | LF | $91,784 | $0.168 | $3,142 | $51,160 | 81.0 | 3,066 |
| 55.0 | | 10.0 | 42 | 12.0 | LF | $117,738 | $0.215 | $6,242 | $37,045 | 57.7 | 6,580 |
| 55.0 | 6 | | 121 | 12.0 | CC | $121,420 | $0.222 | $3,024 | $82,322 | 100 | 0 |
| 115 | | | 261 | 15.0 | CC | $196,683 | $0.360 | $7,178 | $103,886 | 100 | 0 |
| | 5 | 10.0 | 87 | 3.00 | CC | $211,601 | $0.387 | $12,146 | $54,580 | 34.0 | 12,170 |

Fig.3. Résultats classés par ordre de rentabilité et de faisabilité.

Suite à la simulation de notre système, il est apparu que HOMER favorise une configuration hybride qui intègre un système solaire de 20 kW, 5 éoliennes de 5.1 kW CA, un générateur électrique de 10 kW, un ensemble de batteries de stockage, ainsi qu'un convertisseur de 12 kW, comme illustré dans la figure 3.

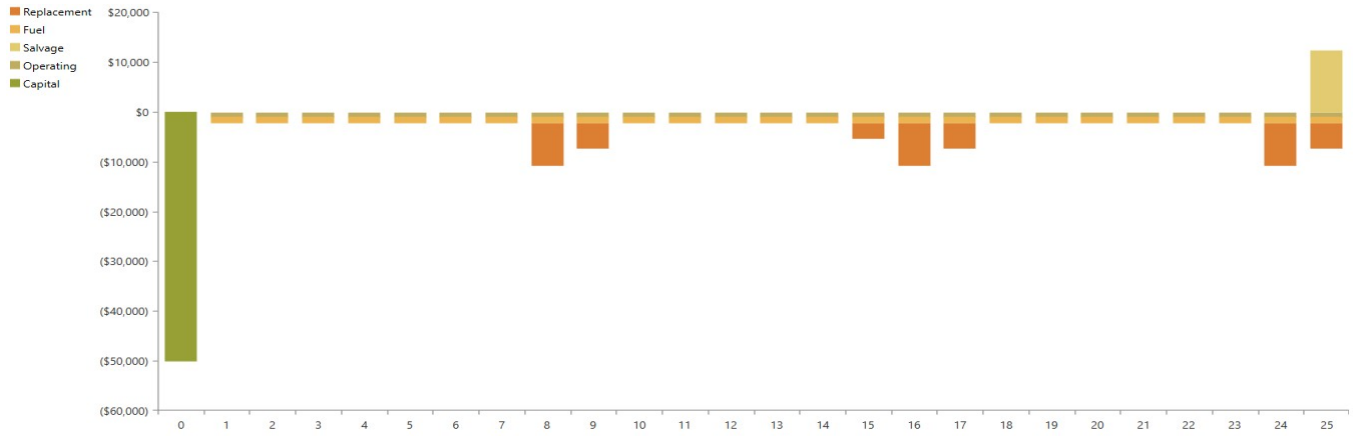


Fig.4. Analyse Économique de Système.

La figure 4 présente une analyse technico-économique de ce système sur une période de 25 ans, englobant l'investissement initial, les remplacements, les coûts d'exploitation et la valeur résiduelle.

[1] H. Oueslati and S. B. Mabrouk. (2023). Techno-economic analysis of an on-grid PV/Wind/Battery hybrid power system used for electrifying building. Energy Sources, Part A: Recovery, Utilization, and Environmental Effects, 45(4), 9880-9893.
[2] M. Jbilou, M.N. Brahami, S. Nemmich, M. Brahami, & A. Tilmatine. (2018). Ozone food storage supplied by photovoltaic energy. Carpathian Journal of Food Science & Technology, 10(4).
[3] T. Adefarati, R. C. Bansal, T. Shongwe, R. Naidoo, M. Bettayeb & A. K. Onaolapo. (2023). Optimal energy management, technical, economic, social, political and environmental benefit analysis of a grid-connected PV/WT/FC hybrid energy system. Energy Conversion and Management, 292, 117390.
[4] A. S. Almashakbeh, A. A. Arfoa & E. S. Hrayshat. (2023). Techno-economic evaluation of an off-grid hybrid PV-wind-diesel-battery system with various scenarios of system's renewable energy fraction. Energy Sources, Part A: Recovery, Utilization, and Environmental Effects, 45(2), 6162-6185.
[5] A.G . Kiliç, K. Al, E. Dağtekin & Ü. Ünver. (2020). Technical, economic and environmental investigation of grid-independent hybrid energy systems applicability: a case study. Energy Sources, Part A: Recovery, Utilization, and Environmental Effects, 1-16.

# A numerical comparative study of the electric field distribution between simple and a multi-tube DBD ozone generators

**GHAITAOUI Essama Ahmed[1], NASSOUR Kamel [1], NEMMICH Said [2], OLAD NAOUI Ibrahim Khalil[2], BOUROUMEID Yassine[1], GHAITAOUI Touhami[3] , TILMATINE Amar[2]**

*[1]ICEPS Laboratory ,Djillali Liabes University of Sidi Bel-Abbes, Sidi Bel-Abbes, Algeria*
*[2]APELEC Laboratory , Djillali Liabes University of Sidi Bel-Abbes, Sidi Bel-Abbes, Algeria*
*[3]LDDI Laboratory, University Ahmed Draia – Adrar , Adrar Algeria*
*Email: oussamaghaitaoui@gmail.com or ahmed.ghaitaoui@univ-sba.dz*

**ABSTRACT**

This paper proposes a comparative study between two ozone generators. The first generator was designed with a cylindrical stainless steel electrode connected to the ground and an inner aluminum electrode connected to high voltage, with a glass tube chosen as a dielectric barrier discharge . The second ozone generator was also designed, called a multi-tube ozone generator. A stainless steel electrode was chosen as the first electrode connected to the ground, and a high-voltage aluminum electrode with a glass tube was chosen as a dielectric barrier discharge. It should be noted that the discharge volume of the two generators is equal and is estimated at 140.74 $cm^3$. The study was carried out using the simulation program Comsol Multiphysics 5.6 . The simulation results of the electric field strength in the two generators showed that the multi-tube ozone generator has a better distribution of the electric field compared to the first ozone generator, which means greater efficiency for generating ozone.

**Keywords:** ozone generator ; electric field distribution ; dielectric ; electrode, multi-tube .

## 1. NUMERICAL MODEL

The study was conducted on two ozone generators. The first is a simple ozone generator. A cylindrical stainless steel electrode was used as the electrode connected to the ground, and an aluminum electrode was connected with high voltage . A glass tube was chosen as a dielectric barrier discharge. Figure 1(a) shows the geometry of the simple generator. The second ozone generator is called a multi-tube ozone generator, where a cylindrical stainless steel electrode was used as a ground electrode and an aluminum electrode as a high-voltage electrode. The generator contains four generators with the mentioned specifications, linked together as shown in Figure 1(b). The two generators studied have the same rated discharge volume of 140.74 $cm^3$

*Fig.1 a) Design of simple ozone generator* *b) Design of multi-tube ozone generator*

Figure 2 shows the computational domain adopted in a simple ozone generator. The domain is divided into four parts: a high-voltage aluminum electrode, glass dielectric layer with a thickness of 2 mm, a discharge gap of 1 mm and a stainless steel grounding electrode with a thickness of 2 mm. The simulation domain is discretized with triangular meshes [1]. Taking into account the grid quality and computation resource[2], [3].

*Fig.2. Computational domain of simple generator*

Figure 3 shows the computational domain adopted in the multi-tube ozone generator. The generator contains four generators, and the computational domain for each of them has four parts. The domain is divided into four parts: a high-voltage aluminum electrode with a thickness of 1 mm, an dielectric layer of glass with a thickness of 2 mm, a discharge gap of 1 mm, and a stainless steel grounding electrode with a thickness of 2 mm. The simulation domain is discretized with triangular meshes[1]. Taking account the grid quality and computation resource[4].

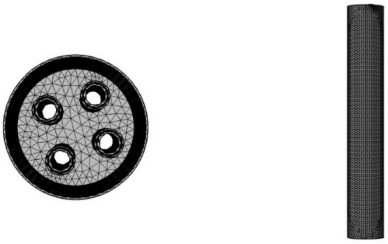

*Fig.3. Computational domain of Multi-tube generator*

**References**

[1] L.-S. Wei, B.-F. Peng, M. Li, and Y.-F. Zhang, "A numerical study of species and electric field distributions in pulsed DBD in oxygen for ozone generation," *Vacuum*, vol. 125, pp. 123–132, Mar. 2016, doi: 10.1016/j.vacuum.2015.12.011.

[2] K. Nassour *et al.*, "Comparative experimental analysis of ozone generation between surface and volume DBD generators," *IEEE Trans. Dielectr. Electr. Insul.*, vol. 25, pp. 428–434, Apr. 2018, doi: 10.1109/TDEI.2017.006600.

[3] S. Nemmich, K. Nassour, N. Ramdani, Y. Bellebna, M. Boukhoulda, and A. Tilmatine, "DEVELOPMENT AND OPTIMIZATION OF AN OZONE FOOD PRESERVATION SYSTEM USING RESPONSE SURFACE MODELLING (RSM)," *Carpathian J. Food Sci. Technol.*, vol. 13, pp. 33–46, Jan. 2022, doi: 10.34302/crpjfst/2021.13.4.4.

[4] L. Tayeb Mehdi *et al.*, "Experimental study of the gas flow path for a dielectric barrier discharge ozone generator using for wastewater fish hatchery depollution," *Int. J. Plasma Environ. Sci. Technol.*, vol. 16, Apr. 2022, doi: 10.34343/ijpest.2022.16.e01005.

# Dynamic Voltage Restorer Based on Direct Matrix converters,

**F. Ghezal[1], S. Hadjeri[1], M. Benghanem[2], S. Zidi[1]**

[1] *Intelligent Control and Electrical Power Systems Laboratory ICEPS Electrical Engineering Faculty, Djillali Liabes university, Sidi Bel Abbes, Algeria*
[2]*AVCIS Laboratory Automatic Control Dep University USTOMohamed boudiaf, Oran , Algeria*
*Email: nour73_fac@yahoo.fr , shadjeri2@yahoo.fr*

**ABSTRACT**

This work presents the Dynamic Voltage Restorer (DVR) based on direct AC/ AC converters. DVR is one of custom power devices used in distribution network. The DVR can resolve some problems of power quality such as: voltage sag, swell and briefs cuts in network. The classical DVR is based on inverter with DC energy storage. To resolve problem of energy storage, the direct AC/AC converters without any energy storage is used in this work. Matrix converters is one of AC/AC converters, based on Venturini algorithm, a closed loop of this work uses classical regulator PI, the DVR in this work can correct the voltage.

The nine firing pulses are generated using simplified Venturini algorithm with 0.86 voltage transfer ratio.

**Keywords:** DVR, voltage sags, voltage swell, matrix converters.

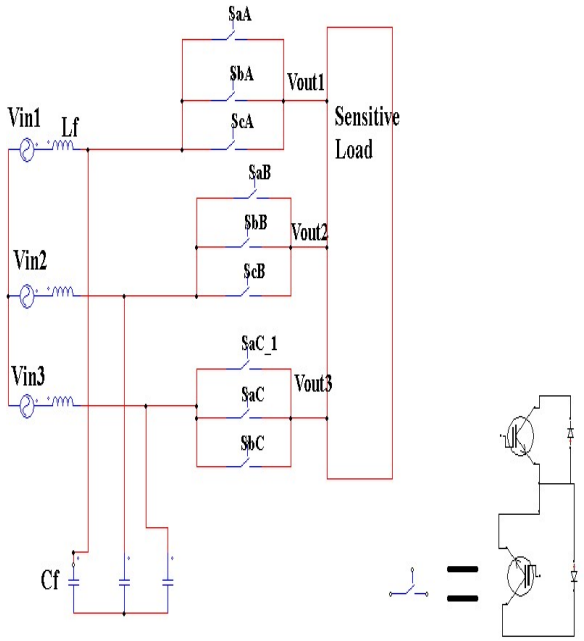


**Fig 1 :** Basic scheme of direct matrix

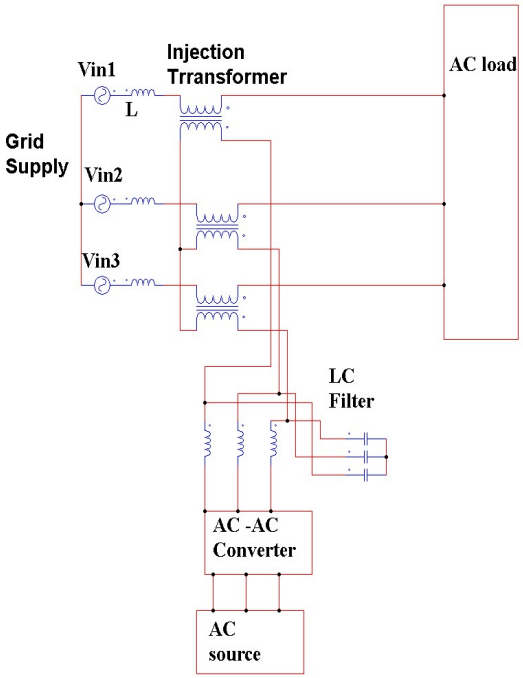


**Fig 2:** DVR scheme of the simulated system

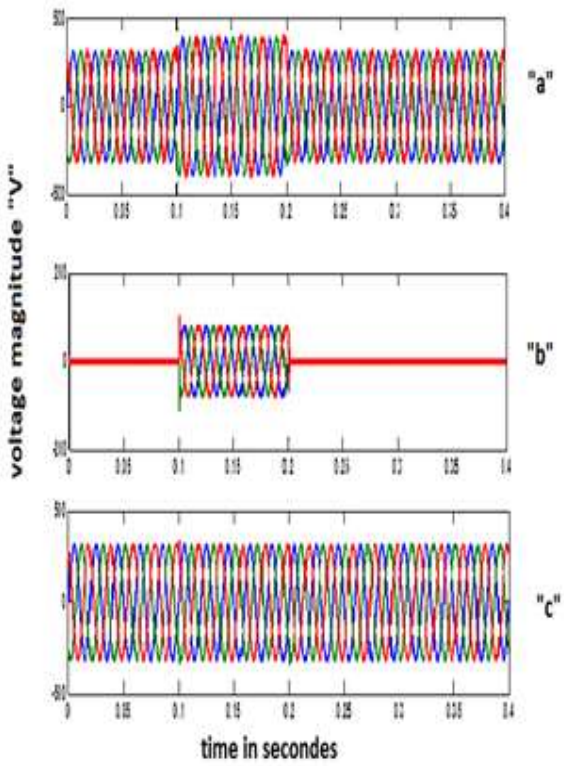


**Figure 3:** 20% swell voltage
"a": voltage source
"b": injected voltage
"c": load voltage

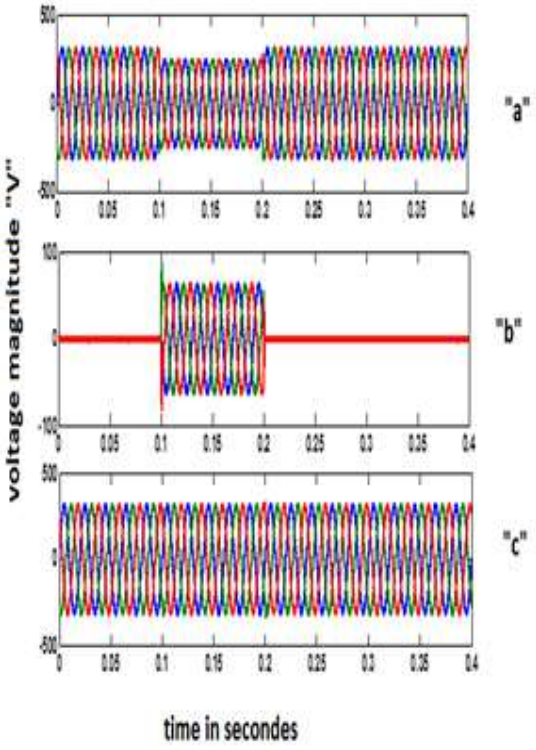


**Figure 4:** 20% sag voltage
"a": voltage source
"b": injected voltage
"c": load voltage

**References**

[1] Muhammad Alif Mansor, Muhammad Murtadha Othman, Ismail Musirin, Siti Zaliha Mohammad Noor«Dynamic voltage restorer (DVR) in a complex voltage disturbance compensation» International Journal of Power Electronics and Drive System (IJPEDS) Vol. 10, No. 4, December 2019, pp. 2222~2230

[2] José M. Lozano, Juan M. Ramirez, Member, IEEE, Rosa Elvira Correa «A novel dynamic voltage restorer based on matrix converters» October 2010, IEEE conference.

[3] M.G.B. Venturini and A.Alesina "Intrinsic amplitude limits and otipmum design of 9-switches direct PWM ac-ac converter" Conf –Rec. IEEE -PESC .1988 PP 1284- 1294

[4] Ghalem BACHIR; Azeddine BENDIABDELLAH; "A Comparative Study between Two Control Strategies for Matrix Converter" Advances in Electrical and Computer Engineering Journal, volume 9, Number 2, 2009

[5] Hulusi Karaca and Ramazan Akkaya «Modeling, Simulation and Analysis of Matrix Converter Using Matlab&Simulink », International Journal of Modeling and Optimization, Vol. 2, No. 3, June 2012, pp. 328-322

# Review of Wind Turbine integration challenges and proposed solutions

**[1]S. Khelifa , [1]A. Semmah**

*[1]ICEPS LAB, faculty of electrical engineering, 22000, SBA, Algeria*
*Email: sihamsiam71@gmail.com*

**ABSTRACT**

The integration of wind turbines into the electrical grid has known a tremendous increase, especially with the policy adopted by the countries to reduce the emissions of gazes mainly CO2, N2O, CH4 that affect the planet's weather causing environmental crises all over the world. The integration of wind turbines participates effectively in generating and ensuring clean energy however the connection of wind turbines to the electrical grid will result in many operational and control challenges that lead to unsuitable power flow throughout the electrical lines, instability, and power quality issues. The purpose of the present paper is to highlight briefly the different issues related to the integration of wind turbines into the electrical grid, and the solutions proposed to deal with these challenges will be presented and explained. This study aims to share a clear overview of wind energy integration technical issues and to enable decision-makers to develop sustainable strategies for tackling them.

**Keywords:** Wind Turbine; power quality; renewable energy; flicker; static compensator; grid code.

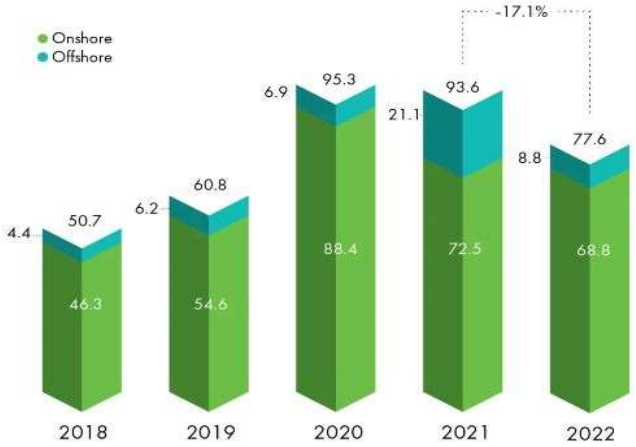


Fig. 1 The growth of wind turbine installed total capacity in the world

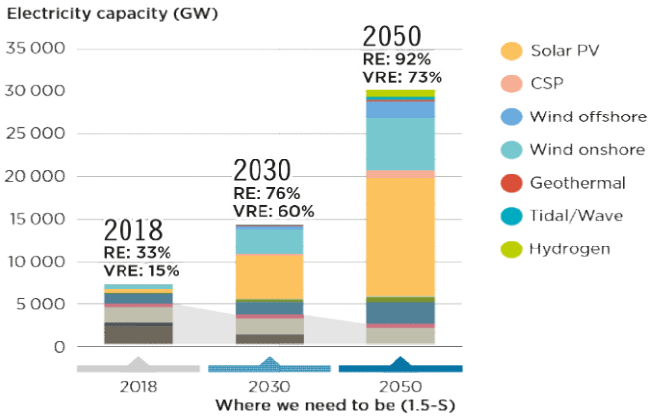


Fig. 2 Wind energy compared to others RE

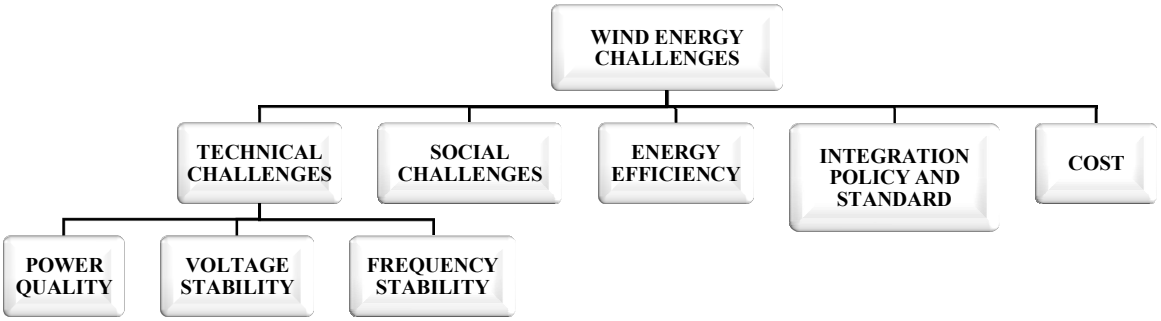


Fig.3 Different challenges of the wind turbine integration

**References**

[1] Catalán, Pedro, et al. "A comprehensive overview of power converter applied in high-power wind turbine: Key challenges and potential solutions." IEEE Transactions on Power Electronics (2023).

[2] Ali, Syed Wajahat, et al. "Offshore wind farm-grid integration: A review on infrastructure, challenges, and grid solutions." *IEEE Access* 9 (2021): 102811-102827.

[3] Al-Shetwi, Ali Q. "Sustainable development of renewable energy integrated power sector: Trends, environmental impacts, and recent challenges." Science of The Total Environment 822 (2022): 153645.

[4] Ahmed, Shakir D., et al. "Grid integration challenges of wind energy: A review." *IEEE Access* 8 (2020): 10857-10878.

[5] Veers, Paul, et al. "Grand challenges in the science of wind energy." Science 366.6464 (2019): eaau2027.

[6] Holttinen, Hannele. "Wind integration: experience, issues, and challenges." Advances in Energy Systems: The Large-scale Renewable Energy Integration Challenge (2019): 341-354.

[7] Rao, K. R. Wind energy for power generation: meeting the challenge of practical implementation. Springer Nature, 2019

[8] Sinsel, Simon R., Rhea L. Riemke, and Volker H. Hoffmann. "Challenges and solution technologies for the integration of variable renewable energy sources—a review." renewable energy 145 (2020): 2271-2285.

[9] Shaw, William, et al. "Scientific challenges to characterizing the wind resource in the marine atmospheric boundary layer." Wind Energy Science Discussions 2022 (2022): 1-47

[10] Guo, Yaohua, Haijun Wang, and Jijian Lian. "Review of integrated installation technologies for offshore wind turbines: Current progress and future development trends." *Energy Conversion and Management* 255 (2022): 115319.

[11] Benzohra, Omar, et al. "Integrating wind energy into the power grid: Impact and solutions." Materials Today: Proceedings 30 (2020): 987-992

[12] Ahmed, Noor A., and Michael Cameron. "The challenges and possible solutions of horizontal axis wind turbines as a clean energy solution for the future." Renewable and Sustainable Energy Reviews 38 (2014): 439-460.

[13] Erdiwansyah, et al. "A critical review of the integration of renewable energy sources with various technologies." Protection and control of modern power systems 6 (2021): 1-18.

# A Comparative study between input-output linearization control and sliding mode control for the doubly fed induction generator applied in a wind energy conversion system

**Mehadjia MESLEM and Youcef DJERIRI**

*ICEPS Laboratory, Faculty of Electrical Engineering, Djilali Liabes University of Sidi Bel Abbes, Algeria*

*Email : mehadjiameslem@gmail.com*

**ABSTRACT :**

In this work we propose a comparative study between two control approaches for the doubly fed induction generator (DFIG) applied in a wind energy conversion system, namely linearization in the input-output sense (IOLC) and sliding mode (SMC), for the independent control of the stator active and reactive power of the DFIG. These techniques are validated by simulation in the MATLAB/SIMULINK environment. The simulation results clearly demonstrate the effectiveness of these control strategies for decoupling the DFIG's stator active and reactive power. They perfectly follow their reference values, with high dynamic and static performances and satisfactory disturbance rejection. A robustness test when the mutual inductance Lm was reduced by 30% and 50% of its nominal value shows that IOLC is highly robust against 30% decrease in the nominal value of the mutual inductance. However, when the mutual inductance decreases by a large proportion, up to 50% of its nominal value, the performances of the IOLC is partially degraded, in contrast to the SMC, where this control exhibits great robustness against a 50% decrease in the nominal value of the mutual inductance. The only drawback of the SMC is the chattering effect.

We can conclude that IOLC is an effective tool for decoupling active and reactive power. However, the control is still relatively sensitive to large parametric variations. Although the performance obtained with SMC is very satisfactory even in the presence of parametric variations, as shown by the trajectory tracking and fast convergence of measured outputs towards their desired reference. Power tracking is without overshoot, decoupling, stability and convergence to equilibrium are assured. What's more, SMC features a very simple robust control algorithm which has the advantage of being easy to implement in an calculator control.

**Keywords:**

Wind energy; Doubly-fed induction machine; Input-output linearization; Sliding mode; Robustness.

**simulation results:**

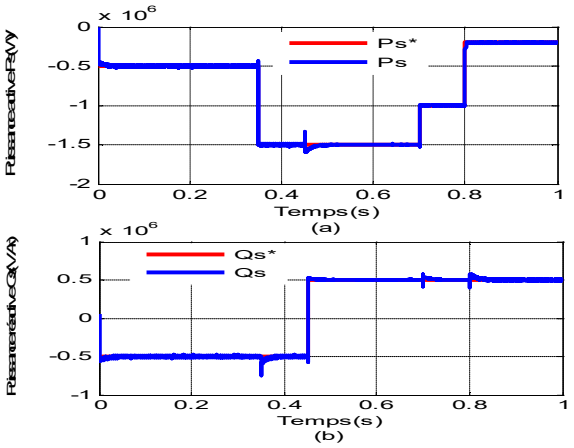


**Figure I :** IOLC of the DFIG at fixed wind speed

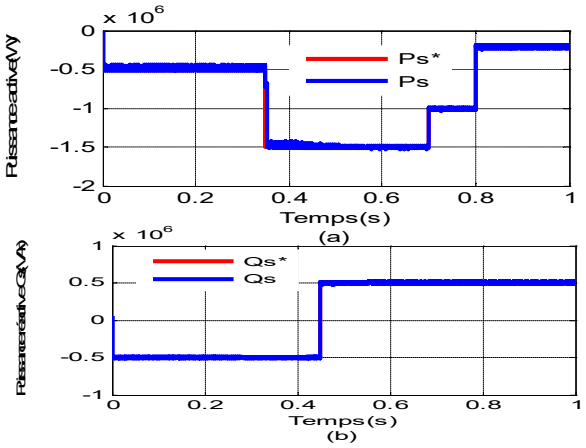


**Figure II:** SMC of the DFIG at fixed wind speed

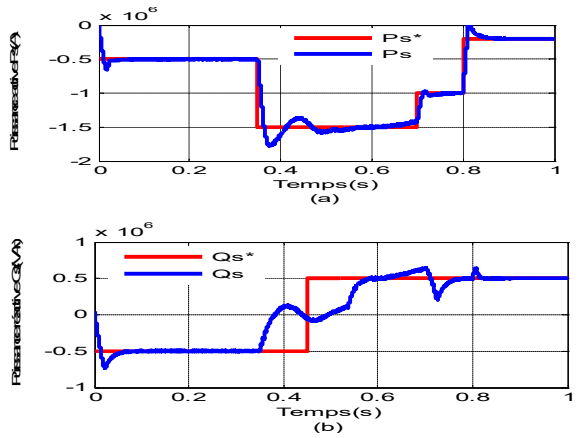


**Figure III :** robustness test of the IOLC

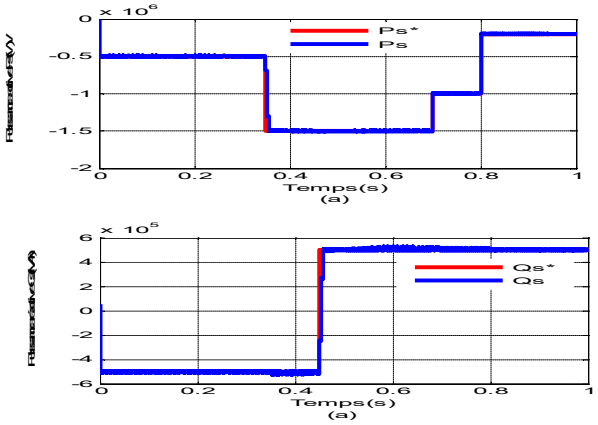


**Figure IV:** robustness test of the SMC

**References :**

[1] MESLEM MEHADJIA, « Commandes non linéaires de la machine asynchrone à double alimentation utilisée dans une chaîne de conversion d'énergie éolienneà vitesse variable» ,Mémoire de Master, Université Djilali Liabes Universityde Sidi Bel Abbes, juin 2018.
[2] BOUSSAID RAFIK , MORAD MOHAMMED ABDELHALIM, «Commandes non linéaires d'une machine asynchrone double alimentation»; Mémoire de Master, Université Abou Bekr Belkaïd de Tlemcen, 20 /06/2016
[3] KENNICHE HANA «Commande par linéarisation entrée/sortie d'une machine asynchrone avec un estimateur d'état du flux rotorique»; Mémoire de Master académique, Universite Kasdi Merbah de Ouargla, 2015.
[4] PAUL ETIENNE, « Commande non linéaire d'une machine asynchrone à double alimentation» ; thèse de Doctorat, Laboratoire d'Electrotechnique et d'Electronique Industrielle de l'ENSEEIHTUMR CNRS N_5828 ,2014.
[5] FENNI ATMANE, « Commande Non Linéaire Par Des Régulateurs En Mode Glissant D'une Machine Asynchrone à Double Alimentation (MADA) »; Mémoire de Magister, Université Mohamed Khider de Biskra, 19/12/2013.

# Combining optimal capacitor placement and optimal reconfiguration for distribution system load flow using ETAP

**Mohamed Ali-DAhmane[1], Farid Benhamida[1], Zegai Amine[2], Rachid Belhachem[2]**

*Irecom laboratory, departement. of electrotechnics*
*UDL university of Sidi Bel Abbes,Algeria*
*Email: Ali.mohamed28@yahoo.fr*

**ABSTRACT**

For the evaluation and operation of a real electrical distribution system the load flow solution is essential, it allows us to validate the sizing of cables, switchgear, transformers and determine the real (kW) and reactive (kvar) power losses at the different branch, magnitudes and voltage angles of the nodes. Load flow studies carried out to obtain suitable voltage profiles and loss rates under different operational conditions, low and high load. The results obtained help us to carry out other studies on the network.

To remedy the problem of high losses rate various approaches are used such as reconfiguration, optimal placement of capacitors, optimal placement of distributed generation and optimal use of electrical equipment.

The load flow analysis is also a starting point for other system studies [1].

1- To calculate the power flow of the branches starting from the last branch to the source in backward direction

$$P_k = P_{k+1} + P_{loss(k,k+1)} + P_{L(k+1)} \qquad Q_k = Q_{k+1} + Q_{loss(k,k+1)} + Q_{L(k+1)}$$

- $P_k$ and $Q_k$ are the active and reactive powers flowing through the branch $l$ from node $k$ to node $k+1$.
- $P_{L(k+1)}$ and $Q_{L(k+1)}$ are a real and a reactive loads powers at bus $k+1$.
- $P_{loss(k,k+1)}$ and $Q_{loss(k,k+1)}$ are real and reactive powers losses in the line connecting buses $k$ and $k+1$ may be computed as

$$P_{loss(k,k+1)} = R_k \frac{P_k^2 + Q_k^2}{V_k^2} \qquad Q_{loss(k,k+1)} = X_k \frac{P_k^2 + Q_k^2}{V_k^2}$$

To find the total power of the system, $P_{T,\,loss}$ by adding the losses of all the system feeders:

$$P_{T,loss} = \sum_{k=1}^{n} P_{loss(k,k+1)} R_k \qquad Q_{T,loss} = \sum_{k=1}^{n} Q_{loss(k,k+1)} R_k$$

2- To calculate the magnitudes and voltage angles of the nodes starting from the source node to the last node in forward direction.

$$V_{k+1} = \left[ V_k^2 - 2(P_k R_l + Q_k X_l) + (R_l^2 + X_l^2) \frac{(P_k^2 + Q_k^2)}{V_i^2} \right]^{1/2} \qquad \delta_{k+1} = \delta_k + \tan^{-1} \frac{(Q_k R_l - P_k X_l)}{\left[ V_k^2 - (P_k R_l + Q_k X_l) \right]}$$

The load flow studies are helpful to confirm selected switchgear, transformer, and cable sizing. These studies should also be used to confirm adequate voltage profiles during different operating conditions, such as heavily loaded and lightly loaded system conditions. Load flow studies can be used to determine the optimum size and location of capacitors for power factor correction. The results of load flow studies are also starting points for other system studies [1].

The management and optimization of the distribution electrical system (i.e., state estimation, VAR planning, etc.) calls for quick, efficient and repetitive load flow solutions.

Load flow analysis requires, first of all, determining all node voltages. The results of the voltages brought back to determine the currents that circulate in the different branches, the power flows, the losses of the system and other quantities in a steady state.

In the operating standards of an electrical distribution network, the voltage delivered to the consumer must vary within +/- 5 percent of the nominal, the voltage drop causes a reactive power flow (vars) for this reason the under-voltage is a serious problem in all public utility systems. The first fast solution is the reconfiguration system RDS, which is the modification of the network topology by changing the state of the switches open and closed taking into consideration the profile of the demand of the different consumers and the supply of all customers. But in some cases where the load conditions are high, the objective is not to reach 100%, so we go to the second solution, is to generate the reactive powers (Var) in proximity to the consumer side with the location of the optimal capacities.

In this paper, using ETAP (Electrical Transient Analyzer Program) to provides reliable and accurate results in realizing the IEEE 33 bus radial distribution system, we combine optimal capacitor placement and reconfiguration to analyze and optimize the IEEE 33 bus radial distribution system to overcome the problem of under voltage and minimize the losses.

Once an optimal topology is obtained for the different power condition and the optimal capacitor locations are achieved, the voltage profile of the system is further improved, the losses are minimized, which leads to an improved and stable system.

**Keywords:** Load Flow Analysis; Radial Distribution System; Optimal Capacitor Placement (OCP); Network Reconfiguration and electrical Transient Analyzer Program (ETAP).

**References**

[1] Rani and Vijaya, "Distribution system loss reduction by capacitors", Proc.of National Conference on Emerging Trends in Engineering(2000), Husur
[2] Rohit Kapahi, "Load Flow Analysis of 132 kV substation using ETAP Software" International Journal of Scientific Engineering Research, vol. 4, issue 2, Feb 2013, pp. 1-5.
[3] Rana A. Jabbar Khan, Muhammad Junaid and Muhammad Mansoor Asgher, "Analyses and Monitoring of 132 kV Grid using ETAP Software", In Electrical and Electronics Engineering, 2009. ELECO 2009. International Conference on, IEEE, 2009, pp. I-113 – I-118.
[4] Bompard, E. Carpaneto," Convergence of the backward/forward sweep method for the load-flowanalysis of radial distribution systems" Electrical Power and Energy Systems 22 (2000) 521–530.
[5] R. SrinivasaRao, K. Ravindra,"Power Loss Minimization in Distribution System Using Network Reconfiguration in thePresence of Distributed Generation" IEEE Transactions On Power Systems, Vol. 28, No. 1, February 2013.
[6] P. M. Anderson, A. A. Fouad, Power System Control and Stability, New York: IEEE Press, 1992.
[7] J. Arrillaga, N.R. Watson "Computer Modelling of Electrical Power Systems", second edition, ISBN: 978-0-471-87249-8, John Wiley and Sons [2001].
[8] Nadia M. Mahdi, "Power flow analysis of Rafah governorate network Distribution using ETAP software", International Journal of Physical Sciences vol. 1(2), pp. 019-026, June 2013.

# Comparaison des Approches de Commande pour la Machine Asynchrone à Double Alimentation : Vectorielle, Mode Glissant, Logique Floue

**AZZEDDINE Yasser Nadhir[1], NACERI Abdelatif[1], DJERIRI Youcef[2]**

[1] *Interaction Réseaux Electriques Convertisseurs Machines – IRECOM – , Laboratory Sidi Bel Abbes – ALGERIA*
[2]*Intelligent Control & Electrical Power Systems – ICEPS – Laboratory Sidi Bel Abbes - 22000 – ALGERIA*
*Email: nadir.azzeddine@gmail.com*

**ABSTRACT**

Ce travail vise à apporter une contribution significative au développement et à la mise en œuvre de stratégies de commande avancées pour la Machine Asynchrone à Double Alimentation (MADA) fonctionnant en mode moteur. La MADA, caractérisée par des enroulements statoriques et rotoriques connectés à deux onduleurs de tension, joue un rôle central dans les efforts de modernisation et d'efficacité énergétique. La motivation de cette recherche réside dans la nécessité d'améliorer la commande de la MADA. Les régulateurs proportionnels-intégrateurs (PI) classiques sont couramment utilisés dans l'approche de la commande vectorielle (Fig.1), mais leurs lacunes, telles que les dépassements indésirables et les erreurs statiques dans les systèmes non linéaires, nous ont amenés à explorer des améliorations. Dans cette étude, nous examinons l'application de la commande par mode glissant (Fig.2) et de la commande par logique floue (Fig.3) en tant que solutions potentielles pour relever ces défis. Notre recherche se penche sur la robustesse du découplage et de la commande, en examinant l'influence des harmoniques et de la Modulation de Largeur d'Impulsion, tout en tenant compte de l'application du mode glissant et de la logique floue. Les résultats indiquent que bien que le système de commande de la MADA montre une certaine résilience, il reste sensible aux perturbations extérieures et aux variations des paramètres de la machine. Les résultats des approches de commande par mode glissant, par logique floue et par la commande vectorielle sont validés par leur mise en œuvre dans l'environnement Matlab/Simulink. Nous évaluons la performance de ces trois approches de commande en termes de robustesse, de gestion des harmoniques, en prenant en compte l'Orientation du Flux Rotorique (Tableau.1).

**Mots-clés** : Machine asynchrone à double alimentation, commande vectorielle, régulateur PI, Modulation de Largeur impulsion, Orientation de Flux Rotorique, Commande par mode glissant, Commande par logique floue.

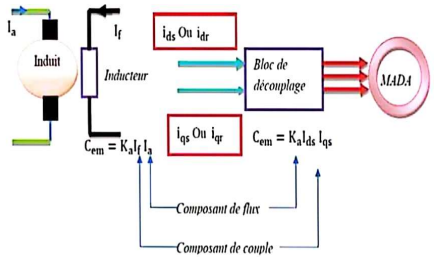


*Fig.1. Principe de la commande vectorielle de la MADA.*

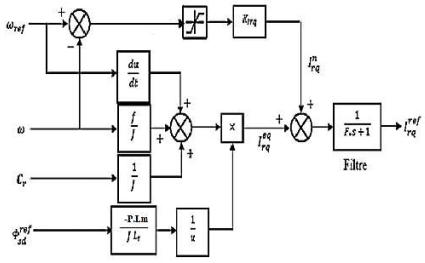


*Fig.2. La structure de régulateur de vitesse à mode glissant*

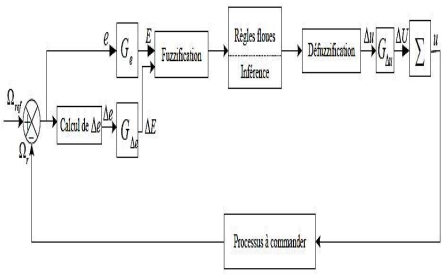


*Fig.3. Schéma synoptique d'un contrôleur flou de vitesse appliqué à la MADA..*

| | Commande vectorielle | Commande par Mode Glissant | Commande par logique floue |
|---|---|---|---|
| **Rapidité (temps de réponse $a^{\pm}$ 5% en seconde)** | 0,105<br>Bonne | 0,00971<br>Très bonne | 0,0003<br>Très bonne |
| **Précision (erreur statique%)** | 0,03%<br>Bonne | 0,019%<br>Très bonne | 0,005%<br>Très bonne |
| **Stabilité (dépassement%)** | 4,39%<br>Acceptable | 0%<br>Très bonne | 1%<br>Très bonne |
| **Complexité d'implémentation** | Forte | Moyenne | Moyenne |
| **Qualité d'énergie (THD %)** | Moyenne<br>30,32% | Mauvaise<br>53,17% | Moyenne<br>37,46% |
| **Robustesse** | Faible | Moyenne | Grande |

*Tableau.1. Comparaison des performances des trois types de commande proposées.*

**References**

[1] Djeriri.Y, « Directe du couple et des puissances d'une MADA associée à un système éolien par les techniques de l'intelligence artificielle » ; Thèse de doctorat en électrotechnique, Université Djillali Liabes de Sidi-Bel-Abbès, 2015.

[2] Djeriri. Y, Boudjema.Z Article, « Commande robuste par la logique floue et les réseaux de neurones artificiels de la GADA : étude comparative » ; Université Djillali Liabès de Sidi Bel-Abbès, Université Hassiba Benbouali, Chlef, 2017.

[3] Bekakra.Y,«Etude et Commande du Moteur Asynchrone à Double Alimentation (MADA) par Différentes Techniques Avancées»; Magister en Electrotechnique université d'el-oued 2010.

[4] Ardjoun.S.A.E, «Commande en vitesse par mode glissant d'une Machine Asynchrone à Double Alimentation»; Mémoire de Magister, Université DjillaliLiabes de Sidi Bel Abbes, 2010.

[5]Allali.A, «Application des techniques avancées pour le contrôle de la Machine Asynchrone Doublement Alimentée»; mémoire magistère en électrotechnique université Djilali Liabes sidi bel Abbés 2013.

[6] Azzeddine.Y.N , Djeffal.A.H ,« Contribution à l'étude et l'amélioration des performances d'un moteur asynchrone à double alimentation MADA»; Mémoire Master, Université Djillali Liabes de Sidi Bel Abbes, 2022.

[7] Ouanjli.N, « Contributions à l'étude et l'amélioration des performances d'une MADA fonctionnent en mode moteurs»;thèse de doctorat en génie électrique, université Sidi Mohamed Ben Abdellah de Fès, Maroc, 2020.

# Innovative Feature Selection Approach based on Metaheuristic Algorithms for Electricity Price Forecasting in Smart Grids

**Abderrahim Bakir[1], Abdelkader Rami[1]**

[1] *IRECOM Laboratory, Electrical Engineering Faculty, Djillali Liabes University, Sidi Bel Abbes, 22000,Algeria*
*Email: abderrahim.bakir@univ-sba.dz*

**ABSTRACT**

Smart Grids (SGs) are a modern approach to energy management that integrates advanced technologies, renewable energy sources, and improved consumer control. In this context, accurate Electricity Price Forecasting (EPF) is essential to enable efficient energy consumption and allocation. Traditional EPF models often struggle to handle large and diverse datasets, primarily owing to the volatility of electricity prices and their complex dependence on numerous variables, including electricity demand, weather conditions, fuel prices, and social and economic factors. Feature Selection (FS) is the process of identifying and selecting a subset of the most relevant features to improve the performance and efficiency of predictive models. FS can be categorized into several techniques. Where, wrapper methods stand out as they evaluate subsets of features using specific machine learning algorithms. An evolving approach to wrapper FS methods is the use of population-based metaheuristic algorithms. These algorithms, inspired by natural phenomena, explore large search space and select subsets that minimize an objective function (fitness). By employing the computational power and adaptive properties of metaheuristics, wrapper methods can efficiently navigate complex feature spaces, making them a promising approach for FS in tasks where traditional methods might fall behind. While metaheuristic methods have gained widespread recognition in classification FS tasks, their potential and capabilities in solving regression tasks such as EPF have remained under-researched, making their adaptation and use to tackle this problem a promising avenue for research and innovation. This study presents a robust and innovative FS approach that addresses a critical industrial need for accurate and efficient energy management in SGs and showcases its potential for significant improvements in short-term EPF. The main objectives of this study are:

Initially, to create a wrapper FS technique suitable for preprocessing SG data before performing EPF, this technique includes a metaheuristic algorithm as a search engine and uses Random Forest (RF) as a learning method. RF is an ensemble machine learning technique that improves predictive accuracy by using multiple decision trees trained on different subsets of data. RF is chosen for its ability to classify selected features according to their influence on the predictions and the overall performance. The population-based metaheuristics used in this study can be classified into five major categories based on their sources of inspiration: Evolutionary-based algorithms that draw on natural selection and evolution, swarm-based algorithms which are inspired by the collective behavior of social organisms, bio-inspired algorithms that mimic biological processes, physics/chemistry-based algorithms which are based on the principles of physics and chemistry, and human-based and plant-based algorithms that take cues from human behavior and the growth patterns of plants. The second objective is to evaluate and compare the performance of 44 different population-based metaheuristic algorithms in the FS context, employing various tasks to rank and evaluate their effectiveness. Task 1 focuses on the quantity of the selected features , while task 2 evaluates their quality. Task 3 focuses on the convergence performance, while task 4 examines the optimization time. Task 5 investigates the balance between exploration and exploitation, while task 6 explores the trade-off between the number of features and model accuracy. Finally, task 7 evaluates the forecasting performance of the selected features on new data. Key parameters for population-based metaheuristics include the number of

populations (representing subsets of features) and the stopping criteria (such as the maximum number of iterations). Applying the same parameter values to all metaheuristics ensures fair evaluation and eliminates potential bias associated with different settings.

The models in this study were developed in MATLAB 2021b and run on a system with an Intel® Core™ i5-6300U CPU processor and 8 GB of RAM, using data collected from the ISO New England SG [1]. The simulation results highlight that features related to electricity price, particularly real-time energy components and lagged prices, exhibit a higher suitability for accurate EPF compared to features related to electricity load, fuel prices, weather conditions, and temporal variables. In addition, the overall FS process reveals that recent metaheuristic algorithms, such as EPO, MPA, MRFO, HGSO, SMA, and GWO, are more effective in addressing electrical engineering challenges, such as selecting relevant SG data for accurate short-term EPF, compared to older metaheuristics, such as CS, PSO BA, FA, GA and SA. The innovative aspect of our approach is the comprehensive evaluation of metaheuristic algorithms across multiple tasks, revolutionizing the FS process. This methodology sets a new standard and reference for accuracy and efficiency in short-term EPF in the SG domain providing researchers and practitioners with valuable insights and techniques to improve their forecasting models.

**Keywords:** Wrapper Feature Selection; Metaheuristic Algorithms; Smart Grid; Electricity Price Forecasting; Random Forest.

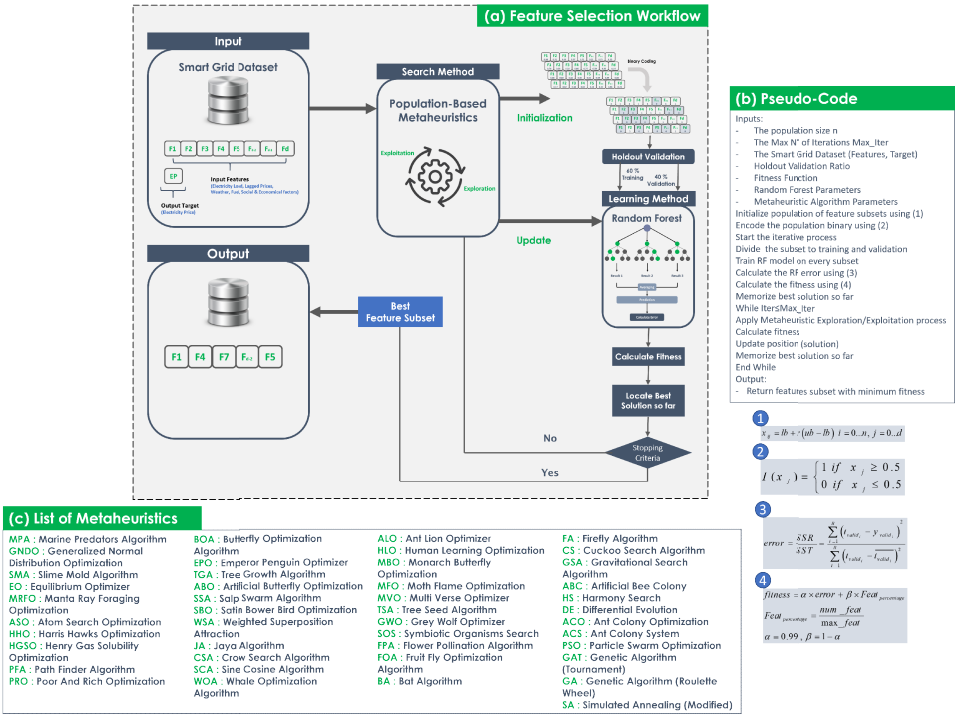


**Fig1.** Proposed Approach, (a) Feature Selection Workflow, (b) Pseudo-Code, (c) List of Metaheuristics.

## References

[1] ISO-NE, "ISO New England," 2016. [Online]. Available: http://www.iso-ne.com/. [Accessed: 15-Aug-2023].

# Optimisation de la Puissance Éolienne par une Nouvelle MPPT sans Asservissement de Vitesse Basée sur le Contrôle non Linéaire

**BOUDJEMAI Hamza[1], ARDJOUN Sid Ahmed El Mehdi[1] et CHAFOUK Houcine[2]**

*[1]IRECOM Laboratory, Faculty of Electrical Engineering, Djillali Liabes University, Sidi Bel-Abbes, Algeria.*
*[2]Normandy University, UNIROUEN, ESIGELEC, IRSEEM, 76000 Rouen, France.*
*Email : boujemaa.hamza802@gmail.com*

**RESUME**

Actuellement, le développement des énergies renouvelables représente l'une des solutions les plus prometteuses qui ont contribué de manière significative à réduire la pollution atmosphérique et environnementale causée par l'exploitation des ressources fossiles, notamment l'énergie éolienne qui monte en puissance de plus en plus.

En ce qui concerne le développement des éoliennes, l'amélioration du rendement de production de cette source d'énergie elle suscite aujourd'hui l'intérêt de nombreux chercheurs et fabricants. Dans le même contexte, le présent travail décrit une étude plus détaillée sur la technique MPPT sans asservissement de la vitesse. Mais contrairement à plusieurs chercheurs qui appliquent cette technique dans le modèle mécanique de système éolien et sans aborder l'effet d'une grande inertie de la turbine éolienne, ni l'influence de la variation de la charge électrique, nous avons choisi dans notre cas de le rendre une solution pratique et efficace pour forcer la turbine éolienne à extraire le maximum de la puissance du vent. Cela est possible en appliquant la commande dans la partie électrique de la chaîne éolienne à travers des contrôleurs non linéaires tels que : le contrôleur backstepping, synergétique et floue.

La modélisation complète du système éolienne étudié avec le schéma de commande proposé est réalisée dans l'environnement MATLAB/Simulink, puis validé expérimentalement via la carte dsPACE1104 sur un banc d'essai expérimental. Plusieurs scénarios ont été adoptés pour la validation, y compris l'influence de la variation de la vitesse du vent et des changements de la charge électrique. Les résultats expérimentaux obtenus sont nettement meilleurs et montrent des très bonnes performances pour le suivi du point de puissance maximale. Non seulement cela, mais également la nouvelle conception de MPPT sans asservissement de la vitesse a l'avantage d'être simple, efficace, robuste et capable de prend en compte les non-linéarités du système éolienne et même l'effet de l'inertie important de la turbine éolienne. Franchement, ces résultats nous motivent à travailler de plus en plus pour les améliorer. Donc, pour les travaux futurs, on voudrait appliquer la technique MPPT étudiée sur une vraie éolienne couplé au réseau électrique. Ainsi, on souhaite aussi d'ajouter un système de surveillance de défaut qui reste une solution efficace pour protéger et réduire les coûts de réparation d'une éolienne.

**MOTS CLES :** Turbine éolienne ; Contrôle non linéaire ; MPPT ; Convertisseur Boost ; MATLAB/Simulink ; dsPACE1104.

**RÉFÉRENCES**

[1] X. Deng, J. Yang, Y. Sun, D. Song, Y. Yang and Y. H. Joo, "An effective wind speed estimation based extended optimal torque control for maximum wind energy capture," IEEE Access, vol. 8, 2020, pp. 65959-65969.

[2] M. Chakib, T. Nasser and A. Essadki, "Comparative study of active disturbance rejection control with RST control for variable wind speed turbine based on doubly fed induction generator connected to the grid," International Journal of Intelligent Engineering and Systems, vol. 13, no. 1, 2020, pp. 248-258.

[3] A. Dahbi, A. Reama, M. Hamouda, N. Nait-Said and M-S. Nait-Said, "Control and study of a real wind turbine," Computers and Electrical Engineering, vol. 80, 2019, pp. 106492.

[4] M. Yin, W. Li, C. Y. Chung, L. Zhou, Z. Chen and Y. Zou , "Optimal torque control based on effective tracking range for maximum power point tracking of wind turbines under varying wind conditions," *IET Renewable Power Generation*, vol. 11, no. 4, pp. 501–510, 2017.

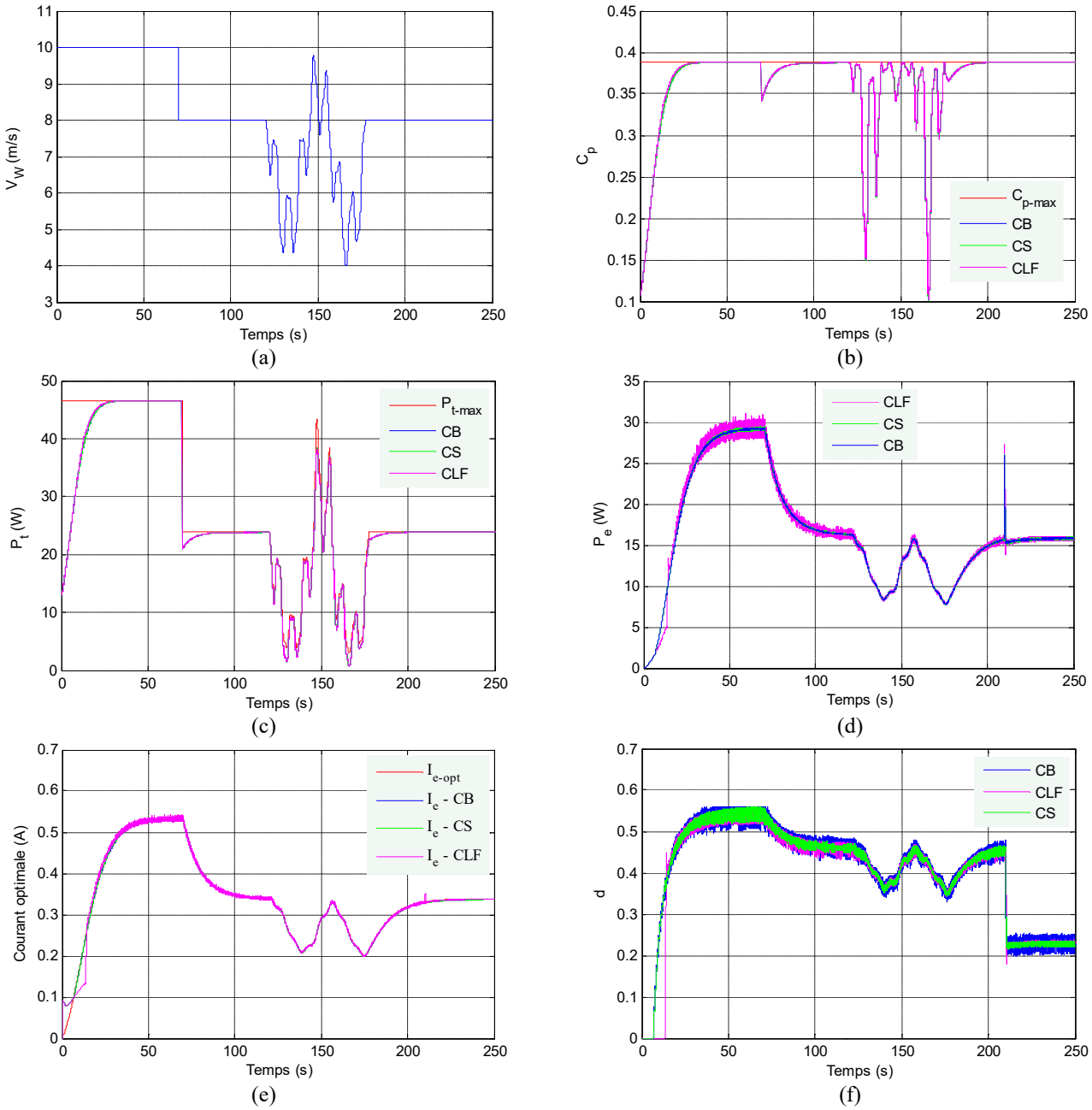


**Fig. 1.** Résultats expérimentaux : (a) profil du vent, (b) coefficient de puissance de la turbine éolienne, (c) puissance de la turbine éolienne, (d) puissance aux bornes de la charge électrique, (e) comparaison entre le courant optimale et les courants à l'entrée du convertisseur Boost, (f) rapport cyclique du convertisseur Boost.

# Optimisation de l'efficacité énergétique des moteurs à induction dans les véhicules électriques : Une approche de commande économe en énergie

**DJELLOULI Younes[1], ARDJOUN Sid Ahmed El Mehdi[1] , CHAFOUK Houcine[2], DENAI Mouloud[3]**

[1] *Laboratoire IRECOM, Faculté de génie électrique Université Djillali Liabes Sidi Bel Abbes, Algérie.*
[2] *Université de Normandie, UNIROUEN, ESIGELEC, IRSEEM, 76000 Rouen, France.*
[3] *École de physique, d'ingénierie et d'informatique, Université de Hertfordshire, Hatfield, Royaume-Uni.*
*Email: djellouli08younes08@gmail.com (Corresponding author's email)*

**RESUME**

L'autonomie est un critère essentiel pour évaluer les performances des véhicules électriques, définie par la distance qu'ils peuvent parcourir. Cette autonomie dépend de divers paramètres, tels que le modèle du véhicule, le type de batterie, le moteur utilisé, entre autres. Pour maximiser l'efficacité énergétique, les systèmes de contrôle peuvent jouer un rôle déterminant en suivant le point de fonctionnement optimal en fonction de la vitesse et de la charge mécanique du moteur.

L'objectif de ce travail est de présenter une approche de contrôle économe en énergie pour les moteurs à induction à enroulement ouvert (OEWIM) utilisés dans les véhicules électriques (VE), en prenant en compte les pertes énergétiques dans le fer du moteur. La commande introduit également un algorithme d'optimisation énergétique visant à réduire les pertes du moteur en calculant le flux statorique optimal en fonction du couple de charge et de la vitesse de rotation, en se basant sur un modèle dynamique amélioré de l'OEWIM, qui inclut les pertes dans le fer.

Les paramètres de performance analysés dans ce travail sont la dynamique du véhicule et son efficacité. Les résultats de simulations confirment l'efficacité de la commande optimisée, avec une amélioration de l'efficacité énergétique et une réduction des pertes de puissance. En outre, ces résultats ont été validés expérimentalement sur un banc d'essai pour confirmer les performances de l'algorithme de minimisation des pertes proposé.

**Mots-clés:** véhicules électriques, OEWIM, efficacité énergétique, flux statorique optimal, contrôle scalaire, dSPACE1104.

**Méthodes :** La technique proposée modifie la référence de flux du stator pour suivre le point de meilleur rendement. Elle se base sur le modèle dynamique amélioré de l'OEWIM utilisé dans les véhicules électriques (VE), qui inclut les pertes de fer. L'algorithme de minimisation des pertes (LMC) calcule le flux de référence selon le point de fonctionnement du moteur en termes de couple et de vitesse, et appliquée à la structure de commande afin d'imposer à la machine un fonctionnement à rendement optimal.

**Résultats Expérimentaux :**

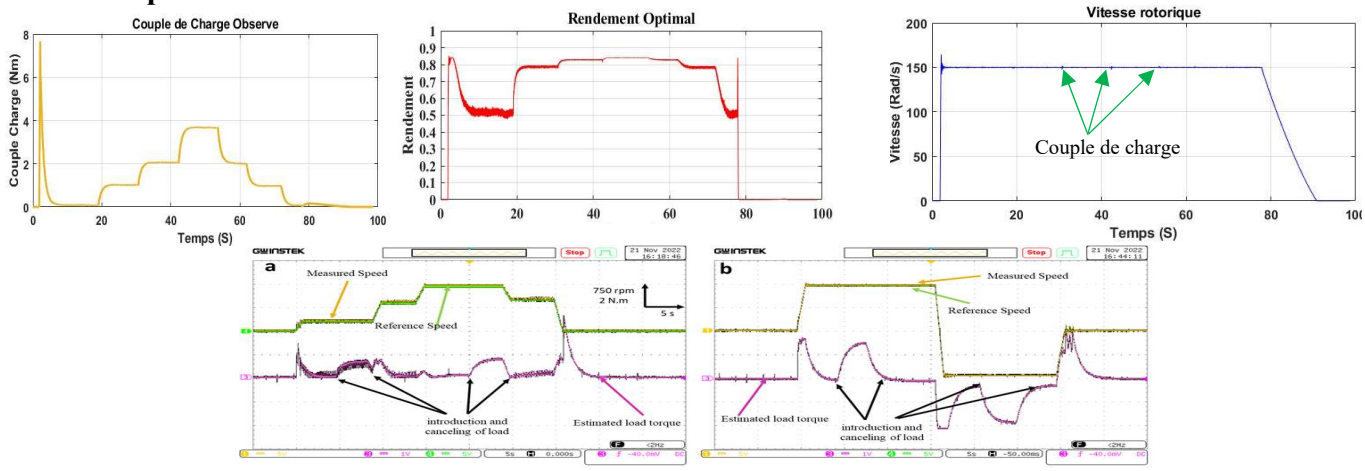

Fig. 1. Résultats expérimentaux.

**Conclusion**

Le travail présenté dans cet papie concerne une approche d'optimisation de l'efficacité énergétique d'un moteur asynchrone à cage d'écureuil, établie et appliquée à une structure de contrôle scalaire.. La technique est basée sur la détermination de valeurs de flux optimales calculées en utilisant un modèle dynamique amélioré qui inclut l'effet des pertes fer.

**References**

[1] M. Zerdani, S. A. E. M. Ardjoun, H. Chafouk, et M. Denaï, « Experimental Investigation of Decoupled Discontinuous PWM Strategies in Open-End Winding Induction Motor Supplied by a Common DC-link », IEEE J. Emerg. Sel. Top. Power Electron., 2023.

[2] Y.-F. Jia et al., « Control strategy for an open-end winding induction motor drive system for dual-power electric vehicles », IEEE Access, vol. 8, p. 8844-8860, 2020.

[3] Z. Yu, C. Gan, K. Ni, Y. Chen, et R. Qu, « A simplified PWM strategy for open-winding flux modulated doubly-salient reluctance motor drives with switching action minimization », IEEE Trans. Ind. Electron., vol. 70, no 3, p. 2241-2253, 2022.

[4] G. Khoury, R. Ghosn, F. Khatounian, M. Fadel, et M. Tientcheu, « Energy-efficient field-oriented control for induction motors taking core losses into account », Electr. Eng., vol. 104, no 2, p. 529-538, 2022.

[5] K. Lee et Y. Han, « Simple Discontinuous Pulse-Width Modulation Scheme for the Loss Reduction of a Dual Inverter Fed an Open-End Winding Induction Motor », IEEE Trans. Energy Convers., vol. 38, no 1, p. 495-506, 2022.

[6] I. J. Smith et J. Salmon, « High-efficiency operation of an open-ended winding induction motor using constant power factor control », IEEE Trans. Power Electron., vol. 33, no 12, p. 10663-10672, 2018.

# Réseaux de Neurones Artificiels pour commander un générateur photovoltaïque avec une batterie de stockage

**A. Ghalem[1], A. Naceri[1], Y. Djeriri[2]**

[1] *Département d'Electrotechnique, Faculté de Génie Électrique, Laboratoire d'Interaction Réseaux-Convertisseurs-Machines (IRECOM), Université Djillali Liabes, Sidi Bel-Abbes, Algérie*
[2] *Département d'Électrotechnique, Faculté de Génie Électrique, Laboratoire de Contrôle Intelligent et des Systèmes Électriques de Puissance (ICEPS), Université Djillali Liabes, Sidi Bel-Abbes, Algérie.*
*Contact: ghalem.abdelhak@yahoo.com*

**RESUME**

Les systèmes photovoltaïques sont couramment utilisés pour convertir l'énergie solaire en électricité, mais leur efficacité est limitée. Cependant, l'utilisation de réseaux neuronaux artificiels pour le suivi du point de puissance maximale (MPPT) permet une réponse rapide et précise aux variations atmosphériques, améliorant ainsi le rendement et la gestion de la puissance dans différentes conditions. Des simulations avec MATLAB/SIMULINK confirment la validité de cette approche.

**Mots cles :** Réseaux neuronaux artificiels ; MPPT ; Générateur photovoltaïque ; Batterie

Cette étude se concentre sur l'utilisation de l'énergie solaire, en particulier la conversion directe en électricité à l'aide de systèmes photovoltaïques, en combinant des réseaux de neurones artificiels pour optimiser la gestion de la puissance maximale et la charge de la batterie, démontrant une précision dans le suivi de la puissance maximale théorique du générateur photovoltaïque dans diverses conditions atmosphériques.

Dans cet article, un réseau neuronal à cinq couches est employé pour suivre le point de puissance maximale, tel qu'illustré dans la Figure 1. Les paramètres d'entrée comprennent la température "T" et l'irradiance "E", tandis que la sortie correspond au signal de contrôle du convertisseur Boost.

Les équations qui définissent le système sont les suivantes : l'équation 1 décrit le modèle moyen du convertisseur, tandis que l'équation 2 modélise le générateur photovoltaïque (GVP).

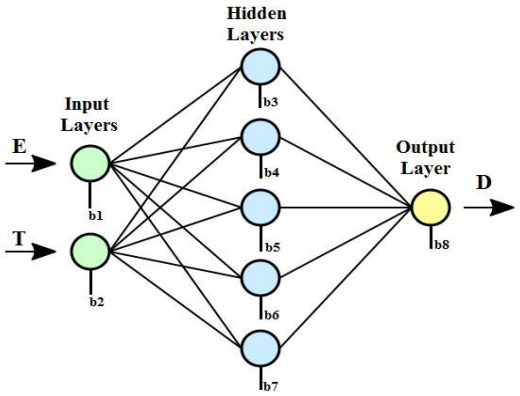


*Fig 1. La structure du réseau neuronal*

$$\begin{cases} \dot{V}_{pv} = \frac{1}{C_1} I_{pv} - \frac{1}{C_1} I_L \\ \dot{I}_L = \frac{1}{L} V_{pv} - \frac{1-\alpha}{L} V_{Dc} \\ \dot{V}_{Dc} = \frac{1-\alpha}{C_2} I_L - \frac{1}{RC_2} V_{Dc} \end{cases} \quad (1)$$

$$I_{pv} = I_{ph} - I_0 \left[ exp\left( \frac{U_{pv} + R_s I_{pv}}{V_t n} \right) - 1 \right] - \frac{U_{pv} + R_s I_{pv}}{R_{sh}} \quad (2)$$

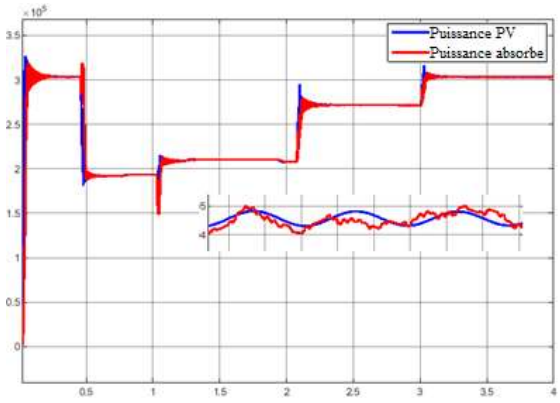


*Fig 2. Puissance du générateur PV et puissance absorbée (puissance de sortie du Boost)*

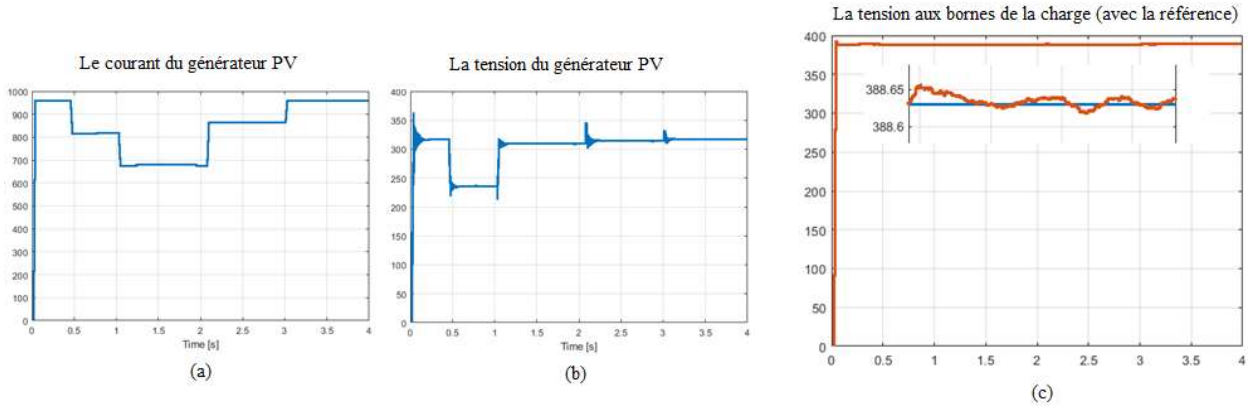


*Fig 3. Résultat de simulation : Courant, Tension PV (a, b) et Tension regelé de la charger (c)*

Les figures de tension et de courant, combinées avec l'utilisation du contrôleur basé sur les Réseaux de Neurones Artificiels (figure 3), démontrent une remarquable stabilité de la tension de charge, avec des perturbations mineures (dans l'ordre de 0,05 Volts). La figure 2 montre clairement que la puissance extraite du générateur PV suit rapidement et précisément le Point de Puissance Maximale (MPP). En conséquence, il est possible de conclure que le système de contrôle basé sur les Réseaux de Neurones Artificiels présente une excellente performance dynamique dans le suivi du point de puissance maximum.

**References**

[1] M. Samir Saadouni, N. Bilad Abdellah et S. Mahmoud, Renewable energies : sources and uses, 1st ed., vol. 1, 1 vol. Al-Yazuri Scientific, 2012.
[2] « Solar Energy Industries Association », Solar Energy Industries Association, https://www.seia.org/
[3] Clean Energy Council, « Approved PV Modules », 24 septembre 2021. [en ligne]. Disponible : https://www.solarsafety.com.au/approved-panels-list
[4] L. ANNE, C. PASCAL, B. JEAN-PAUL, and F. BENJAMIN, Cellules solaires Les bases de l'énergie photovoltaïque, 5th ed. Paris: Dunod, 2010.
[5] A.-R. Haitham, M. Mariusz et A.-H. Kamal, Power Electronics for Renewable Energy Systems, Transportation and Industrial Applications-Wiley (2014). Royaume-Uni : IEEE, 2014.
[6] R. MUHAMMAD H, Power Electronics Handbook, 892 vol. Auburn University : Academic Press Series in Engineering.

# Post-contingency Assessment by Sensitivity Factors for Power System Congestion

**Haba Mekki[1], Benhamida Farid[1], Souag Slimane[1] , Bouddou Riadh[1] , M. Ali-dahmane[1]**

[1] *Irecom laboratory, dept. of electrotechnics UDL University of Sidi Bel Abbes, Sidi Bel-Abbes, Algeria*
*Email:mekki_haba@yahoo.com*

**ABSTRACT**

This paper outlines a calculation method for ac load flow program for post-contingency based on a sensitivity factor for power system security calculated from dc power flow and implemented in a Matlab environment for post-contingency assessment. Power system congestion happens when insufficient power transmission system capacity is low to satisfy the electricity demand. It can occur for several reasons, including rising electricity demand, declining generation capacity, or transmission equipment constraints. Congestion can result in a number of problems, such as voltage dips, power shortages, and even blackouts. Congestion can also lead to increased electricity costs in impacted areas, as electricity providers must pay more to supply electricity to clients. The contingency analysis is critical in ensuring power system safe, reliable, and efficient operation. It helps power system engineers identify potential problems and develop effective strategies for preventing or mitigating the impact of these problems on the power system and which can assist in balancing the demand and supply of electricity, thereby enabling the efficient and reliable operation of the power system [1], [2]. Electrical system safety requires procedures to keep the system running during component failure. For example, a production unit can be shut down due to a failure of secondary equipment, or a transmission line can be damaged by a weather storm and shut down by an emergency relay. When one failure results in another failure in the system, it is called cascading failure, which leads to a system blackout. System security is classified into three major functions, which are carried out in an operation control center. These are System monitoring (SCADA, state estimation), Contingency analysis, and Security constrained OPF (SCOPF) [2]. a next step, the second main safety task is contingency analysis. Results from this kind of analysis enable systems to be exploited protectively. Most problems in a power system can result in severe problems in such a short period that the system operator cannot react quickly. Often this is the case with failures in sequence. Due to this feature of the system operation, modern operating systems are provided with contingency software to analyze potential problems in the system. Such reports are built on a pattern of the electrical system and are employed to examine failures and warn operators of possible overloading or out-of-range voltages. The optimal power flow under safety constraints is considered a third safety function of the method. This option combines a contingency analysis with an optimal power flow that attempts to adjust the optimal output dispatch, along with other corrections. When a safety analysis occurs, no contingency leads to a safety violation.

The power system's operational states can be split into four different states: Optimal economic dispatch, Post-contingency, Safe dispatch, Post-contingency security. The impact of the incident on a system is assessed using the Line Failure Distribution Factor named *d*-factors or LODF and the generation shift distribution factor called *a*-factors or GSDF. Contingency analysis linear methods have been utilized for several years [2], [3] in the assessment of the LODF matrix [4] and in the production shift distribution factor approximation. The present paper reports a computational program implemented within Matlab for possible post-emergency scenarios based on the sensitivity factor to power system security, estimated utilizing the dc power flow [5]-[6]. In common, failure affects any given system by shifting the energy flowing on the interrupted elements in conditions before the failure to other locations in the system. Such variations can either decrease or increase the power flow on the facilities depending on the system architecture, load, and generation allocation. Computationally, dc load flow has many distinct advantages over

conventional N-R power flow. As a result, DC power flow can be anticipated to be approximately ten times faster than regular power flow [7], [8]. Therefore, the DC power flow is used to estimate the *a* and *d* sensitivity matrices, which are the focus of the developed post-contingency analysis program, more quickly [9],[10]. DC power flow provides a more straightforward approach to power flow by performing several approximations and simplifies the power flow process to a simple equation system. To this end, we have developed a Matlab program appropriate for contingency studies considering line outage distribution factors (LODFs) and generation Shift distribution factors (GSDFs). The programs in Matlab are built to perform two-way communication between a load flow and contingency analysis routine. To validate the proposed algorithm, comparisons are made between the ac power flow from PowerWorld and approximated solution obtained by our algorithm. The accuracy of the proposed approach is demonstrated by applying it to a 6-bus test system. The calculation outcomes indicate an improved efficiency of the developed method concerning the execution time and the quality of the results.

**Keywords:** system congestion, contingency analysis; sensitivity matrices.

**References**

[1] Daniel S. Kirschen, Goran Strbac, Fundamentals of Power System Economics, 2nd Edition, John Wiley & Sons, New York, 2019.

[2] P. Venkatesh, B. V. Manikandan, S. Charles Raja, A. Srinivasan, Electrical power systems: analysis, security and deregulation, PHI Learning Pvt. Ltd., 2nd edition, 2017 - 576 pages

[3] M. Shahidehpour, H. Yamin, Z. Li, Market Operations in Electric Power Systems: Forecasting, Scheduling, and Risk Management, John Wiley and Sons, New York, 2002.

[4] M. Giuntoli, V. Biagini and K. Schönleber, "Novel Formulation of PTDF and LODF Matrices for Security Constrained Optimal Power Flow for Hybrid AC and DC Grids," 2019 IEEE PES Innovative Smart Grid Technologies Europe (ISGT-Europe), Bucharest, Romania, 2019, pp. 1-5, doi: 10.1109/ISGTEurope.2019.8905672.

[5] B. M. Weedy, and B. J. Cory, Electric Power System, 5th Eds., John Wiley and Sons, New York, 2012.

[6] A. J. Wood, and B.F. Wollenberg, Power Generation, Operation and Control, 2nd Eds., John Wiley & Sons, New York, 1996.

[7] H. Saadat, Power System Analysis, Eds. McGraw-Hill, NY, 1999.

[8] J. Duncan Glover and Sarma. 2017. Power System Analysis and Design, SI Edition. Cengage Learning, USA.

[9] R. Vykuka and L. Nohácová, "Sensitivity factors for contingency analysis," 2015 16th International Scientific Conference on Electric Power Engineering (EPE), Kouty nad Desnou, Czech Republic, 2015, pp. 551-554, doi: 10.1109/EPE.2015.7161162.

[10] H. Zhou, K. Yuan and C. Lei, "Security Constrained Unit Commitment Based on Modified Line Outage Distribution Factors," in IEEE Access, vol. 10, pp. 25258-25266, 2022, doi: 10.1109/ACCESS.2022.3156081.

# Experimental Analysis of Factors Affecting the Separation of Electrical Cable Waste in an Electrostatic Plate Separator

**A. Lahcen[1], S. Touhami[1], M. Maammar[1], W. Aksa[1], A.Timatine[2]**
[1] *IRECOM Laboratory, University of Sidi-Bel-Abbes, 22000 Sidi-Bel-Abbes, Algeria*
[2] *APELEC Laboratory, University of Sidi-Bel-Abbes, 22000 Sidi-Bel-Abbes, Algeria*
*Email : seddik.touhami@gmail.com*

## ABSTRACT

This article presents the results of an experimental study on the separation of waste electrical cables using an electrostatic separator based on innovative technology. Recently developed and protected by a patent in the name of the APELEC laboratory of the University of Sidi Bel Abbés, this installation has shown promising results in the separation of waste electrical cables characterized by a wide particle size range. The particle size characteristics of the cable waste processed in this facility constitute the main advantage compared to conventional devices such as roll-type electrostatic separators. In addition, this installation exhibits exceptionally high productivity, making it suitable for use in the industrial sector. The operation of this installation is based on the use of a plate conveyor, each plate being equipped with two electrodes powered by an alternating high voltage source. This conveyor ensures the attachment of conductive particles to its surface, which facilitates the separation of the mixture by aspirating the insulating particles. In this study, the effects of the effective voltage, product flow rate, and aspirator rotation speed were analyzed using the experimental design methodology. The results obtained indicate that these factors have a significant influence on the separation efficiency. The experimental models developed during this study were utilized with optimization methods to identify the optimal operating point of the installation.
**Keywords:** Electrostatic Separation; Experimental Design; Optimization.

## I. INTRODUCTION

The electrostatic plate separator (Figure 1) is considered as a new installation resulting from the improvement of aspiration separation systems [1-2], widely used in the electrical cable waste recycling industry. The improvements made to this installation result in the integration of electrostatic techniques aimed at increasing the adhesion of conductive particles to the surface of the conveyor plates. This approach facilitates the aspiration of insulating particles while minimizing losses of conductive material. The performance of the new system is influenced by multiple factors. To achieve the optimal operational configuration for the installation, we conducted an experimental parameter adjustment, using the experimental design method [3].

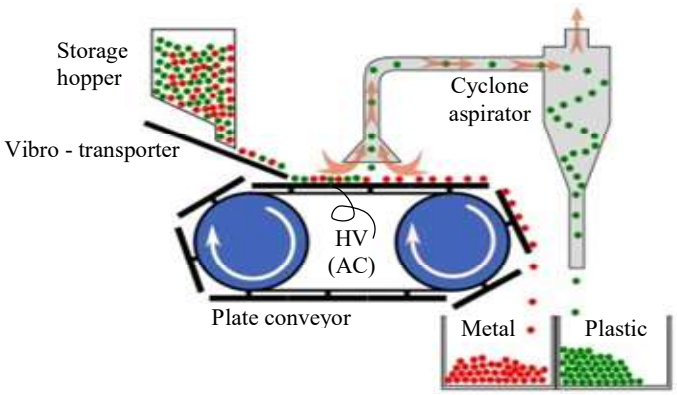


*Figure 1. Descriptive diagram of the electrostatic plate separator.*

## II. EXPERIMENTAL METHODS

The experiments were carried out using a laboratory prototype shown schematically in Figure 1. The system offers the possibility of adjusting several parameters, including the flow rate of the product (*D*), the rotation speed of the aspiration motor (*N*) and the high voltage applied to the conveyor plates (*U*). The material sorted in this study is supplied by an Algerian company specialized in recycling waste electrical cables. This waste category, labeled as an insulating product within the company, is recovered using a conventional aspiration separation system.

## III. RESULTS

The results of the experimental study carried out using a face-centered composite plane demonstrated that increasing the rotation speed of the aspiration motor (*N*) has a positive effect on PVC recovery (Figure 2.b) but has a negative effect on copper recovery (Figure 2.a). On the other hand, the influence of high voltage (*U*) manifests itself in the opposite way for copper and is less significant in relation to the rotation speed of the suction motor for PVC.

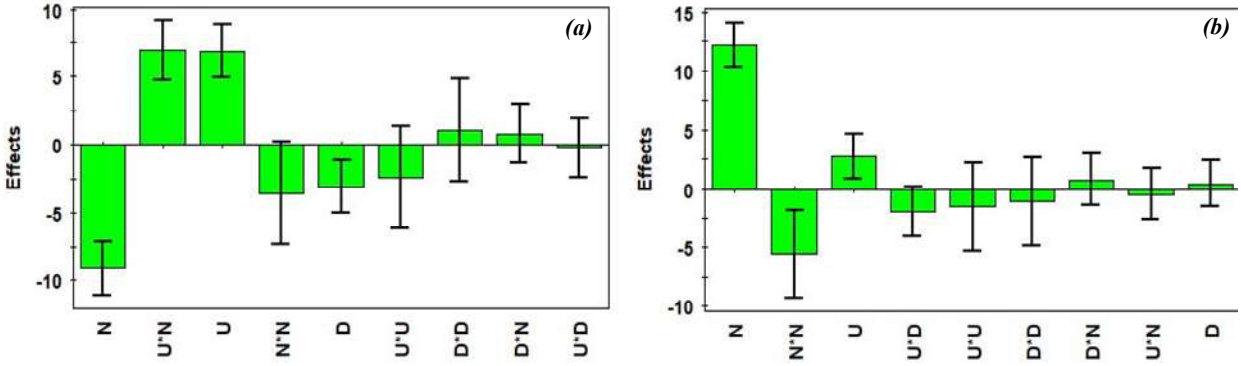


*Figure 2. Effects of factors U, N, and D on the recovery of copper (a) and PVC (b)*

## IV. CONCLUSION

An experimental study was carried out to examine the impact of product flow rate (*D*), aspiration motor rotation speed (*N*), and high voltage applied to the conveyor plates (*U*). The results obtained were used to formulate mathematical models capable of predicting the recovery of copper and PVC. These models are then used to determine the optimal operating point of the installation. Analysis of the effects of factors on copper recovery revealed that an increase in voltage leads to improved copper and PVC recovery. However, increasing the aspiration motor speed has a contradictory impact by reducing copper recovery while improving PVC recovery. Therefore, to optimize the operation of the installation, we optimized both criteria simultaneously.

### References

[1] N.E. Menad, Physical Separation Processes in Waste Electrical and Electronic Equipment Recycling. WEEE Recycling, (2016) 53.
[2] M. Kaya, Current WEEE recycling solutions. Waste Electrical and Electronic Equipment Recycling, (2018) 33.
[3] L. Eriksson, E. Johansson, N. Kettaneh-Wold, C. Wikström, S. Wold, Design of Experiments. Principles and Applications, Sweden, Stockholm:Learnways AB, (2000).

# Estimation of the purity and recovery of non ferrous metal separation system using the capacitance of an industrial capacitor

**M. Louahedj[1], W. Aksa[1], F. Miloua[2], S. Touhami[1], M. Rezoug[1]**

[1]*IRECOM laboratory, university of Djillali Liabbes, 22000 Sidi-Bel-Abbes, Algeria*
[2]*APELEC laboratory, university of Djillali Liabbes, 22000 Sidi-Bel-Abbes, Algeria*
*Contact: louahedjmustafa22@gmail.com*

**ABSTRACT**

A separation system requires an effective control strategy to determine the quality of the recovered products, as any system, regardless of its nature, is unable to consistently produce the exact same product. Given the customers demands for high-quality products, the task for manufacturers becomes a bit challenging, as they need to optimize the product recovery system to the maximum, which requires control techniques in case of machine performance degradation. It is in this context that the objective of our project has been focused, by developing a new control and quantification device for the concentrations of compounds in a granular mixture, be it insulator-insulator or conductor-insulator. The prototype that has been developed (parallel plate capacitor) can function as a capacitive sensor, capable of continuously providing information on the purity of the recovered products as well as the overall system status. Estimating purity and recovery using this prototype may be more appropriate as a fast and preliminary method of quality control. Several experimental tests have been conducted in the laboratory within this framework.

**Keywords:** Separation system; capacitor; control; quantification; purity; recovery.

## I. INTRODUCTION

The estimation of the purity and recovery of non-ferrous metal separation system refers to the process of determining the effectiveness of a system designed to separate non-ferrous metals from mixed materials. The primary objective of this estimation is to assess the efficiency and accuracy of the separation system in terms of both purity and recovery. The estimation process involves various techniques and methodologies, including data analysis, statistical modeling, and physical testing, to quantify the purity and recovery rates. Accurate estimation of the purity and recovery of non-ferrous metal separation systems is crucial for industries involved in metal recycling, mining, and waste management.

## II. EXPERIMENTAL METHODS

We have prepared the model, which is a parallel plate capacitor (PPC), which has metal plates covered with a black ribbon arranged in notches on either side of a rectangular-shaped tray. Each pair of plates thus forms a capacitor. The distance between the plates of each pair is e = 11 mm and each armature is connected to the measuring device via a connection terminal. All plates have the same surface dimension (length * width) = (230 * 140) mm2.

Before starting the capacity measurements with this model, we tried to see the response of the different capacity measuring instruments (the multimeter as an example) before choosing the right instrument, and this for different classes of materials (physical nature and size). Preliminary measurements were made on a small capacitor which has two armatures of the same surface separated by a distance e = 14 mm. Each plate is insulated with a black tape to prevent short circuit in the case of a conductive material. These preliminary measurements will guide us to make a good sizing of our sensor.

During all subsequent experiments, the weighing of the masses of the pure or mixed granulated products is carried out using a precision 0.4 g balance. For continuous data acquisition, we used a 500khz LC meter connected to a computer. The Vibro-Transporter is used to transport our product and deposit it in the PPC.

*Fig 1: the separation control prototype plus a vibro-transporter, digital scale and LC meter*

All we have to do now is notice the change in capacitance when the amount of mass of the insulator and conductor is changed together. First, the variation in the value of insulator-insulator capacity (granules) that have the same permittivity was investigated using the two products, Acrylonitrile butadiene styrene (ABS) and polycarbonate (PC), are two solid insulators of the thermoplastic polymer family. The capacity of the mass range from 0 to 200 g is measured with a pitch of 20 g separately for the two products, the capacitance of the capacitor is then calculated by mixing the two products. At the end, the three curves of the three tests are drawn and the variation of the capacity as a function of the mass of the products is analyzed. In a second step, the same tests were carried out to see the evolution of the value of the capacitance of the conductor-insulator mixture, this time the two mixed products are Cu copper and ABS.

## III. RESULTS

To find the purity of the product, we used three methods, each of which was better than the other in terms of approaching the true value of the purity of the product. The first method is the determination of the purity of copper by calculating the capacitive ratio, the second is the determination of the purity of copper by differential measurement, And recently, a mathematical model has been found that can determine the purity result based on the value of the measured capacity:

$$Cm - d = Ccu \times \frac{Mcu}{Mtot} + Cabs \times \frac{Mabs}{Mtot}$$

$C_{m\text{-}d}$: the value of the capacity of the mixture deducted in pF; $C_{cu}$: the value of pure copper capacity in pF; $C_{abs}$: the value of pure ABS capacity in pF; $M_{cu}$: the mass of copper in g; $M_{abs}$: ABS mass in g; $M_{tot}$ : the total mass of the copper-ABS mixture in g.

With: $P_{cu} = M_{cu}/M_{tot}$ and $P_{abs} = M_{abs}/M_{tot}$; $P_{CU}$, $P_{abs}$: purity of copper and ABS respectively in %

## IV. CONCLUSION

The experiments carried out have given us several conclusions, the most important of which is that we can know the purity of a mixture of two different products provided that we know the total mass of the two products.

### References

[1] A.N.E.I Ayad, A. Ayad, H. Boudjela, Electromagnet Separator of Different Particles, 5 (2018) 22-31.
[2] J. Zheng, J. Ruan, L. Dong, T. Zhang, M. Huang, Z. Xu, Hollow Aluminum Particle in Eddy Current Separation of Recovering Waste Toner Cartridges, 5 (2017) 161-167.
[3] B. Niu, Z. Chen, Z. Xu, Recovery of Valuable Materials from Waste Tantalum Capacitors by Vacuum Pyrolysis Combined with Mechanical−Physical Separation, 5, 3 (2017) 2639-2647.
[4] Y. Qin, J. Wu, Q. Zhou, Z. Xu, Quadratic nonlinear models for optimizing electrostatic separation of crushed waste printed circuit boards using response surface methodology, 167 (2009) 1038-1043.

# Efficient Green Hydrogen Production in Seawater Desalination Plant

**A. Zeggai[1], F. Benhamida[1], M. Ali-dahmane[1] R. Belhachem[1] , M. Haba[1]**

[1] *IRECOM laboratory, Faculty of Electrical Engineering, University Djilali Liabes of Sidi Bel Abbes*
*Contact: zeggai-amine13@hotmail.com*

**ABSTRACT**

However, the hydrogen and water sectors will need to take an integrated approach and carefully consider the implications of water for each form or "color" of hydrogen production. The color of hydrogen production depends on the production method used, but hydrogen remains the same product for every process. This includes the supply, disposal and management of water without affecting or exacerbating local water security issues, and without having a negative impact on the environment, local communities and industries. As with most forms of hydrogen production, green and blue hydrogen systems rely on demineralized water (typically <0.5 uS/cm) which, depending on the water source, often requires desalination, second-pass RO and other demineralization steps. Consequently, the complexities associated with brine management are a major consideration for any desalination process. This work quantifies the current and future costs and environmental burdens of hydrogen production systems. Water electrolysis currently accounts for just 0.1% of global hydrogen production, but installed capacity and the number of projects announced have grown rapidly in recent years. Around 600 projects with a combined capacity of over 160 GW have been announced since the 2022 World Hydrogen Conference. By the end of 2022, the worldwide installed capacity of water-based electrolyzers for hydrogen production had reached almost 700 MW, an increase of 20% on the previous year, green hydrogen produced by water electrolysis has a very high purity, greater than 99.9%, thus avoiding additional cleaning steps.

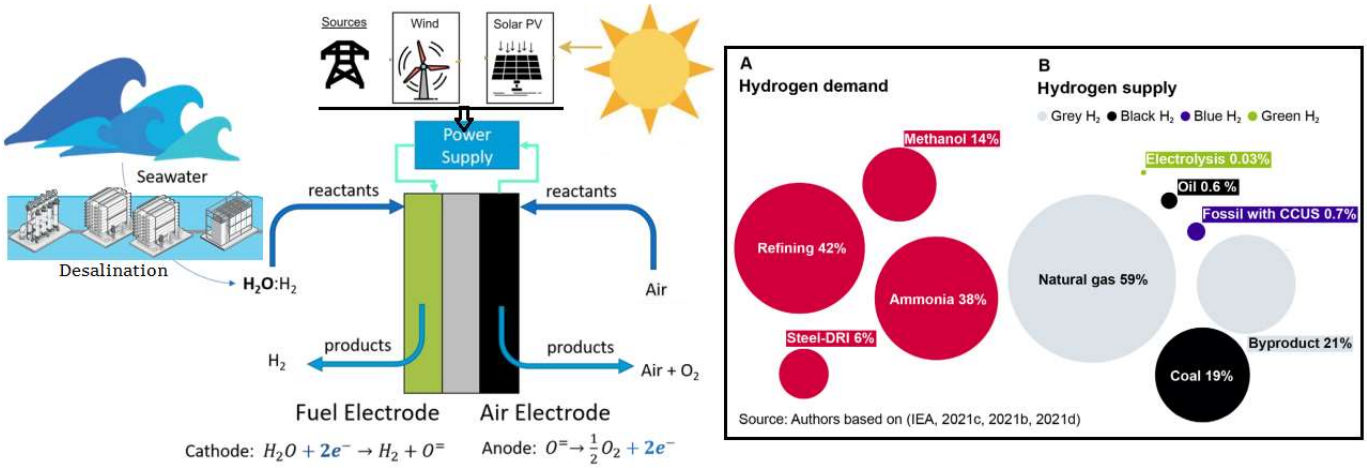


**Fig 1:** Operation scheme Electrolysis, Hydrogen demand by area (A) and supply by production (B) technology in 2020

The cost of hydrogen production depends on the technology and the cost of the energy source used, which generally varies considerably from region to region. Before the global energy crisis triggered by Russia's invasion of Ukraine, the levelized cost of hydrogen production from untouched fossil sources was in the order of USD 1.5-1.0-3.0/kg H2. In 2021, these production routes offered the cheapest option for producing hydrogen, compared with the most expensive option. the cheapest option for producing hydrogen, compared

with using fossil fuels with CCUS technology (1.5-3.6 USD/kg H2) or using electrolysis with low-emission electricity (3.4-12 USD/kg H2). The cost of hydrogen produced by electrolysis is determined by the capital cost of electrolyzers and the cost of electricity used to power the electrolyzer. As mentioned above, the capital costs of electrolyzers should fall considerably in the short term, thanks to economies of scale and continued technological innovation. The cost of renewable electricity has already fallen sharply over the past decade (80% reduction in the cost of solar modules between 2010 and 2020). Recent rises in raw material prices may slow the decline in costs in the short term, but are unlikely to halt it completely in the long term. If large-scale deployment takes place as predicted in the NZE scenario, the cost of producing electrolytic hydrogen from solar photovoltaic electricity could fall to 1.6 USD/kg H2 by 2030 in regions with excellent sunshine, such as Africa, Australia, Chile, China and India. Green hydrogen therefore seems to be the best option when economically and financially feasible.

The objective of this study, in particular, is to analyze the distribution network behavior of a seawater desalination plant (seawater is one of the most abundant resources on the planet), it is promising both as a source of drinking water and as a source of low-carbon (green) hydrogen by electrolysis of water using renewable energy (wind or photovoltaic) through the power flow and voltage profile, with different load scenarios (full load, full load N-1, low load, emergency system), by ETAP simulation software, The hybrid configuration consists of a grid connection as well as a direct connection to renewable electricity sources. The main motivation for this configuration is that hybrid systems integrate renewable energy sources (at low cost) and use the power grid as a supply and storage (cheap), which could reduce costs and lower environmental loads when coupled to a low-GHG-intensity power grid. In this particular case, the grid can be used as a source of backup power in the absence of wind or photovoltaic generation, and as a buffer - i.e. a potential storage medium - in the event of excess electricity production. An additional storage medium, such as a battery, is therefore not envisaged in this configuration.

**Keywords:** Hydrogen; Power Flow; Different Contingency; Water; Renewables.

**References**

[1] Ying Zhou, Ruiying Li, Zexuan Lv, Jian Liu, Hongjun Zhou, Chunming Xu, Green hydrogen: A promising way to the carbon-free society, Chinese Journal of Chemical Engineering, Volume 43, 2022, Pages 2-13, ISSN 1004-9541, Https://doi.org/10.1016/j.cjche.2022.02.001.
[2] T.O. Ozan Akdağ, The operation and applicability to hydrogen fuel technology of green hydrogen production by water electrolysis using offshore wind power, Journal of Cleaner Production, Volume 425, 2023, 138863, ISSN 0959-6526, Https://doi.org/10.1016/j.jclepro.2023.138863.
[3] Mohamed Nasser, Hamdy Hassan Egyptian green hydrogen Atlas based on available wind/solar energies: Power, hydrogen production, cost, and CO2 mitigation maps, International Journal of Hydrogen Energy, 2023, issn 0360-3199 Https://doi.org/10.1016/j.ijhydene.2023.09.127
[4] Nattapol Srettiwat, Mohammadhosein Safari, Hakan Olcay, Robert Malina, A techno-economic evaluation of solar-powered green hydrogen production for sustainable energy consumption in Belgium, International Journal of Hydrogen Energy, 2023,ISSN 0360-3199, https://doi.org/10.1016/j.ijhydene.2023.09.159.
[5] Ozan Akdağ, The operation and applicability to hydrogen fuel technology of green hydrogen production by water electrolysis using offshore wind power, Journal of Cleaner Production, Volume 425, 2023, 138863, ISSN 0959-6526, Https://doi.org/10.1016/j.jclepro.2023.138863.
[6]IEA (2023), Global Hydrogen Review 2023, IEA, Paris https://www.iea.org/reports/global-hydr ogen-review-2023, License: CC BY 4.0

# Influence de la MLI Découplée sur les Systèmes à Double Onduleurs Alimentés par un Bus Continu Commun : Validation Expérimentale

**ZERDANI Mohammed[1,2], ARDJOUN Sid Ahmed El Mehdi[1], CHAFOUK Houcine[2], Denaï Mouloud[3], MOHAMED Metwally Mahmoud[4]**

*[1] IRECOM Laboratory, University of Djillali Liabes, Sidi Bel-Abbes 22000, Algeria.*
*[2] IRSEEM/ESIGELEC Laboratory, Normandy University of Rouen, 76000 Rouen, France*
*[3] School of Physics, Engineering and Computer Science, University of Hertfordshire, AL10 9AB Hatfield, U.K.*
*[4] Department of Electrical Engineering, Faculty of Energy Engineering, Aswan University, Aswan 81528, Egypt.*
*Email : ardjoun.s.e.m@gmail.com (Corresponding author: ARDJOUN Sid Ahmed El Mehdi)*

**RESUME**

Dans le domaine industriel, les entraînements électriques à vitesse variable sont largement utilisés dans diverses applications, et le développement technologique des variateurs ne cesse de croître. Il est bien établi que l'élément clé du développement de ces variateurs réside dans l'association électronique de puissance et de machines électriques. Cependant, cette association a des effets sur la qualité et l'efficacité énergétique de ces variateurs [1][2]. De nombreuses recherches ont donc été adoptés pour améliorer les performances de ces variateurs en termes de qualité et d'efficacité énergétique. Ces axes de recherche se divisent en trois catégories : (i) l'utilisation de filtres (actifs/passifs), (ii) la reconfiguration de l'électronique de puissance, (iii) l'amélioration des lois de commande de modulation de largeur d'impulsion (MLI).

En ce qui concerne l'utilisation des filtres, bien que cela soit une solution classique, elle présente de nombreux inconvénients tels que son coût élevé, son encombrement et sa consommation énergétique élevée [3][4]. C'est pourquoi la plupart des chercheurs préfèrent se concentrer sur la reconfiguration de l'électronique de puissance et l'amélioration des lois de commande.

Il convient de noter qu'il existe plusieurs topologies pour l'association de l'électronique de puissance avec les machines électriques dans les variateurs de vitesse. Parmi celles-ci, la proposition de H. Stemmler et P. Guggenbach [5] retient l'attention. Leur idée consiste à ouvrir le point neutre des enroulements statoriques au lieu de les coupler en étoile/triangle, permettant ainsi l'alimentation des enroulements par deux onduleurs distincts (un pour chaque côté). Cette structure est appelée moteur à stator ouvert avec double onduleurs (OEWM-DI). Ces derniers temps, cette structure suscite un intérêt particulier en raison de ses avantages tels que la simplicité du circuit de puissance [6], l'absence de fluctuations du point neutre [7], la tolérance aux pannes [8] et une tension de bus continue réduite [9]. Cependant, cette configuration présente quelques inconvénients, notamment la tension de la composante homopolaire (ZSV) due à la connexion directe des deux onduleurs [10], et la présence d'une tension de mode commun (CMV) due à la commutation à haute fréquence des interrupteurs des onduleurs [11][12][13].

Dans la littérature, trois structures à double onduleurs sont répertoriées (à bus continu commun, à deux sources de bus continu isolées, à bus continu avec une capacité flottante). Dans notre étude, la structure à bus continu commun (voir Figure 1) [14] a été sélectionnée. L'objectif de ce travail est de faire une analyse expérimentale de l'impact de la modulation de largeur d'impulsion découplée (MLI-D) sur les différentes performances (THD, CMV, ZSV et vitesse de rotation) du système OEWM-DI. L'analyse de cette stratégie a

été mise en œuvre expérimentalement sur une carte dSPACE 1104 et appliquée à un moteur de 1,5 kW (voir Figure 2).

**Mots-clés :** Bus continu commun, tension de mode commun (CMV), modulation de largeur d'impulsion découplée (MLI-D), onduleur double (DI), moteur à induction à enroulement ouvert (OEWIM), distorsion harmonique totale (THD), composante homopolaire (ZSV).

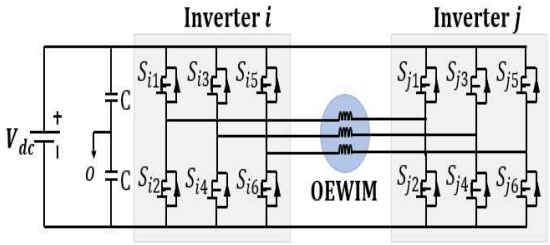


**Fig 1 :** Configuration de l'alimentation de l'OEWIM-DI avec un seul bus continu.

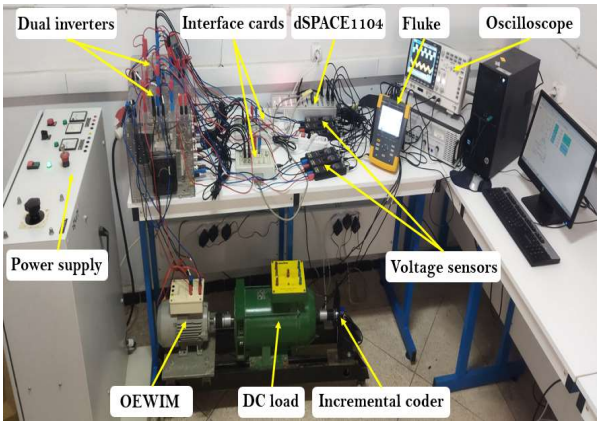


**Fig 2 :** Dispositif expérimental d'un moteur à induction à enroulement ouvert alimenté par deux onduleurs

## References

[1] Kyrylenko, O. V.,"passiModeling of energy processes in energy supply systems in solving energy saving problems", Pratsi Instytutu elektrodynamiky NAN Ukrainy, Elektrodynamika: Zbirnyk naukovykh prats – Kyiv: IED NAN Ukrainy, 2001.– P. 87–91

[2] Sychenko, V. H., "Influence of electric power processes in traction power supply systems on the quality of electric energy", Hirnycha elektromekhanika ta avtomatyka: Naukovo – tekhnichnyi zbirnyk NHU. –Dnipropetrovsk.: Vypusk: 2015. №1(94).– P.25-30.

[3] J. C. Das, "Passive filters - potentialities and limitations," in IEEE Transactions on Industry Applications, vol. 40, no. 1, pp. 232-241, Jan.-Feb. 2004..

[4] Fuchs, Ewald F., and Mohammad AS Masoum. *Power quality in power systems and electrical machines*. Academic press, 2011, pp 359-395.

[5] H. Stemmler and P. Guggenbach, "Configurations of high-power voltage source inverter drives," in *1993 Fifth European Conference on Power Electronics and Applications*, Sep. 1993, pp. 7–14 vol.5

[6] S. Srinivas and K. Ramachandra Sekhar, "Theoretical and Experimental Analysis for Current in a Dual-Inverter-Fed Open-End Winding Induction Motor Drive With Reduced Switching PWM," *IEEE Transactions on Industrial Electronics*, vol. 60, no. 10, pp. 4318–4328, Oct. 2013.

[7] V. T. Somasekhar, S. Srinivas, and K. K. Kumar, "Effect of Zero-Vector Placement in a Dual-Inverter Fed Open-End Winding Induction-Motor Drive With a Decoupled Space-Vector PWM Strategy," IEEE Trans. On Ind. Electron., vol. 55, no. 6, pp. 2497–2505, Jun. 2008

[8] N. K. Nguyen, F. Meinguet, E. Semail, and X. Kestelyn, "Fault-Tolerant Operation of an Open-End Winding Five-Phase PMSM Drive With Short-Circuit Inverter Fault," IEEE Trans. on Ind. Electron., vol. 63, no. 1, pp. 595–605, Jan. 2016.

[9] A. Dehghani kiadehi, K. El Khamlichi Drissi and C. Pasquier, "Angular Modulation of Dual-Inverter Fed Open-End Motor for Electrical Vehicle Applications," in *IEEE Transactions on Power Electronics*, vol. 31, no. 4, pp. 2980-2990, April 2016.

[10] A. D. Kiadehi, K. E. K. Drissi and C. Pasquier, "Voltage THD Reduction for Dual-Inverter Fed Open-End Load With Isolated DC Sources," in IEEE Transactions on Industrial Electronics, vol. 64, no. 3, pp. 2102-2111, March 2017.

[11] S. Chen, T. A. Lipo, and D. Fitzgerald, "Source of induction motor bearing currents caused by pwm inverters," IEEE Trans. Energy Conv., vol. 11, no. 1, pp. 25–32, Mar. 1996.

[12] Erkuan Zhong and T. A. Lipo, "Improvements in emc performance of inverter-fed motor drives," IEEE Trans. Ind. Appl., vol. 31, no. 6, pp. 1247–1256, Nov. 1995.

[13] J. Kalaiselvi and S. Srinivas, "Bearing Currents and Shaft Voltage Reduction in Dual-Inverter-Fed Open-End Winding Induction Motor With Reduced CMV PWM Methods," in IEEE Transactions on Industrial Electronics, vol. 62, no. 1, pp. 144-152, Jan. 2015.

[14] M. Zerdani, S. A. E. M. Ardjoun, H. Chafouk and M. Denaï, "Experimental Investigation of Decoupled Discontinuous PWM Strategies in Open-End Winding Induction Motor Supplied by a Common DC-link," in IEEE Journal of Emerging and Selected Topics in Power Electronics, doi: 10.1109/JESTPE.2023.3258799.

# Experimental analysis of the force of attraction applied on metal particles using an electrostatic device

**Ait Yahia Abdellah Walid [1], Tilmatine Amar [1], Zelmat Mohamed El mouloud [2]**
[1] *APELEC Laboratory , Faculty of Electrical Engineering, University Djillali Liabes, Sidi-Bel-Abbes, Algeria*
[2] *Mohamed Boudiaf University USTMB, Oran, Algeria*
*Email: aityahia.walidabdellah@gmail.com*

**ABSTRACT**

Rapid technological change, the increasing pace of household appliance production, and the shorter lifespan of these appliances are all factors that lead to a significant production of electrical and electronic waste (WEEE). The recycling of this WEEE is therefore becoming a fundamental challenge to support a global vision of sustainable development. Processing WEEE has environmental, economic and health dimensions [1]. It not only reduces emissions and protects people from the dangers of specific components contained in this waste, but also helps to contain this waste and create jobs. This recovery operation requires the use of various techniques and processes, including electrostatic separators.

Electrostatic separators play a vital role in industry by contributing to the efficient separation of charged particles,making them valuable in solving contemporary environmental and industrial challenges.electrostatic separation is the process of sorting and separating particles or materials according to their electric charge characteristics [2]. It is based on the principles of electrostatics, which studies the behavior of electric charges. In this process, particles are electrically charged and then subjected to an electric field. Particles react according to their electrical charge: oppositely charged particles are attracted to each other, while similarly charged particles repel each other. This electrical interaction enables them to be effectively separated . Electrostatic separation is widely used in various industrial applications, such as recycling, mineral processing, e-waste recycling,air and water purification, and other material separation processes.It is appreciated for its versatility and efficiency , particularly in fields where it is essential to sort materials according to their electrical properties, such as charge. New electrostatic separation techniques for metal/plastic and metal/metal mixtures. Their principle is based on the displacement of granular or micronized plastic particles for metal/plastic separation, and on the conductivity of metals for metal/metal separation [3].

The aim of the work is to create an experimental device used for separating metal particles from millimeter-sized plastic particles. The device consists of a blower with maximum air flow and an double-sided electric curtain made up of a series of parallel segment electrodes of width l and distance d. Built on a surface of a dielectric layer which is separated by a small gap of mm between the electrodes and fed by a polyphase voltage in the form of a square wave where each electrode was fed by a voltage amplifier. The square-wave voltage signals applied to the electrodes were visualized using a digital oscilloscope The sample used millimeter-sized copper particles were deposited in a monolayer When the particles had settled on its surface, the blower was activated At the end of the experiment the mass of metal particles remaining on the surface were weighed by a digital balance,An experimental analysis was carried out to analyze the influence of different factors on the influence of this new separator. In this study two factors were analyzed: air flow and supply voltage, the influence of these factors on the Attractive force of copper particles was analyzed.

In our work, the results obtained revealed the existence of attraction, with the force of attraction applied to the metal particles depending mainly on the amplitude of the applied voltage. The analysis revealed an intense electric field at the edges of the electrode segments, causing the metal particles to adhere due to the electric charge induced on these particles. the experimental results pointed out the feasibility of metal/plastic particles separation using such actuator with high values of recovery and purity

**Keywords:** WEEE; electrostatic separators; Separation of particles; particles; Attraction force

**References**

[1] H. Louati, A. Tilmatine, R. Ouiddir, A. Alibida, et N. Zouzou, « New separation technique of metal/polymer granular materials using an electrostatic sorting device », Journal of Electrostatics, vol. 103, p. 103410, janv. 2020, doi: 10.1016/j.elstat.2019.103410.
[2] A. Alibida et al., « Experimental analysis of a new attraction force applied on metal particles », Particulate Science and Technology, vol. 38, no 4, p. 505-510, 2020.
[3] R. Sayah, A. Semmak, M. Bouhmama, et F. Miloua, « Experimental analysis of a new separation technique of metal/plastic particles using a double-side electrostatic actuator ».

**Fig 1 . Schematic description**

| Air flow rate | 0,26 | 0,58 | 0,74 | 1,04 | 1,3 |
|---|---|---|---|---|---|
| remaining copper mass (voltage 2kv) | 1,5 | 1,5 | 1,48 | 0,83 | 0,09 |
| remaining copper mass (voltage 0v) | 1,5 | 1,47 | 0 | 0 | 0 |

Table1 : represents the variation of the mass of copper particles as a function of air flow

| Voltage(v) | 0 | 400 | 800 | 1200 | 1600 | 2000 |
|---|---|---|---|---|---|---|
| remaining copper mass(g) | 0,29 | 0,76 | 1,43 | 1,47 | 1,49 | 1,5 |

Table 2 : represents the variation of the mass of copper particles as a function of the applied voltage

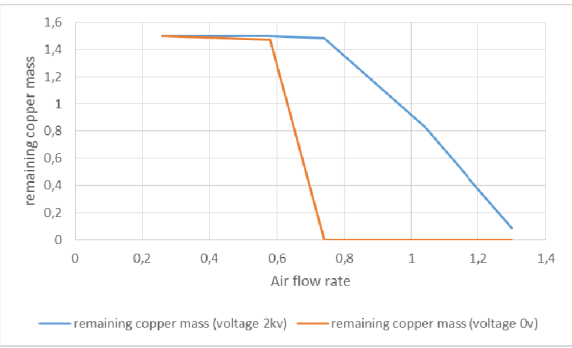


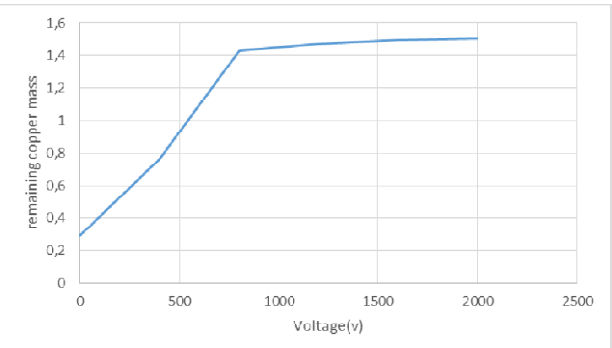

# Evaluation de l'impact de la Tension d'alimentation sur les EMI d'un Convertisseur DC/DC Alimentant un Moteur à Courant Continu

**Mohcine AMARA[1], Houcine MILOUDI[1], Abdelber BENDAOUD[1], Mohamed MILOUDI[1], Mohammed Hamza BERMAKI[1]**

[1]*Laboratory of Applications of Plasma, Electrostatics and Electromagnetic Compatibility (APELEC), DjilaliLiabés University,Sidi Bel Abbès, 22000 Algeria*
mohmohcinam@gmail.com

**RESUME**

Les convertisseurs DC/DC, composants électroniques omniprésents utilisés dans une grande variété d'appareils, peuvent générer des interférences électromagnétiques (EMI) qui peuvent perturber le fonctionnement d'autres appareils.Cette étude a examiné l'influence de la tension d'alimentation sur les EMI générées par un convertisseur DC/DC alimentant un moteur à courant continu. Un convertisseur DC/DC a été utilisé pour alimenter un moteur à courant continu de 24 V. La fréquence de commutation du convertisseur a été fixée à une valeur constante et la tension d'alimentation a été variée de 9 à 22 V. Les EMI ont été mesurées à l'aide d'un analyseur de spectre.Les résultats ont montré que les EMI augmentaient avec la tension d'alimentation. La principale source d'EMI était la commutation du convertisseur DC/DC. Les harmoniques de commutation étaient responsables de l'augmentation des EMI.

Cette étude a montré que les EMI générées par un convertisseur DC/DC alimentant un moteur à courant continu peuvent être importantes. Les résultats de cette étude peuvent être utilisés pour concevoir des convertisseurs DC/DC plus efficaces et générant moins d'EMI.

**Mots clés:**Convertisseur DC/DC; EMI; Tension d'alimentation;Moteur à courant continu.

## INTRODUCTION

Les convertisseurs DC-DC sont utilisés pour convertir l'énergie électrique d'un niveau de tension à un autre.[1] Ils fonctionnent en commutant des quantités électriques à des fréquences élevées [1][2], ce qui peut générer des interférences électromagnétiques (EMI). Les EMI peuvent se propager dans l'environnement et perturber le fonctionnement des appareils électriques à proximité [2].

## COMPOSITIONDU BANC DE MESURE

Le montage expérimental consiste en un hacheur série statique avec une tension d'entrée de 24 V et unetension de sortie variable pouvant être inférieure à 24 V.

Le convertisseur (Hacheur série) est connecté à un réseau de stabilisation d'impédance de ligne d'entrée (RSIL) par le câble 1, et à une charge fixe par le câble 2. Un analyseur de spectre a été utilisé pour mesurer la réponse en fréquence de l'ensemble du système.

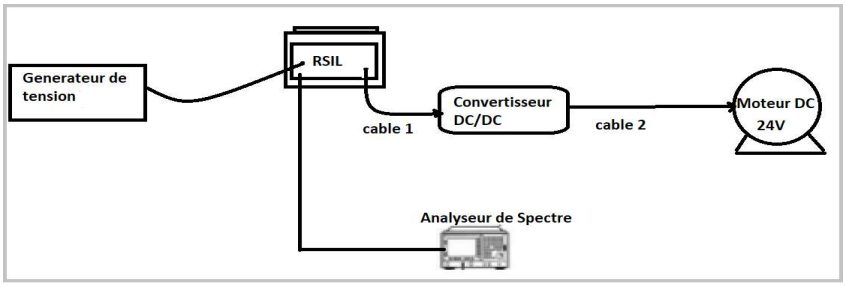


Fig 1 :Diagramme en bloc du montage expérimental

**RESULTATS ET INTERPRETATIONS**

La fréquence de commutation a été fixée à 16 kHz et la tension d'entrée a été variée. Les PEM ont été mesurés àchaque tension d'entrée. La figure 3 montre la réponse en fréquence de la tension RSIL en fonction de la tension d'alimentation du convertisseur.

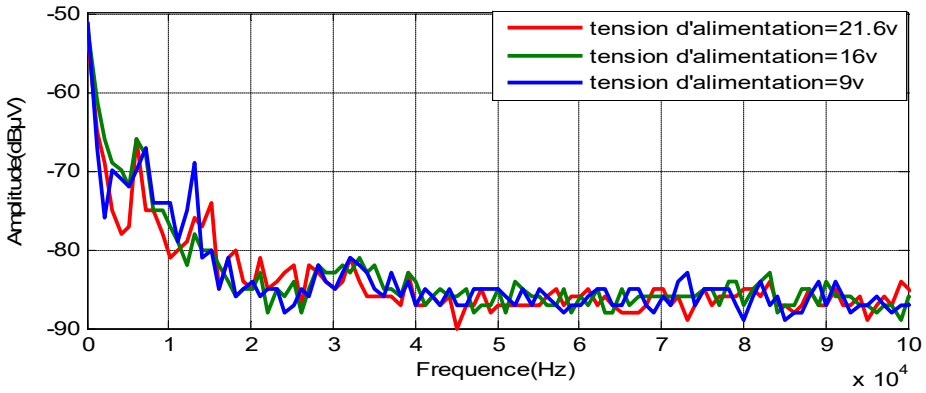


Fig 2 :la réponse fréquentielle de la tension RSIL en fonction de la fréquence

Il est clair que la variation de la tension d'alimentation a un effet significatif aux basses fréquences. Cependant, de faibles effets sont observés aux hautes fréquences.

L'utilisation des convertisseurs de puissance est largement répandue en raison de leur rendement élevé. Cependant, ils sont également une source d'interférences électromagnétiques (EMI). Ce travail porte sur l'analyse des EMI dans les convertisseurs DC-DC alimentant un moteur à courant continu de 24 V, en fonction de l'influence des variations de tension d'alimentation. L'influence du facteur étudié sur le convertisseur DC-DC se situe dans la bande de basse fréquence.

**References**

[1] Payami, S., Behera, R. K. Iqbal, A. Al-Ammari R., Common-ModeVoltage and Vibration Mitigation of a Five-Phase Three-Level NPCInverter-Fed Induction Motor Drive System, IEEE Journal of Emergingand Selected Topics in Power Electronics, Vol.3, no.2, pp.349-361, Juin2015..
[2] Zeghoudi, A., Bendaoud, A., Slimani, H., Benazza, B., & Bennouna, D.(2022). Determination of Electromagnetic disturbances in a buckchopper. Australian Journal of Electrical and Electronics Engineering,19(2), 149-157.

# The effect of increasing the number of pole pairs on non-ferrous particle (aluminum, copper, silver, and zinc) separation in a magnetic drum separator

**Abderrahmane Bettache[1], Salah-Eddine Bendimerad[1], Wafa Krika[1] , Abdelghani Ayad[1] , Ahmed Nour El Islam Ayad[2] , Kadda Khellaf[1]**

[1]*Department of Electrical Engineering Djillali Liabes University APELEC Laboratory, Algeria*
[2]*Kasdi Merbah University, Department of Electrical Engineering, Ouargla, Algeria,*
*email of corresponding author: abderrahmane.bettache@univ-sba.dz*

## ABSTRACT

In this paper, we simulate a magnetic drum separator made of permanent magnets with alternating polarity. The study aims to investigate the effects of changing the number of pole pairs in the magnetic drum separator on the separation of non-ferrous particles.Using the 2D Finite Element Method Magnetics (FEMM) software, we carried out a thorough simulation analysis to examine how these non-ferrous particles behaved in response to the magnetic field produced by the permanent magnets with alternating polarity. Finally, the differences between these materials and the relationship between the number of pole pairs and the separation efficiency are all presented in this paper.

**Keywords:** Magnetic Separation, Magnetic Drum, Non-Ferrous Particules.

## INTRODUCTION

To extract non-ferrous metals (Cu, Al, Ag and Zn) from solid wastes, eddy-current separation techniques are employed [1]. The working principle creates an eddy current in conductive particles that are passed by a magnetic field, based on the electromagnetic induction phenomenon.The repulsive force that caused the separation was created by the interaction between the magnetic field that was applied and the magnetic field that the particles produced.[2]

## DESCRIPTION OF SYSTEM

The magnetic drum separator for recycling particles is shown in Figure 1. The system consists of a cylinder with alternating-polarity permanent magnets attached to its surface. Eddy currents are produced by an alternating magnetic field both within and outside of conductive particles such as copper, zinc, silver and aluminum.The rotor's magnetic field interacts with this secondary magnetic field to produce the Lorentz force, which is an opposing force. The conductive particles are repelled or deflected by this force away from the material flow. In eddy current magnetic separation, the conductivity to density ratio acts as an index to show how much a material will be impacted by the repulsive force. [3]

*Table 01: Conductivity-to-density ratio of some conductive materials.*

| metals | Electrical conductivity. $\sigma$ ($10^7$ S/m) | Mass density $\rho$ ($10^3$ Kg/m$^3$) | Ratio ( $\sigma$ / $\rho$) $10^3$ (m$^2$ /$\Omega$.Kg) |
|---|---|---|---|
| **Aluminum** | 3.5 | 2.7 | 13 |
| **Copper** | 5.9 | 8.9 | 6.7 |
| **Silver** | 6.3 | 10.5 | 6.0 |
| **Zinc** | 1.7 | 7.1 | 2.4 |

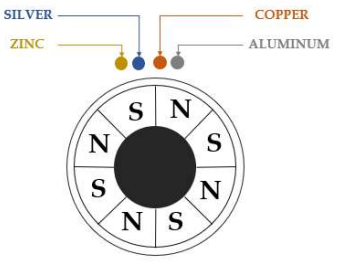


*Fig 1: The magnetic drum separator*

## IMPLEMENTATION IN FEMM 2D

Our objective was to analyze the behavior of numerous particles (Al, Cu, Ag and Zn ) in the presence of varying magnetic fields. Utilizing the features of the FEMM 2D software, we carried out an extensive simulation. We were able to study and extract the magnetic field profiles related to each individual particle.

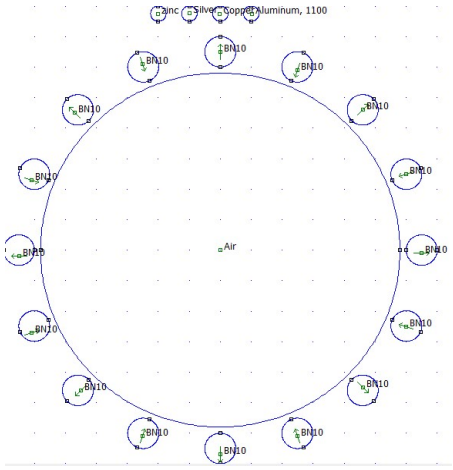


*Fig 2 : The magnetic drum separator with 16 pole pairs*

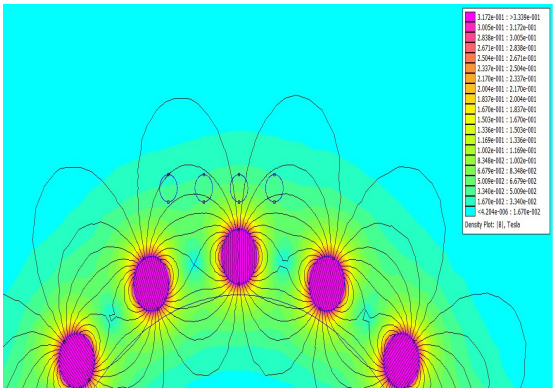

*Fig 3: Distribution of the Magnetic Flux Density Around Particles*

## CONCLUSION

The goals of this work are to demonstrate the influence and distribution of magnetic field lines around the non-ferrous particles (Al, Cu, Ag and Zn) near to the separator, as well as to simulate the properties of magnetic fields using FEMM.

In addition to that, the aim of this work is to investigate the effects of changing the number of pole pairs in the magnetic drum separator on the separation of non-ferrous particles. We used the following scenarios to achieve this goal: 8 pole pairs, 16 pole pairs, and 32 pole pairs.

The results of the simulation provide an explanation of the phenomenon of magnetic separation as well as the variables that affect it, including the position of the particles, their distance from the separator, and the magnetic field's powerful force. When these factors are realized, the separations give good results. There are many other factors affecting the separation that may be studied in the future.

### References

[1]. Schlett, Z., et al., A new static separator for metallic particles from metal–plastic mixtures, using eddy currents. Minerals Engineering, 2002. 15(1-2): p. 111-113.

[2]. Smith, Y.R., J.R. Nagel, and R.K. Rajamani, Eddy current separation for recovery of non-ferrous metallic particles: A comprehensive review. Minerals Engineering, 2019. 133: p. 149-159.

[3]. AYAD, A.N.E.I., Etude et Réalisation d'un séparateur à induction électromagnétique. 2017.

# Modeling electromagnets for separation of non-magnetic materials (aluminum, copper)

**KHELLAF Kadda[1], AYAD Abdelghani[1], BENDIMERAD Salaheddine [1], BETTACHE Abderrahman[1]**

[1] *Electrical Engineering Department, Djillali Liabes University, Sidi Bel Abbes, Algeria*
[2] *APELEC Laboratory, Djillali Liabes University, Sidi Bel Abbes, Algeria*
*Email: khellafkadda1234@gmail.com*

**ABSTRACT**

Magnetic field separation is an effective method in the field of separation of industrial waste containing several materials in particle form. Using electromagnet for separation gives good and efficient results, because the intensity of the magnetic field is controlled, which is a very important feature, where we have the possibility of changing the magnetic induction. This work presents a simulation of our electromagnet for the separation of non-ferrous materials. The results obtained are consistent with the theoretical analysis.

**Keywords:** Electromagnetic separation, Electromagnet, Aluminum, Copper.

## 1. INTRODUCTION:

Magnetism is a manifestation of moving electrical charges. A conductor carrying a current is a source of magnetic fields. [1]
The electromagnet, unlike a permanent magnet, has the advantage of attracting ferromagnetic substances when a current flows in the solenoid and of not attracting them when the coil is not powered by a current. This is a very important characteristic of electromagnets [2].

## 2. DEFINITION OF THE MAGNETIC FIELD:

We consider a point particle q placed at point M. In the vicinity of a magnet or a conductor carrying a current, it is subjected to a magnetic force:

$$\vec{f} = q\vec{v} \wedge \vec{B}$$

This force makes it possible to define the magnetic field B (T). [1]

## 3. SIMULATION WORK:

In this simulation we use 'femm' software and work on two materials which are non-ferromagnetic materials (Aluminum (Al) and Copper (Cu))
After the simulation we note the curves of the induction B in the electromagnet and (Al) and (Cu).

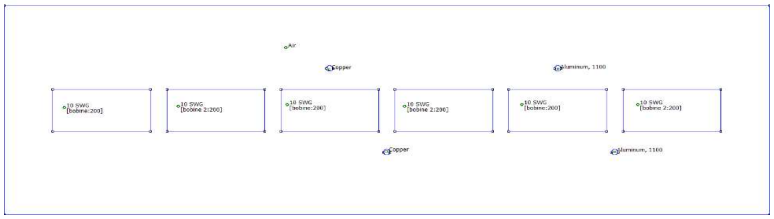

*Figure 1: Geometry of the problem*

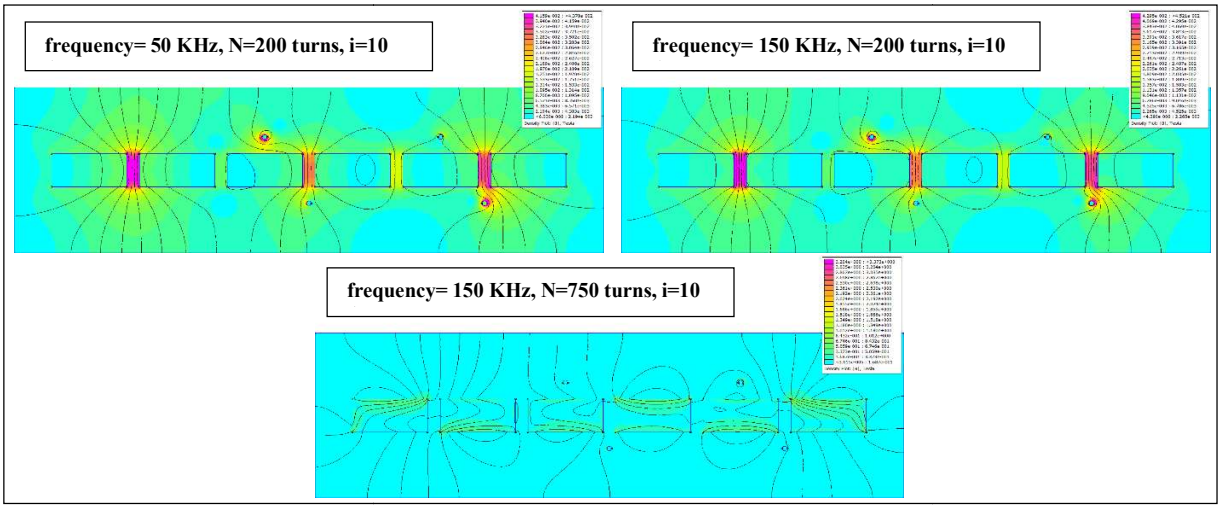


*Figure 2: the lines of magnetic induction B*

## 4. INTERPRETATION:

From the results obtained in the figures we notice that there is a proportional relationship between the magnetic induction (B) and the frequency (f), the current (i) and the number of turns (N) according to the following equation:
Ampère's theorem:

$$FMM = \int H.l = N.i \Rightarrow H.l = N.i$$

$$H = \frac{N.i}{l}; B = \mu.H$$

$$B = \frac{\mu.N.i}{l}$$

We make a comparison between Aluminum (Al) and Copper (Cu) according to the following table:

| Metal | Conductivity (σ) [$10^6$ S/m] | Density (ρ) [$10^3$ Kg/m³] | σ/ ρ [$10^3$ S.m²/kg] | B[T] |
|---|---|---|---|---|
| Al-1100 | 34.45 | 2.7 | 12,76 | 0.39 |
| Copper | 58 | 9 | 6,44 | 0.26 |

*Table 01: Electrical conductivity and mass density for the metals.*

## 5. CONCLUSION:

Based on the concept of the hypothesis of non-ferrous particles as induced magnetic pole. This simulation was carried out of the repulsive force generated between aluminum and copper particles and an electromagnet. The goal is to know the intensity of the necessary magnetic field that acts on these particles. In addition, we deduce the effect of the number of turns, the intensity of the current and the frequency on the variation of the intensity of the magnetic field in the non-ferrous particles.

### References

[1] Olivier GRANIER, Le champ magnétique La loi de Biot et Savart.
[2] Alain St-Pierre, Le champ magnétique, Électricité et magnétisme- Automne 2012.

# Analyse des Perturbations Rayonnées Générées par les Composants Utilisés dans un Hacheur Buck

**Naima Miloudi[1], Abdelber Bendaoud[1], Mohamed Miloudi[2], Abdelhakim Zeghoudi[1], Houcine Miloudi[1]**

[1]*Laboratoire APELEC, Département de génie électrique, Université Djilali Liabès, Sidi Bel-Abbès*
[2]*Laboratoire APELEC, Département de génie électrique, Université Ahmed Zabana, Relizane*

naimamiloudi@yahoo.fr

**RESUME**

La compatibilité électromagnétique apparait aujourd'hui comme l'une des contraintes majeures de la conception des structures de l'électronique de puissance et plus précisément dans les hacheurs. Cependant, leur avancée technologique, notamment avec l'utilisation des MOSFETs et des IGBTs pour augmenter leur rendement et leur capacité, a engendré des perturbations électromagnétiques. La propagation des perturbations se fait soit en mode rayonné (champ magnétique et /ou champ électrique), soit en mode conduit (mode commun et /ou mode différentiel). Le but de ce travail est d'étudier les émissions rayonnées (champ électrique) générées par chaque composant (diode, MOSFET, IGBT) utilisé dans le hacheur série pour les différentes distances (1 cm, 2 cm et 3 cm) par rapport à la sonde de mesure. Les résultats expérimentaux ont montré que l'augmentation de la distance du point de mesure entraine une diminution du champ électrique.

**Mots clés:** Compatibilite Electromagnetique; Hacheur Série; MOSFET; IGBT; Diode; Emissions Rayonnées.

## INTRODUCTION

De nos jours les convertisseurs statiques sont fortement répandus dans les appareillages modernes, néanmoins ils engendrent des perturbations électromagnétiques [1, 2]. Les convertisseurs statiques sont constitués de commutateurs électronique (diode, IGBT, MOSFET), ces composants augmentent les niveaux d'émissions conduites et rayonnées à cause des vitesses de commutation plus élevées (forts di/dt ou dv/dt) [3, 4, 5]. L'objectif de ce travail est d'évaluer l'impact de la distance entre le point de mesure et la surface des composants électroniques sur émissions rayonnées.

## METHODES ET MESURES

La figure 1(a) montre le circuit électrique utilisé pour l'équipement sous test (hacheur série) par contre la figure1(b) montre une photographie du banc de mesure du champ électrique proche dans un hacheur série.

(a)

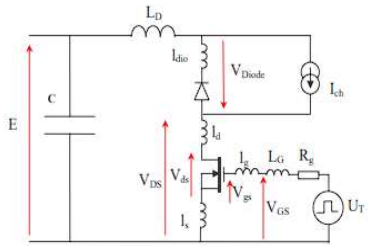


(b)

*Fig 1. Convertisseur buck (hacheur) : (a) Schéma de montage ; (b) photographie du banc de mesure des perturbations.*

Dans le banc de mesure, l'analyseur de spectre et la sonde électrique sont utilisés afin de mesurer et visualiser le champ électrique dans le convertisseur de type buck en particulier la diode, le MOSFET et l'IGBT en fonction de la fréquence. Le hacheur est alimenté par une source continue.

## RESULTATS

Les figures 2, 3 et 4 montrent respectivement le champ électrique émis par les composantes (diode, MOSFET, IGBT) en fonction de la distance entre le point de mesure et le dispositif sous test où l'on voit clairement qu'avec l'augmentation de la distance au point de mesure le champ électrique diminue, car la surface du dipôle de mesure est très petite.

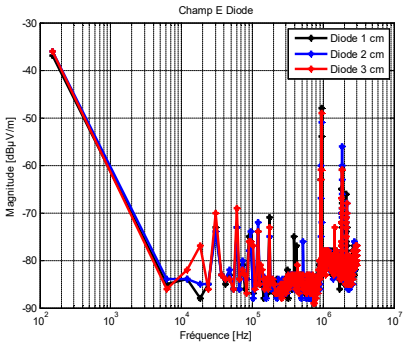


*Fig 2. Champ électrique en fonction de la distance pour la diode*

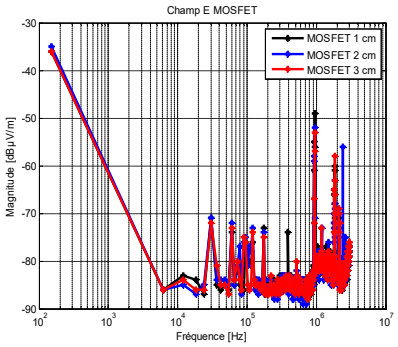


*Fig 3. Champ électrique en fonction de la distance pour MOSFET*

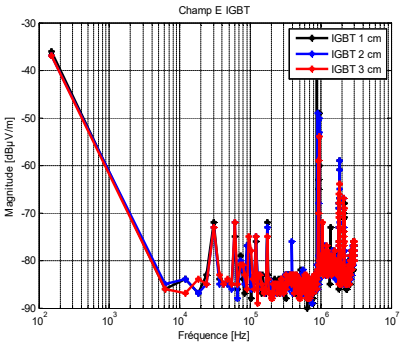


*Fig 4. Champ électrique en fonction de la distance pour IGBT*

## CONCLUSION

À partir des résultats obtenus nous pouvons dire que la variation de la distance entre le point de mesure et le circuit sous test influent sur les perturbations rayonnées (champ électrique) généré par les composants électroniques en particulier (la diode, le MOSFET et l'IGBT) utilisé dans le hacheur série. Ces mesures sont importantes pour atténuer efficacement les perturbations rayonnées, offrant ainsi des perspectives prometteuses pour l'amélioration des performances et de la fiabilité des hacheurs Buck.

## REFERENCES

[1] M. Miloudi, Perturbations électromagnétiques dans les alimentations à decoupage, Thése de doctorat en électrotechnique, Université de Sidi Bel-Abbes, 2018.
[2] A. Lakrim, D. Tahri, Modélisation et simulation par les éléments finies d'un cable électrique à 4 conducteurs soumis aux contraintes générées par les convertisseurs d'électronique de puissance, Revue des energies renouvelables Vol. 18 N°2(2015) 247-255.
[3] C. Marlier, Modélisation des perturbations électromagnétiques dans les convertisseurs statiques pour des applications aéronautiques, Thése de doctorat, Université de Lille1, 2013.
[4] A. Zeghoudi, A. Bendaoud, B. Baghdadi, B. Benazza, S. Bechekir, H. Miloudi, Measurement and analysis of commom and differential modes conducted emissions generated by an AC/DC converter. Electrical Engineering and Electromecanics, 2022, no.4, pp.63-67.

# Ozone Treatment for Enhanced Food Safety and Shelf Life in Cereal Products

**[1]OULAD NAOUI Brahim el Khalil , [1]NEMMICH Said , [2]NASSOUR Kamel, [2]GHAITAOUI Essama Ahmed, [2]BOUROUMEID Yassine, [2]KHELIFI Elmabrouk ,[2]JBILOU mokhtaria, [2]BRAHAMI Mohamed nadjib, [1] TILMATINE Amar**

*[1]APELEC Laboratory, Djillali Liabes University of Sidi Bel-Abbes, Algeria*
*[2]ICEPS Laboratory, Djillali Liabes University of Sidi Bel-Abbes, Algeria*
*Email: oladnaoui45@gmail.com*

**ABSTRACT**

In this experimental study, we delve into the innovative utilization of ozone generated through dielectric barrier discharge for the preservation and disinfection of ground grain products. Ozone, recognized as a potent oxidizing agent, takes the center stage in our exploration, as we seek to not only extend the shelf life of these products but also ensure their microbial safety. The results unveiled in this research reveal a remarkable achievement: the application of ozone significantly extends the preservation duration by an impressive three months. This promising breakthrough stands as a potent and impactful solution, offering substantial potential for enhancing the overall quality and safety of ground grain products. The implications of this research resonate significantly within the food industry and agricultural practices, promising a transformative approach to product preservation and safety.

**Keywords:** Ozone ; Dielectric Barrier Discharge; Ground Grain Products ;Preservation; Disinfection Shelf Life Extension; Food Safety;

**Methods and Materials :**

**Experimental Device:**

The experimental setup used for ozone treatment of milled cereal products comprises several key components. At its core, the device relies on a plasma electrical discharge system designed to efficiently generate ozone. The major elements of this device include ***Fig.1***:

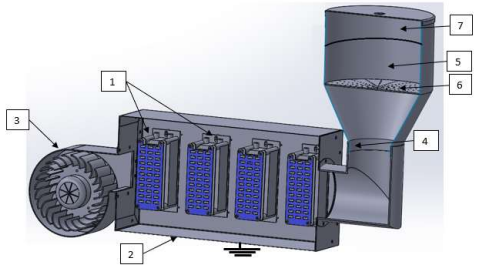


***Fig.1.*** *Comprehensive Schematic Description of the Ozone Treatment-Based Device for Enhancing the Quality and Preservation of Ground Cereal Products (Interior View).*

Ceramic Surface Dielectric Barrier Ozone Generators: Four ceramic surface dielectric barrier ozone generators (1) are fixed inside a metal cabinet (2).

These generators are responsible for ozone production from oxygen. They are made from ceramic, ensuring high resistance to corrosion and high temperatures, guaranteeing stable and reliable ozone production.[1] [2]Air Pump: To supply the ozone generators with oxygen, an air pump (3) is installed inside the metal cabinet. This pump ensures a continuous supply of oxygen required for ozone production, enabling precise control of ozone concentration.

Milled Cereal Product Treatment Chamber: The treatment chamber (5) is designed to accommodate the milled cereal products to be treated. At its lower part, a permeable fabric support (6) is positioned to secure the products in place. Ozone is evenly distributed inside this chamber, ensuring uniform disinfection of the products.
Residual Ozone Venting Channel: Once the ozone and milled cereal product reaction is complete, residual ozone is vented outside through a removable channel (7), ensuring optimal environmental safety.
Programmable Control System: The device is equipped with a programmable and automatic control system (8) that allows the adjustment of ozone concentration and treatment duration. This provides significant flexibility and precision in managing the treatment process.

**Experiments and Results:**

In our study, the experimental device was employed to investigate its effectiveness in eliminating insects from wheat and semolina, and to extend the shelf life of semolina.

**1-Insect Elimination:**

The device was initially applied to eliminate insects from both wheat and semolina.

**a. Complete Insect Eradication:** After the first 36-hour ozone treatment at 1000 ppm, the presence of insects in the cereal products was completely eliminated. This confirmed the high efficacy of the ozone treatment in eradicating insect infestations in the wheat and semolina.

***Tab.1.*** *Elimination of Insects in Cereal Products*

| Processing Time (hours) | Ozone Concentration (ppm) | Insect Presence (Before Treatment) | Insect Presence (After Treatment) |
|---|---|---|---|
| 36 | 1000 | Oui | Non |

**2-Shelf Life Extension:**

Subsequently, we explored the potential of the ozone treatment to enhance the shelf life of semolina.

**a. Prolonged Shelf Life:** The semolina treated with ozone exhibited a significantly extended shelf life. It retained its quality and freshness for over three months, compared to untreated semolina, which experienced quality deterioration and spoilage after a much shorter period.

***Tab.2.*** *Shelf Life of Ozone-Treated Semolina Compared to Untreated Semolina"*

| Type of semolina | Shelf life without treatment (months) |
|---|---|
| **Untreated** | 3 |
| **Ozone-treated** | 6 |

These experiments clearly demonstrate the dual functionality of the experimental ozone treatment device. It not only effectively eliminates insect infestations in cereal products but also significantly extends the shelf life of semolina, ensuring the preservation of product quality for an extended period. This highlights the device's potential to enhance food safety and storage efficiency in the cereal industry.[3]

**References :**

[1] S. Nemmich, K. Nassour, N. Ramdani, Y. Bellebna, M. Boukhoulda, et A. Tilmatine, « DEVELOPMENT AND OPTIMIZATION OF AN OZONE FOOD PRESERVATION SYSTEM USING RESPONSE SURFACE MODELLING (RSM) », *Carpathian J. Food Sci. Technol.*, vol. 13, p. 33-46, janv. 2022, doi: 10.34302/crpjfst/2021.13.4.4.
[2] K. Nassour *et al.*, « Comparative experimental analysis of ozone generation between surface and volume DBD generators », *IEEE Trans. Dielectr. Electr. Insul.*, vol. 25, n° 2, p. 428-434, avr. 2018, doi: 10.1109/TDEI.2017.006600.
[3] M. J. Khan, V. Jovicic, A. Zbogar-Rasic, V. Zettel, A. Delgado, et B. Hitzmann, « Influence of Non-Thermal Plasma Treatment on Structural Network Attributes of Wheat Flour and Respective Dough », *Foods*, vol. 12, n° 10, p. 2056, mai 2023, doi: 10.3390/foods12102056.

# Experimental analysis of a new electrostatic separator using a rotating actuator

**I. Zennani [1,2], S. Zelmat[1], A. Tilmatine[2]**

[1]*Belhadj Bouchaib University of Ain-Temouchent, Algeria*
[2]*APELEC Laboratory, Djillali Liabes University of Sidi-Bel-Abbes, Algeria*
*Contact: zennani.imane37@gmail.com*

**ABSTRACT**

The purpose of this work is to analyse experimentally a new method of separating plastic and metal particles by using a rotating actuator device. Samples of millimeter-sized plastic and copper particles obtained from electrical cable wastes were used in the investigation (Fig 1).


**Fig 1:** Sample of copper and plastic particles.

A rotating actuator device was used in this paper to separate metal / plastic mixture. The actuator is a 200 mm in diameter and 2 mm thick circular printed circuit board (PCB) substrate. A 1 mm-wide helical electrode with a 2 mm space between neighbouring circles covered the top surface of the disc. There was a round grounded electrode on the bottom (Figure 2). Then, in order to stop electrical breakdown between electrodes and metal particles, an insulating coating of acrylic varnish was applied to the upper surface of the actuator. Voltage amplifiers capable of delivering up to 2kV were used to provide various wave shapes of voltage to the actutor's electrodes. By using a vibrating feeder with a regulated flow rate, the plastic/metal mixture was deposited on the actuator's upper surface. Utulising a controlled speed electric motor, the actuator was spun throughout the separation process, and the plastic particles were drawn out using a suction blower. Because of the electro-adhesion force, the metal particles are attched to the actuator surface [1-4]. These particles were separated from the actuator surface and gathered in a box using a brush (Figure 3).

The acquired results demonstrated that excellent recovery and purity rates up to 90% and 98%, respectively, were attained. The voltage level, rotation speed, vibration feeding rate, and air suction

flowrate are the primary factors influencing the new separator's performance. The degree of humidity was another factor that was thought to have an impact on these results.

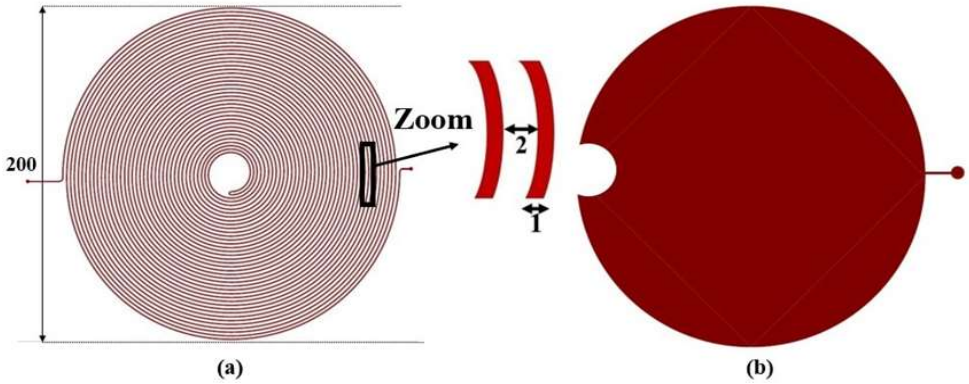


**Fig 2.** Copper electrode configuration on both sides of the rotating actuator
a) Top side. b) Bottom side.

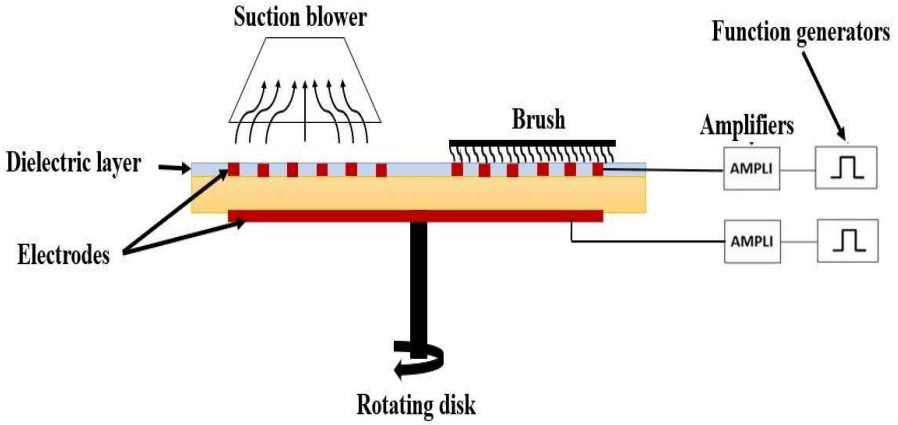


**Fig 3.** Illustration of the experimental setup.

**Keywords:** Adhesion force; Electrostatic separation; Rotating actuator, vaccum blower.

**References**

[1] A. Tilmatine, A. Alibida, S. Zelmat, H. Louati, Y. Bellebna, and F. Miloua, "On the attraction force applied on metal pieces in a traveling wave conveyor," Journal of Electrostatics, vol. 96, pp. 64–68 (Dec. 2018).
[2] A. Alibida et al., "Experimental analysis of a new attraction force applied on metal particles," Particulate Science and Technology, vol. 38, no. 4, pp. 505–510 (May 2020).
[3] H. Louati, N. Zouzou, A. Tilmatine, A. Zouaghi, and R. Ouiddir, "Experimental investigation of an electrostatic adhesion device used for metal/polymer granular mixture sorting," Powder Technology, vol. 391, pp. 301–310 (Oct. 2021
[4] S. Louhadj et al., "Experimental analysis of the attraction force applied on metal particles using a double-side electrical curtain," Journal of Electrostatics, vol. 105 (May 2020).).

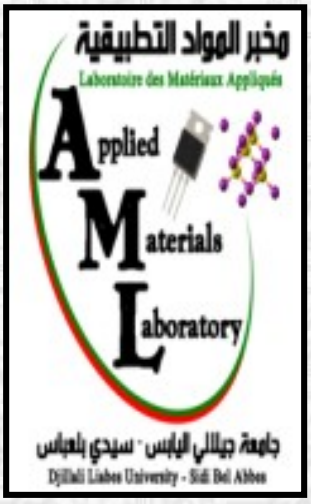
مخبر المواد التطبيقية
Laboratoire des Matériaux Appliqués
Applied
Materials
Laboratory
جامعة جيلالي اليابس - سيدي بلعباس
Djillali Liabes University - Sidi Bel Abbes


E
C
M


RCAM
Laboratory
Réseaux de Communication,
Architecture et Multimédia

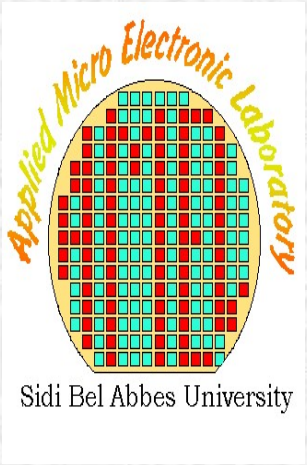
Applied Micro Electronic Laboratory
Sidi Bel Abbes University


APELEC


Lab
IRECOM
Intéraction Réseaux Electriques
Convertisseurs Machines


LTTNS

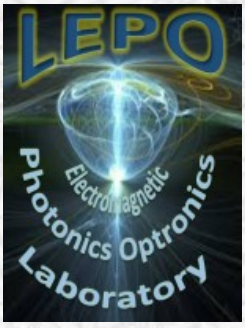
LEPO
Electromagnetic
Photonics Optronics
Laboratory